How breast cancer cells survive the epigenetic disruption caused by histone deacetylase inhibitors



Mairi Elizabeth MacRae

Institute of Cancer and Genomic Sciences
University of Birmingham

A thesis submitted for the degree of
Doctor of Philosophy
March 2023

UNIVERSITY OF
BIRMINGHAM

University of Birmingham Research Archive

e-theses repository

This unpublished thesis/dissertation is copyright of the author and/or third parties. The intellectual property rights of the author or third parties in respect of this work are as defined by The Copyright Designs and Patents Act 1988 or as modified by any successor legislation.

Any use made of information contained in this thesis/dissertation must be in accordance with that legislation and must be properly acknowledged. Further distribution or reproduction in any format is prohibited without the permission of the copyright holder.

Abstract

Histone deacetylase inhibitors (HDACi) have had a patchy history as anti-cancer treatments, only showing efficacy against specific haematological tumours. They have as yet shown no benefit when used in solid tumours. Previous work in our lab has shown that a specific transcriptional mechanism enables some cells to survive in the presence of an HDACi – a response termed the *HDACi survival response*. The coordinated change in the cell's gene expression pattern allows it to survive the epigenetic disruption caused by global protein hyperacetylation.

The work reported here sets out to identify the genes and signalling pathways that were crucial in allowing cells to survive the toxic effects of HDAC inhibition and explore the extent to which these key genes are mutated in cancer. This was done by analysing genes responding rapidly following SAHA (suberoylanilide hydroxamic acid) treatment of an HDACi sensitive (MDA-MB231) and more HDACi resistant (MCF7) cell-line. Factors predicted to drive this response were selected and their role validated through knockdown. This work identified key differences between our cell-lines. The knockdown of *ATF4* and *CREB3L4* increased the HDACi sensitivity of MCF7 cells, while *POU2F2, ATF4* and *ATF5* knockdown further enhanced the sensitivity of MDA-MB231 cells.

Reduced Representation Bisulfite Sequencing (RRBS) analysis showed that there was no evidence DNA methylation was involved in the early transcriptional response following HDACi treatment. However, it did show that HDACi inhibition induced a dynamic change in methylation in both cell-lines.

The CBioPortal database was used to compare our cell-lines to a breast cancer patient cohort. This analysis confirmed that MCF7 and MDA-MB231 cells were representative of their luminal A and triple-negative molecular subtypes in terms of expression of the key genes we have identified. Based on this and our experimental data, we hypothesised that triple-negative tumours may be more receptive to these drugs. Additionally, the genes selected for analysis appeared to be differentially expressed by subtype. Therefore, transcriptional profiles could

potentially be used to indicate a subpopulation of triple-negative tumours more likely to respond to HDAC inhibition.

Acknowledgments

I would firstly like to thank Bryan Turner and John Halsall for all their guidance and support; not only helping with lab techniques, but also helping me understand the real-world application of my project. I learned a lot and grew hugely in confidence, which I owe to you both. This extends out to all past and present lab members– thank you very much for working and laughing alongside me over the years.

Thank you to the BBSRC for funding this project – and to the MIBTP programme for the opportunity to do this work.

I would also like to thank Zymo Research. Thank you to Dr Yang, Dr Chen, and Dr Xu for carrying out the RNA-Sequencing and RRBS Analysis with us and providing valuable guidance on how to analyse these results.

Thank you to Claire Palles, Peter Keane, and Alex Maytum for your help with the Bioinformatics. A general shout out to everyone in WX2.03 and WX2.05 over the years. It has been such a help to have friendly faces in the office and the lab.

Finally, I would not have made it through without the support of my friends and family. To the girls, thank you for always being there for me. A special shout out to my mum, dad, Andrew, Jane, and Jetta. You do not know how much you did for me. You answered the phone, visited, and hugely supported me during this time. Thank you for listening attentively to descriptions of things that probably never made sense and always acting as though it was interesting. And to Jack, thanks for being there with me during the hardest bits.

Table of Contents

1. INTRODUCTION 1

1.1 The promise of HDACi therapy in cancer 1

1.2 Epigenetics in Cancer 1

1.3 Chromatin Structure 3

1.4 Histone Modifications 4

1.5 Histone Acetylation 5

1.5.1 Histone Acetyltransferases 7

1.5.2 Histone Deacetylases 8

1.5.3 Histone Deacetylase Inhibitors 10

1.6 Histone Methylation 12

1.7 DNA Methylation 13

1.7.1 DNA Methyltransferase Inhibitors 15

1.8 HDACi Survival Response 16

1.9 Crossover between HDAC and DNMT inhibition 22

1.10 HDACi in combination therapy 24

1.10.1 DNMT inhibitors 25

1.10.2 Radiotherapy 26

1.10.3 Hormonal therapies: 26

1.10.4 HER2 therapies: 27

1.11 Personalised HDACi treatment: 28

1.12 Project Aims and Objectives 29

2. MATERIALS AND METHODS 31

2.1 Cell Culture 31

2.2 Annexin V Assay 31

2.3 MTS Assay 32

2.4 Primer Design 33

2.5 Quantitative Polymerase Chain Reaction (qPCR) 36

2.6 POU2F2 splice variant expression 37

2.7 POU2F1 splice variant expression 39

2.8 Cell Cycle Analysis following DAC or SAHA treatment 39

2.9 Western Blotting 40

2.10 Flow Cytometry analysis of acetylation 42

2.11 RNA Synthesis Assay 44

2.12 Sample Preparation for Next Generation Sequencing (with Zymo Research) 44

2.12.1 RNA-sequencing sample preparation 44

2.12.2 RRBS sample preparation 45

2.13 RNA Sequencing 45

2.14 Analysis of RNA-sequencing data 46

2.15 Reduced Representation Bisulfite Sequencing (RRBS)....48
2.16 Analysis of RRBS data....49
2.17 Plasmid transformation....50
2.18 Transfection Optimization....50
2.19 Serum Response Factor (SRF) knockdown....51
2.20 SMARTpool siRNA formulations....51
2.21 Individual gene siRNA knockdown....52
2.22 Double siRNA knockdown....53
2.23 Triple siRNA knockdown....53
2.24 Analysis of target gene expression using CBioPortal....54
3. DEVELOPMENT OF A SOLID TUMOUR MODEL OF RESPONSE AND RESISTANCE TO HDACi TREATMENT....56
3.1 Initial identification of HDACi sensitive and resistant cell-lines....56
3.1.1 Breast cancer cell-line characteristics....57
3.2 Annexin V Assays showed that MDA-MB231 cells were more sensitive to treatment with DAC and SAHA....59
3.3 SAHA and DAC reduced the metabolic potential of MDA-MB231 cells....65
3.4 Cell cycle disruption does not explain the remarkable sensitivity of MCF10A cells in the DAC MTS Assay....68
3.5 MCF7 and MDA-MB231 cells exhibited the same cell-cycle alterations in response to SAHA treatment....71
3.6 Histone modifications occur within minutes of SAHA exposure in both HDACi sensitive and resistant cell-lines....75
3.7 Histone hyperacetylation occurred dynamically across the cell-cycle....77
3.8 The SAHA-induced transcriptional response was not observed against the background of overall RNA change....82
3.9 Chapter conclusions....84
4. WHOLE GENOME TRANSCRIPTOMIC AND EPIGENOMIC ANALYSIS OF MCF7 AND MDA-MB231 CELL-LINES FOLLOWING SAHA TREATMENT....86
4.1 A larger transcriptional response was induced in MCF7 cells following 2-hour SAHA treatment....86
4.2 Ontology suggested a common response, occurring earlier in MCF7 cells....95
4.3 Specific patterns of gene expression were induced in response to SAHA treatment..100
4.3.1 HAT gene expression was downregulated in response to HDACi treatment....100
4.3.2 The identified SAHA-responsive transcription factor genes were upregulated in MCF7 cells....106
4.3.3 Heat shock protein genes were variably expressed basally....109
4.4 Motif analysis identified factors driving early gene expression change....113
4.4.1 Predicted binding sites for ATF1, SRF and OCT6 were found in genes differentially expressed by 30-minutes in MCF7 cells....113
4.4.2 The predicted binding site for NFY was enriched among genes upregulated at 60-minutes in MCF7 cells....115

4.4.3 Sp1, NFY and ATF binding sites were enriched among MCF7 genes upregulated at 120-minutes 116
4.4.4 Significantly enriched motifs were only identified among genes upregulated at 120-minutes in MDA-MB231 cells 117
4.4.5 No common binding sites were identified among downregulated HAT genes 118
4.4.6 Chapter Conclusions 119

5. DOES DNA METHYLATION LOCK IN THE LONG-TERM SURVIVAL RESPONSE TO AN HDACi? 120

5.1 A greater number of differentially methylated CpG sites were identified in MDA-MB231 cells 121

5.2 A greater number of regions were differentially methylated in MDA-MB231 cells in response to SAHA treatment 125

5.3 Ontology confirmed that methylation was not related to coordinated gene expression changes 130

5.4 Motif analysis indicated that the methylation response was not TF specific 131

5.5 Are MCF7 cells inherently better at regulating methylation changes? 133

5.6 Chapter conclusions 134

6. DOES POU2F2 PLAY A ROLE IN THE HDACi SURVIVAL RESPONSE? 136

6.1 Identification and verification of targets for knockdown 136
6.1.1 SRF was identified among genes upregulated by 30-minutes in MCF7 cells 137
6.1.2 SMAD Family Member were similarly expressed in both cell-lines 137
6.1.3 The expression of POU2F2 differed between our cell-lines 139

6.2 SRF knockdown did not affect the SAHA sensitivity of MCF7 cells 143

6.3 POU2F2 transcript variant expression 145
6.3.1 Dream Taq DNA Polymerase amplified the POU2F2 coding sequence 147
6.3.2 TV5 was not expressed in MDA-MB231 cells 148
6.3.3 MDA-MB231 cells express four POU2F2 transcript variants 149
6.3.4 MDA-MB231 cells express TV1, 2, 4 and 7 150

6.4 MCF7 and MDA-MB231 cells express distinct POU2F1 transcript variants 152

6.5 POU family member knockdown 154
6.5.1 POU2F2 knockdown resulted in MDA-MB231 cells more sensitive to HDAC inhibition 154
6.5.2 POU2F1 knockdown did not affect the SAHA sensitivity of MCF7 cells 158
6.5.3 POU2F1 knockdown did not affect the SAHA sensitivity of MDA-MB231 cells 160
6.5.4 Double knockdown did not additionally increase the SAHA sensitivity of MDA-MB231 cells. 162

6.6 Was a transcriptional response induced through POU2F2? 165
6.6.1 HAT gene downregulation following HDACi treatment was maintained until 48-hours 166
6.6.2 POU2F2 knockdown did not affect the SAHA-induced HAT gene downregulation at 2-hours in either cell-line 168
6.6.3 The expression of POU2F2 regulated genes was affected by SAHA following knockdown 170

7. DO ATF FACTORS PLAY A ROLE IN THE HDACi SURVIVAL RESPONSE? 174

7.1 Activating Transcription Factors were differentially expressed in MCF7 and MDA-MB231 cell-lines 174

7.2 Knockdown of ATF/CREB family members in the resistant line 178
7.2.1 ATF5 knockdown did not affect the SAHA sensitivity of MCF7 cells 179
7.2.2 CREB3L4 knockdown enhanced the SAHA sensitivity of MCF7 cells 180

7.2.3 ATF4 knockdown enhanced the SAHA sensitivity of MCF7 cells....182
7.2.4 Double ATF4 and CREB3L4 knockdown did not increase the SAHA sensitivity of MCF7 cells above individual knockdown....184
7.2.5 The addition of ATF5 did not enhance on the response observed in MCF7 cells following ATF4 knockdown....185
7.3 Knockdown of ATF/CREB family members in the sensitive line....187
7.3.1 ATF5 knockdown enhanced the SAHA sensitivity of MDA-MB231 cells....188
7.3.2 CREB3L4 knockdown did not enhance the sensitivity of MDA-MB231 cells to SAHA treatment 189
7.3.3 ATF4 knockdown enhanced the SAHA sensitivity of MDA-MB231 cells....191
7.3.4 Double ATF4 and ATF5 knockdown was not additive in MDA-MB231 cells....193
7.3.5 The additional knockdown of CREB3L4 did not increase the loss in viability over double ATF4 and ATF5 knockdown....195
7.4 Was a transcriptional response to SAHA induced through ATF?....197
7.4.1 An ATF regulated response was observed in MDA-MB231 cells following 48-hour SAHA treatment....198
7.4.2 An ATF driven transcriptional response was observed in MCF7 cells following 2-hour SAHA treatment....199
7.4.3 ATF knockdown did not prevent SAHA-induced HAT gene downregulation....204
7.5 Knockdown across resistance pathways....208
7.5.1 ATF4 and POU2F2 appeared to converge on the same apoptotic pathways by 48-hours....209
7.5.2 The effect of ATF4 knockdown was lost in MCF7 cells with SRF also knocked down....213
7.6 Our model system was representative of the comparison between luminal A and triple-negative tumours....216
8. DISCUSSION....225
8.1 Are there multiple drivers of the HDACi survival response?....227
8.2 Is our goal still achievable?....229
8.3 Could HDAC inhibitors be targeted to triple-negative tumours?....230
8.4 What is the future for HDAC inhibitors in the clinic?....234
9. LIST OF REFERENCES....236
10. APPENDICES....260
10.1 Treatment with DAC for less than 96-hours did not induce apoptosis in our cell-lines 260
10.2 Both cell-lines responded similarly to SAHA treatment at the level of the cell-cycle.261
10.3 2-hour SAHA treatment induced histone hyperacetylation in both cell-lines....262
10.4 IgG and C-terminal staining were not affected by SAHA treatment....264
10.5 Correlation was observed between the MDA-MB231 timepoint samples in the RNA-Sequencing....265
10.6 The Lipofectamine 3000 transfection protocol was optimised for use in MCF7 and MDA-MB231 cells....266
10.7 Primers were designed to identify the unique exon structures of the POU2F2 transcript variants....269
10.8 Primers were designed to identify the unique exon structures of the POU2F1 transcript variants....270

List of Abbreviations

ANOVA: Analysis of Variance

AP-1: Activator Protein 1

APC- Allophycocyanin

ATF: Activating Transcription Factor

Bp: base pair

BL: Burkitt Lymphoma

bZIP: Basic Leucine Zipper Domain

cDNA: Complementary DNA

CDS: Coding Sequence

ChIP: Chromatin immunoprecipitation

CREB: cAMP Response Element-Binding Protein

CREB3L4: CAMP Response Element-Binding Protein 3 Like 4

CTCL: Cutaneous T-cell lymphoma.

DAC: Dacinogen

DEG: Differentially expressed gene

DMR: Differentially Methylated Region

DMS: Differentially Methylated Site

DNA: Deoxyribonucleic acid

DNMT: DNA methyltransferase

DNMTi: DNA methyltransferase inhibitor

EGR: Early Growth Response Protein

EPC1: Enhancer of Polycomb Homolog 1

EPC2: Enhancer of Polycomb Homolog 2

ER: Oestrogen Receptor

FBS: Foetal Bovine Serum

GFP: Green fluorescent protein

HAT: Histone Acetyltransferase

HDAC: Histone deacetylase

HDACi: Histone deacetylase inhibitor

HER2: Human epithelial receptor 2

HSP: Heat Shock Protein

HSPA1A: Heat Shock Protein Family A (Hsp70) Member 1A

HSPA1B: Heat Shock Protein Family A (Hsp70) Member 1B

HSPA5: Heat Shock Protein Family A (Hsp70) Member 5

HSPA13: Heat Shock Protein Family A (Hsp70) Member 13

HSPA14: Heat Shock Protein Family A (Hsp70) Member 14

IER: Immediate Early Response

IgG: Immunoglobulin G

ING5: Inhibitor of Growth Family Member 5

JADE: JADE Family PHD Finger

KAT6B: Lysine Acetyltransferase 6B (MYST2)

KAT7: Lysine Acetyltransferase 7 (MYST4)

KMT: Lysine methyltransferase

LCL: human lymphoblastoid cell-lines

LIN54: Lin-54 DREAM MuvB Core Complex Component

LRT: Likelihood ratio test

MBP: Methyl binding protein

MDS: Multidimensionality Scaling

mRNA: messenger ribonucleic acid

NFAT: Nuclear factor of activated T-cells

NF-κB: Nuclear Factor-κB

NFY: Nuclear Transcription Factor Y

NFYC: Nuclear Transcription Factor Y Subunit Gamma

NR4A: Nuclear Receptor Subfamily 4 Group A

NuRD: Nucleosome remodelling and deacetylase complex

OCT6: Octamer Binding Transcription Factor 6

OSR1: Odd-Skipped Related Transcription Factor 1

PBS: Phosphate-buffered Saline

PCR: Polymerase Chain Reaction

POU: Pit-1, Oct1/2, Unc-86 domain family

POU2F1: POU Class 2 Homeobox 1

POU2F2: POU Class 2 Homeobox 2

PR: Progesterone Receptor

P/S: Penicillin Streptomycin

PTCL: Peripheral T-cell lymphoma

PTM: post translational modifications

qPCR: Quantitative Polymerase Chain Reaction

RNA: Ribonucleic acid

rRNA: Ribosomal RNA

RPM: rotations per minute

RRBS: Reduced Representation Bisulfite Sequencing

RT: room temperature

SAHA: Suberanilohydroxamic acid (Vorinostat)

SD: Standard Deviation

SEM: Standard Error of the Mean

siRNA: Small interfering ribonucleic acid

Six4: SIX Homeobox 4

SMAD: SMAD Family Member

SOX2: SRY-Box Transcription Factor 2

Sp1: Sp1 Transcription Factor

SRE: Serum Response Element

SRF: Serum Response Factor

STAT3: Signal transducer and activator of transcription 3

TEB: Triton extraction buffer

TET: ten-eleven translocation

TF: Transcription Factor

TGF-β: transforming growth factor beta

tRNA: Transfer RNA

TSS: Transcription start site

TSA: Trichostatin A

TV: Transcript variant

UP: ultra-pure

VPA: Sodium Valproate/Valproic Acid

ZNF341: Zinc Finger Protein 341

List of Figures

Figure 1.1: 'Beads on a string' is the simplest chromatin conformation 4

Figure 1.2: Histone tails are subject to a variety of post translational modifications 5

Figure 1.3: Structure of human histone acetyltransferase complexes 8

Figure 1.4: Structure of human histone deacetylase complexes 10

Figure 1.5: Structure of SAHA 11

Figure 1.6: Decitabine structure 15

Figure 1.7: HDACi treatment induces a specific transcriptional response in LCL cells 17

Figure 1.8: HDAC inhibitors can be used in combination with many cancer therapies 25

Figure 3.1: Microscope images of MCF7 and MDA-MB231 cells 58

Figure 3.2: MDA-MB231 cells were more sensitive to 48-hour SAHA treatment 62

Figure 3.3: 96-hour DAC treatment induced apoptosis in MDA-MB231 cells 63

Figure 3.4: MDA-MB231 cells were sensitive to treatment with a histone deacetylase and DNA methyltransferase inhibitor 64

Figure 3.5: The metabolic potential of MDA-MB231 cells was most sensitive to treatment with SAHA 66

Figure 3.6: Treatment with DAC had little effect on the metabolic potential of MCF7 cells 68

Figure 3.7: 96-hour DAC treatment did not alter the cell-cycle profile of MCF10A cells 69

Figure 3.8: DAC treatment altered the cell-cycle distribution of MDA-MB231 cells 71

Figure 3.9: MCF7 and MDA-MB231 cells exhibited the same cell-cycle alterations in response to 48-hour SAHA treatment 72

Figure 3.10: MCF7 and MDA-MB231 cells exhibited similar cell-cycle alterations in response to SAHA treatment 73

Figure 3.11: 48-hour SAHA treatment induced a G2 cell-cycle block in MCF7 and 74

MDA-MB231 cells

Figure 3.12: SAHA treatment induced changes in histone acetylation and methylation by 120-minutes 77

Figure 3.13: SAHA treatment induced H3K27 hyperacetylation in MCF7 and MDA-MB231 cells 80

Figure 3.14: SAHA induced H3K27 hyperacetylation across the cell-cycle in both cell-lines 82

Figure 3.15: The SAHA-induced transcriptional response was not observed against the overall RNA content of the cells 84

Figure 4.1: SAHA induced a greater transcriptional response in MCF7 cells by 120-minutes 89

Figure 4.2: A rapid transcriptional response was induced in MCF7 cells in response to SAHA treatment 93

Figure 4.3: A greater number of genes were differentially expressed in MCF7 cells following SAHA treatment 95

Figure 4.4: A common set of genes respond to SAHA treatment in MCF7 and MDA-MB231 cells 96

Figure 4.5: Similar GO Terms were identified in MCF7 and MDA-MB231 cells in response to 2-hour SAHA treatment 99

Figure 4.6: SAHA treatment resulted in the downregulation of HAT complex component genes in MCF7 and MDA-MB231 cells 102

Figure 4.7: HAT component genes were downregulated after an initial 30-minute upregulation in both cell-lines following SAHA treatment 103

Figure 4.8: SAHA treatment significantly altered the expression of HDAC genes in MCF7 cells 105

Figure 4.9: HDAC gene expression was not affected by SAHA treatment in either cell-line 105

Figure 4.10: SAHA induced a greater upregulation of transcription factor genes in MCF7 cells 107

Figure 4.11: The identified SAHA-responsive transcription factor genes were more highly expressed basally in MCF7 cells 107

Figure 4.12: The selected SAHA-responsive transcription factor genes were 109

upregulated following SAHA treatment in both cell-lines

Figure 4.13: A greater number of heat shock protein genes were significantly upregulated in the MCF7 cell-line after SAHA treatment 110

Figure 4.14: Heat shock protein genes were variably expressed in response to SAHA 111

Figure 4.15: HSP genes were variably expressed basally in MDA-MB231 cells 112

Figure 4.16: Predicted SRF and ATF1 binding sites were enriched in genes upregulated at 30-minutes in MCF7 cells 114

Figure 4.17: An OCT6 predicted binding site was identified among MCF7 genes downregulated at 30-minutes 115

Figure 4.18: The NFY binding site was identified in genes upregulated at 60-minutes in MCF7 cells 116

Figure 4.19: Sp1, NFY and ATF binding sites were identified in genes upregulated at 120-minutes in MCF7 cells 117

Figure 4.20: Binding sites for NFY and Sp1 were found among MDA-MB231 genes upregulated at 120-minutes 118

Figure 4.21: No significant binding site was identified among the downregulated HAT genes 118

Figure 5.1: SAHA treatment progressively altered the methylated fraction of the MCF7 and MDA-MB231 genomes 122

Figure 5.2: A greater number of CpG sites in MDA-MB231 cells exhibited differential methylation after SAHA treatment 123

Figure 5.3: SAHA treatment induced an initial loss in methylation at 24-hours 125

Figure 5.4: More differentially methylated regions were identified in MDA-MB231 cells 126

Figure 5.5: At 24-hours DMRs in MDA-MB231 cells exhibited a strong loss in methylation 127

Figure 5.6: More differentially methylated regions in MDA-MB231 cells were located at promoters 128

Figure 5.7: A greater number of DMRs located at promoter regions in MDA-MB231 cells exhibited a loss in methylation 129

Figure 5.8: OSR1 and SOX2 binding sites were enriched among the 48-hour DMRs in MDA-MB231 cells 131

Figure 5.9: DMRs located at promoters were enriched for LIN54, ZNF341 and NFAT binding sites 132

Figure 5.10: TET and DNMT genes were more highly expressed basally in MCF7 cells 134

Figure 6.1: SMAD transcription factor genes were similarly expressed in MCF7 and MDA-MB231 cells 139

Figure 6.2: POU2F2 was expressed alongside POU2F1 in MDA-MB231 cells 141

Figure 6.3: POU2F2 was expressed only in MDA-MB231 cells 142

Figure 6.4: SRF knockdown was most efficient on Day 1 post-transfection 144

Figure 6.5: SRF knockdown did not affect the apoptotic response in MCF7 cells treated with SAHA 145

Figure 6.6: POU2F2 mRNA was expressed only in MDA-MB231 cells 148

Figure 6.7: Four POU2F2 transcript variants were identified in MDA-MB231 cells for sequencing 148

Figure 6.8: Four POU2F2 transcript variants from MDA-MB231 cells were sequenced 150

Figure 6.9: Exon boundary primers quantified the expression of TV1,2,4 and 7 151

Figure 6.10: TV1 was the dominant POU2F2 variant expressed in MDA-MB231 cells 152

Figure 6.11: MCF7 and MDA-MB231 cells express different POU2F1 transcript variants 153

Figure 6.12: POU2F2 expression was reduced in MDA-MB231 cells following knockdown 155

Figure 6.13: POU2F2 knockdown enhanced the late-apoptotic population of MDA-MB231 cells 156

Figure 6.14: POU2F2 knockdown significantly increased the late apoptotic population following SAHA treatment of MDA-MB231 cells 157

Figure 6.15: POU2F1 expression was reduced in MCF7 cells following knockdown 158

Figure 6.16: POU2F1 knockdown did not affect the SAHA sensitivity of MCF7 cells 159

Figure 6.17: POU2F1 expression was reduced in MDA-MB231 cells following knockdown 160

Figure 6.18: POU2F1 knockdown did not affect the SAHA sensitivity of MDA-MB231 cells 161

Figure 6.19: POU2F1 and POU2F2 expression was reduced in MDA-MB231 cells following double knockdown 162

Figure 6.20: Knocking down POU2F1 with POU2F2 in MDA-MB231 cells did not enhance on the apoptotic response observed following POU2F2 knockdown 164

Figure 6.21: POU2F2 knockdown did not prevent SAHA induced HAT gene downregulation in MDA-MB231 cells at 48-hours 167

Figure 6.22: POU2F1 knockdown did not prevent SAHA induced HAT gene downregulation in MCF7 cells at 48-hours 167

Figure 6.23: POU2F2 was upregulated in the presence of SAHA 168

Figure 6.24: HAT gene downregulation was greater following POU2F2 knockdown at 2-hours in MDA-MB231 cells 170

Figure 6.25: ATXN7L2 and JMJD8 expression was dysregulated following POU2F2 knockdown 172

Figure 6.26: The expression of MEPCE and MIR17HG was reduced by SAHA Treatment irrespective of POU2F2 knockdown 172

Figure 7.1: ATF4, ATF5 and CREB3L4 were selected as targets for knockdown 176

Figure 7.2: The expression of ATF4, ATF5 and CREB3L4 differed in our cell-lines 177

Figure 7.3: ATF5 knockdown did not increase SAHA induced apoptosis in MCF7 cells 180

Figure 7.4: CREB3L4 knockdown significantly increased the number of late apoptotic MCF7 cells following SAHA treatment 181

Figure 7.5: ATF4 knockdown significantly increased SAHA-induced apoptosis in MCF7 cells 183

Figure 7.6: Double ATF4 and CREB3L4 knockdown did not increase the SAHA sensitivity of MCF7 cells above individual knockdown 185

Figure 7.7: The additional knockdown of ATF5 did not enhance the apoptotic response induced in MCF7 cells following ATF4 knockdown 187

Figure 7.8: ATF5 knockdown significantly reduced the viable and increased the apoptotic MDA-MB231 population remaining after SAHA treatment 189

Figure 7.9: CREB3L4 knockdown did not affect the sensitivity of MDA-MB231 cells to SAHA treatment 190

Figure 7.10: ATF4 knockdown enhanced the apoptosis induced in MDA-MB231 cells treated with SAHA 192

Figure 7.11: ATF4 knockdown significantly reduced the number of viable MDA-MB231 cells remaining after SAHA treatment 193

Figure: 7.12: Knockdown of ATF4 with ATF5 did not significantly increase the SAHA-induced loss in viability when compared with individual knockdown 194

Figure 7.13: The additional knockdown of CREB3L4 did not increase the loss in viability over double ATF4 and ATF5 knockdown 196

Figure 7.14: ATF regulated expression of HSPA5 was lost following 48-hour SAHA treatment in MDA-MB231 cells 199

Figure 7.15: SAHA treatment downregulated ATF4 expression in MCF7 cells 200

Figure 7.16: ATF regulated genes responded similarly to SAHA treatment following ATF4 knockdown in MCF7 cells 202

Figure 7.17: SAHA treatment did not affect ATF4 expression in MDA-MB231 cells 203

Figure 7.18: No ATF4 dependent transcriptional regulation was observed in MDA-MB231 cells 204

Figure 7.19: HAT gene downregulation was still observed in MCF7 cells following ATF4 knockdown 206

Figure 7.20: ATF4 knockdown did not affect HAT gene downregulation in MDA-MB231 cells 208

Figure 7.21: Triple pathway knockdown enhanced the proportion of MDA-MB231 cells present in late-apoptosis 211

Figure 7.22: The knockdown of POU2F2 with ATF4 in MDA-MB231 cells was neither additive not protective 212

Figure 7.23: The effect of ATF4 knockdown was lost in MCF7 cells with SRF also knocked down 214

Figure 7.24: Genes of interest were predominantly amplified in breast cancer samples 218

Figure 7.25: Commonly amplified genes are located at similar chromosomal positions 219

Figure 7.26: The molecular subtypes were not associated with a gene copy number of mutation signature 220

Figure 7.27: A gene expression signature was evident in triple-negative and luminal A samples 221

Figure 7.28: The selected TF genes were differentially expressed between triple-negative and luminal A samples 222

Figure 7.29: Heat shock protein genes were differentially expressed in triple-negative and luminal A patient samples 223

Figure 7.30: HSPA1A, HSP90B1 and HSP90AB1 were differentially expressed in triple-negative and luminal A samples 224

List of Tables

Table 1.1: Licensed HDAC inhibitors 11

Table 1.2: Transcriptional changes observed in the presence of HDAC inhibitors 21

Table 2.1: Primers designed for qPCR analysis of gene expression 34

Table 2.2: Reddy Mix 40-cycle thermal profile 38

Table 2.3: Pfu DNA Polymerase 35-cycle thermal profile 38

Table 2.4: Dream Taq DNA Polymerase 35-cycle thermal profile 38

Table 2.5: Antibodies used for Western Blot analysis of acetylation and Methylation changes 41

Table 2.6: Antibodies used for flow cytometry analysis of acetylation 43

Table 2.7: SMARTpool siRNA formulations 52

Table 3.1: SAHA IC50 values per cell-line 66

Table 3.2 DAC IC50 values per cell-line 68

Table 7.1: Knockdown efficiency observed with ATF/CREB factors 196

Table 7.2: Knockdown efficiency in triple pathway knockdown 215

Table 8.1: Summary of gene knockdown effect in each cell-line 227

1. INTRODUCTION

1.1 The promise of HDACi therapy in cancer

Histone deacetylase inhibitors (HDACi) have had a long, yet not very successful, history as anti-cancer therapies. Interest in targeting the histone deacetylase (HDAC) enzymes stemmed from their involvement in important cellular processes such as cell-cycle regulation, proliferation, and the deoxyribonucleic acid (DNA) damage response (Thiagalingam *et al.,* 2003; Minucci and Pelicci, 2006). Additionally, they play important roles in cancer through their regulation of histone and non-histone protein acetylation (Alseksek *et al.,* 2022). These forms of therapy were of particular interest as it had been discovered that epigenetic dysregulation occurred during the initiation of cancer (Nepali and Liou, 2021). HDACi demonstrated antitumour activity *in vivo*, inducing cell-cycle arrest, reactive oxygen species (ROS) production and apoptosis (Chun, 2015; Singh *et al.,* 2018). They were successful initially in some haematological tumours, which led to the belief that HDACi would be effective in all cancers. However, these drugs do not work in solid tumours (Fantin and Richon, 2007). This is surprising as the increase in histone and non-histone protein acetylation induced by these drugs was expected to affect gene regulation and epigenetic processes.

1.2 Epigenetics in Cancer

Cancer was initially understood as a disease of genetic origin (Vogelstein and Kinzler, 2004; Hanahan and Weinberg, 2011). However, it is now recognised that epigenetics is also essential during the initiation and development of cancer (Damaskos *et al.,* 2017;

Baylin and Jones, 2011). Epigenetics involves the modification and maintenance of genetic information through gene expression changes, without any alteration to the underlying DNA sequence (Jones and Laird, 1999). Gene expression is epigenetically controlled through the regulation of chromatin structure – which involves histone modifications, long non-coding ribonucleic acid (lncRNA), and DNA methylation (Esteller, 2008). This differs from genetics, in which information is directly inherited from the DNA sequence (Jones and Laird, 1999). The important therapeutic distinction between them is that epigenetic modifications are reversible. Though gene expression has been altered, the underlying DNA structure has not changed. The clinical interest in epigenetic drugs stems from the belief that these changes could be pharmacologically manipulated to re-express genes which have been silenced during tumour development (Issa and Kantarijan, 2009).

DNA methylation was the earliest epigenetic modification linked with cancer. This was initially observed in colorectal cancer tissue, which exhibited a reduction in DNA methylation compared with normal tissue from matched patients (Feinberg and Vogelstein, 1983; Gama-Sosa *et al.,* 1983). Dysregulated DNA methylation as well as disordered chromatin structure are often observed prior to the development of genetic mutations (Flavahan *et al.,* 2017; Feinberg, 2005; Feinberg *et al*., 2006). The aberrant activity and altered expression of HDACs, an enzyme family which will be discussed later, has been observed in many cancers (Suraweera *et al.,* 2018; Alseksek *et al.,* 2022). The upregulation of HDAC expression has been associated with a poorer prognosis (Witt *et al.,* 2009; Marks, 2010). For example, HDAC1, 2 and 3 overexpression are correlated with a worse prognosis in ovarian or gastric cancer (Weichert *et al.,* 2008a; Weichert *et al.,* 2008b). However, there is no definitive answer on how HDACs are expressed in cancer and whether their expression is associated with a worse prognosis (Alseksek *et al.,* 2022). For

example, HDAC1 and HDAC6 expression correlate with longer disease-free survival in breast cancer (Krusche *et al.,* 2005; Zhang *et al.,* 2004; Zhang *et al.,* 2005; Seo *et al.,* 2014).

1.3 Chromatin Structure

Chromatin consists of eukaryotic DNA associated with histone and non-histone proteins (Hull *et al.,* 2016). Histones are the basic proteins around which the DNA strand is wound for efficient packaging into the nucleus (Annunziato, 2008). The nucleosome is the simplest unit of chromatin, composed of a core subunit attached to linker DNA (Cutter and Hayes, 2015). This subunit consists of 147 DNA base pairs wound around a histone octamer containing two copies of histone H2A, H2B, H3 and H4 (Luger *et al.,* 1997). There is a fifth histone, H1, which does not form part of the core octamer. This linker histone binds externally to the core subunit and influences nucleosome spacing in higher eukaryotes (Fan *et al.*, 2003). The simplest chromatin conformation, 'beads on a string', consists of nucleosomes and their associated linker DNA (Figure 1.1; van Holde, 1989; Bell *et al.,* 2011).

The N-terminal histone tails exist outside the core and are largely unstructured (Cutter and Hayes, 2015; Luger *et al.,* 1997). This leaves them subject to post translational modifications (PTM) such as acetylation or methylation (Shahbazian and Grunstein, 2007). These modifications create new protein binding sites on the nucleosomes. Non-histone proteins bind at these newly created sites, thus any PTMs will affect where proteins can bind (Nightingale *et al*., 2006). In addition, these modifications induce structural changes by altering the interaction of histones with the DNA. For example, acetylation of a lysine

residue neutralises its positive charge, which is thought to reduce its interaction with the DNA (Chueh *et al.,* 2015). Though observed *in vitro* – there is limited *in vivo* evidence of this occurring (Chueh *et al*., 2015). N-terminal histone tails do not mediate core-residue interactions, so it is not clear how these changes would be involved in regulating chromatin structure (Turner *et al.,* 1990).

'Beads on a string' is the simplest chromatin conformation

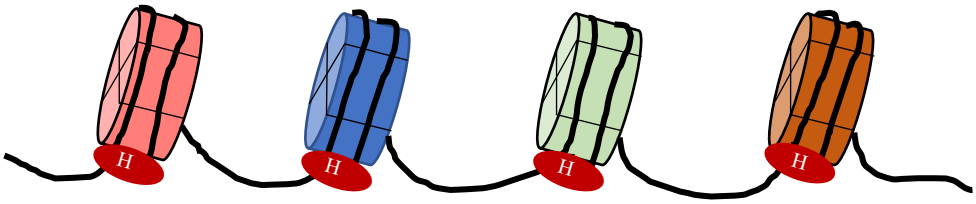


Figure 1.1: The 'beads on a string' structure depicts nucleosomes separated by linker DNA. *Shown is the position of four nucleosomes on the DNA strand. The nucleosome core consists of a histone octamer – around which the DNA is wound twice. Adapted from Luger et al., 2012.*

1.4 Histone Modifications

Histones are important signalling molecules, not only structural proteins (Turner, 2014). They are subject to a variety of reversible PTMs. This enables the enzymes responsible for these modifications to influence gene expression (Bassett and Barnett, 2014). Histones can be modified on multiple sites, so all modifications are influenced by those occurring on adjacent residues (Figure 1.2; Workman and Kingston, 1998; Strahl and Allis, 2000). Though primarily recognised on histone tails, core residues can also be modified. However, much less is known about how these affect the DNA structure. Acetylation of H3K115 and H3K122, which are located at the DNA-histone interface of the nucleosome, reduces the interaction between the histone and the DNA (Hyland *et al.,* 2005; Manohar *et al.,* 2009).

Histone tails are subject to a variety of post translational modifications

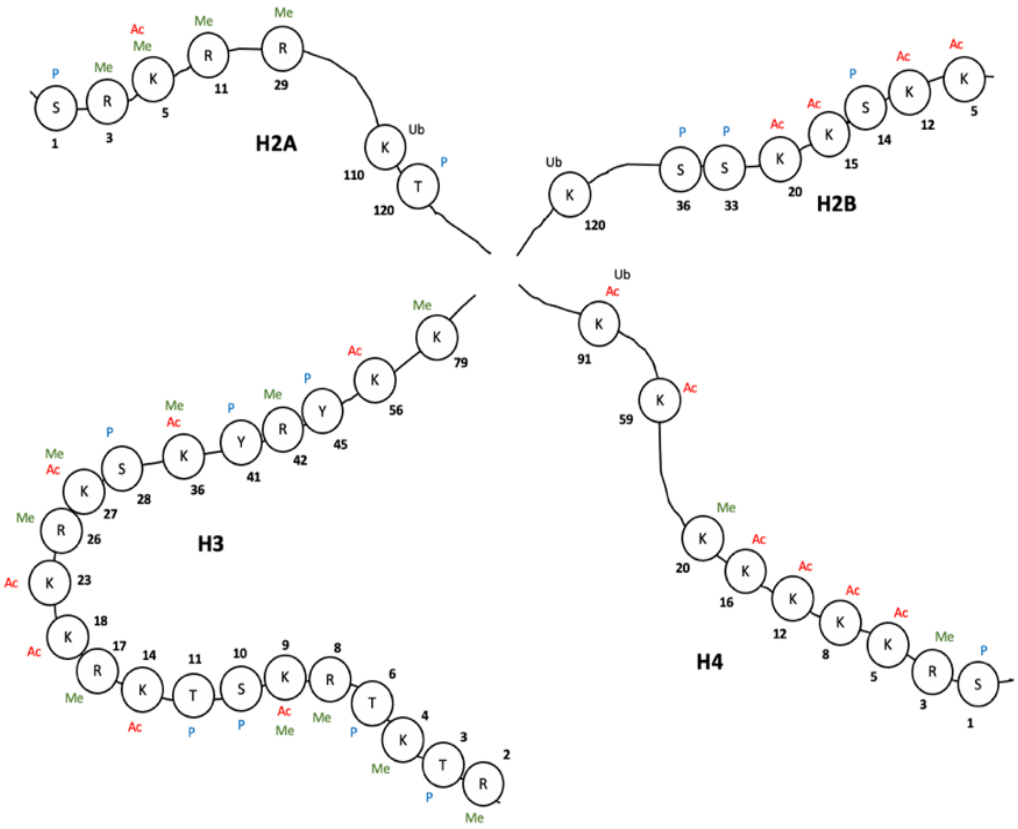


Figure 1.2: Residues on each histone tail can be modified. *Shown are the protruding N-terminal tails of the four-histone core subunits; H2A, H2B, H3 and H4. The numbers indicate their position on each tail. Ac depicts residues which can be acetylated, Me depicts those methylated, P phosphorylated and Ub ubiquitinated.*

1.5 Histone Acetylation

Catalysed by histone acetyltransferase (HAT) enzymes, acetylation involves the transfer of an acetyl group ($COCH_3$) from acetyl-CoA onto a lysine residue (Bojang and Ramos, 2014). This is directly balanced by HDACs, which catalyse the removal of acetyl groups from lysine (Richon, 2006). Allfrey *et al.,* in 1964 were the first to suggest that histone acetylation may regulate gene expression. As acetylation is highly dynamic, environmental

changes can alter acetylation levels and thereby potentially modify gene expression (Suraweera *et al*., 2018).

Acetylation is historically associated with an increase in gene transcription. This was thought to occur through a disruption of the interaction between histones and DNA, opening the chromatin to allow access for the transcription machinery (Bassett and Barnett, 2014; Shahbazian and Grunstein, 2007). This is exemplified by the acetylation of H4K16, which disrupts higher order chromatin structure (Turner, 2014; Shogren-Knaak *et al.,* 2006).

It is through the creation of new receptor sites on nucleosomes that histone modifications influence transcription (Turner, 1993; Cheung *et al.,* 2000). These receptor sites are recognised by binding proteins which act to initiate downstream biological processes, such as transcription (Strahl and Allis, 2000). This mechanism was initially proposed by Turner (Turner *et al.,* 1992; Turner, 1993). This association was confirmed using acetyl-lysine antibodies (Turner, 1993; Turner and Jeppesen, 1993). The link between histone modification and transcription regulation was then proven when the initial protein with acetylase activity was identified (Brownell *et al.,* 1996). This was followed by the discovery of the first mammalian histone deacetylase, HDAC1 (Taunton *et al.,* 1996). The "language of histones" metaphor put forward by Strahl and Allis in 2000 extended this idea. This recognised that many proteins were involved in processing the information contained in these PTMs. Enzymes such as HATs, which laid down PTMs were referred to as 'writers' while enzymes removing these modifications were referred to as 'erasers'. (Nightingale, 2016). Proteins termed 'readers' recognise and bind at these modified sites (Yun *et al.,* 2011). They use them as docking sites to recruit complexes which mediate

downstream biological changes (Strahl and Allis, 2000). An important example of which are bromodomain containing proteins, which bind to acetyl-lysine (Winston and Allis, 1999). For example, bromodomain-containing protein 4 (BRD4) binds acetylated H4K5, 8 and 12 to initiate transcriptional elongation (Chueh *et al.,* 2015). It is through these interactions that epigenetic modification of histone tails leads to transcriptional change.

HATs are interchangeably referred to as lysine acetyltransferases (KAT), as they can acetylate not only histones – but also many non-histone proteins (Yang and Seto, 2008). Acetylation influences protein stability and function as well as protein interactions (Glozak *et al*., 2005). For example, acetylation of transcription factors (TF) affects their cellular location and their ability to interact with DNA. This is seen with signal transducer and activator of transcription 3 (STAT3) and nuclear factor-κB (NF-κB), which shuttle between the cytoplasm and nucleus based on their acetylation (Seidel *et al.,* 2012; Chueh *et al.,* 2015). For example, NF-κB is removed from the DNA once K122 and 123 in its p65 subunit have been acetylated (Kiernan *et al.,* 2003).

1.5.1 Histone Acetyltransferases

HAT enzymes can be separated into two groups based on their cellular location. Type B exist in the cytoplasm and acetylate newly synthesised histones before they are incorporated into DNA (Parthun *et al.*, 1996). On the other hand, Type A enzymes acetylate histones and non-histone proteins in the nucleus (Wapenaar and Dekker, 2016). Nuclear HATs can be further subdivided into families based on sequence homology. The largest is MYST, named after its members MOZ, Ybf2/Sas3, Sas2 and Tip60 (Marmostein, 2001). The Gcn5-related-N-acetyltransferase (GNAT) family –

includes enzymes such the p300/CBP-associated factor (PCAF) (Neuwald and Landsman, 1997). p300/CBP, consisting of CBP and p300, make up the final HAT family (Ogryzko *et al.,* 1996). Additionally, it has been shown that some transcription and steroid receptor co-activators exhibit acetyltransferase activity alongside their primary function (Marmostein, 2001).

HATs exist within protein complexes, with their histone residue specificity influenced by the additional subunits they contain (Figure 1.3; Carrozza *et al.,* 2003; Lee and Workman, 2007). For example, MOF can acetylate free histones H4, H2B and H3 but can only acetylate H4K16s as part of the MSL complex (Carrozza *et al.,* 2003; Figure 1.3B).

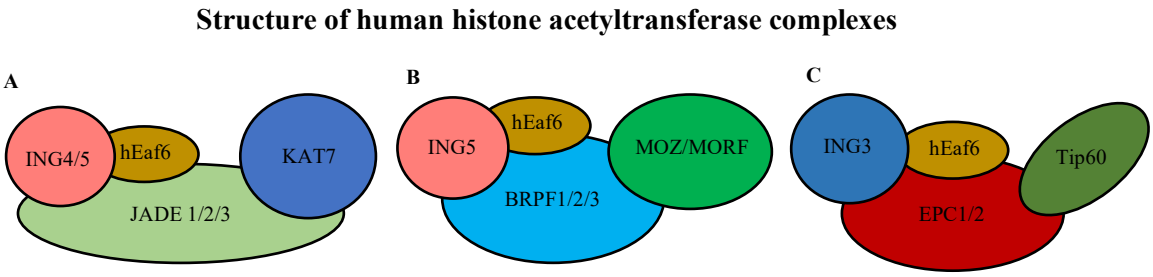


Figure 1.3: Structure of three human histone acetyltransferase complexes. *Shown are the subunits and proposed structures of three HAT complexes containing A. Lysine Acetyltransferase 7 (KAT7) B. Monocytic leukemic zinc-finger/monocytic leukemic zinc-finger related factor (MOZ/MORF) and C. Tat interactive protein 60 (Tip60). Adapted from Avvakumov et al., 2012.*

1.5.2 Histone Deacetylases

HDACs are generally viewed as transcriptional repressors. Deacetylation, and the removal of acetyl groups from lysine residues, was thought to increase the positive charge on a histone. Historically, this was associated with chromatin condensation and restricted access to the DNA (Bassett and Barnett, 2014; Richon, 2006). HDACs were

thought to be bound at repressed genes and then replaced by HATs following gene activation (Xu *et al.,* 1999). However, it has been shown that HDACs can also be bound at active genes alongside HATs. This suggests that they are involved in removing acetyl groups to reset chromatin modifications following gene activation (Wang *et al.,* 2009; Dovey *et al.,* 2010).

There are four distinct classes of HDAC enzyme. Class I consists of HDAC1, 2, 3 and 8. These enzymes are nuclear, more ubiquitously expressed than other HDAC Classes and contain a zinc dependent active site (Bertrand, 2010). Class II enzymes are also zinc dependent, but they are larger in size (Thiagalingam *et al.,* 2003). They can be further subdivided into IIa (HDAC4, 5, 7 and 9) and IIb (HDAC6 and 10) based on sequence homology (Park and Kim, 2020). Class IIb enzymes are primarily found in the cytoplasm. Class III are homologous to the yeast SIR2 protein and instead depend on nicotinamide adenine dinucleotide (NAD) for activation (Imai *et al.*, 2000). Class IV consists only of HDAC11 (Bertos *et al*., 2001).

HDAC enzymes cannot directly bind DNA. Those in Class I are recruited to genes primarily through their incorporation into large multiprotein transcriptional complexes (Millard *et al*., 2017). HDAC1 and HDAC2 exist as homo or heterodimers in the NuRD (nucleosome remodelling and deacetylase), CoREST and Sin3 complexes (Kelly and Cowley, 2012; Figure 1.4). On the other hand, HDAC3 seems to be recruited only to the silencing mediator of retinoic acid (SMRT)/nuclear receptor corepressor (NCoR) complexes (Wen *et al.,* 2000; Figure 1.4D). These complexes are then recruited to the DNA by TFs (de Ruijter *et al.,* 2003; Yang and Seto, 2008). The additional components in these complexes regulate the activity of the HDAC and their targeting to specific

cellular or genomic locations (Sengupta and Seto, 2004). Importantly, histones are not the only target of HDACs (Minucci and Pelicci, 2006; Gregoretti *et al.,* 2004). HDACs can also deacetylate many non-histone proteins, including signalling molecules and TFs such as p53 or STAT3 (Glozak *et al.,* 2005).

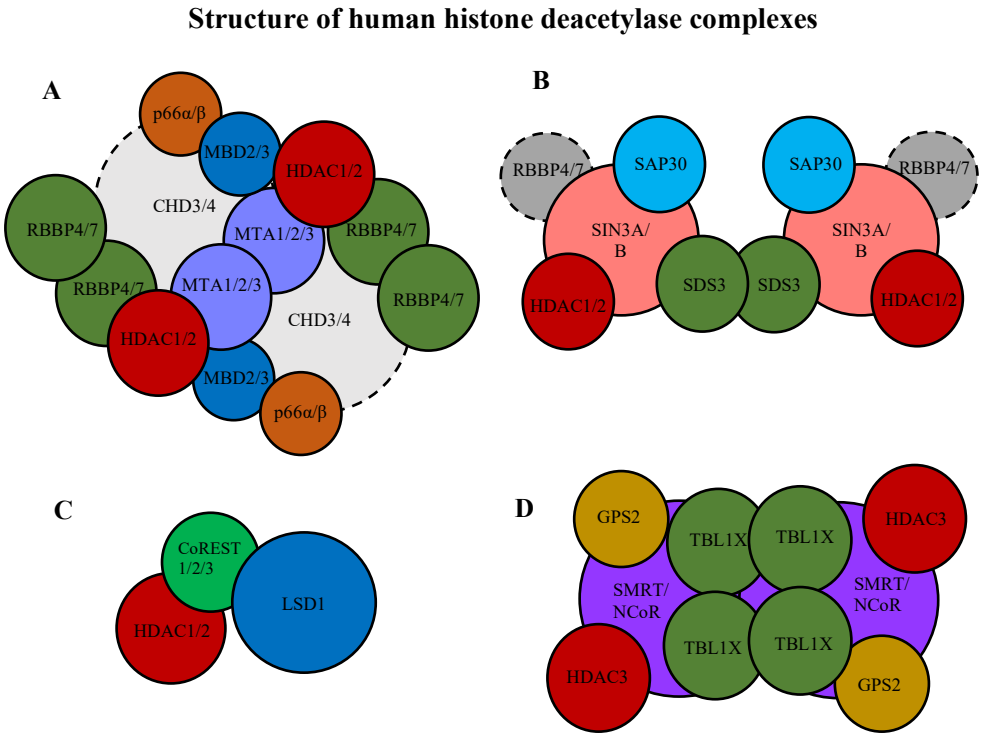


Figure 1.4: Structure of four histone deacetylase complexes. *Shown are the subunits and proposed structures of the A. Nucleosome remodelling and deacetylase (NuRD) B. Sin3 C. CoREST and D. Silencing mediator of retinoic acid (SMRT)/ nuclear receptor co-repressor (NCoR) HDAC complexes. Image adapted from Millard et al., 2017.*

1.5.3 Histone Deacetylase Inhibitors

There are four types of HDACi inhibitor: hydroxamic acid, cyclic peptide, benzamide and aliphatic acid (Bassett and Barnett, 2014). Suberoylanilide hydroxamic acid (SAHA) also known as vorinostat and marketed by Merck as Zolinza was the first HDACi licensed for use, approved to treat cutaneous T-cell lymphoma (CTCL) (Mann *et al.,* 2007). Four further HDACi have been licensed for peripheral T-cell lymphoma

(PTCL), pre-treated multiple myeloma and refractory PTCL (Smalley *et al.,* 2020; Table 1.1).

Table 1.1: Licensed HDAC inhibitors

Drug	Cancer Type	Inhibitor Type	Reference
Vorinostat	CTCL	Hydroxamic acid	Mann *et al.,* 2007
Romidepsin	CTCL and PTCL	Cyclic peptide	Piekarz *et al.,* 2011
Belinostat	Refractory PTCL	Hydroxamic acid	Lee *et al.,* 2015
Panobinostat	Pre-treated multiple myeloma	Hydroxamic acid	Laubach *et al.,* 2015
Tucidinostat	PTCL	Benzamide	Lu *et al*., 2016

The active site of the zinc (Zn^{2+}) dependent Class I and Class II HDAC enzymes is a tubular pocket. Two adjacent histidines, two aspartic residues, a tyrosine and the Zn^{2+} ion at the base of the pocket create a charge relay system (Finnin *et al.,* 1999). It is the zinc ion which hydrolyses the acetyl-lysine bond. Cells in this project were treated with SAHA, which is a hydroxamic acid inhibitor (Figure 1.5). The acid component chelates the Zn^{2+} ion at the base of the pocket, with the attached hydrophobic chain then blocking the space where the acetyl lysine would normally bind (Finnin *et al*., 1999; Villar-Garea and Esteller, 2004).

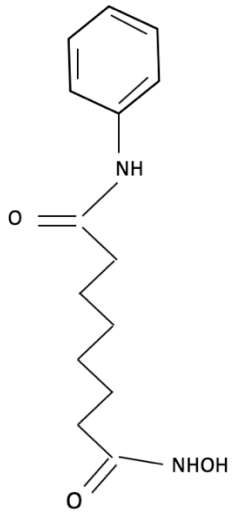


Figure 1.5: Structure of SAHA. *The acid component binds zinc in the HDAC active site, and the hydrophobic side chain then fills the active site. Adapted from Villar-Garea and Esteller, 2004.*

Some tumour cells are more sensitive than normal cells to HDACi treatment. SAHA treatment arrests the growth of normal cells but does not induce apoptosis as it does in cancer cells (Ungerstedt *et al.,* 2005; Marks *et al.,* 2001). However, this was not believed to be due to a lack of HDAC inhibition. Thioredoxin, a redox protein involved in protecting against oxidative stress, was shown to be more highly expressed in normal cells (Minucci and Pelicci, 2006). Transfection of thioredoxin siRNA (small interfering ribonucleic acid) into normal cells increased both oxidative stress and cell death - suggesting that thioredoxin may usually protect them from HDACi induced damage (Ungerstedt *et al.,* 2005; Robey *et al.,* 2011).

1.6 Histone Methylation

Histone methylation is mediated through lysine methyltransferases (KMT) and lysine demethylases (KDM) (Bannister and Kouzarides, 2011). As methylation does not affect the charge on the amino-acid side chain, the outcome depends on the downstream effector molecules recruited to specific sites (Hyun *et al.,* 2017). Thus, methylation can lead to gene activation or silencing. For example, methylation of H3K4 or H3K36 is associated with gene activation (Rada-Iglesias *et al.,* 2007; Bernstein *et al.*, 2006). Trimethylation of H3K4 promotes the binding of chromatin re-modellers such as chromodomain-helicase-DNA binding domain 1 (CHD1), while preventing the binding of repressors such as the NuRD complex **(**Flanagan *et al*., 2005; Nishioka *et al.,* 2002). On the other hand, methylation of H3K27 and H3K9 are associated with gene silencing (Black *et al.,* 2012; Kuzmichev *et al.,* 2002).

1.7 DNA Methylation

DNA methylation involves the addition of a methyl (CH_3) group onto position 5 of the cytosine pyrimidine ring, creating 5-methyl-cytosine (Santini *et al*., 2001). This is catalysed by the DNA-methyltransferase (DNMT) family of enzymes, which consists of three important enzymes: DNMT1, DNMT3a and DNMT3b. DNA methylation is laid down by the *de novo* enzymes, DNMT3a and DNMT3b, primarily during embryonic development while DNMT1 ensures methylation patterns are passed to daughter cells during replication (Okano *et al.,* 1999; Bestor, 2000). All three DNMT enzymes are expressed in embryonic and post-natal tissue, meaning that DNMT3a/3b also contribute to methylation after embryonic development (Okano *et al.,* 1999).

DNMT1 is the best studied of this family. Its C-terminus contains the catalytic domain, while its N-terminus contains important regulatory domains –involved in processes such as nuclear import (Bestor, 2000). Deacetylation regulates the activity of the DNMT1 protein. This is most clearly demonstrated by the degradation of DNMT1 following HDAC inhibition (Zhou *et al.,* 2008). HDACs have been shown directly interacting with DNMT1. This led to the discovery of 12 new lysine residues on DNMT1 which are subject to acetylation (Peng *et al.,* 2011). These exist across the three domains of the protein. Four of these residues exist in the N-terminal region, while a further six are in the central region of the protein (Peng *et al.,* 2011). The final two lysine residues are in the catalytic domain, with their deacetylation shown to enhance the methyltransferase activity of DNMT1 (Peng *et al*., 2011).

What is interesting about the pattern of DNA methylation in the genome is the presence of CpG islands, regions of the DNA containing a high CpG frequency (Momparler and Bovenzi, 2000; Deaton and Bird, 2011). The majority of CpG dinucleotides in the genome are methylated, while CpG islands remain predominantly unmethylated (Smith and Meissner, 2013). Around 50% of mammalian genes have CpG islands in their promoter regions (Santini *et al.,* 2001; Wang and Leung, 2004). Methylation of CpG islands is therefore associated with the silencing of genes (Santini *et al.,* 2001). In a direct sense, methylation would alter the accessibility of CpG islands to TFs and the transcription machinery (Kass *et al.,* 1997). However, this is a minor mechanism by which methylation is believed to silence gene expression. What methylation does is enable the recruitment of additional transcriptionally repressive proteins to CpG islands (Momparler and Bovenzi, 2000). Methyl binding proteins (MBPs) bind to these regions. These proteins then recruit other histone modifying enzymes, such as HDACs or KMTs, which will further modify the chromatin to maintain it (Nan *et al.,* 1998). For example, methyl-CpG- binding protein (MeCP2) has been shown to recruit the Sin3 HDAC complex to methylated chromatin (Jones *et al*., 1998).

Cancer cells exhibit alterations in their DNA methylation. Tumour cells exhibit global DNA hypomethylation as well as DNMT1 overexpression alongside CpG island hypermethylation (Baylin *et al.,* 1998). CpG island methylation occurs early in cancer development, with 5-10% of normally unmethylated CpG islands becoming methylated (Jones and Baylin, 2002; Feinberg and Tycko, 2004; Bird, 2002). Methylation of CpG islands enables tumour cells to shut down the transcription of tumour suppressor (TS) genes, allowing unchecked growth (de Bustros *et al.,* 1988; Berger, 2007). This is observed in renal cancer with the Von-Hippel-Lindau *(VHL)* gene (Baylin and Jones,

2011). Inhibition of DNMT1 may, therefore be able to restore TS function (Santini *et al.,* 2001).

1.7.1 DNA Methyltransferase Inhibitors

Two cytidine analogue DNMT inhibitors (DNMTi), 5-azacytidine and 5-aza-2'-deoxycytidine, have been approved for use in treating myelodysplastic syndrome (Fandy, 2009). Decitabine, 5-aza-2'deoxycytidine (DAC) was used in this project (Oki *et al.,* 2007). This drug differs from cytosine by having a nitrogen at position 5 of the pyrimidine ring instead of carbon (Santi *et al.,* 1984; Figure 1.6). Cytosine analogues were initially tested at high concentrations – which inhibited DNA synthesis (Santini *et al.,* 2001). Follow up studies induced hypomethylation and reactivated silenced genes by using lower doses, which did not inhibit DNA synthesis (Issa and Kantarjian, 2009).

DAC is phosphorylated inside cells into its active triphosphate form, which enables it to be incorporated into DNA during replication (Yang *et al.,* 2010). Once incorporated into the DNA strand, this analogue is recognised by DNMT1. The presence of the nitrogen at position 5 enables an irreversible bond to be created with DNMT1 (Santi *et al.,* 1984). This results in the degradation of DNMT1, causing a widespread loss in DNA methylation (Yang *et al.,* 2010). This may not be its only mechanism of action. Based on their incorporation into DNA during replication, these drugs should require an entire cell-cycle to be incorporated. However,

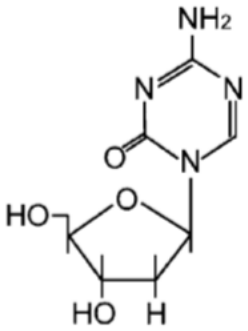


Figure 1.6: Decitabine structure. *DAC is a deoxyribonucleoside. It incorporates into DNA during the S-phase, covalently binding and trapping DNMT1. Taken from Oki et al., 2007.*

some of the DAC-induced gene expression changes have been shown to operate independently of growth stage (Gius *et al.,* 2004).

1.8 HDACi Survival Response

Epigenetic therapies were initially successful in the treatment of PTCL and CTCL but not in trials against many other tumour types (Nervi *et al.,* 2015; Majchrzak-Celińska *et al.,* 2021). It has been hypothesised that cells are intrinsically resistant to HDAC inhibition (Halsall and Turner*,* 2016). Previous work characterised an innate response – termed the HDACi survival response – in which cells survive in the presence of an HDACi by initiating a specific transcriptional response (Halsall *et al*., 2012). This response was identified in Lymphoblastoid (LCL), and Burkitt Lymphoma (BL) cell-lines treated with SAHA for 2-hours. It can be characterised by the downregulation of growth promoting cytokines, such as growth differentiation factor 9 (GDF9), and the up-regulation of TFs and DNA-binding proteins (Halsall *et al.,* 2012; Halsall *et al.,* 2015; Figure 1.7). In addition, genes encoding components of HAT complexes are consistently downregulated following HDACi treatment (Halsall *et al*., 2012). This was believed to allow cells to reset their gene expression patterns and balance the induced hyperacetylation, which could explain how acetylation levels return to normal after prolonged HDACi exposure (Halsall *et al.,* 2015).

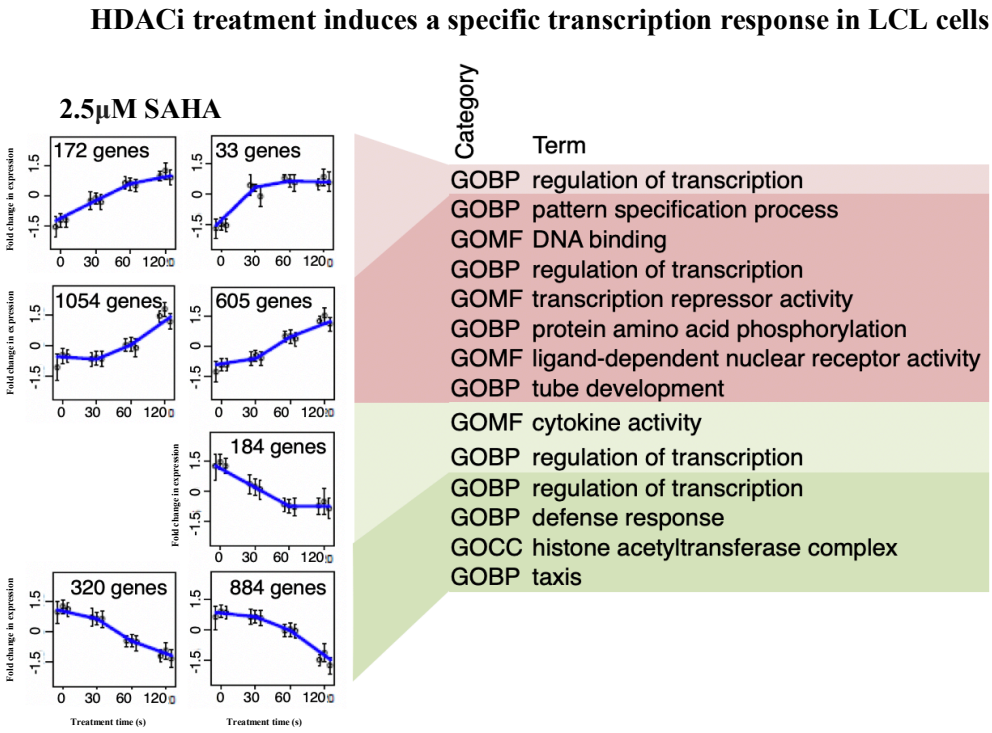


Figure 1.7: Characterisation of the HDACi survival response in LCL cells. *Shown are genes exhibiting a greater than 1.5-fold-change in expression after treatment with 2.5 μM SAHA. Genes are clustered based on whether they are upregulated or downregulated which either occurs rapidly, or more progressively. Shown alongside are the ontology terms from DAVID associated with each gene cluster. Taken from Halsall et al., 2015.*

It had been expected that the hyperacetylation induced following HDAC inhibition would result in uncontrolled gene transcription. However, rather than inducing widespread effects - the expression of only a limited subset of genes was altered (Marks *et al.,* 2004; Table 1.2). Van Lint *et al*., were the first to show in 1996 that following Trichostatin A (TSA) treatment, only 2% of the 340 genes analysed exhibited a change in expression. Additionally, equal number of genes were up and downregulated following 2-hour HDACi treatment. This argued against the idea that HDACi operate only through the opening of chromatin and increasing the accessibility to the DNA or recruiting activating TFs. This indicated that the key substrates of gene regulation were not the histones themselves, leading to the hypothesis that it is non-histone protein acetylation that drives this response

(Halsall *et al.,* 2012; Halsall and Turner, 2016). This is interesting considering that Hansen *et al.* showed in 2019 that most cellular acetylation occurs at a stoichiometry <1% and would not affect protein activity. They showed that most high stoichiometry acetylation in human cervical cancer (HeLa) cells occurred on the N-terminal H2B, H3 and H4 histone tails. This suggests that non-histone protein acetylation would have to occur to a high degree to affect protein activity.

Promoter acetylation cannot explain the HDACi-induced transcriptional changes. Though genes responding to SAHA are often located in highly acetylated chromatin, no change in promoter acetylation is then identified among genes responding to HDACi treatment (Halsall *et al*., 2015). Chueh *et al.,* showed in 2015 that most gene promoters hyperacetylated following HDACi treatment did not exhibit an associated change in their expression. Ellis *et al*., showed in 2008 that the extent of histone acetylation induced in response to TSA did not relate to the transcriptional activity of a promoter.

On the other hand, it should be acknowledged that hyperacetylation disrupts the activity of super enhancers (SEs) (Gryder *et al.,* 2019). SEs are formed by core regulatory (CR) TFs, which determine the location of these large histone acetylation deposits, which drive cell-type specific gene expression (Whyte *et al.,* 2013; Saint-André *et al.,* 2016). Contrary to the belief that acetylation is associated with transcription, greater expression from SEs is predicted by increased HDAC binding (Gryder *et al.,* 2019). Hyperacetylation prevents transcription from CR TFs, with SE activity lost following HDACi treatment (Gryder *et al.,* 2019).

Gene repression was also observed by Mitsiades *et al.,* in 2004 – agreeing with the idea of a selective transcriptional response not driven purely through histone acetylation. Govers *et al*, in 2019, carried out a chromatin immunoprecipitation (ChIP) experiment assessing the presence of H3K27ac at the promoters of genes differentially expressed following treatment of CD34+ progenitor cells with two HDAC inhibitors: MS-275 and SAHA. H3K27ac was significantly increased at the promoters of up-regulated genes and reduced at the promoters of down-regulated genes in response to MS-275 treatment – as would be predicted. However, H3K27ac was not associated with the direction of change following SAHA treatment. Promoters of genes which were downregulated in response to SAHA exhibited greater H3K27 acetylation (Govers *et al.,* 2019). There was also a selectivity in the genes transcribed, which may reflect the regulation of TF complexes which control their expression (Wilson *et al.,* 2010). It is believed that the structurally different HDACi initially alter an overlapping set of common target genes, with the response then diverging as time progresses (Peart *et al.,* 2005).

Few RNA-Sequencing experiments have investigated gene expression changes induced in response to shorter SAHA treatment times. The available analysis suggests that around 30% of genes exhibit a change in their expression after 12 or 24-hour SAHA treatment (Table 1.2). The greater percentage of genes indicated from the RNA-Sequencing versus Microarray analysis, could relate to the difference in their normalization methods. A criticism of Microarray techniques is that the median and spread of signal are normalized to fit the assumption that only a small number of genes change in expression (Jaksik *et al*., 2015). Thus, progressive up or downregulation in expression as well as widespread change in either direction would be normalized out in this analysis. RNA-Sequencing is believed

to be more sensitive, reproducible, and to display a greater dynamic range over which expression can be detected (Wang *et al.,* 2010).

The time chosen for HDACi treatment is also an important consideration. Transcriptional changes have been suggested to occur as little as 15-minutes post treatment (Chambers *et al*., 2003). Many of the experiments discussing HDACi-induced transcriptional change in Table 1.2 analysed gene expression after 24-hours. These changes would represent downstream effects that were being mediated through early responding genes.

It is hypothesised that this specific transcriptional response enables cells to survive and continue to grow in the presence of an HDACi (Halsall and Turner, 2016). Cells susceptible to HDACi are believed to have lost key components of this response, through mutation in the necessary pathways (Halsall and Turner, 2016). The acetylation of histones themselves does not seem to be important in regulating how cells respond to HDAC inhibition. Thus, the focus is now on non-histone protein acetylation in response to early HDACi treatment.

Table 1.2: Transcriptional changes observed in the presence of HDAC inhibitors

Study	Inhibitor	Cell-line	Technique	Treatment time	Genes altered
Van Lint *et al.,* 1996	TSA	Jurkat, SupT1	Differential display PCR detection	2,4,8 hours	2%
Glaser *et al.,* 2003	SAHA, TSA, MS-27-275	MDA 468/435, T24	Microarray	24 hours	8-10%
Lee *et al*., 2002	TSA	SNU1	Microarray	24 hours	5%
Gray *et al.,* 2004	TSA, SAHA, 4-phenyl butyrate	ACHN, CNE-2 Hep3B	Microarray	16 hours	<2%
Moore *et al.,* 2004	TSA	PaCa44	Microarray	8 hours	3.4%
Chambers *et al.,* 2003	TSA	CCRF-CEM, HL-60	Microarray	0, 0.25, 1, 2, 4, 6 and 8 hours	9%
Sasakawa *et al.,* 2005	FK228	PC-3, ACHN, U937	Microarray	24-hours	3% (common to all)
Mariadason *et al.,* 2000	Butyrate	SW620 colon carcinoma cells	Microarray	0.5, 2, 12, 16, 24 and 48-hours	7%
Boudadi *et al.,* 2013	VPA	Mouse ES lines (CCE/R, J1)	Microarray	2,4,8 hours	2.4%
Mazzio and Soliman, 2018	TSA	SK-MEL-3 cells	Microarray	24-hours	3.4%
Peart *et al.,* 2005	SAHA/ Depsipeptide	CEM cells	Microarray	1,2,4,8,16-hours *>1.5fold-change*	22.1% or 24.8%
Halsall *et al.,* 2012	VPA, SAHA and TSA	HL60	Microarray	1 and 8-hours	~9%
Halsall *et al., 2015*	SAHA, VPA	Human lymphoblastoid cells	Microarray	30, 60 and 120-minutes	7%
Cusack *et al.,* 2020	TSA	J1 mouse embryonic stem cells	RNA-Sequencing	24-hours, assessed at 36	20%
Rafehi *et al.,* 2014	TSA/SAHA	Aortic endothelial cells	mRNA-Sequencing	12-hours	30%
Sato *et al.,* 2017	Depsipeptide	YB5, MCF7, HL60	RNA-Sequencing	24-hours	30.4% (combined)

1.9 Crossover between HDAC and DNMT inhibition

This project treated cells with both an HDAC and DNMT inhibitor. This was because of the crosstalk identified between histone acetylation and DNA methylation – with HDACi and DNMTi shown to act together to reactivate silenced genes (Yang *et al.,* 2001; Ghoshal *et al.,* 2002). Interestingly, the gene expression changes induced in response to DNMTi treatment were more similar to those induced following HDACi treatment than following DNMT knockout (Gius *et al.,* 2004). This suggested that there may be a crossover in their mechanism of action. Similar effects were observed on Day 1 and Day 5 of DNMT inhibition, which does not fit with the view that DNMTi affect gene expression purely through their incorporation into DNA during replication (Gius *et al.,* 2004). By this mechanism, further rounds of cell division would progressively remove DNMTi and dilute out its inhibitory effect with time. This suggests that an alternative mechanism exists through which DNMTi induce shorter-term transcriptional change. 5-aza-CdR and valproic acid (VPA) also induced a common set of genes, suggesting DNA demethylation is involved in the mechanism of HDACi action. This may be how VPA exerts longer-term transcriptional change (Milutinovic *et al*., 2007).

The relationship between DNA methylation and histone deacetylation was traditionally described as unidirectional. DNA methylation led to chromatin alterations and gene repression, through the recruitment of HDACs to methylated chromatin (Nan *et al.,* 1998). This indicated that DNA methylation preceded chromatin change. However, recent work presents a different view and suggests that this relationship is bidirectional, with DNA methylation operating alongside histone acetylation. In this model, histone deacetylation initiates gene silencing and leads to DNA hypermethylation (Vaissière *et al.,* 2008). This mechanism may operate through DNMTs targeting regions of chromatin which have

already been deacetylated (Fuks *et al*., 2000). Additionally, DNMT enzymes can be recruited to genes by chromatin silencing proteins (Brenner *et al.,* 2005; Viré *et al.,* 2006). For example, Bachman *et al.* in 2003 investigated silencing of the *p16* gene using somatic knockout cells. They showed that chromatin modifications could initiate gene silencing, without relying on DNA methylation having occurred first. Along similar lines, it was also shown that Interkekin-2 Receptor (*IL2R)* silencing was induced following histone modification (Mutskov and Felsenfeld, 2004). Leu *et al.,* in 2004 showed that DNA methylation occurred after histone modifications and the inactivation of some ERα target genes. In addition, H3 deacetylation was shown to occur prior to DNA methylation during the inactivation of the Ras association domain family member 1 (*RASSF1A)* gene (Strunnikova *et al.,* 2005). Taken together, these suggest that DNA methylation may occur after histone modifications and act to lock in gene silencing.

Cells treated with TSA exhibit a decrease in DNMT1 protein expression (Arzenani *et al.,* 2011). As HDACi treatment did not affect the expression of *DNMT1* mRNA (messenger ribonucleic acid), it is most likely that this reduction in expression occurs through protein modification (Zhou *et al.,* 2008). HDACs have been shown directly interacting with and stabilising DNMT1 (Peng *et al.,* 2011). Their deacetylation activity is important in mediating DNMT1 protein stability (Zhou *et al.,* 2008). Acetylation of DNMT1 targets it for ubiquitination and subsequent proteasomal degradation (Du *et al*., 2010; Zhou *et al.,* 2008). Thus, treatment with an HDACi and the subsequent increase in acetylation leads to the degradation of DNMT1. Additionally, DNMT1 protein is stabilised through its interaction with heat-shock protein 90 (HSP90). Hyperacetylation of HSP90 in response to HDAC inhibition disrupts it its interaction with DNMT1 and, therefore, allows its degradation via the ubiquitin-proteasome pathway (Zhou *et al.,* 2008). Loss of DNMT1

leads to a significant decrease in global methylation – similar to the loss of methylation observed following DNMT inhibition (Ou *et al*., 2007).

1.10 HDACi in combination therapy

Though epigenetic drugs show promise in the treatment of some haematological malignancies, their responses in solid tumour have been poor (Fantin and Richon, 2007; Huang *et al.,* 2018). This may relate to the more complex range of molecular alterations driving solid tumours (Kalebic, 2003). The genetic diversity exhibited in most solid tumours by the time they are detected, prevents single agent therapies from being effective (Kitano, 2003). Additionally, many haematological malignancies are epigenetically driven. HDACi may be so effective in tumours, such as B-cell lymphoma which express the highest levels of HDAC1 and DNMT1 (Mohammad *et al.,* 2019).

Disappointing clinical trial outcomes considering HDACi for single agent therapy have led many researchers to employ them in combination therapies (Nolan *et al.,* 2008). Due to their relatively safe toxicity profiles, HDACi could be used in combination to lower the dose of cytotoxic drugs needed (Mokhtari *et al.,* 2017). Though there are numerous examples of cancer therapies with which HDAC inhibitors could be combined, only radiotherapy and hormonal and HER2 therapies will be discussed. For a more comprehensive review, see Suraweera *et al.* 2018 and Hontecillas-Prieto, 2020 (Figure 1.8).

HDAC inhibitors can be used in combination with many cancer therapies

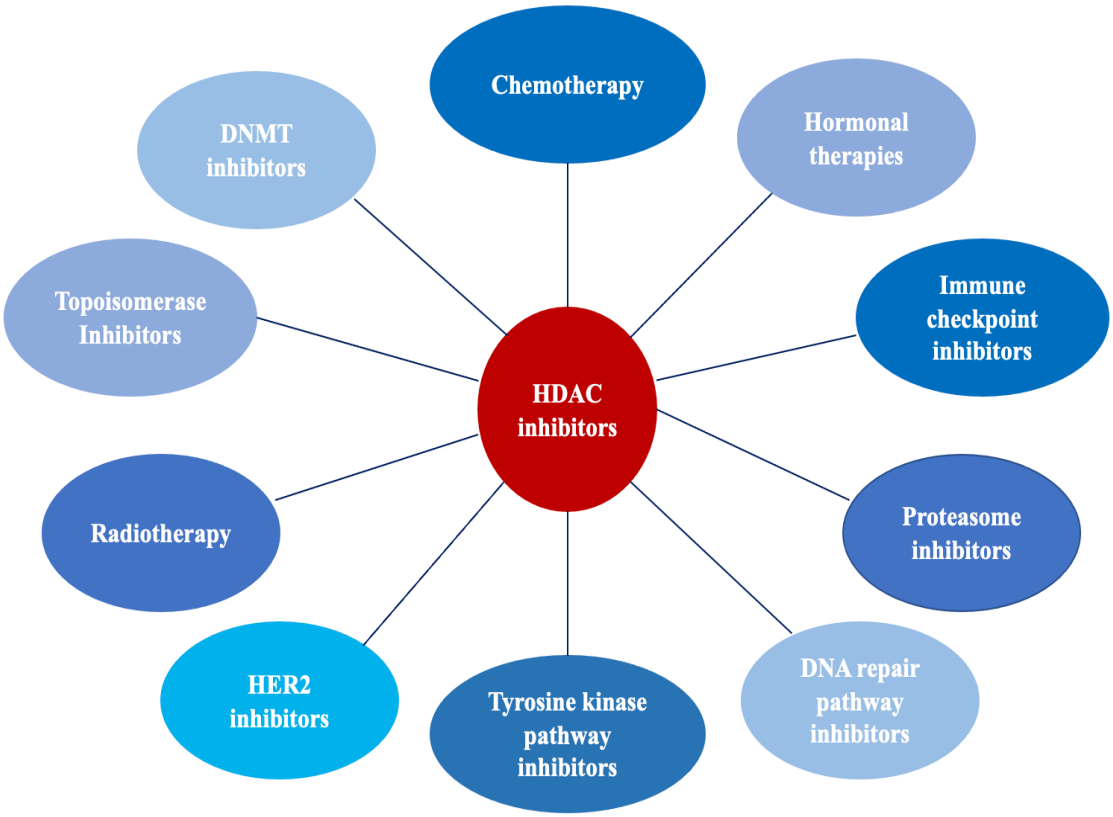


Figure 1.8: Cancer treatments that have been assessed in combination with HDAC inhibitors. *Information adapted from Suraweera et al., 2018.*

1.10.1 DNMT inhibitors

As mentioned previously, the crossover demonstrated between HDACi and DNMTi has led to an interest in their combined use in the clinic. As both enzymes play a role in gene expression silencing, their combined use could result in the re-expression of genes silenced during tumour development (Sarkar *et al.,* 2013). This would be especially important for enhancing tumour suppressor gene expression in cancer (Hontecillas-Prieto, 2020).

1.10.2 Radiotherapy

Radiotherapy is one of the most common cancer treatments available. It operates through inducing double-strand DNA breaks (Cannan and Pederson, 2017). The rationale for this combination is that HDACs are involved in several DNA-damage signalling and repair pathways (Groselj *et al.,* 2013). HDAC inhibition reduces the capacity of tumour cells to repair radiation-induced DNA damage – which leaves them more sensitive to radiation (Karagiannis and El-Osta, 2006; Thurn *et al.,* 2011). For example, HDACs are involved in ataxia telangiectasia-mutated protein (ATM)-mediated DNA damaging signalling (Suraweera *et al.,* 2018). HDAC1 interacts with ATM, with this interaction enhanced following ionising radiation (Kim *et al.,* 1999). Following HDAC inhibition, ATM was downregulated which diminished DNA damage signalling (Thurn *et al.,* 2013). This combination manifests in cells displaying a greater number of γ-H2AX foci. In addition, the expression of repair proteins such as Ku70 was reduced in HDACi treated cells experiencing radiation-induced DNA damage (Munshi *et al.*, 2005).

1.10.3 Hormonal therapies:

HDAC inhibitors show promise in combination with hormonal therapies for breast cancer. Munster *et al* in 2011 evaluated the combination of an HDAC inhibitor and anti-oestrogen (tamoxifen) in patients with advanced ER-positive breast cancer. This built on previous work showing that HDACi could enhance the anti-tumour effects of tamoxifen, through modulation and post translational modification of the Oestrogen Receptor (ER) (Yang *et al*., 2001; Kawai *et al.,* 2003). It has been shown that HDACi could re-establish ER expression in ER-negative cell-lines, such as MDA-MB231

(Zhou *et al.,* 2007). This means that HDACi are capable of reversing tamoxifen resistance and preventing the development of hormone therapy resistance (Yang *et al.,* 2001; Thomas *et al.,* 2011). Tamoxifen primarily operates as an anti-proliferative drug, but apoptosis was more often observed when used in combination with an HDACi (Munster *et al.,* 2011). Treatment of receptor-positive breast cancer with Vorinostat and tamoxifen prolonged disease stabilisation and reduced tumour growth (Munster *et al.,* 2011).

1.10.4 HER2 therapies:

Trastuzumab is a humanised monoclonal antibody targeted to human epithelial receptor 2 (HER2), which is overexpressed in certain breast cancers (Iqbal and Iqbal, 2014). This drug binds to the receptor at domain IV, preventing HER2 from being able to form homodimers (Gajria and Chandarlapaty, 2011). These Her2 dimers normally induce signalling through pro-survival pathways such as phosphatidylinositol 3-kinase (PI3K) and mitogen-activated protein kinase (MAPK) (Harari and Yarden, 2000; Hynes and Lane, 2005). Trastuzumab not only internalises and degrades the Her2 receptor but prevents these important signalling pathways (Nahta and Esteva, 2006). Combined HDAC inhibition would further enhance this effect, as HDACi reduce PI3K signalling (Kawamata *et al.,* 2007). Additionally, this combination may prevent trastuzumab resistance – which develops through these signalling pathways (Albanell and Baselga, 2001). HDACi also complement trastuzumab by reducing *HER2* mRNA and enhancing the degradation of the HER2 protein (Scott *et al.,* 2002; Fuino *et al.,* 2003). HER2 is normally protected from proteasomal degradation through its binding to the HSP90 chaperone (Fuino *et al.,* 2003). HDACi prevent this interaction by acetylating HSP90.

Through these mechanisms, treatment with an HDACi alongside Trastuzumab significantly increases the apoptotic response (Fuino *et al.,* 2003; Bali *et al.,* 2005).

1.11 Personalised HDACi treatment:

A necessary next step in improving the use of HDAC inhibitors in the clinic involves their personalisation. HDACi have a long and patchy history in cancer, starting back with sodium valproate (Göttlicher *et al.,* 2001). Their use in cancer stemmed from the original simple hypothesis that histone acetylation was associated with an increase in gene transcription (Allfrey *et al.,* 1964). Additionally, their role in many important cellular processes linked them mechanistically to cancer (Chun, 2015). HDACi exhibited promising results in the treatment of some haematological cancers, such as CTCL (Chun, 2015). However, they do not work in solid tumours (Fantin and Richon, 2007).

Why does treating patients with these drugs not shut down the activity of all cells? Some patients can take HDACi their entire lives with minimal side-effects. For example, sodium valproate is used as an anti-epileptic (Goldenberg, 2010). This was explained with the discovery of an inherent survival response used by many cells to tolerate the disruption caused by an HDACi (Halsall *et al.,* 2015). We are still trying to identify what initiates this pathway in cells and how sensitive cells are less able to induce this response. This project looked for differences in how our resistant and sensitive cell-line responded to SAHA, with the aim of identifying a gene or signalling pathway that could be exploited therapeutically to enhance the sensitivity of cells to HDAC inhibition.

HDACs are differentially expressed across breast molecular subtypes. Park *et al* observed in 2011 that HDAC1 and HDAC2 were similarly expressed in MCF7 and MDA-MB231 cells. However, additional work showed that HDAC2 and HDAC3 were expressed in more aggressive tumour subtypes while HDAC1 was expressed in hormone receptor positive tumours (Müller *et al*., 2013). Krusche *et al* in 2005 additionally correlated HDAC1 and HDAC3 expression with receptor positive tumours. Finally, HDACs 4, 6 and 8 – which are associated with tumour cell invasion – were shown to be more highly expressed in MDA-MB231 cells (Park *et al.,* 2011). This variability in HDAC expression could explain why HDACi have been less successful clinically than had been expected. These drugs could be more useful in the clinic if mechanisms were developed to target them to more HDACi-sensitive tumours.

1.12 Project Aims and Objectives

A specific transcriptional mechanism enables some cells to survive in the presence of an HDACi. Our hypothesis is that the acetylation of non-histone proteins is what drives this survival response. This work, therefore, aimed to identify genes and signalling pathways that were crucial in allowing cells to survive the toxic effects of HDAC inhibition. This was investigated using a solid tumour model system, characterised by assessing the apoptosis induced in cells following treatment with an HDACi (SAHA) and DNMTi (DAC). Cells were treated with both drugs based on unpublished work from the lab suggesting a crossover in sensitivity to them. This work aimed to identify genes responding rapidly following SAHA treatment. Knocking down factors that we hypothesise are responsible in allowing some cells to survive HDACi treatment, would validate the roles of these selected TFs in mediating the survival response. Gene

expression patterns in a breast cancer patient cohort were analysed using CBioPortal to validate our model system. This also explored whether our cell-lines were representative of their molecular subtype and whether differential gene expression was evident between subtypes.

2. MATERIALS AND METHODS

2.1 Cell Culture

U2OS cells were donated by J. Schwabe (Leicester University), MDA-MB231 and MCF10A cells by P.S Jayaraman and MCF7 cells by the Tomlinson Lab (University of Birmingham). U2OS and MCF7 cells were cultured in Gibco Dulbecco's Modified Eagle Medium (DMEM) with 4.5 g/L D-glucose and L-glutamine, supplemented with 10% foetal bovine serum (FBS, Sigma-Aldrich) and 50 units/ml penicillin and 50 μg/ml streptomycin (P/S, ThermoFisher Scientific). MDA-MB231 cells were cultured in Gibco Roswell Park Memorial Institute (RPMI) 1640 medium with L-glutamine, supplemented with 10% FBS and P/S. MCF10A cells were cultured in Gibco DMEM F12 Nutrient Mix supplemented with 5% horse serum, 20 ng/ml Epidermal Growth Factor, 0.5 μg/ml Hydrocortisone, 100 ng/ml Cholera toxin, 10 μg/ml insulin and P/S. Cells were grown at 37°C in a humidified atmosphere containing 5% CO_2 and passaged using 0.05% Trypsin (Corning/Gibco). Cells were treated with 2.5 μM Suberoylanilide hydroxamic acid (SAHA, Merck) or 1 μM 5-aza-2' deoxycytidine (DAC, Sigma-Aldrich) for 30, 60, 120-minutes, 24, 48, 72 or 96-hours. SAHA and DAC were both diluted in dimethyl sulfoxide (DMSO) – and made up to 2.5 mM and 1 mM working stocks respectively, for use in cell culture.

2.2 Annexin V Assay

The Annexin V Assay was used to determine the sensitivity of cell-lines to treatment with the HDACi (SAHA) for 48-hours or the DNMTi (DAC) for 96-hours. This enabled their characterisation as more resistant or more sensitive to HDACi treatment. MCF7 cells were seeded at a density of approximately $2.8x10^5$, MDA-MB231 at $1.9x10^5$ and MCF10A at

$1.8x10^5$ cells per well and treated with a final drug concentration of 2.5 μM SAHA for 48-hours. MCF7 cells were seeded at $1.6x10^5$, MDA-MB231 at $1x10^5$ and MCF10A at $1.4x10^5$ cells per well and treated with a final drug concentration of 1 μM DAC for 96-hours. Cells were centrifuged at 300 g for 5 minutes (5810R, Eppendorf) and washed in 1 ml Phosphate buffered Saline (PBS). They were washed in 1 ml 1x Annexin V Binding Buffer (ThermoFisher Scientific) and centrifuged as before.

Cells were re-suspended in 100 μl binding buffer and incubated for 15-minutes with 5 μl Annexin V (eBioscience) before being spun at 1800 rotations per minute (RPM) for 5 minutes (Heraeus Fresco 17 Microcentrifuge) and washed in 300 μl binding buffer. Cells were re-suspended in 250 μl binding buffer, incubated with 5 μl Propidium Iodide (PI, eBioscience), and stored in the dark. Cells were analysed on the Beckman Coulter CytoFLEX flow cytometer. Whole cells were gated using forward versus side scatter light and doublets excluded by gating pulse width. Allophycocyanin (APC) fluorescence was plotted against PC5.5 to quantify the proportion of viable, apoptotic, and necrotic cells using CytExpert 2.3 Software. The difference in apoptosis between treated and untreated populations was compared using a paired, one-tailed T-test setting $p<0.05$ as significant. Graphs were created using GraphPad Prism 8.

2.3 MTS Assay

The MTS Assay was used to determine whether at sub-lethal concentrations SAHA and DAC affected cellular metabolic potential. This assay enabled IC_{50} values to be calculated, comparing the sensitivity of our cell-lines to treatment with SAHA and DAC. MCF7, MDA-MB231 and MCF10A cells were seeded into 96-well plates at a final density of

8000 cells per well for SAHA treatment or 3000 cells per well for DAC treatment. Cells were incubated with two-fold dilutions of SAHA and DAC (40 μM-0.0195 μM) for 48-hours or 96-hours respectively. An equal volume of DMSO was added to control wells and medium only wells seeded to account for background absorbance. Cells were incubated for 3-hours with 20 μl of a 5% phenazine methosulfate (PMS) in MTS (3-(4,5-Dimethylthiazol-2-yl)-5-(3-carboxymethoxyphenyl)-2-(4-sulfophenyl)-2H-tetrazolium) solution (2 mg/ml). Absorbance was measured at 490 nm using the EnSpire Multimode Plate Reader spectrophotometer (Tecan). The half maximal inhibitory concentrations (IC_{50}) values were determined by fitting Nonlinear regression curves in GraphPad Prism 8. Standard Deviation (SD) error bars were then applied to these curves.

2.4 Primer Design

Primers were designed to carry out qPCR (quantitative polymerase chain reaction) analysis of the expression of genes identified from the RNA Sequencing as well as to validate the expression of targets of interest for knockdown work. Primers were designed to HAT, HDAC, TF and heat shock protein (HSP) genes identified as differentially expressed between SAHA treatment timepoints in MCF7 cells (Table 2.1). Gene transcript variants (TV) were analysed using the UCSC Genome Browser. Primer 3 software was used for primer design, selecting regions common to all variants. The sequences were input into Primer Blast for confirmation. Primers were similarly designed to verify the expression of *POU* and *ATF/CREB* (Activating transcription factor, cAMP response element-binding protein) family members. Primers were also designed to identify the distinct TVs of POU Class 2 Homeobox 1 and 2 genes (*POU2F1* and *POU2F2)*. The NCBI database was used to identify the differences in their exon structure and primers designed to distinguish each

variant based on exon inclusion. Primers were also designed to downstream *POU2F2* target genes to observe how they were initially regulated by *POU2F2* and how this regulation changed upon knockdown.

Table 2.1: Primers designed for qPCR analysis of gene expression

Primer	Forward Sequence (5'-3')	Reverse Sequence (5'-3')
UBC	GGGTCGCAGTTCTTGTTTGT	TCCAGCAAAGATCAGCCTCT
HPRT1	TTTACTGCCGATGTCAATAGGA	AAGATGGTCAAGGTCGCAAG
B2M	GAGGTTTGAAGATGCCGCAT	TAAGTTGCCAGCCCTCCTAG
YWHA	TGGCCCTTAACTTCTCTGTG	CAGCTTCGTCTCCTTGGGTA
EPC1	TGTCAAGTTTCCAAGGTCCCA	TGCTGCTTTCCATCATCCCT
EPC2	GACTTCAGCACCATCGCCAA	ATCAGCACAGGTCAGAGCCA
ING5 (1)	GGTTTCACTTTGCCTGCGTG	TTGCGACACGAATGAAGGGA
ING5 (2)	CTGGCCATGCAGACCTACG	CCTCTGATGTCCTCCTGCCT
KAT6B	GAGACGGCTGTGAATCCTGT	CTGGCTCGGAATGACAGGTC
KAT7	TGCTTCAAGAATGCTGACCCT	TGGCGGGGTGTACAAATTCA
HDAC2	AAGACAGTGGAGATGAAGATGG	CCACTGTTGTCCTTGGATTTATC
HDAC3	TGTGATCGATTGGGCTGCTT	ATTGTCTGGCGGATCTGGTC
HDAC5	CCCAGCAGGCGTTCTACAAT	TGAGAACTCGTGGGCAATGG
HDAC7	AGGGCTGATCTATGACTCGGT	TCCCGTTGTCCAGTTTGAGG
JADE1	CTGATGGTGAGGACGGCAAT	TAGCTCCACCCTTCTTCGGA
HSPA1A	CTGCGACAGTCCACTACCTT	GTTCCCTGCTCTCTGTCGG
HSPA1B	AAATGAATCAACACTGCCACC	AAACATACATTCCCAGCCTTTG
HSPA5	TGTTCTTGTTGGTGGCTCGA	TGACACCTCCCACAGTTTCAA
HSPA13	ATGTTGGCTCTCGACTATTGTTG	CTCCGCCCAAGTCTATCACC
HSPA14	CCCTCCTGATGAAGTGATCCC	TCTTCGAGCTGGCAAAGGAG
EGR1	AGCCCTACGAGCACCTGAC	TGGGTTGGTCATGCTCACTA
EGR2	TTGACCAGATGAACGGAGTG	ACCAGGGTACTGAGGGTCAA
EGR3	CTATGACCGGCAAACTCGC	TCCCAAGTAGGTCACGGTCT
NR4A1	GGCATGGTGAAGGAAGTTGT	CGGAGAGCAGGTCGTAGAAC
NR4A3	CTCGCTCTAAAGACGGAACC	AGCGGAGGCTGAGAGTGTAG

POU2F1	GGAGGAGCAATCTCAACAGC	GCGTCAAAGTAAGCCCAGTT
POU2F2	AGCATGGTTCACTCCAGCAT	GGGTCTTCAGCCTTGATCTTT
POU5F1	GAAGGATGTGGTCCGAGTGT	GTGAAGTGAGGGCTCCCATA
POU3F1	AAAGCGACAGGTAACGCAGT	CGAGAGGCTCCACGAATAAA
ATF4	TCAAACCTCATGGGTTCTCC	GTGTCATCCAACGTGGTCAG
ATF5	TGCTACAGCCATGTCACTCC	TCGCTCAGTCATCCAGTCAG
CREB3L4	GAGACACCAAACCCTCAGGA	GGATTCCGAGATCCATGCT
Oct2 TV5	GAAGACAGCGGCGCCTAC	
Oct2 TV1-10	GAAGCAAGGTCTGGACTCCC	
Oct2 R		AGAGGTAGGGTAAGGGCAGG
Bentrari CDS	ATGGTTCACTCCAGCATGGGG	AGGCTGGTAAGGGGCAGGG
162F/R	CCTGCTCAGTTCCTGCTACC	CTCCAGCTCCTCCAGATCAC
TV5 154F/R	GAAGACAGCGGCGCCTAC	TTCGGTGTCTGTGTGCTCTG
Oct2 CDSb R		TGCCATCAAGGCTGGTAAGG
TV4 66F	AAGCTTCCAGCAGTCTGAGC	
TV1xx F/R	TTCCCACACAGGCCGTGAC	GCCGCACTGCAGGGGT
TV2xx F	CTTCCCACACAGCCCCC	
POU2F2 xx R		GCCCAGCATGATTCAAGAAG
TV2xx F/R	CACTTTCCACCCTACGCAAC	TTGCCATCTCCACTCTCCAT
TV136xx F/R	CAGCAGCAGACTCAAGAATGA	AGGTTCTCTGCATCATTTAGCCA
TV5xx F/R	AGCAGCAGCTACTACTGGG	TGTTGAAGCTGTTGCAGTTGT
ATXN7L2	CACTGCGAAAGAAGACATGG	GTCTTCTCAGGAGGCTGGTG
INO80E	AATCTGAAGCGGAAGCTCAA	ATGATGCAGTGGCATCTGAG
JMJD8	ACCTACGCGGAGTTCGTG	AAGGGCAAGTCCACTTTGTG
MATR3	TGGAGCAAGTCACAGTCGTC	TCTGCCTTTCTGCATGTGTC
MED10	CTGCTGGTTGAGGCTGTGT	AGCTGCTGTCTGCACTTGTC
MEPCE	AGCGGACACATCAGTCTTCC	GGTAGATCCGGCGAAACAT
MIF	TTCATCGTAAACACCAACGTG	TGCTGTAGGAGCGGTTCTG
MIR17HG 2	CCTGTTGAGTTTGGTGGGGA	CAAATCTGACACGCAACCCC
PPP1R14B	CAGGACCACGCGTCTACTTT	CTTCCTGGCAGTCGTAGAGG
RPL36	ATGGCCCTACGCTACCCTAT	ATAAATTTGAGGGCCCGTTT

2.5 Quantitative Polymerase Chain Reaction (qPCR)

qPCR was used to assess the expression of key genes of interest in MCF7 and MDA-MB231 cell-lines. Cells were seeded at a density of approximately $1.3x10^6$ MDA-MB231 and $3.5x10^6$ MCF7 cells per T75 flask and treated with 2.5 μM SAHA for 30, 60 or 120-minutes, 24 or 48-hours – in line with the experimental protocol. Cells were harvested and spun at 300 g for 5-minutes prior to being frozen at -80°C.

RNA (ribonucleic acid) was extracted from cell pellets using the Isolate II RNA Mini Kit (Bioline Meridian Bioscience) or RNeasy Mini Kit (QIAGEN) according to the manufacturer's instructions, including on column DNA digest using RNase-Free DNAse I (QIAGEN). RNA concentration (μg/μl) and purity were then determined using the IMPLEN Nanophotometer P-Class, P300. cDNA (complementary DNA) was synthesised from the extracted RNA using the Tetro cDNA Synthesis Kit (Bioline Meridian Biosciences), as per the manufacturer's instructions. The amount of RNA converted depended on how much was available. Most experiments converted 5 μg of RNA using Oligo (dT) as a primer. Some used less than 5 μg of RNA, but the volume was kept consistent within experiments. Reactions were incubated at 45°C for 30 minutes and 85°C for 5 minutes on the PTC-200 Thermal Cycler (MJ Research). cDNA was then stored at -20°C.

qPCR was performed using PowerUp SYBR Green Master Mix, (Applied Biosystems) with 0.5 μl of 10 μM forward and reverse primer per reaction. Plates were read on the ABI 7900 HT or Quant Studio 5 384-well PCR machine. Reactions were incubated at 94°C for 2-minutes, prior to 40 cycles of 94°C for 15 seconds and 60°C for 1-minute. Dissociation then proceeded at 95°C for 15 seconds, 60°C for 15 seconds and 95°C for 15 seconds.

Each plate included three technical replicates. Results were analysed by the Standard Curve Method using SDS2.4 or ThermoFisher Data Connect Software. qPCR data was normalized to the expression of housekeeper genes. Data was presented as a fold-change difference from the normalized expression values calculated at Time 0. Error bars depicting Standard Error of the Mean (SEM) were applied. Significant differences in expression between cell-lines were compared using an unpaired, one or two-tailed T-test. Gene expression changes in one cell-line were compared using a paired, one or two-tailed T-test setting $p<0.05$ as significant.

2.6 POU2F2 splice variant expression

To determine the difference in *POU2F2* expression between the cell-lines, expression of *POU2F2* splice variants was assessed by PCR amplification and subsequent gel analysis. Two sets of primers were firstly designed to amplify the coding sequence (CDS) of either TV1-4, 6-10 or TV5, and amplified for 40-cycles using ReddyMix at 60°C annealing (Table 2.2). Primers specified in the Bentrari *et al*., 2015 publication were amplified in this manner with Reddy Mix initially and then with Pfu DNA Polymerase at 62°C annealing (Table 2.3). The Bentrari primers were then amplified using DreamTaq DNA Polymerase (ThermoFisher) at 66°C or 68°C and run on a Gel Red stained 1.5% Agarose gel alongside a 100 bp DNA ladder (New England Biosciences; Table 2.4). Product from the gel bands of interest was extracted using a needle and re-amplified with Dream Taq Mastermix at 66°C. Following clean up using the Wizard SV PCR clean-up kit, 10 ng/µl DNA product was sent for sequencing with 3.2 pmol/µl forward and reverse primer (Bentrari F/R and Bentrari F/Oct2 CDS R). The sequencing results were analysed using Nucleotide Blast. Additional primers (162F/R, TV1 154F/R, TV4 66F, TV1xx F, TV2xx F) were generated

to the exon differences identified in specific splice variants and amplified and analysed in the same manner (Appendix 10.7).

Table 2.2: Reddy Mix 40-cycle thermal profile

Process	Temperature	Time	Number of Cycles
Initial denaturation	95°C	2 minutes	1 cycle
Denaturation	95°C	25 seconds	40 cycles
Annealing	60°C	35 seconds	40 cycles
Extension	72°C	2 minutes	40 cycles
Final extension	72°C	5 minutes	1 cycle
Soak	4°C	indefinite	1 cycle

Table 2.3: Pfu DNA Polymerase 35-cycle thermal profile

Process	Temperature	Time	Number of Cycles
Initial denaturation	95°C	2 minutes	1 cycle
Denaturation	95°C	30 seconds	35 cycles
Annealing	62°C	30 seconds	35 cycles
Extension	72°C	3 minutes 45 seconds	35 cycles
Final extension	72°C	5 minutes	1 cycle
Soak	4°C	indefinite	1 cycle

Table 2.4: Dream Taq DNA Polymerase 35-cycle thermal profile

Process	Temperature	Time	Number of Cycles
Initial denaturation	95°C	2 minutes	1 cycle
Denaturation	95°C	30 seconds	35 cycles
Annealing	60-68°C	30 seconds	35 cycles
Extension	72°C	30 seconds- 2 minutes	35 cycles
Final extension	72°C	5 minutes	1 cycle
Soak	4°C	indefinite	1 cycle

2.7 POU2F1 splice variant expression

The *POU2F1* splice variants expressed in each cell-line were then assessed using PCR amplification and gel analysis. Three primer sets designed to identify the specific exon structure of the five *POU2F1* variants (Table 2.1; Appendix 10.8). They were amplified using DreamTaq DNA Polymerase (ThermoFisher) at 64°C and 66°C annealing and run on a Gel Red stained 1.5% Agarose gel alongside a 100 bp DNA ladder (New England Biosciences; Table 2.4).

2.8 Cell Cycle Analysis following DAC or SAHA treatment

The effect of drug treatment on cell cycle progression was analysed by flow cytometry using DNA content as a measure of cell cycle stage. To identify any cell-cycle specific changes in histone modification, modification specific antibodies were used in combination with the DNA binding dye. Cells to be treated with DAC were seeded more thinly to allow for a longer time-course. MCF7 cells were seeded at $1.6x10^5$, MDA-MB231 at $1x10^5$ and MCF10A at $1.4x10^5$ cells per well and treated with a final drug concentration of 1 μM DAC for 96-hours. MCF7 and MDA-MB231 cells were seeded at $4.5x10^5$ and $2.2x10^5$ cells per well respectively and treated with 2.5 μM SAHA for 48-hours.

Cells were harvested and centrifuged at 300 g for 5-minutes. They were then washed in PBS before being fixed in 1 ml 80% Methanol and stored at -20ºC. Following PBS washing, cells were suspended in 500 μl of Analysis Buffer (100 μM Vybrant Violet, 250 μg/ml RNAse A in PBS) at 37ºC for 30 minutes. Cells were then analysed on the CytoFLEX (Beckmann Coulter) with DNA content assessed using PB450 signal. These

results were analysed using CytExpert software, and the percentage per phase of the cell-cycle graphed using GraphPad Prism. Error bars depicting SEM were applied. The Chi-squared test was used to investigate the difference in the cell-cycle distribution after DAC or SAHA treatment, setting $p<0.05$ as significant. Differences in individual phases in response to SAHA were assessed using a paired, two-tailed test with $p<0.05$ set as significant.

2.9 Western Blotting

Antibodies to key histone modifications of interest were used to investigate whether differences in methylation and acetylation were observed in MCF7 and MDA-MB231 cells following 2-hour SAHA treatment. $3.5x10^6$ MCF7 and $1.3x10^6$ MDA-MB231 cells were seeded in T75 flasks and treated with 2.5 μM SAHA for 30, 60 or 120 minutes. Cells were harvested and centrifuged at 300 g for 5-minutes, washed in PBS-Butyrate (5 mM sodium butyrate in 1xPBS) and re-centrifuged. Cells were resuspended in Triton Extraction Buffer (TEB, 0.5% Triton X-100, 2 mM PMSF, 0.02% Sodium Azide, 10% PBS in ultra-pure (UP) water) left on ice for 10 minutes then centrifuged at 2000 RPM for 10-minutes. The pellets were resuspended in TEB and centrifuged. Cells were resuspended in 0.4 N Hydrochloric Acid at 4ºC overnight. The cells were centrifuged as before, and the supernatant stored at -20ºC.

Protein concentrations were calculated against the absorbance obtained from a Bovine Serum Albumin (BSA) standard curve. 25 μg of histone was made up with 10 μl Sample Reducing Agent (Novex, Life technologies), 25 μl Bolt LDS Sample Buffer to 100 μl in UP water and heated at 70ºC for 10 minutes. 5 μl of pre-stained protein ladder (PageRuler

Plus, Thermo Fisher Scientific) and 40 µl of histone sample were loaded into 12% Bolt Bis-Tris Plus Gels (Invitrogen) and run at 165V for 45 minutes in Bolt MES SDS running buffer (Thermo Fisher Scientific) in a Mini-Gel Tank (Life Technologies). Gels were transferred using the Mini Blot Module (Life Technologies) and run at 10V for 60 minutes with Transfer Buffer (5% 20X Bolt Transfer Buffer, 1% Methanol, 0.1% Tween). Ponceau solution was used to visualize bands. Membranes were cut, rinsed in TBS/T (1% Tween-20 in 1x tris-buffered saline (0.2 mM Tris, 150 mM sodium chloride, pH7.4)) and blocked overnight at 4ºC in 25 ml milk (10% milk powder TBS/T). Membranes were then incubated in 5 ml 10% milk TBS/T containing primary antibody (H3 C-terminal (ab1791, Abcam) at 1:5000, H3K27ac (ab4729, Abcam), H3K27me3 (07-449, EMD Millipore Corp), H4K16ac (ab109463, Abcam) at 1:1000 and the in-house antibodies H3K9ac, H3K14ac, H4K5ac, H4K16ac or H3K4me3 at 1:500 for one hour (Table 2.5). Membranes were rinsed three times in TBS/T. Secondary anti-rabbit antibody (IRDye® 800CW Goat anti-Rabbit Immunoglobulin (IgG) Secondary Antibody, 926-32210, Li-Cor) was then added at 1:5000 for one-hour. Membranes were rinsed three times in TBS/T and scanned on the Li-Cor Odyssey infrared imager.

Table 2.5:Antibodies used for Western Blot analysis of acetylation and methylation changes

Antibody target	Antibody name	Source
H3 C-terminal	ab1791	Abcam
H3K27ac	ab4729	Abcam
H3K27me3	07-449	EMD Millipore Corp
H4K16ac	ab109463	Abcam
H3K9ac	R607	Turner lab
H3K14ac	R224	Turner lab
H4K5ac	R41	Turner lab
H4K16ac	R251	Turner lab

H3K4me3	R612	Turner lab
Secondary anti-rabbit	926-32210 IRDye® 800CW goat anti-rabbit	Li-Cor

2.10 Flow Cytometry analysis of acetylation

H4K16ac and H3K27ac antibodies were used to investigate the occurrence of acetylation across the two-hour SAHA treatment time-course and determine whether acetylation was affected by cell-cycle phase. Cells were seeded at a density of approximately $1.3x10^6$ for MDA-MB231 and $3.5x10^6$ cells per T75 flask for MCF7 and treated with 2.5 µM SAHA for 0, 30, 60 or 120-minutes. Cells were harvested and spun at 1500 RPM for 7-minutes. Cells were aliquoted into $1x10^6$ cells/sample portions. 1 ml PBS-BSA (1 mg/ml BSA in PBS-Butyrate (5 mM sodium butyrate in 1xPBS)) was added per aliquot. Cells were centrifuged at 2000 RPM for 5-minutes and the supernatant removed. 100 µl CSK buffer (1 M HEPES, Sucrose, 5 M NaCl, 1 M $MgCl_2$, Triton X-100) was added and cells incubated for 10 minutes on ice. 900 µl of PBS-BSA was added slowly and the cells centrifuged at 2500 RPM for 3-minutes. 500 µl of 80% ice cold methanol was added and cells stored at -20ºC.

Cells were resuspended in washing buffer (2% BSA, 0.1% Tween-20 in PBS) and centrifuged at 2000 RPM for 5-minutes. Cell pellets were resuspended in 50 µl of washing buffer containing primary antibody (H4K16ac (ab109463, Abcam), H3K27ac (ab4729, Abcam), Anti-Histone H3 Phospho S10 (ab14955, Abcam), H3 C-terminal (ab1791,

Abcam), IgG (EMD Millipore Corp) or Normal Mouse IgG (12-370, EMD Millipore Corp) all at 1:25)) for 1 hour at room temperature (RT) (Table 2.6).

500 µl of washing buffer was added, the cells centrifuged as before, and the supernatant removed. Pellets were then resuspended in 50 µl of washing buffer containing secondary antibody (APC-conjugated goat anti-rabbit IgG, F0111 or anti-mouse IgG APC conjugate, F0101B (R&D Systems)) at 1:5 for 0.5 hours in the dark. 500 µl of washing buffer was added, cells centrifuged as before, and supernatant removed. Pellets were resuspended in 300-500 µl Analysis Buffer (1% Vybrant Violet and 1.25% RNAse-A in PBS) and incubated at 37ºC for 30-minutes prior to analysis on the CytoFLEX (Beckmann Coulter). Figures were generated using CytExpert 2.3 software. The distribution of hyperacetylated cells across the cell-cycle was displayed as the percentage of hyperacetylated MCF7 or MDA-MB231 cells compared with the total number of cells identified in G1, S or G2/M-phase. The percentage of hyperacetylated cells per phase was assessed in each cell-line using a two-way ANOVA, considering cell-phase and treatment time.

Table 2.6: Antibodies used for flow cytometry analysis of acetylation

Antibody Target	Antibody name	Source
H4K16ac	ab109463	Abcam
H3K27ac	ab4729	Abcam
H3 C-terminal	ab1791	Abcam
IgG (rabbit)		EMD Millipore Corp
Secondary anti-IgG	Goat anti-rabbit APC	R&D Systems

2.11 RNA Synthesis Assay

The Abcam RNA Synthesis Assay kit was used to investigate whether the specific transcriptional response occurring in response to SAHA was observed on a global scale. $4.5x10^5$ MCF7 and $2.2x10^5$ MDA-MB231 cells per well were seeded into 6-well plates. 48-hours later, cell medium was replaced with 400 µl fresh medium. The RNA label, 5-EU (Ethynyl uridine) was diluted 1:100 into the medium and incubated for 30-minutes at 37ºC in treatment and positive control wells. Treatment wells were treated with a final concentration of 2.5 µM SAHA for 30, 60 or 120-minutes. The experiment was terminated by removing the medium and rinsing cells with 500 µl PBS. Cells were harvested using Trypsin, 600 µl fresh medium added and cells centrifuged at 300 g for 5-minutes (Heraeus Fresco 17 Microcentrifuge, ThermoFisher Scientific). Cells were incubated in 200 µl Fixative Solution for 15-minutes at RT, protected from light. Samples were then washed with 400 µl Wash Buffer and incubated with 200 µl Permeabilization Buffer for 10-minutes at RT. 200 µl Reaction Cocktail (2X) (1% Copper Agent, 1% Fluorescent Azide and 5% Reducing Agent in PBS) was added per well. Samples were incubated for 30-minutes at RT, protected from light. Cells were washed in 400 µl Wash Buffer and incubated with 200 µl 1µM DAPI (4′,6-diamidino-2-phenylindole) in PBS prior to analysis on the CytoFLEX. Figures were generated using CytExpert 2.3 software.

2.12 Sample Preparation for Next Generation Sequencing (with Zymo Research)

2.12.1 RNA-sequencing sample preparation

An RNA-Sequencing experiment was carried out assessing gene expression changes induced in MCF7 and MDA-MB231 cells following short SAHA treatments. MCF7 and

MDA-MB231 cells were seeded at a density of approximately $3.5x10^6$ and $1.3x10^6$ cells per T75 flask, respectively. 48-hours later, cells were treated with 2.5 μM SAHA for 30, 60, 120-minutes or left untreated. Following treatment, cells were harvested into fresh media and centrifuged at 300 g for 5 minutes at 4ºC. Cells were resuspended in 1 ml cold PBS and transferred into 1.5 ml eppendorfs and centrifuged again. Cells were counted by hematocytometer and resuspended in an appropriate volume of DNA/RNA Shield (Zymo Research) and stored at -80ºC.

2.12.2 RRBS sample preparation

An RRBS experiment was carried out assessing the methylation changes induced in MCF7 and MDA-MB231 cells following treatment with SAHA for 24 or 48-hours. Cells were seeded as before. 24-hour samples were incubated with 2.5 μM SAHA for 24-hours. 48-hour samples were treated twice with 2.5 μM SAHA, with fresh media added prior to re-treatment at 24-hours. Cells were harvested into fresh media, centrifuged at 300 g for 5 minutes at 4ºC and processed in the same manner as the RNA-Sequencing samples.

2.13 RNA Sequencing

Two sample replicates per timepoint were processed and analysed at Zymo Research, Irvine, CA. RNA was extracted from human samples stored in DNA/RNA shield using *Quick*-RNA MicroPrep according to the manufacturer's instructions. *RNA-Seq Library preparation:* Total RNA-Seq libraries were constructed from approximately 100 ng of total RNA. The method described by Bogdanova *et al*. (2011) was followed, with some modifications to remove rRNA (ribosomal RNA). Libraries were prepared using the

Zymo-Seq RiboFree Total RNA Library Prep Kit (Cat # R3000) according to the manufacturer's instructions. RNA-Seq libraries were sequenced on an Illumina NovaSeq to a sequencing depth of ~40-50 million read pairs (150 bp paired-end sequencing) per sample. *Sequence Data Alignments and Differential Expression Analysis:* Illumina NovaSeq paired-end 150 bp reads from Total RNA-Seq data files were first adaptor trimmed and then analysed using the STAR program (version 2.6.1d) for alignment of short reads to the GRCh38 *homo sapiens* reference genome. Transcript counts were inferred from alignment files. All transcripts with either 0 or 1 counts were removed. Gene expression was measured using EdgeR. The DESeq2 R package was used for differential expression analysis using the gene feature.

2.14 Analysis of RNA-sequencing data

The RNA-Sequencing data was analysed, to identify the differences in response between MCF7 and MDA-MB231 cells. The initial sample analysis was carried out at Zymo Research. The Sample Similarity matrices were created by plotting the Pearson correlation coefficient between samples (Boslaugh and Waters, 2008). Each dot in the Multidimensionality Plot (MDS) represents a sample, with the distance between them indicating differences in their gene expression patterns (Mead, 1992). Top Gene Expression Heatmaps were created plotting Log2values of the fold change in expression of the top 100 genes with the highest variance against their mean expression levels among all samples. Differential Gene Expression analysis was carried out using DESeq2 (Love *et al.,* 2014). Genes significantly differentially expressed between the treatment timepoints in each individual cell-line were identified, setting the threshold as $p<0.05$. DESeq2 was also used at Zymo to carry out the Likelihood Ratio Test. This is an alternative form of testing

when evaluating expression across more than two levels. It operates like an analysis of variance test (ANOVA) to indicate genes with the greatest variation across time. Ontology analysis was also carried out using g:Profiler (Raudvere *et al.,* 2019).

DAVID Bioinformatics Resources 6.8 was used for subsequent Ontology analysis (Huang *et al.,* 2009a; Huang *et al.,* 2009b). This analysis identified genes of interest annotated with functions that we predict to be important in the response. Interesting patterns of change in MCF7 cells, among genes including *HSPs, HATs, HDACs* and *TFs* were identified. Their basal expression and expression following SAHA treatment was analysed from the RNA-Sequencing data. Their expression was then followed up by qPCR in the MCF7 and MDA-MB231 cell-lines (Materials and Methods 2.5). HOMER software was used to carry out motif analysis to identify potential driver TFs of the survival response. Genes significantly differentially regulated following 30, 60 or 120-minute SAHA treatment in either cell-line were analysed. This was followed up with analysis of those significantly differentially regulated and exhibiting a fold-change>2. The expression of the individual *POU* and *ATF/CREB* family members was then assessed from the RNA-Sequencing data. These were validated by qPCR prior to selection of genes whose involvement in the survival response would be tested by knockdown. Figures were generated using GraphPad Prism. qPCR data was normalized to the expression of housekeeper genes, and fold-changes calculated from normalized pre-treatment expression presented graphically. Differences in basal expression were assessed using an unpaired, one-tailed T-test with $p<0.05$ set as significant. Differences in expression between treatment timepoints in one cell-line were assessed using a paired two-tailed T-test ($p<0.05$).

2.15 Reduced Representation Bisulfite Sequencing (RRBS)

Two replicates per timepoint were processed and analysed using the Methyl-MiniSeq® Service at Zymo Research, Irvine, CA. DNA was extracted using the protocol associated with the Quick-DNA/RNA Plus Kit Miniprep Kit (Zymo Research). *RRBS Library Preparation:* 300 ng of starting input genomic DNA was digested with 30 units of MspI (NEB). Fragments were ligated to pre-annealed adapters containing 5'-methyl-cytosine instead of cytosine according to Illumina's specified guidelines. Adaptor-ligated fragments ≥50 bp in size were recovered using DNA Clean & ConcentratorTM-5 (Cat#: D4003). The fragments were then bisulfite-treated using EZ DNA Methylation-LightningTM Kit (Cat#: D5030). Preparative-scale PCR was performed, and the resulting products were purified with DNA Clean & ConcentratorTM-5 (Cat#: D4003) for sequencing on an Illumina platform. *Sequence alignment and data analysis:* Sequence reads from bisulfite-treated RRBS libraries were identified using standard Illumina base calling software and the raw FASTQ files were quality trimmed using TrimGalore 0.6.4 to remove adapters and filled-in nucleotides. FastQC 0.11.8 was used to assess the effect of trimming and overall quality distributions of the data. Alignment to the hg19 reference genome was performed using Bismark 0.19.0. Methylated and unmethylated read totals for each CpG site were called using MethylDackel 0.5.0 (Ryan, 2022). The methylation level of each sampled cytosine was estimated as the number of reads reporting a C, divided by the total number of reads reporting a C or T. ANOVA and T-test were performed on each CpG site that had at least five reads coverage. A 10% difference in methylation value between groups and a p-value (unadjusted) of <0.05 was used to identify significantly differentially methylated cytosines. Promoter, gene body, and CpG island annotations were added for each CpG included in the comparison.

2.16 Analysis of RRBS data

The RRBS data was analysed to investigate whether DNA methylation occurred downstream of the initial acetylation induced by SAHA treatment and to determine any differences in the response of MCF7 and MDA-MB231 cells. Heatmaps, depicting the change in differentially methylated sites (DMS) in the MCF7 and MDA-MB231 genome, were generated by Zymo Research. These heatmaps included CpG sites which exhibited the greatest change in their methylation state across 48-hours, grouped by site and clustered by timepoint similarity. The DMS were firstly considered, which are individual CpG sites exhibiting significant difference in their methylation state between the SAHA treatment timepoints. The number of DMS in the 0 v 24-hour, 24 v 48-hour and 0 v 48-hour comparisons were analysed to indicate whether SAHA treatment resulted in changes in methylation downstream following the initial acetylation changes. The methylation state of each DMS following treatment was calculated selecting CpG sites exhibiting a difference in methylation >0.5 or <-0.5. These sites were then filtered to select only those located at promoter region. This enabled the percentage of DMS identified at promoter regions in each timepoint comparison to be calculated.

The differentially methylated regions (DMR) were then investigated. These are regions which contain several CpG sites exhibiting a similar significant difference in their methylation state in response to SAHA treatment (Rakyan *et al.,* 2011). Their methylation post SAHA treatment was then considered selecting those with a difference in methylation >0.5 or <-0.5. These sites were then filtered to select only those located at promoters. Using an areaStat cut-off >10 or <-10, the methylation change observed in DMRs at promoters was shown graphically in pie-charts generated using GraphPad Prism. Motif

Analysis, using the default parameters, was carried out using HOMER software. DMRs identified in the 0 v 24-hour or 0 v 48-hour comparison in each cell-line exhibiting an areaStat value >10 or <-10 were analysed. Next considered were the DMRs with these criteria also located at promoter regions. The analysis was also repeated applying a difference in methylation >0.4 or <-0.4 as the inclusion cut-off. All figures were generated using GraphPad Prism 9.

2.17 Plasmid transformation

A GFP expressing plasmid was generated to optimize the transfection protocol in MCF7 and MDA-MB231 cells. 5 ng of pmax green fluorescent protein (GFP) vector (Lonza, 1 µg/µl) was diluted 1:1000 in UP water and added to 50 µl DH5α (Invitrogen), mixed briefly and incubated on ice for 30 minutes. Cells were heated to 42ºC for 20 seconds and then placed on ice for 2 minutes. 950 µl of prewarmed LB broth was added, and cells incubated at 37ºC for 1 hour at 225 RPM. 20 µl of cells were streaked onto Kanamycin selective agar plates and stored at 37ºC overnight. One colony was selected and added to 20 ml of LB broth, containing 100 µg/ml Kanamycin, overnight. Plasmid DNA was extracted using the protocol associated with the QIAPrep Spin Miniprep Kit (QIAGEN).

2.18 Transfection Optimization

A GFP expressing plasmid was used to determine the optimal Lipofectamine concentration, incubation time and seeding density in MCF7 and MDA-MB231 cells. Approximately $4x10^5$ MCF7 and $2.7x10^5$ MDA-MB231 cells per well were seeded into 6-well plates. The following day, cells were transfected using 2.5, 5 or 7 µl Lipofectamine

3000 (Invitrogen) with 2.5 µg pmax GFP plasmid DNA. After 4-hours the medium was replaced. After 24-hours, transfection efficiency was analysed by Flow Cytometry using the FIT-C channel to gate GFP incorporation from the untransfected population.

2.19 Serum Response Factor (SRF) knockdown

SRF was knocked down in MCF7 cells to determine whether this affected their HDACi sensitivity. MCF7 cells were seeded into 6-well plates in DMEM/FBS at a density of approximately $2.5x10^5$ cells per well. On the following day they were transfected with 10 nM SRF siRNA (ORIGENE), or Cy-3 labelled fluorescent transfection control siRNA duplex (ORIGENE) using 2.5 µl Lipofectamine 3000 (Invitrogen). After 4-hours, fresh DMEM was added. The following day, cells were treated with a final concentration of 2.5 µM SAHA. 48-hours later, one set of plates was harvested and used to assess *SRF* expression by qPCR. RNA was extracted from cell pellets following the protocol associated with the RNeasy Mini Kit (QIAGEN) and converted to cDNA using the Tetro cDNA synthesis kit (Bioline Meridian Biosciences). qPCR was run as detailed in Materials and Methods 2.5. The second plate was used for the Annexin V assay, assessing the effect of knockdown on SAHA sensitivity using the CytoFLEX (Beckman Coulter). Figures were generated using GraphPad Prism.

2.20 SMARTpool siRNA formulations

250 µL of UP water was added to 5 nmol of SMARTpool siRNA (Dharmacon, Horizon Discovery Biosciences Ltd; Table 2.7) to create a 20 µM stock solution. This was diluted to 5 µM working stocks and cells treated with a final concentration of 25 nM siRNA.

Table 2.7: SMARTpool siRNA formulations

Gene Targeted	siRNA formulation	Catalogue ID
SRF	SMARTpool ON-TARGET siRNA against Human SRF	L-009800-00-0005
Scrambled	ON-TARGETplus Non-targeting Pool	D-001810-10-05
POU2F1	ON-TARGETplus Human POU2F1 siRNA	L-019689-00-0005
POU2F2	ON-TARGETplus Human POU2F2 siRNA	L-019690-00-0005
ATF4	ON-TARGETplus Human ATF4 siRNA	L-005125-00-0005
ATF5	ON-TARGETplus Human ATF5 siRNA	L-008822-00-0005
CREB3L4	ON-TARGETplus Human CREB3L4 siRNA	L-010738-02-0005

2.21 Individual gene siRNA knockdown

POU or ATF/CREB genes were individually knocked down in MCF7 or MDA-MB231 cells and the effect this had on their HDACi sensitivity assessed using the apoptosis assay after 48-hour SAHA treatment. MCF7 and MDA-MB231 cells were seeded into 6-well plates in 1 ml DMEM/FBS or RPMI/FBS at an approximate density of $2.5x10^5$ or $1.4x10^5$ cells per well. The following day, MCF7 and MDA-MB231 cells were transfected with 25 nM POU2F1, POU2F2, ATF4, ATF5, CREB3L4 (cAMP Response element-binding protein 3 like 4) or scrambled siRNA using 2.5 µl (MCF7) or 5 µl (MDA-MB231) Lipofectamine 3000 (Invitrogen). After 4-hours, 2 ml fresh DMEM/RPMI was added. The next day, treatment wells were treated with 2.5 µM SAHA. 48-hours later, cells were harvested, and knockdown gene expression assessed by qPCR (as detailed in Materials and

Methods 2.5). Apoptosis was analysed using the Annexin V Assay. Figures were generated using CytExpert 2.4 software and GraphPad Prism. Error bars depicting SEM were applied. Significance was determined by comparing the late apoptotic or viable population following treatment in knockdown versus scrambled samples using a one-tailed, paired T-test setting $p<0.05$ as significant.

2.22 Double siRNA knockdown

Two genes from either the POU or ATF/CREB family were knocked down together in MCF7 and MDA-MB231 cells to determine whether this enhanced their HDACi sensitivity. MCF7 and MDA-MB231 cells were seeded as before. The following day, MCF7 cells were transfected using 2.5 µl and MDA-MB231 cells using 5 µl Lipofectamine 3000 (Invitrogen). Both cell-lines were transfected with 25 nM POU2F1 and 25 nM POU2F2. MCF7 cells were transfected with 25 nM ATF4 and 25 nM CREB3L4 siRNA while MDA-MB231 cells were transfected with 25 nM ATF4 and 25 nM ATF5 – alongside scrambled siRNA. After 4-hours, 2 ml fresh DMEM/RPMI was added. The next day 2.5 µM SAHA was added to treatment wells. 48-hours later, cells were harvested for qPCR assessment of *POU2F2, POU2F1, ATF4, ATF5* or *CREB3L*4 expression following knockdown. RNA was extracted and converted to cDNA as stated previously. Apoptosis was analysed and tested statistically as previously described.

2.23 Triple siRNA knockdown

Three genes were knocked down from either the ATF/CREB family or from distinct resistance pathways to investigate whether this enhanced the sensitivity of MCF7 and

MDA-MB231 cells to HDACi treatment. MCF7 and MDA-MB231 cells were seeded as before. The following day, MCF7 cells were transfected using 2.5 µl and MDA-MB231 cells using 5 µl Lipofectamine 3000 (Invitrogen). Both cell-lines were incubated with 25 nM ATF4, POU2F2, SRF siRNA alongside scrambled siRNA. MDA-MB231 cells were additionally transfected with 25 nM ATF4, ATF5, CREB3L4 siRNA. After 4-hours, 2 ml fresh DMEM/RPMI was added. The next day 2.5 µM SAHA was added to treatment wells. 48-hours later, cells were harvested for qPCR assessment of knockdown gene expression. RNA was extracted and converted to cDNA as stated previously. Apoptosis was analysed and tested statistically as previously described.

2.24 Analysis of target gene expression using CBioPortal

MCF7 and MDA-MB231 cell-lines were compared to a patient cohort in CBioPortal to understand whether they were representative of their molecular subtype and investigate whether our TF genes of interest were differentially expressed by subtype. CBioPortal was used to observe the expression and mutation profiles of *SRF, CREB3L4, ATF1, ATF3, ATF4, ATF5, ATF6, POU2F1* and *POU2F2* genes in breast cancer cells. All 25 breast cancer studies (11632 samples) were queried for copy number variations and mutations in these nine genes. The associated oncoprint was analysed and the significant co-occurrence assessed. Following this, the chromosomal position of the nine genes was investigated from literature. The Cancer Genome Atlas (TCGA) Nature 2012 database was then queried to see whether mutation or copy number signatures could be assigned to molecular subtypes. This study was chosen as it contains copy number, mutation, gene expression and receptor status information for each sample. The 482 samples were queried for the nine genes of interest. Tracks for Oestrogen (ER), Progesterone (PR) and Human

Epithelial receptor 2 (HER2) status were incorporated in the oncoprint. Sorting the tracks by receptor status showed the patterns observed in triple-negative and luminal A patient samples. The next step involved the analysis of gene expression data in this dataset, again separating samples by receptor status. The database was queried for gene expression changes in these nine genes, which was visualized in a heatmap generated using z-scores relative to the diploid samples. The mRNA data (from microarrays) associated with each patient sample was then used to plot Violin plots of gene expression in triple-negative samples versus luminal A samples using Prism 9. Significance was determined using an unpaired T-test with Welch's correction. The expression of heat shock protein genes; *HSPA1A, HSP90AA1, HSP90AB1* and *HSP90B1* were then assessed in triple-negative and luminal A samples in the TCGA Nature 2012 database. The associated mRNA data from microarrays was then used to plot Violin plots of gene expression per molecular subtype in Prism 9.0, with significance determined using an unpaired T-test and Welch's correction.

3. DEVELOPMENT OF A SOLID TUMOUR MODEL OF RESPONSE AND RESISTANCE TO HDACi TREATMENT

This chapter focussed on developing the solid tumour model of resistance to HDACi treatment, with the aim of identifying an HDACi sensitive and HDACi resistant cell-line for comparison. Cell-lines were initially identified using the Annexin V and MTS Assays – characterising their sensitivity to both an HDACi (SAHA) and DNMTi (DAC). The model was then verified through an analysis of DAC and SAHA induced cell-cycle changes, as well as the RNA synthesis and histone acetylation induced in response to SAHA. Their molecular response to SAHA treatment would then be compared through RNA-Sequencing and RRBS, with these analyses also used to identify potential driver proteins mediating cellular resistance to HDAC inhibitors.

3.1 Initial identification of HDACi sensitive and resistant cell-lines

The initial step in this project involved establishing a solid tumour model of HDACi resistance, with the aim of defining an HDACi resistant and HDACi sensitive cell-line. This followed on from previous work in our lab characterising the HDACi resistance of BL and LCL cells. A panel of adherent cell-lines was initially assessed. MCF7, MDA-MB231, MCF10A and U2OS cells were selected as they could be acquired from colleagues at Birmingham or Leicester University. It had been expected that a much larger screening panel would have been required to identify an HDACi resistant and HDACi sensitive cell-line. However, this solid tumour model system was fortunately located very quickly. Of the four cell-lines selected, it happened that the sensitivity of the MCF7 and MDA-MB231 cells – as determined by the Annexin V and MTS Assays - differed

significantly. This led to the establishment of our model system, consisting of the more HDACi sensitive MDA-MB231 and the more HDACi resistant MCF7 cells. MCF10A cells were additionally included as an immortalised but non-transformed cell-line, representing the closest comparison to a normal cell-line.

3.1.1 Breast cancer cell-line characteristics

MCF7 cells were isolated from a pleural effusion of a primary invasive ductal carcinoma (Soule *et al.,* 1973; Figure 3.1A). They represent a Luminal A subtype and express the Oestrogen receptor (ER^{+}), often alongside the Progesterone receptor ($PR^{-/+}$) (Riaz *et al.,* 2013). MCF7 cells do not express amplified HER2 and express wild type p53 (Riaz *et al.,* 2013; Troester *et al.,* 2006). This cell-line displays features of differentiated mammary epithelium, expressing epithelial markers such as E-cadherin and B-catenin (D'Anselmi *et al.,* 2013). MCF7 cells are less invasive (Gest *et al.,* 2013). This relates to their lower expression of vascular endothelial growth factor (VEGF), a factor known to induce migration and invasion (Comsa *et al*., 2015). They are aneuploid and exhibit genomic instability. They display chromosome numbers varying from 60-140, with a modal chromosome number of 82 (Comsa *et al*., 2015; Lee *et al.,* 2015).

The MDA-MB231 triple-negative epithelial cell-line was established from the pleural effusion of a metastatic mammary adenocarcinoma (Cailleau *et al.,* 1978; Riaz *et al.,* 2013; Figure 3.1B). It is highly invasive, poorly differentiated, and often associated with a poorer prognosis (Chavez *et al.,* 2010; Prat *et al*., 2010). MDA-MB231 cells

exhibit stem cell characteristics, specifically $CD44^+$ and $CD24^-$ low phenotypes (Prat *et al.,* 2010). They also express p53 mutated at residue 280 (Walerych *et al.,* 2012).

The MCF10A cell-line was derived from benign proliferative breast tissue spontaneously immortalized without defined factors (Soule *et al.,* 1990). They represent pre-neoplastic mammary epithelial cells – which are immortalised but non transformed. These cells have a stable diploid karyotype (Puleo and Polyak, 2021).

Microscope images of MCF7 and MDA-MB231 cells

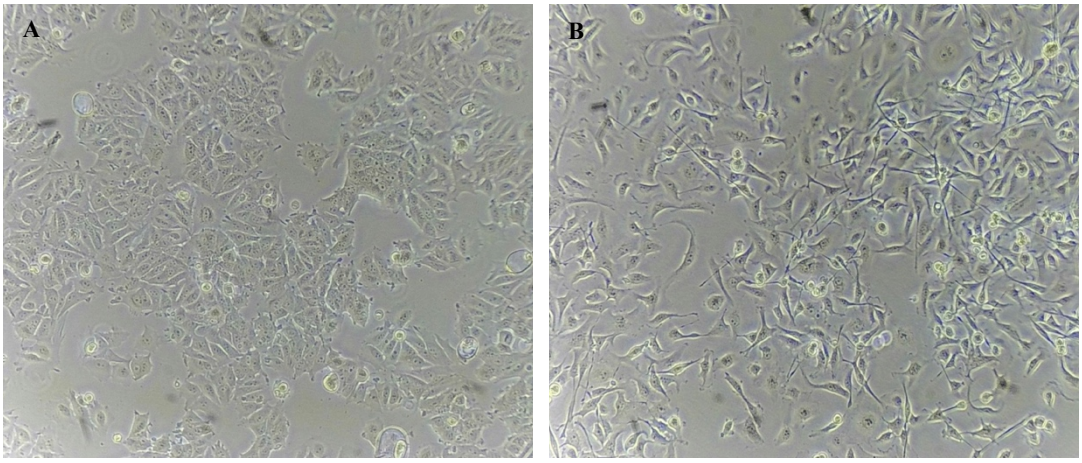


Figure 3.1: Microscope images of MCF7 and MDA-MB231 cells grown in the lab. *Images of A. MCF7 cells seeded at a density of $6x10^6$ cells and B. MDA-MB231 cells seeded at a density of $5x10^6$. Acquired at x10 objective on the EVOS Microscope.*

This project focussed on the transcriptional changes induced in our more HDACi resistant cell-line following 2-hour SAHA treatment. However, this work also aimed to link these early gene expression changes with the occurrence of apoptosis 48-hours after treatment. Different experimental techniques were used to investigate these two separate issues. The occurrence of cell death at 48-hours was assessed through the Annexin V Assay, while qPCR was used to analyse the shorter-term transcriptional response. Apoptosis at 48-

hours was selected as a measurable endpoint, representative of the knockdown affecting cell viability – suggesting genes of interest for qPCR follow up.

3.2 Annexin V Assays showed that MDA-MB231 cells were more sensitive to treatment with DAC and SAHA

The sensitivity of our solid tumour cell-lines to treatment with an HDACi (SAHA) and DNMTi (DAC) was assessed using the Annexin V Assay. Cells were treated with either of the two drugs to follow up on unpublished work from our lab, which had shown that cells sensitive to SAHA were also sensitive to DAC. This suggested that common pathways were being utilised in response to these drugs. Based on previous work in the lab, cells were treated with 2.5 μM SAHA, 1 μM DAC or an equivalent volume of DMSO for 48-hour or 96-hours respectively. This SAHA concentration was chosen as it was deemed therapeutically achievable and because profound growth effects are observed in response to higher concentrations (Munster *et al*., 2001).

The apoptosis assay uses Annexin V to detect the presence of phosphatidylserine (PS) outside the plasma membrane of a cell. This protein is externalised on the membrane of cells during the initial stages of apoptosis. Double staining with Propidium Iodide (PI) is then used to distinguish the necrotic from the apoptotic population. PI enters cells through permeable cell membranes. Its presence within cells indicates that the membrane has been damaged, suggesting that necrosis has occurred. Considering Figure 3.2A, cells in the bottom left quadrant are Annexin V and PI negative and represent the viable population. Cells in the bottom right quadrant are Annexin V positive only, representing the early apoptotic population. Cells in the top right quadrant are PI and Annexin V positive and

represent the late apoptotic population. Cells in the top left quadrant are PI positive, representing the necrotic population.

An initial 24-hour SAHA experiment was set up, based on the timing which has been used previously for BL cell-line characterisation. However, little apoptosis was induced in our solid tumour cell-lines by this time. Analysis of the literature confirmed that longer SAHA treatment times should be tested. For example, it has been shown that apoptosis was induced in MCF7 cells following 48-hour SAHA treatment (Huang and Pardee, 2000). This led to cells being treated with SAHA for 48-hours. As shown in Figure 3.2A, MDA-MB231 cells were most sensitive to 48-hour SAHA treatment. Their viable cell population was reduced from 91.21% in untreated cells to 50.88% in those treated with 2.5 μM SAHA. Comparison of this 40.3% loss in viability with a loss of 9.2% in MCF7, and 10% in MCF10A highlighted the greater HDACi sensitivity displayed by MDA-MB231 cells (Figure 3.2). Comparing this with values quoted in literature, the sensitivity of MCF7 cells correlated with the 8.4% loss in viable population reported by Marchion *et al*., in 2004 after 48-hour SAHA treatment. These results were an early indication of the difference in SAHA sensitivity evident between our cell-lines, concluding that MDA-MB231 cells were more sensitive than MCF7 cells to HDAC inhibition.

Based on the suggestion of a crossover in the pathways used in response to an HDACi and DNMTi, the apoptosis induced following DAC treatment was then investigated (Yang *et al*., 2001). MCF7, MDA-MB231 and MCF10A cells were initially treated with 1 μM DAC for 48-hours. This, however, had no effect on their viability (Appendix 10.1). As the mechanism of action of this inhibitor involves its incorporation during cell-division, cells were then treated with DAC for 72-hours. However, even treatment for this length of time

had little effect on their viability (Appendix 10.1). This led to cells finally being treated with 1 μM DAC for 96-hours. DAC treatment did not reduce the viability of MCF7 cells within this time, while the viability of the MCF10A cells was reduced by only 2% (Figure 3.3B/C). MDA-MB231 cells were more sensitive to DNMT inhibition, exhibiting a reduction in their viable population from 95.84% in untreated to 72.25% in DAC treated cells (Figure 3.3A). This 23.59% loss in viability was smaller than that observed following SAHA treatment. The Annexin V assays concluded that only MDA-MB231 cells were sensitive to treatment with a DNMTi. Importantly, this highlighted that the MDA-MB231 cell-line was sensitive to both an HDACi and DNMTi – as had been shown in previous unpublished work from the lab.

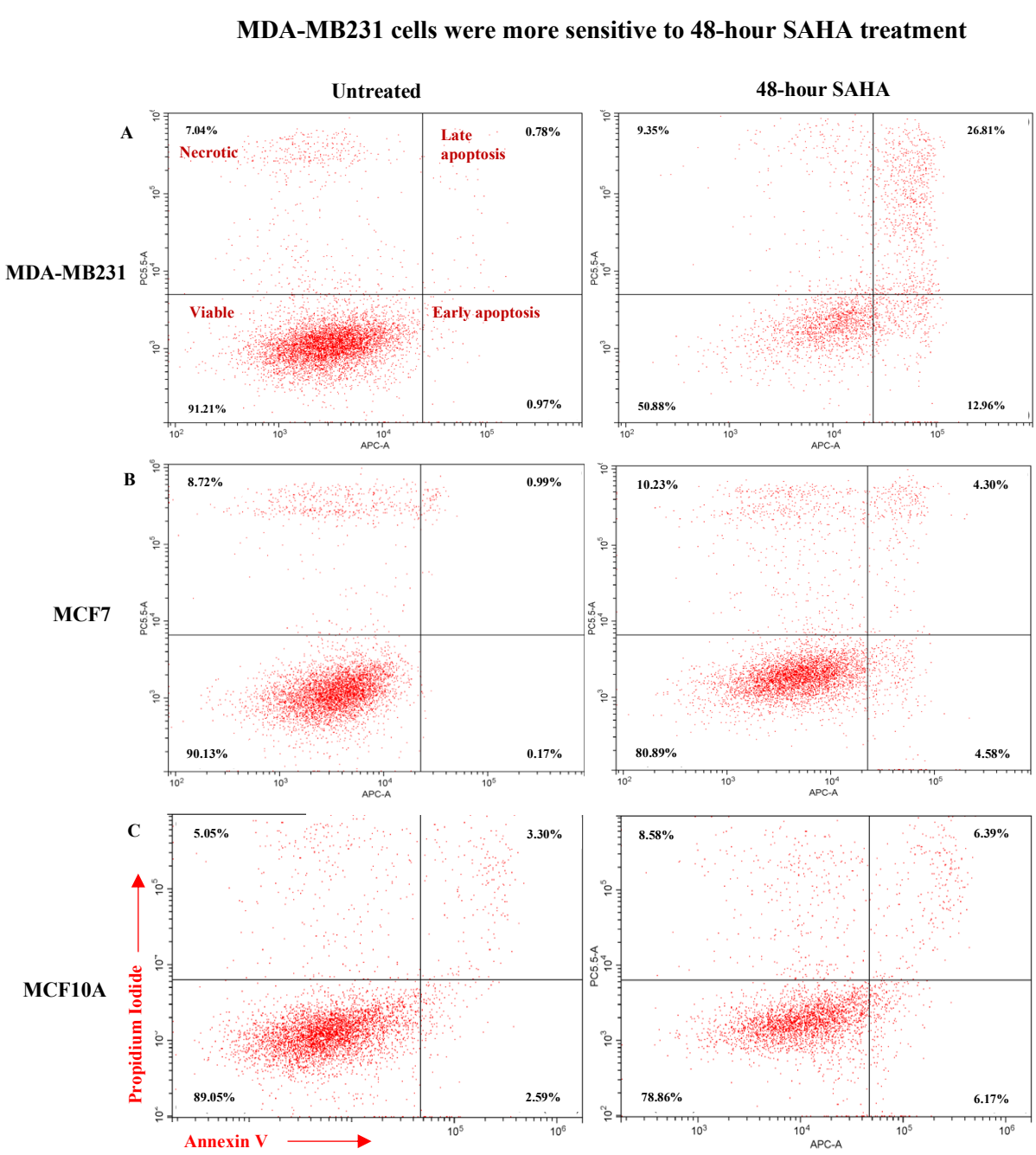


Figure 3.2: MDA-MB231 cells were more sensitive to 48-hour SAHA treatment. *Apoptosis was assessed using the Annexin V/Propidium Iodide assay in A. MDA-MB231, B. MCF7 and C. MCF10A cells following treatment with 2.5 μM SAHA or DMSO for 48-hours.*

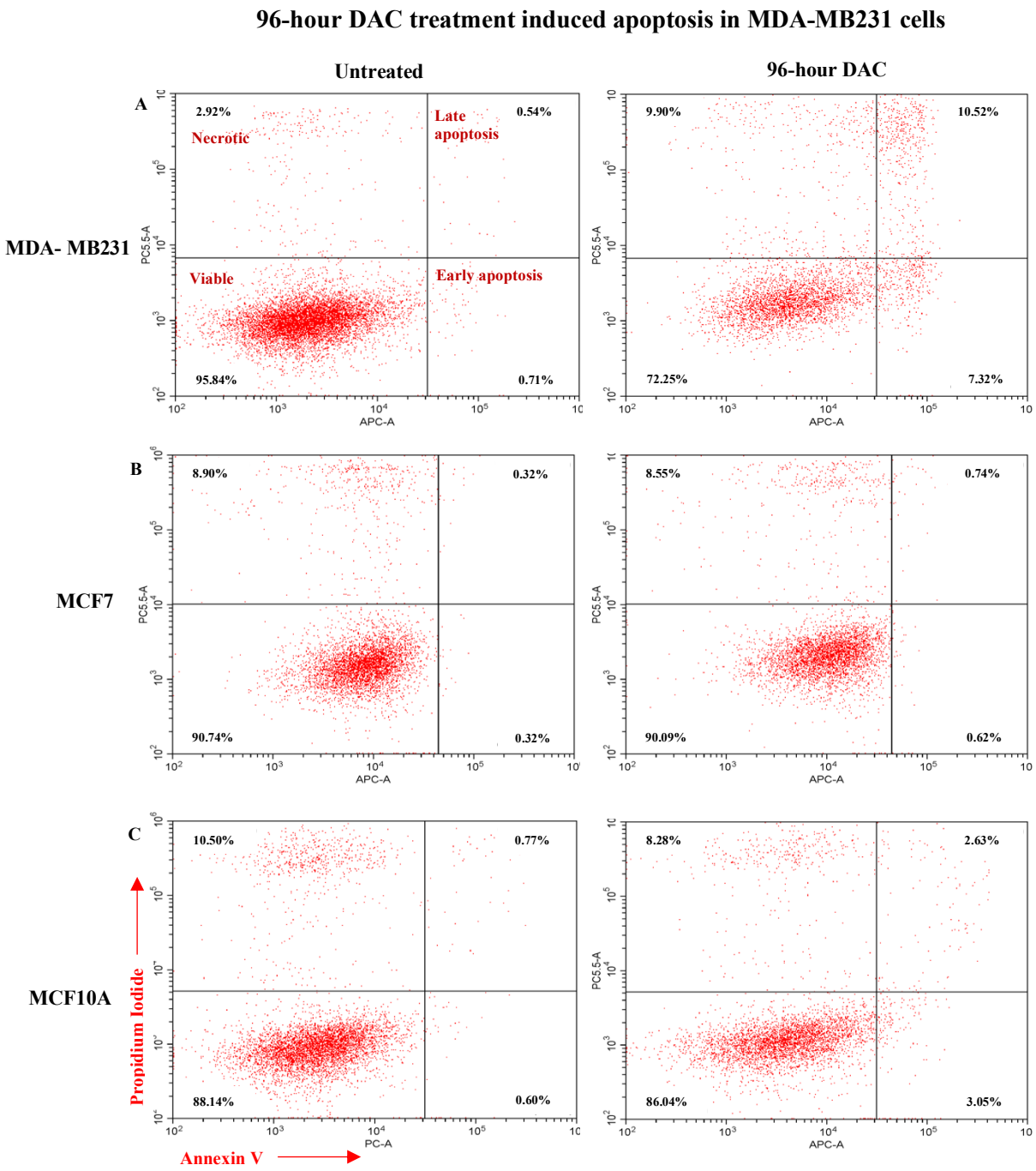


Figure 3.3: MDA-MB231 cells were most sensitive to 96-hour DAC treatment. *The apoptosis induced in A. MDA- MB231, B. MCF7 and C. MCF10A cells treated with 1 μM DAC or DMSO for 96-hours was assessed using the Annexin V/Propidium Iodide Assay.*

The viable population of all three cell-lines was significantly reduced following 48-hour SAHA treatment (Figure 3.4A). The viable population of MDA-MB231 cells was reduced by 32.7%, the MCF7 population by 9.58% and the MCF10A population by 10.41%. This highlighted that MDA-MB231 cells were the most sensitive to HDACi treatment. Figure 3.4B indicated that DAC treatment had less effect on the viability of all cell-lines tested. The viable population of MDA-MB231 cells was significantly reduced, exhibiting a loss of 24.8%. The viable population of MCF7 cells was reduced by 5.2% and MCF10A cells by 4.1%. This showed that MDA-MB231 cells were most sensitive to 48-hour SAHA and 96-hour DAC treatment. The limited effect on cell viability observed in the MCF10A and MCF7 cell-lines suggested that they were more resistant to HDACi and DNMTi treatment. This characterised our model system as one containing the more HDACi sensitive MDA-MB231, the more HDACi resistant MCF7 and the non-transformed MCF10A cells.

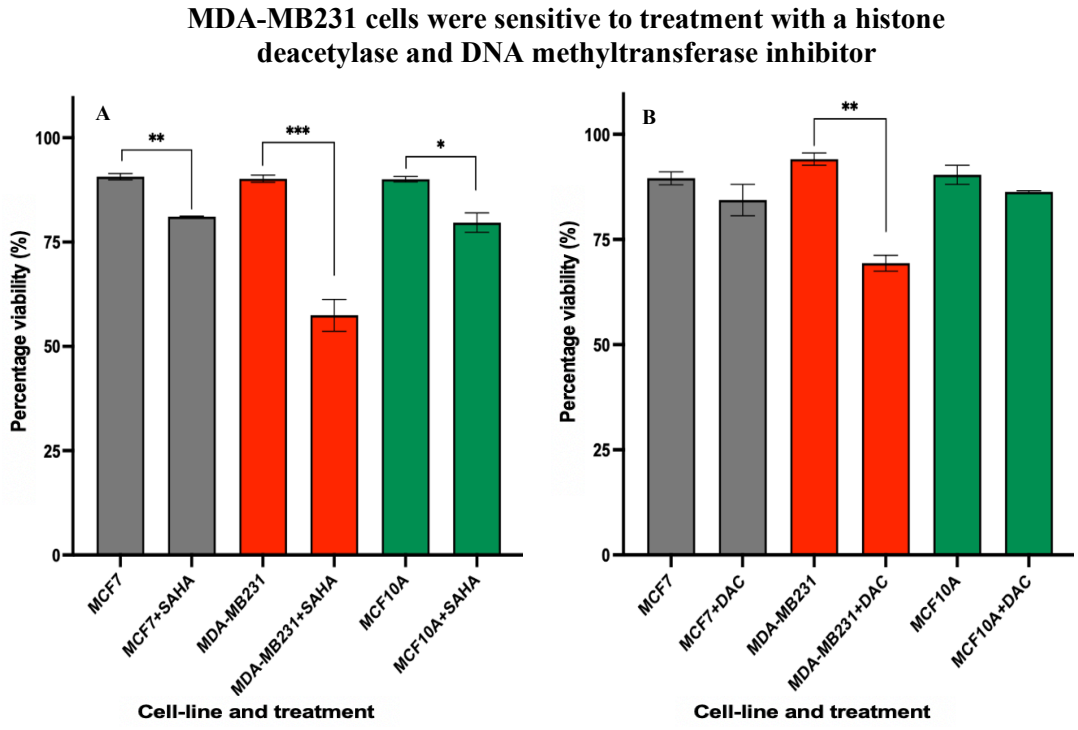


Figure 3.4: MDA-MB231 cells were more sensitive to HDAC and DNMT inhibition. *The viable population remaining following A. 48-hour treatment with 2.5 μM SAHA and B. 96-hour treatment with 1 μM DAC was compared with that in untreated MCF7, MDA-MB231 and MCF10A cells using the Annexin V/ Propidium Iodide apoptosis assay. Paired, one-tailed T-test *p<0.05, **p<0.01, ***p<0.001. Error bars depict SEM of independent experiments (N=3).*

3.3 SAHA and DAC reduced the metabolic potential of MDA-MB231 cells

It had not been expected that these solid tumour cell-lines would be so resistant to HDACi treatment. This led to the MTS assay being carried out, investigating the hypothesis that at sub-lethal concentrations SAHA and DAC reduced cellular metabolic capacity. Though measuring the metabolic potential of the cells, this assay is also dependent on cell number. This assay also allowed IC_{50} values to be calculated for SAHA and DAC in each cell-line and confirm the concentrations chosen for treatment in this project.

The MTS Assay is a colorimetric assay, reflecting the number of viable cells in a population (Mossman, 1983). MTS, in the presence of the intermediate electron donor phenazine methosulfate (PMS), is reduced by metabolically active cells into the insoluble formazan product (Stockert *et al.,* 2018). This is associated with a colour change from yellow to purple, which is quantified by spectrophotometry at an absorbance of 490nm.

MCF7, MDA-MB231 and MCF10A cells were treated with two-fold dilutions of SAHA (40 μM to 1.25 μM) for 48-hours. This affected the metabolic potential of MCF7 and MCF10A cells, however, MDA-MB231 cells were extremely sensitive to these concentrations (Figure 3.5). Thus, they were treated with four lower SAHA concentrations (0.625 μM – 0.078 μM) in subsequent experiments. The IC_{50} values highlighted the sensitivity of MDA-MB231 cells to SAHA treatment (Table 3.1). The IC_{50} value calculated for MCF7 cells was three times greater, and the value for MCF10A cells was more than four times greater than that observed in MDA-MB231 cells. To conclude, the SAHA MTS Assay confirmed that MCF7 and MCF10A cells were more HDACi resistant while MDA-MB231 cells were more HDACi sensitive.

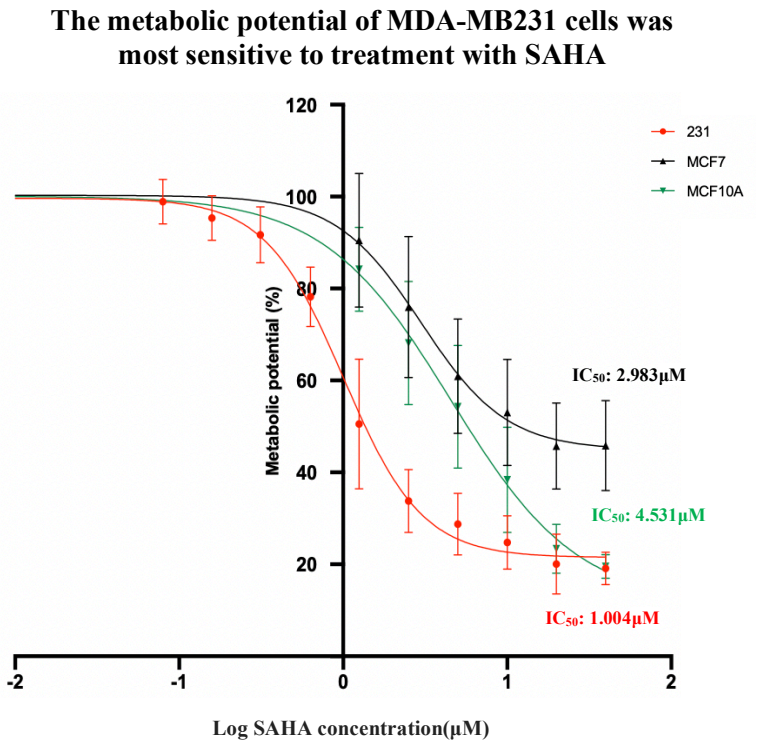


Figure 3.5: MDA-MB231 cells were more sensitive than MCF7 and MCF10A cells to SAHA treatment. *The metabolic potential of MCF7, MDA-MB231 and MCF10A cells incubated with two-fold dilutions of SAHA from 40 µM to 0.078 µM for 48-hours was assessed using the MTS Assay. The Dose Response Curve was generated using GraphPad Prism 8. Error bars depict Standard Deviation (SD) of independent experiments (MDA-MB231 N=5, MCF7 N=4, MF10A N=3).*

Table 3.1: SAHA IC_{50} values per cell-line

Cell-line	IC_{50}
MDA-MB231	1.004 µM
MCF7	2.983 µM
MCF10A	4.531 µM

MCF7, MDA-MB231 and MCF10A cells were then treated with two-fold dilutions of DAC (40 µM to 1.25 µM) for 96-hours. The metabolic potential of MCF7 cells was unaffected by this treatment, while the metabolic potential of MDA-MB231 cells was reduced in the presence of higher DAC concentrations (Figure 3.6). Unusually, the metabolic potential of MCF10A cells was reduced to around 40% of the control across all concentrations tested, which led to them being treated with six lower DAC concentrations (0.625 µM – 0.00195 µM) in subsequent experiments (Figure 3.6). As DAC had little effect on the metabolic potential of MCF7 cells, their IC_{50} value was over three hundred times greater than that calculated for MDA-MB231 cells. The IC_{50} values highlighted that

DAC had less effect on cell metabolic potential than SAHA, while showing that MDA-MB231 cells were more sensitive to DNMTi treatment than MCF7 cells (Table 3.2). The calculated SAHA IC_{50} values also provided confidence in the SAHA concentration chosen for this work, with 2.5 μM between the IC_{50} of our sensitive and resistant cell-line.

The MCF7 and MDA-MB231 findings agreed with the results obtained from the Annexin V Assay. MDA-MB231 cells were more sensitive to both HDAC and DNMT inhibition, while the MCF7 cells were more resistant to treatment with both. This also confirmed that SAHA reduced cell viability and metabolic potential to a greater extent than DAC in all cell-lines tested. A two-fold difference in IC_{50} value was evident between the resistant and sensitive line, as had been observed in previous unpublished work in the lab characterising HDACi resistant and sensitive BL cell-lines. It is important to consider SAHA treatment time when comparing these IC_{50} values to those in the literature. Our cell-lines were treated with SAHA for 48-hours. However, an IC_{50} value of 0.75 μM was reported for MCF7 treated with SAHA for 120-hours and 0.577 μM for MDA-MB231 cells treated with SAHA for 96-hours (Munster *et al.,* 2001; Wawruszak *et al.,* 2015).

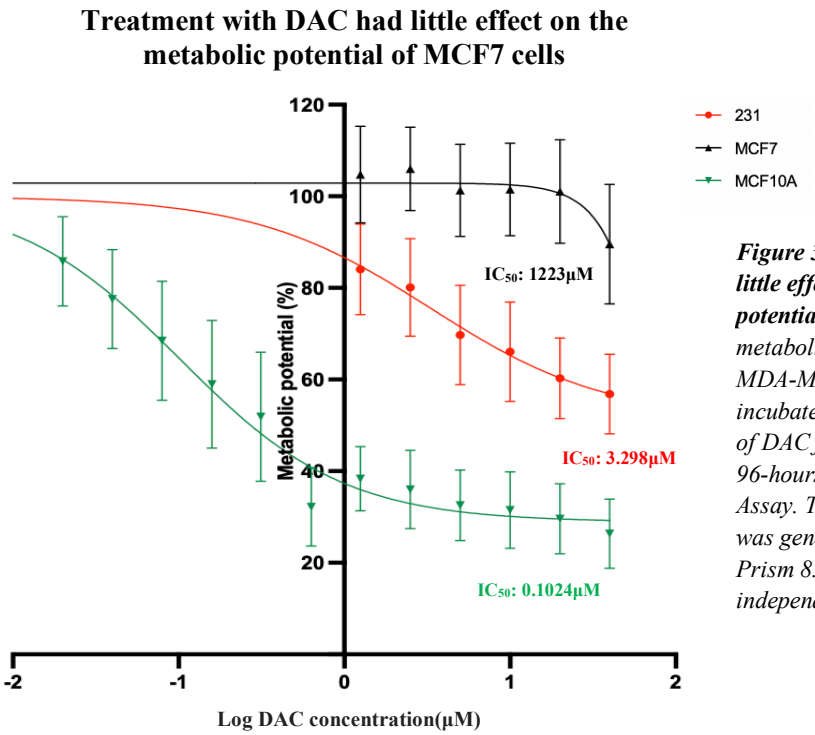


Figure 3.6: DAC treatment had little effect on the metabolic potential of MCF7 cells. *The metabolic potential of MCF7, MDA-MB231 and MCF10A cells incubated with two-fold dilutions of DAC from 40 µM to 1.25 µM for 96-hours was assessed in the MTS Assay. The Dose Response Curve was generated using Graph Pad Prism 8. Error bars depict SD of independent experiments (N=5).*

Table 3.2: DAC IC_{50} values per cell-line

Cell-line	IC_{50}
MDA-MB231	3.298 µM
MCF7	1223 µM
MCF10A	0.1024 µM

3.4 Cell cycle disruption does not explain the remarkable sensitivity of MCF10A cells in the DAC MTS Assay

Cell-cycle analysis post DAC treatment was then carried out to follow up on the unusual MCF10A sensitivity observed in the MTS assay. It was hypothesised that their sensitivity may have been the result of a G2 cell-cycle block. MCF7, MDA-MB231 and MCF10A cells were treated with 1 µM DAC for 96-hours. Vybrant Violet, a cell permeable DNA dye that emits fluorescence proportional to the DNA mass, was then added. This allowed the distribution of cells per cell-cycle phase to be analysed by Flow Cytometry.

The more HDACi and DNMTi sensitive cell-line, MDA-MB231, exhibited the greatest change in its cell-cycle profile following DAC treatment (Figure 3.7C/D). Flow Cytometry analysis indicated that a 24% loss in the number of cells in G1 was accompanied by a 13% increase in G2/M. On the other hand, neither the cell cycle profile of the MCF7 or MCF10A cells was significantly altered in response to 96-hour DAC treatment (Figure 3.7B/F). MCF7 cells exhibited only a 2% loss in the number of cells in G1, accompanied by a 1% gain of those in G2/M.

96-hour DAC treatment did not alter the cell-cycle profile of MCF10A cells

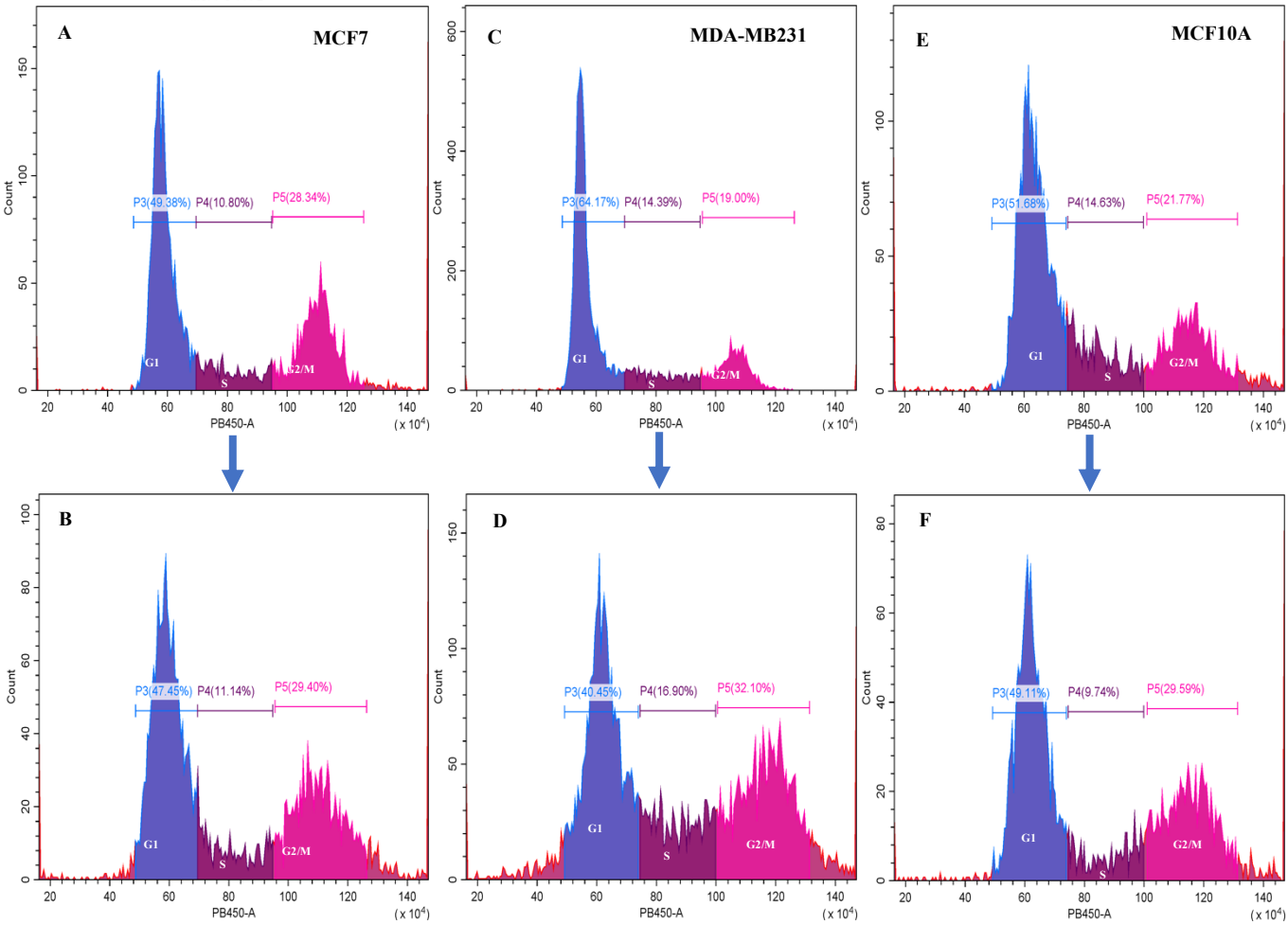


Figure 3.7: The cell-cycle profile of the MCF10A cells was not affected by DAC treatment. *The percentage of A. untreated and B. 96-hour DAC treated MCF7, C. untreated and D. 96-hour DAC treated MDA-MB231, E. untreated and F. 96-hour DAC treated MCF10A cells per phase of the cell-cycle was assessed using Flow Cytometry analysis of Vybrant Violet incorporation.*

Considering the results across both replicates – the cell-cycle distribution of MDA-MB231 cells was significantly altered following DAC treatment, X^2 (4, N=3) =12.6, p=0.006. A 21% loss in G1 was accompanied by an 8.8% increase in G2/M (Figure 3.8). Cells present in sub-G1 reflected the apoptosis induced in response to DAC treatment. MDA-MB231 cells exhibited the greatest increase in their apoptotic population, correlating with the results of the Annexin V Assay (Figure 3.3). DAC treatment did not significantly affect the distribution of MCF7 cells per cell-cycle phase X^2 (4, N=3) =1.2, p=0.76. Cells exhibited a 6.2% loss in G1, accompanied by a small gain in G2/M. The cell-cycle profile of MCF10A cells was not affected by DAC treatment, suggesting that a G2 block was not responsible for their unusual sensitivity in the MTS assay. The MTS assay is sensitive to pH and the depletion of essential nutrients. Perhaps a change in pH resulting from cellular metabolism altered the ability of the cells to produce formazan (Riss *et al.,* 2013). This hypothesis could be confirmed using the Trypan blue assay. This was not followed up as this project focussed on the comparison between an HDACi resistant and sensitive cell-line. MCF10A cells were only included as a comparison to a more karyotypically normal cell-line.

In conclusion, DAC treatment did not induce a cell-cycle block in MCF10A cells. The greatest change in cell-cycle profile was observed in the more HDACi and DNMTi sensitive, MDA-MB231 cells. They exhibited a loss in G1 alongside a gain in G2/M and S-phase. The sub-G1 population was used an indicator of apoptosis – with this population only increasing in MDA-MB231 cells following DAC treatment.

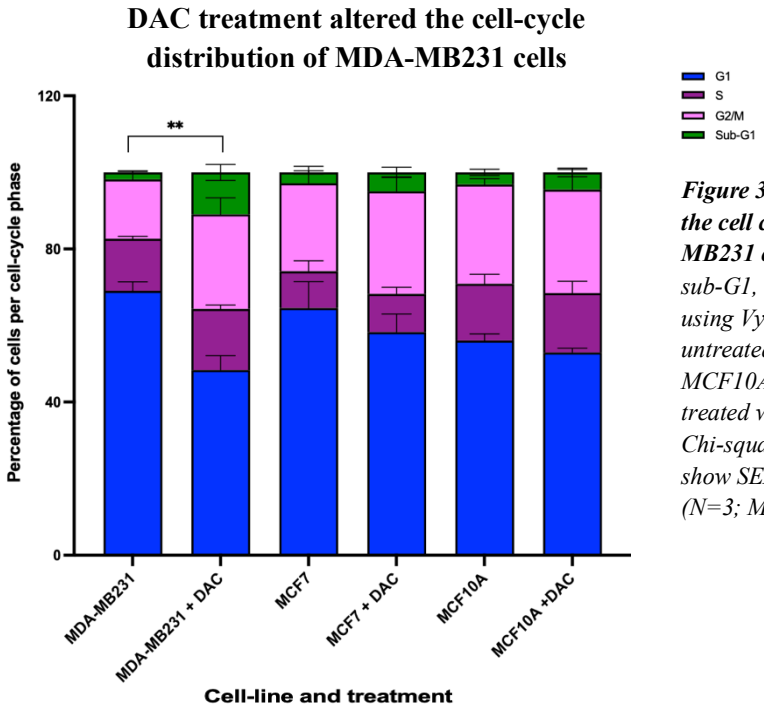


Figure 3.8: DAC treatment affected the cell cycle distribution of MDA-MB231 cells. *The percentage of cells in sub-G1, G1, S or G2/M were assessed using Vybrant Violet incorporation in untreated MDA-MB231, MCF7 and MCF10A cells compared with cells treated with 1 μM DAC for 96-hours. Chi-squared test **p<0.01. Error bars show SEM of independent experiments (N=3; MCF10A N=2).*

3.5 MCF7 and MDA-MB231 cells exhibited the same cell-cycle alterations in response to SAHA treatment

Our next consideration was whether the MCF7 and MDA-MB231 cell-cycle distributions differed in response to SAHA treatment. This aimed to investigate whether differences at the level of the cell-cycle could explain why MCF7 cells were more resistant to HDACi treatment. MCF7 and MDA-MB231 cells were treated with 2.5 μM SAHA for 48-hours, prior to Vybrant Violet staining which indicated their distribution by cell-cycle phase.

48-hour SAHA treatment affected the cell-cycle distributions of both cell-lines (Figure 3.9). A significant change was evident in the percentage of MDA-MB231 cells in all phases of the cell-cycle (p<0.05; Appendix 10.2). G1 was reduced by 35% and S by around 8%, while the number of cells in G2/M increased by around 18% (Figure 3.9C/D). S-phase was diminished but still maintained, suggesting that MDA-MB231 cells were

progressing more slowly through the cell-cycle. The greatest change was observed in the presence of a sub-G1 population, representing an increase in the number of apoptotic cells. Their chi-squared distribution significantly differed following treatment X^2 (4, N=4) =45.8, p= 6.13E^{-10} (Figure 3.10). Though showing an increase in the proportion of cells in G2/M, this assay could not indicate whether this was due to a G2 or mitotic block. It was hypothesised that this increase resulted from a G2 block, which prevented cells from re-entering the cell-cycle. This was investigated by analysing Phospho-S10 staining on Histone H3. This histone modification indicates the onset of mitosis (Crosio *et al.,* 2002). Analysis of its presence before and after SAHA treatment would show whether cells were blocked in G2 or mitosis. Loss of the mitotic cells following treatment suggested that SAHA induced a G2 cell-cycle block in MDA-MB231 cells (Figure 3.11C/D).

MCF7 and MDA-MB231 cells exhibited the same cell-cycle alterations in response to 48-hour SAHA treatment

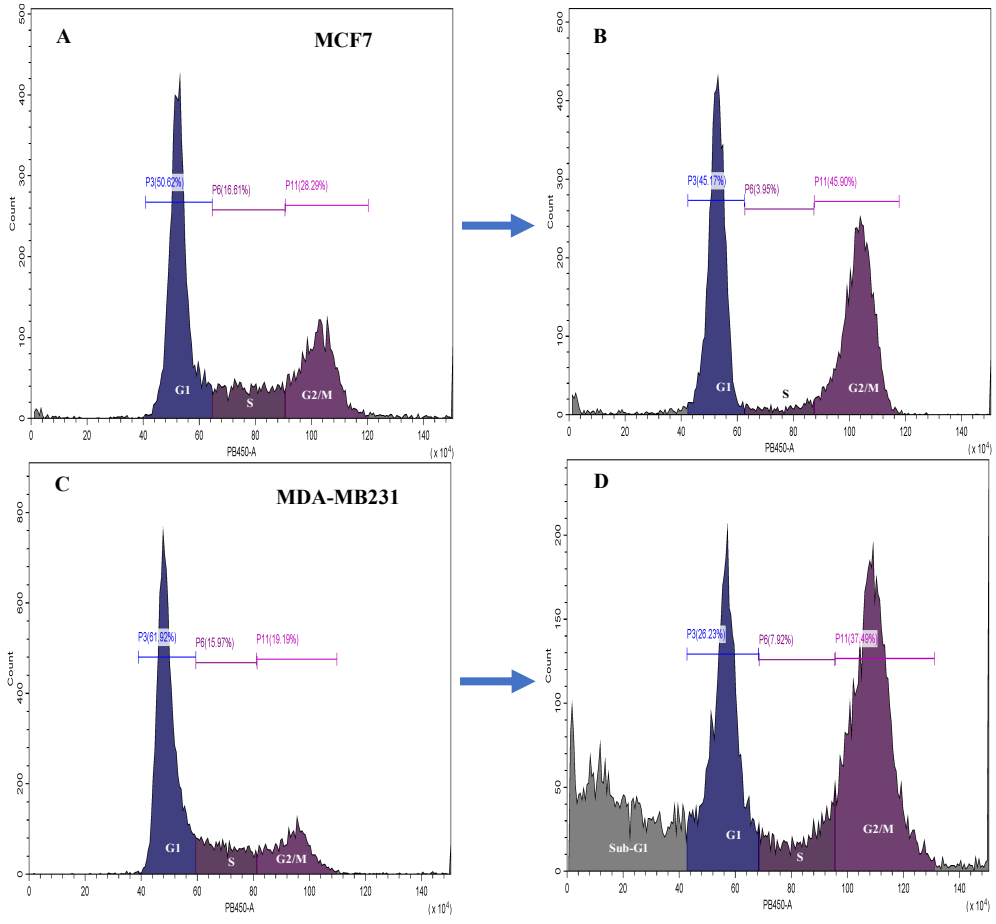


Figure 3.9: SAHA treatment induced similar cell-cycle alterations in MCF7 and MDA-MB231 cells. *The percentage of A. untreated and B. 48-hour SAHA treated MCF7, C. untreated and D. 48-hour SAHA treated MDA-MB231 cells per phase of the cell-cycle was assessed using Flow Cytometry analysis of Vybrant Violet incorporation.*

SAHA treatment significantly altered the proportion of MCF7 cells in S and G2/M (Appendix 10.2). The cells exhibited an almost complete loss of S-phase, from 16.16% down to 3.95% following SAHA treatment. This was observed alongside an increase of around 17% in the proportion of cells in G2/M (Figure 3.9A/B). There were no cells in sub-G1, correlating with the limited SAHA-induced apoptosis observed in this cell-line. The MCF7 cell-cycle significantly differed following SAHA treatment X^2 (4, N=4) =10.4, p=0.02 (Figure 3.10). The increase in the proportion of cells in G2/M was again hypothesised to be the result of a SAHA-induced G2 cell-cycle block. Phospho-S10 staining on Histone H3 showed that no mitotic cells were observed following SAHA treatment. This suggested that a G2 block was preventing cells from being able to re-enter the cell-cycle (Figure 3.11A/B). This had been observed previously in cells treated with SAHA (Blagosklonny *et al*., 2002; Noh and Lee, 2003).

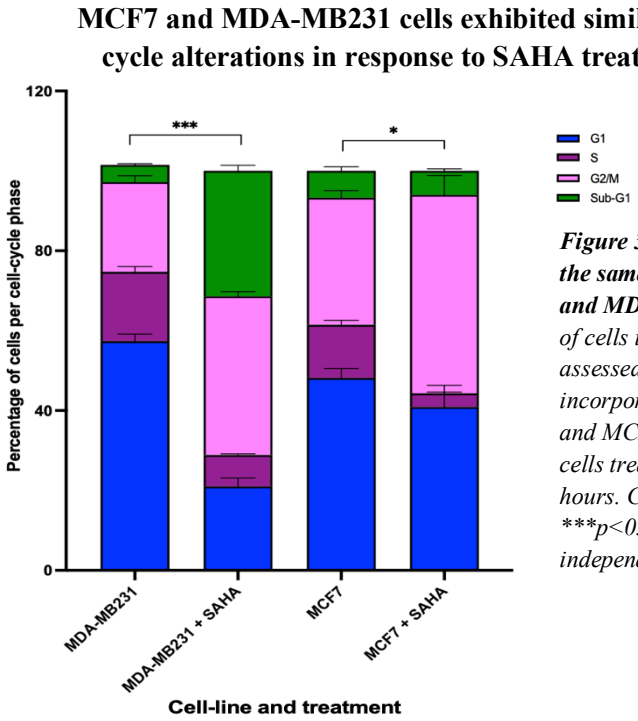


Figure 3.10: SAHA treatment induced the same cell cycle changes in MCF7 and MDA-MB231 cells. *The percentage of cells in sub-G1, G1, S or G2/M were assessed using Vybrant Violet incorporation in untreated MDA-MB231 and MCF7 and cells compared with cells treated with 2.5 μM SAHA for 48-hours. Chi-squared test *p<0.05, ***p<0.001. Error bars show SEM of independent experiments (N=4).*

To conclude, our cell-lines exhibited the same cell-cycle alterations in response to 48-hour SAHA treatment. Thus, no cell-cycle change induced in response to SAHA could explain why MCF7 cells were more resistant and MDA-MB231 cells more sensitive to HDACi.

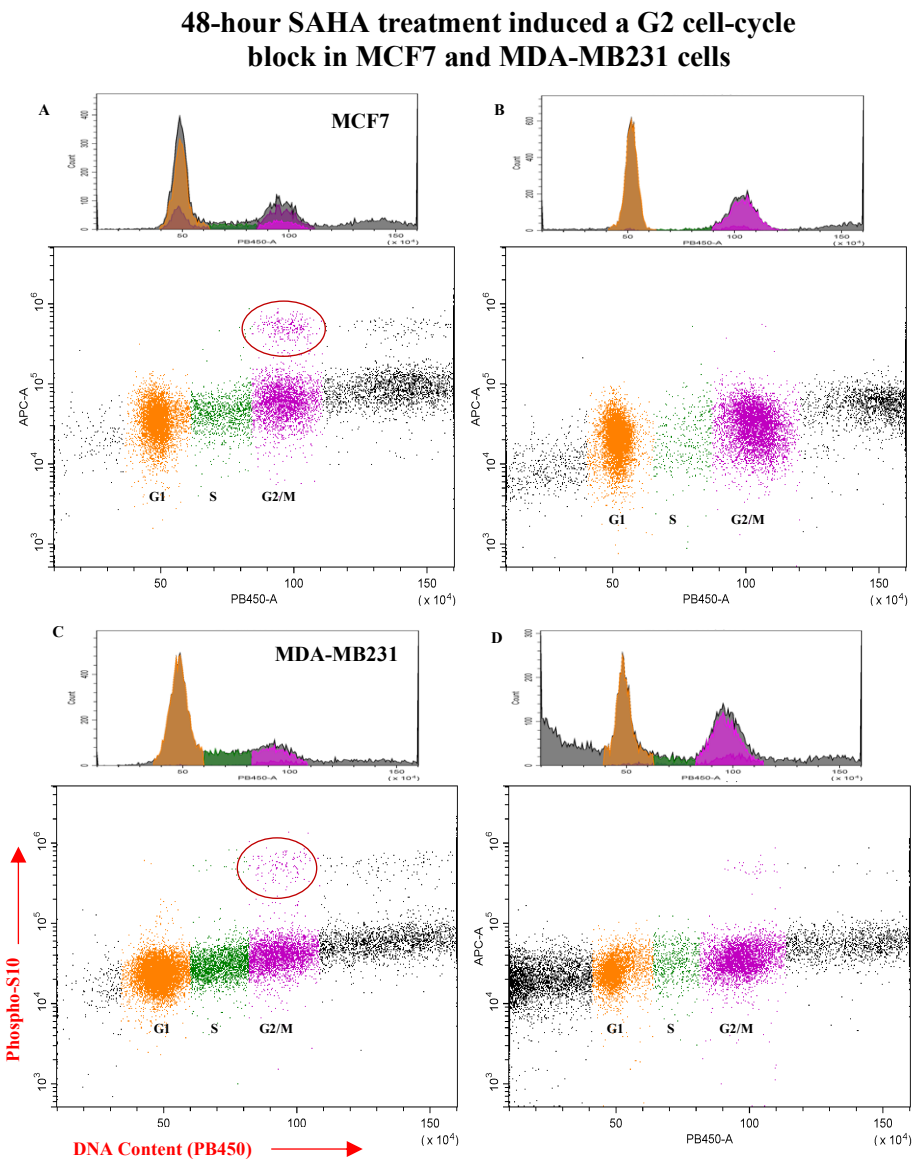


Figure 3.11: The mitotic population was lost following 48-hour SAHA treatment*. Phospho-S10 staining intensity was assessed in A. untreated MCF7, B. MCF7 cells treated with 2.5 μM SAHA for 48-hours, C. untreated MDA-MB231 and D. MDA-MB231 cells after 48-hour treatment with 2.5 μM SAHA. The red circles depict the mitotic populations observed in untreated cells. Images representative of N=3.*

3.6 Histone modifications occur within minutes of SAHA exposure in both HDACi sensitive and resistant cell-lines

The next question asked was whether resistance related to SAHA not acetylating core histones in MCF7 cells. Western Blotting was used to visualise the acetylation and methylation patterns on histone residues in MCF7 and MDA-MB231 cells treated with 2.5 μM SAHA for 30, 60 or 120-minutes. Acetylation changes were known to be rapid (Covault and Chalkley, 1980; Zentner and Henikoff, 2013). However, it was not known whether any observable histone methylation changes would occur in response to SAHA treatment with 2-hours.

An antibody against the H3 C-terminal was used as the loading control. This showed that an equal amount of histone was loaded for each sample. The H3 C-terminal is not known to be acetylated, so this also confirmed the specificity of these results (Figure 3.12G).

The acetylation profile of H3K27 was similar in both cell-lines, with hyperacetylation observed as early as 30-minutes following SAHA treatment (Figure 3.12A). Hyperacetylation was then maintained until 120-minutes. Interestingly, the level of acetylation appeared to be greater in the MCF7 cells than the MDA-MB231 cells. Though the H4K16ac bands were less clear at early treatment time-points, acetylation on H4K16 appeared greater by 120-minutes in both cell-lines (Figure 3.12B). H3K9 acetylation increased steadily with time, though there were differences evident in the extent and speed of acetylation between our cell-lines. H3K9 was acetylated to a greater extent in the MCF7 cells at all timepoints, with hyperacetylation apparent at 30-minutes (Figure 3.12C). MCF7 cells also exhibited a more rapid increase in H3K14 acetylation- with hyperacetylation evident by 60-minutes (Figure 3.12D). The increase in acetylation in MDA-MB231 cells

was much slower, with hyperacetylation not observed until 120-minutes. The H4K5 acetylation response was similar in both cell-lines (Figure 3.12D). Acetylation was enhanced at this residue in the presence of increasing SAHA treatment time, with hyperacetylation observed at 120-minutes. It was important to see that acetylation of this site occurred more slowly, as this site is known to be last acetylated on H4 (Davie, 1997).

The most notable difference between the cell-lines was observed in the trimethylation of H3K27 and H3K4 (Figure 3.12E/F). In MDA-MB231 cells the presence of H3K27me3 appeared to decrease by 120-minutes, while H3K4me3 was constant across the 120-minutes. In MCF7 cells, there was little change in H3K27me3 observed across the 120-minutes. The occurrence of H3K4me3 was initially lower in MCF7 cells. A progressive increase in methylation was then observed, with hypermethylation at this residue evident at 60-minutes. This increase in H3K4me3 following HDACi has been observed in many tumour cells; closely associated with the occurrence of H3 acetylation (Nightingale *et al.,* 2007). Bradbury *et al.,* reported in 2005 an increase in di- and trimethylated H3K4 after HDACi treatment at a similar rate to histone acetylation.

These results showed that MCF7 histones were acetylated, confirming that their resistance was not due to a lack of acetylation. Analysis of these histone modifications confirmed that acetylation occurred in both cell-lines within 120-minutes and suggested early transcriptional differences in how both cell-lines responded to SAHA. For example, the increase in H3K4me3 alongside H3K9ac suggested that a greater transcription response was induced in MCF7 cells following SAHA treatment.

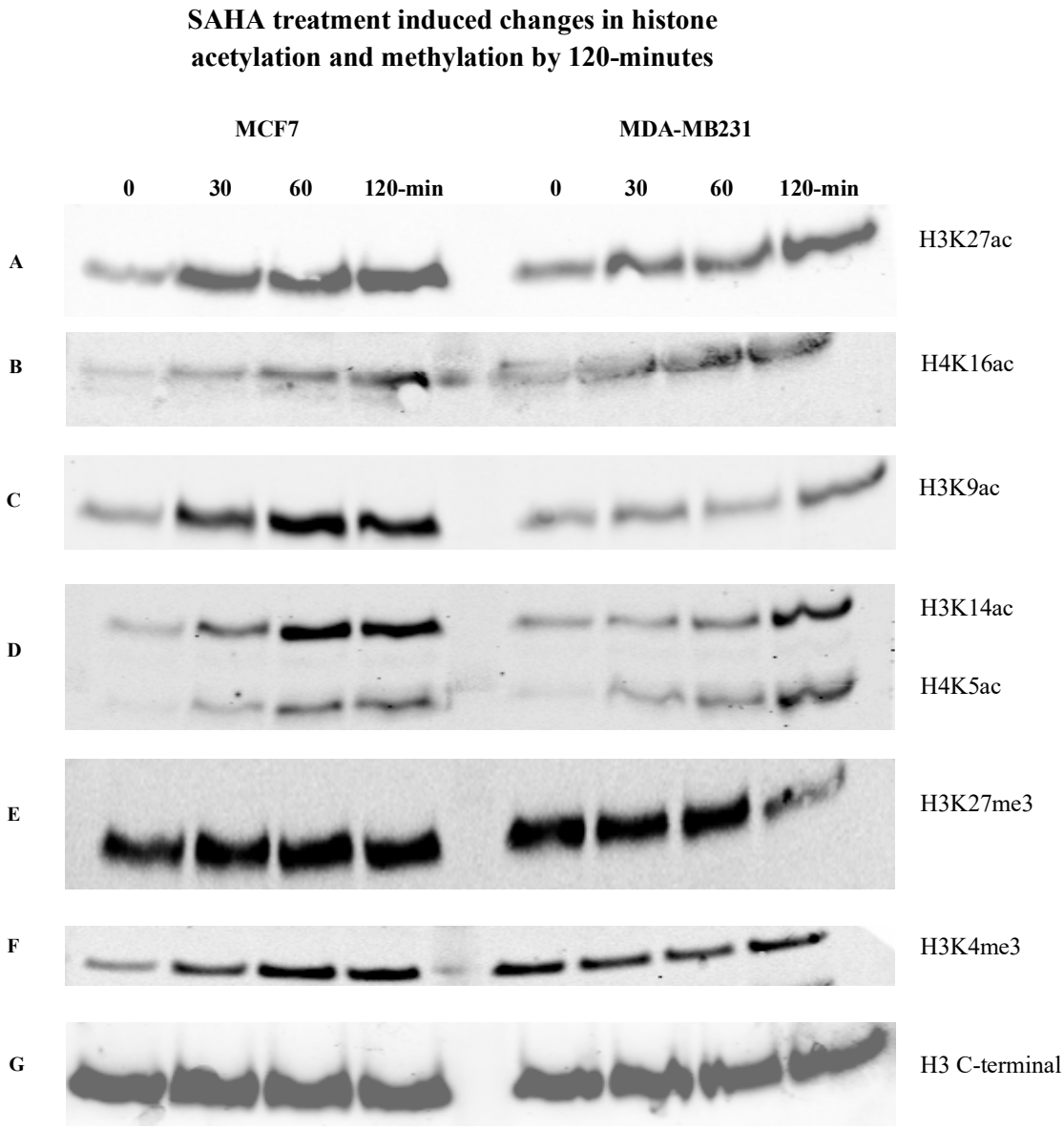


Figure 3.12: SAHA treatment induced global histone acetylation and changes in histone methylation by 120-minutes in MCF7 and MDA-MB231 cells. *Western blots showing changes in the acetylation of A. H3K27 B. H4K16 C. H3K9 D. H3K14 and H4K5 and trimethylation of E. H3K27 and F. H3K4 after treatment for 0, 30, 60 or 120-minutes with 2.5 μM SAHA. G. H3 C-terminal domain staining was used as a loading control. Images visualized using the Licor Infrared Scanner. Images representative of N=2.*

3.7 Histone hyperacetylation occurred dynamically across the cell-cycle

The acetylation of H4K16 and H3K27 was also analysed by Flow Cytometry. Western Blotting had been used to examine population wide effects, while Flow Cytometry would

enable the variation within the cell population to be observed. This experiment would also determine whether acetylation was affected by cell-cycle phase. The acetylation induced in response to the 2-hour SAHA treatment time-course was assessed, alongside IgG and H3 C-terminal antibody controls.

IgG was used to set the voltage. The position of the cell-cycle boxes and location of hyperacetylated cells was set using the baseline IgG signal (Appendix 10.4). Any increase above this central line, and a shift of signal from the bottom to the top box suggested an enrichment of this histone modification. In addition, it was important to see that no increase in signal was observed with the IgG control across the 2-hour time-course. An H3 C-terminal antibody control was also used to determine how readily the chromatin bound antibody (Appendix 10.4). This binding did not increase with SAHA treatment time, confirming that the signal increase did not relate to more open chromatin and that changes were specific to the chosen histone modifications.

Initial experiment analysed the acetylation of H4K16 and H3K27, at 0-hours and then again after 2-hour SAHA treatment. Acetylation changes were similar in MCF7 and MDA-MB231 cells; with hyperacetylation observed by 2-hours in both (Appendix 10.3). However, we were interested in determining how acetylation changed within the 2-hour SAHA treatment time course - not only at 2-hours. We looked at how quickly these changes occurred following SAHA treatment; considering cells treated with SAHA for 30, 60 and 120-minutes. In both MCF7 and MDA-MB231 cells, H3K27 was rapidly acetylated as SAHA treatment time increased – with hyperacetylation observed after only 30-minutes (Figure 3.13). These experiments showed that rapid hyperacetylation of H3K27 occurred in both cell-lines.

As they use different methods, Western Blotting and Flow Cytometry results inherently differ. What was important was that histone acetylation was observed in both cell-lines within the 2-hour SAHA treatment timeframe. Interestingly, these changes appeared to occur more quickly in MCF7 cells, a theme that will continue through this project in relation to their HDACi response.

The distribution of H3K27 acetylation per phase of the cell-cycle was then considered to assess whether this modification was evident across the cell-cycle. Figure 3.14 shows the percentage of the total number of MCF7 and MDA-MB231 cells present in G1, S or G2/M exhibiting hyperacetylation. This clearly shows that H3K27 acetylation occurred across the entire cell-cycle. A two-way ANOVA was performed to analyse the effect of cell-cycle phase and timepoint on H3K27 hyperacetylation. This revealed no significant interaction between cell-cycle phase and timepoint ($F(6, 18) = 1.967$, $p=0.12$). Simple main effects analysis showed timepoint and cell-cycle phase had a statistically significant effect on H3K27 hyperacetylation ($p=0.0004$, $p=0.03$). The cell cycle significance exists in both untreated and treated cells – with an increase in signal evident comparing G1, S and G2/M. This suggests that the increase in acetylation relates to DNA replication, resulting in an increased signal as cells progress through the cell-cycle. The small size of the error bars with MDA-MB231 cells, show that their acetylation response was more consistent. Across all three phases, the percentage of hyperacetylated cells increased between 0- and 30-minutes. There was then little increase evident up till 120-minutes. A similar percentage of cells in G1, S and G2/M display H3K27 hyperacetylation (Figure 3.14).

SAHA treatment induced H3K27 hyperacetylation in MCF7 and MDA-MB231 cells

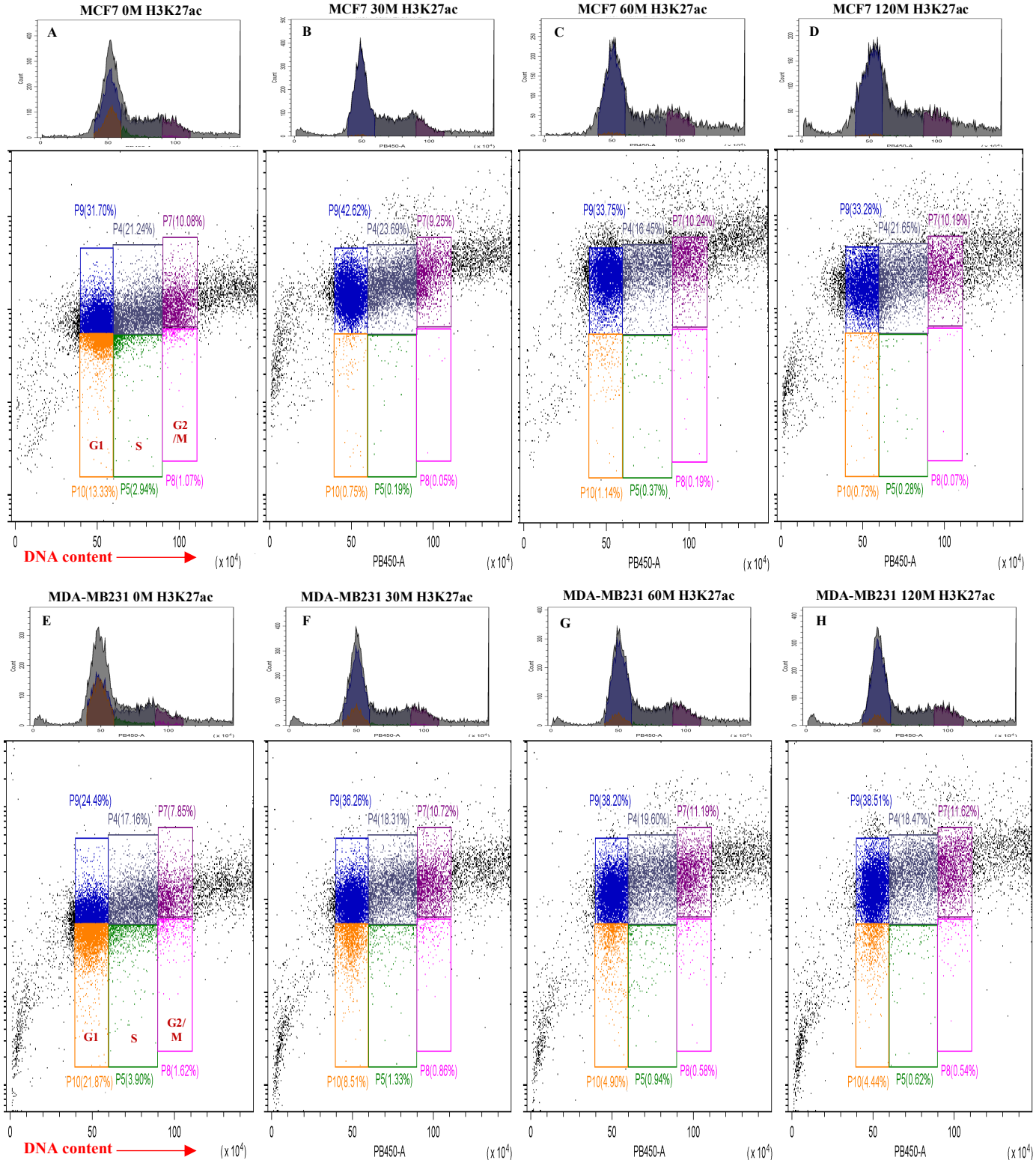


Figure 3.13: H3K27 hyperacetylation was observed in both cell-lines following 2-hour SAHA treatment. *Flow Cytometry analysis of H3K27 acetylation in A. untreated and MCF7 cells treated with 2.5μM SAHA for B. 30-minutes, C. 60-minutes and D. 120-minutes and E. untreated and MDA-MB231 cells treated with 2.5 μM SAHA for F. 30-minutes, G. 60-minutes and H. 120-minutes. IgG signal was used to set the location of the cell-cycle boxes with cells above the central line displaying hyperacetylation.*

The magnitude of the acetylation response in MCF7 cells was less consistent across replicates, evident in the size of the error bars in the earlier SAHA treatment timepoints. A two-way ANOVA revealed no significant interaction between cell-cycle phase and timepoint ($F(6, 18) = 0.08$, $p=0.98$). Simple main effects analysis showed that timepoint had a statistically significant effect on H3K27 hyperacetylation ($p=0.03$). Again, the percentage of hyperacetylated cells increased from 0 to 30-minutes. This percentage remained similar through to 60-minutes, before exhibiting a final increase at 120-minutes – matching that observed in MDA-MB231 cells. A similar percentage of cells across all cell-cycle phases exhibited H3K27 hyperacetylation.

This analysis concluded that hyperacetylation on H3K27 occurred throughout the cell-cycle. It also showed a slower initiation of acetylation in G1 in both cell-lines, with a low percentage of hyperacetylated cells observed at 0-minutes. This suggested that an early cohort of cells were under acetylated but recover in G1 prior to entering the cell-cycle. The 0-minute signal in G2/M was around twice the size of the signal observed in G1. This most likely reflects the doubling in chromatin between G1 and S-phase. What was interesting was the remarkable consistency across the time course and between the timepoint replicates.

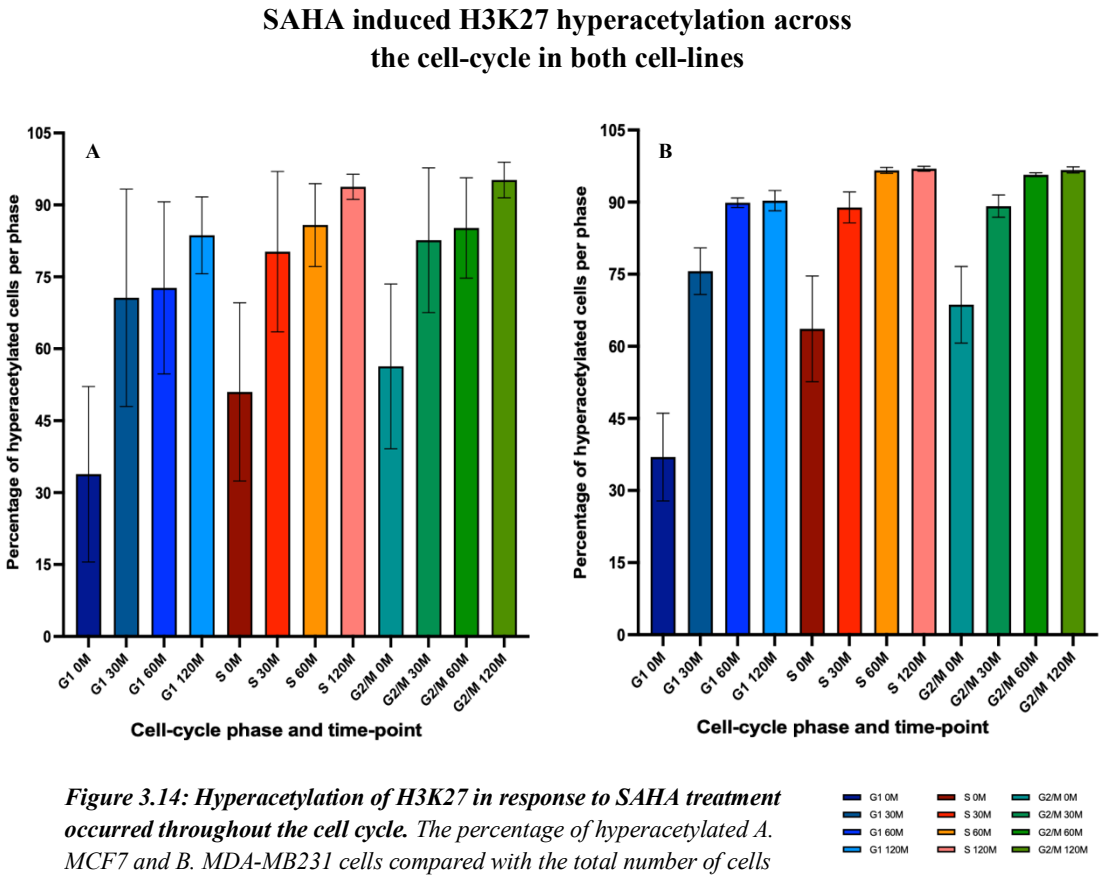


Figure 3.14: Hyperacetylation of H3K27 in response to SAHA treatment occurred throughout the cell cycle. *The percentage of hyperacetylated A. MCF7 and B. MDA-MB231 cells compared with the total number of cells identified in G1, S or G2/M phase of the cell-cycle from Flow Cytometry analysis. Two-way ANOVA showed timepoint and cell-cycle phase significantly affected hyperacetylation in MDA-MB231 cells and timepoint significantly affected hyperacetylation in MCF7 cells. Error bars show SEM of independent experiments (N=3).*

3.8 The SAHA-induced transcriptional response was not observed against the background of overall RNA change

A final consideration was whether the specific transcriptional response occurring in response to SAHA could be visualized on a global scale. It was hypothesised that a larger transcriptional response was induced in MCF7 cells in response to 2-hour SAHA treatment. Global changes in transcription following 30, 60 or 120-minute SAHA treatment were assessed through incorporation of an RNA label. This investigated the global response induced in both cell-lines and assessed the early acetylation driven

increase in transcription at 30 and 60-minutes, which will be discussed with the RNA-Sequencing analysis. As the Abcam RNA Synthesis Assay cannot quantify transcriptional change, it was likely that little difference would be evident between our cell-lines even though greater changes in gene expression were believed to occur in MCF7 cells.

Following optimisation of the assay for use in adherent cell-lines, cells were incubated with the RNA label for 30-minutes. This meant that the transcription induced in both cell-lines following treatment with the established SAHA time-course (30, 60 or 120-minutes) could be assessed. Cells in positive control wells were incubated with the RNA label only, and those in negative control wells were incubated without SAHA or the RNA label. As shown in Figure 3.15, a clear separation was observed between the positive and negative control peaks. However, in both cell-lines all SAHA treatment timepoints overlapped with the positive control - indicating that SAHA did not affect the total RNA content of the cell. We were looking for changes in the mRNA population, occurring alongside changes in rRNA and transfer RNA (tRNA) – which are much more abundant in cells. It was concluded that the specific transcriptional response hypothesised to occur in MCF7 cells, was not obvious against a background of overall change in rRNA transcription occurring.

This hypothesis could be followed up by gel analysis. The specific SAHA-induced increase in mRNA population would be more easily observed with each individual RNA population (tRNA, rRNA and mRNA) separated out by weight. Though not qualitative, this analysis would show if there was a difference in the size of the mRNA population of both cell-lines following SAHA treatment.

The SAHA-induced transcriptional response was not observed against the overall RNA content of the cells

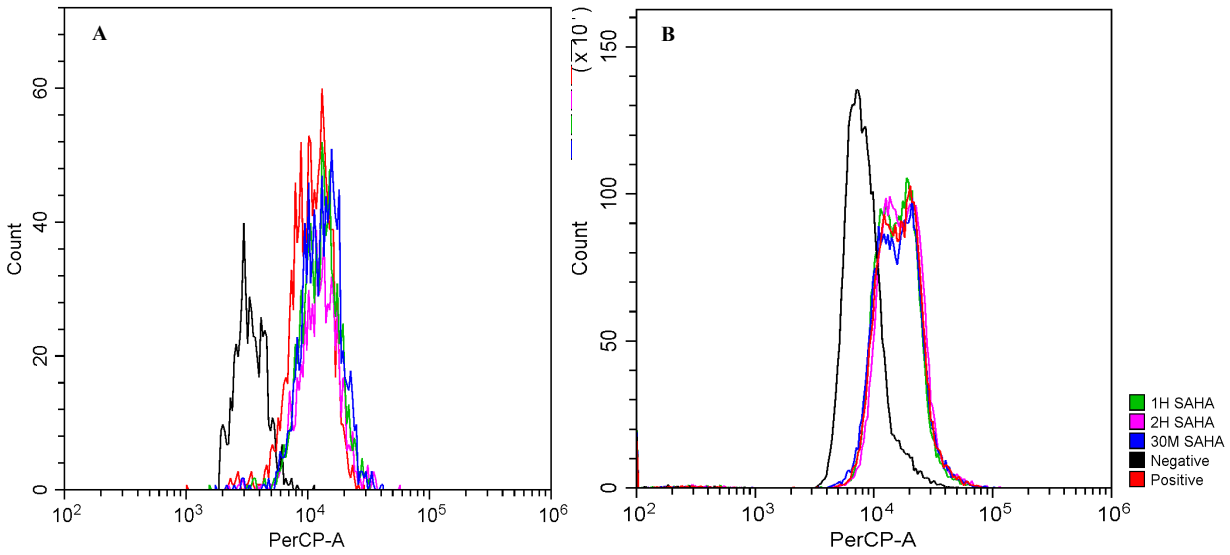


Figure 3.15: The transcriptional response induced in cells in response to SAHA treatment was not observed against the overall RNA content of the cell. *Flow Cytometry analysis of the signal obtained following RNA label incorporation in A. MCF7 and B. MDA-MB231 cells treated with 2.5 μM SAHA for 0, 30, 60 or 120-minutes alongside the positive (RNA label only) and negative (no RNA label or SAHA treatment) control.*

3.9 Chapter conclusions

This chapter described the development of a solid tumour model of HDACi resistance. Cell-lines were treated with an HDACi (SAHA) and DNMTi (DAC), and their sensitivity determined using the Annexin V and MTS Assay. This enabled the selection of a breast line model - consisting of the more HDACi sensitive MDA-MB231, more HDACi resistant MCF7, alongside the immortalised but non-transformed MCF10A cells.

Their response to SAHA treatment was then compared. This involved an analysis of the cell-cycle alterations induced in response to SAHA and DAC. The same alterations were observed in both cell-lines in response to SAHA, confirming that MCF7 resistance could not be explained by a difference at the level of the cell-cycle. This was followed by Western Blot analysis of the methylation and acetylation of histone residues as well as

Flow Cytometry analysis of H3K27ac. These confirmed that acetylation occurred in both cell-lines within 2-hour SAHA treatment. The RNA synthesis induced in response to HDACi treatment was then assessed in both cell-lines, though no difference was observed against the background of overall rRNA change.

By identifying the general properties observed in our cells when they were treated with SAHA, this chapter verified our chosen HDACi resistance model. Nothing in this initial comparison of how they responded to SAHA could pin down a key difference between our cell-lines. As they respond in the same way, there is no strong evidence that the induced acetylation explains this difference in their sensitivity.

4. WHOLE GENOME TRANSCRIPTOMIC AND EPIGENOMIC ANALYSIS OF MCF7 AND MDA-MB231 CELL-LINES FOLLOWING SAHA TREATMENT

This chapter focussed on analysing the results of an RNA-Sequencing experiment carried out to compare the response of our HDACi sensitive (MDA-MB231) and more HDACi resistant (MCF7) cell-lines to treatment with SAHA for 30, 60 or 120-minutes. This experiment assessed two replicates at each timepoint. The number of genes exhibiting differential expression following SAHA treatment was assessed, indicating the size of transcriptional response induced in both cell-lines. SAHA-induced gene expression patterns identified from the RNA-Sequencing were then investigated, looking closely at how *HAT, HDAC, TF* and *HSP* genes' expression was affected. Finally, motif analysis was used to investigate the TFs driving early gene expression change in MCF7 cells – which could point towards potential drivers mediating their resistance to HDACi treatment.

4.1 A larger transcriptional response was induced in MCF7 cells following 2-hour SAHA treatment

In collaboration with Zymo Research, an RNA-sequencing experiment was carried out, analysing two replicates of a short SAHA treatment time-course (30, 60 and 120-minutes) in MCF7 and MDA-MB231 cells. The aim of this experiment was to assess the early gene expression changes induced following SAHA treatment in the HDACi sensitive and more HDACi resistant cell-line. In addition, identifying the TFs driving these early gene expression changes could potentially point to drivers of the HDACi survival response.

A Sample Similarity Matrix and Multidimensional Scaling (MDS) Plot were produced by Zymo. These were used initially to compare the treatment timepoints and replicates. All analysed genes are incorporated in the Sample Similarity Matrix. This matrix depicts the Pearson correlation coefficient between samples and with most not expected to significantly differ between treatments; sample coefficients are usually close to 1 (Boslaugh and Waters, 2008). Thus, any deviation from 1 indicates differences in their gene expression patterns following SAHA treatment. The MDS Plot is a form of non-linear dimensionality reduction. Each dot represents a sample, with the distance between them indicating differences in their gene expression (Mead, 1992).

Figure 4.1A shows that the effects induced in the resistant line were relatively mild, though clear differences were evident between treated and untreated samples. This was visualised in the hierarchical clustering, which distinguished replicates by timepoint. It was important to see that all MCF7 timepoint replicates paired first. The earlier time-points grouped together and were kept distinct from those at 120-minutes. Interestingly, the 30 and 60-minute samples clustered closest together with the next closest being 0-minutes. This suggested a two-stage response, with an early change occurring at 30-minutes, followed by a second response at 120-minutes. The MDS Plot showed that the 0-minute replicates were distinct, with the subtle overlap of the other time points suggesting that SAHA had a progressive effect on transcription with time (Figure 4.1A). This plot also highlighted that there was a significant difference in the gene expression patterns comparing 0 with 120-minutes. Taken together, they indicated that SAHA induced a rapid and progressive change in gene expression in MCF7 cells within 120-minutes.

The Sample Similarity Matrix in Figure 4.1B showed a less clear distinction between the MDA-MB231 time-point replicates. The intermixing of samples within the hierarchical clustering, suggested a high degree of similarity in their gene expression. In addition, all the timepoint replicates overlapped in the MDS Plot with no separation evident between the untreated and treated samples. This suggested that either the replicates did not correlate or that little transcriptional change occurred in these cells by 120-minutes. To further investigate this, scatterplots comparing the individual timepoints were analysed. These confirmed correlation between the replicates (Appendix 10.5) leading to the conclusion that SAHA induced little transcriptional change in MDA-MB231 cells by 120-minutes.

SAHA induced a greater transcriptional response in MCF7 cells by 120-minutes

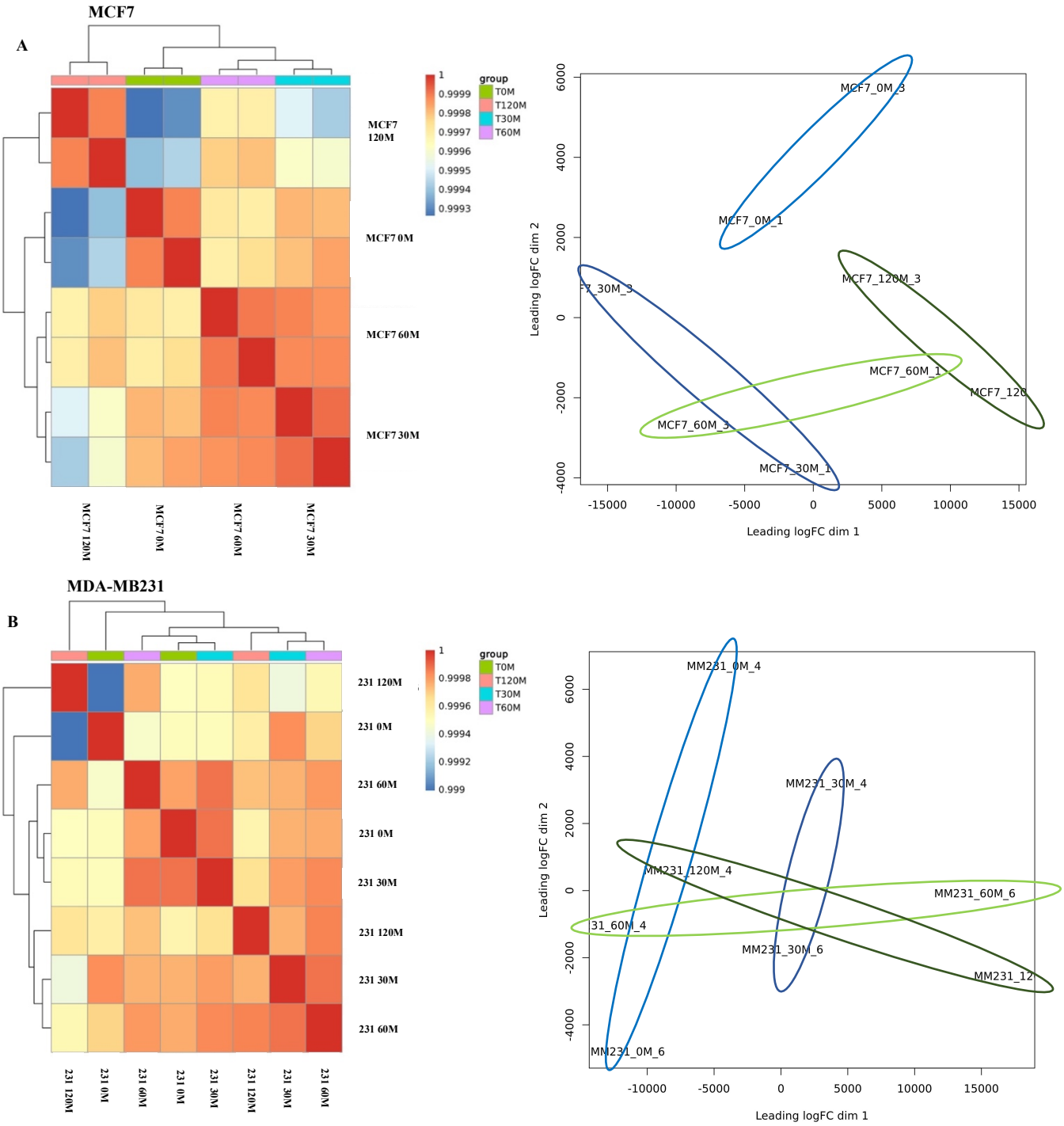


Figure 4.1: SAHA induced greater transcriptional change in the resistant MCF7 cell-line compared with the sensitive MDA-MB231 cell-line, within 120-minutes. *Sample Similarity Matrix and MDS Plot generated for A. MCF7 and B. MDA-MB231 RNA-Sequencing sample replicates following treatment with 2.5 μM SAHA for 0, 30, 60 or 120-minutes. Plots generated by Zymo Research.*

To conclude, the sample level comparisons indicated that a greater transcriptional response was induced in the more resistant MCF7 cells following 120-minute SAHA treatment. The hierarchical clustering and degree of overlap in the MDS Plot indicated that little difference was evident between the MDA-MB231 timepoint replicates. In contrast, the MCF7 cells displayed a clear separation by timepoint and progressive change in gene expression pattern with increasing treatment time. SAHA induced a stronger effect in the MCF7 cells, making these results clearer and easier to observe. However, as fewer changes were observed in the MDA-MB231 cells – the scale was more difficult to understand. Interestingly, these cell-lines respond to SAHA treatment in a different manner than we would have expected given their subtype and characteristics. MDA-MB231 cells, which react more slowly, represent a more invasive and aggressive triple negative tumour cell-line. In comparison, the more responsive MCF7 cells represent the less aggressive luminal A subtype. The difference in their response does not relate to their speed of growth, lending confidence to the use of this model in understanding the molecular resistance to HDAC inhibition.

To further explore the difference between our cell-lines, the magnitude of gene expression change was considered. Heatmaps were plotted at Zymo using the Log2 value of the fold change in expression of the top 100 genes with the highest variance against their mean expression levels among all samples. Positive (red) indicated high expression levels, while negative (blue) indicated low expression levels. Genes were clustered by timepoint similarity using hierarchical clustering. These heatmaps give an overview of the expression patterns among genes with the most significant changes in their expression across the 120-minute SAHA treatment time-course (Figure 4.2).

Hierarchical clustering grouped MCF7 samples by timepoint (Figure 4.2A). 30 and 60-minutes were clustered closest, then joined by 120-minutes with the 0-minute time-point kept distinct. This suggested treatment related expression changes, with an opposing expression pattern observed comparing 0 and 120-minutes. This clustering also highlighted the occurrence of a two-stage response, as was suggested in the Sample Similarity Matrix (Figure 4.1A). The expression changes established at 30-minutes were maintained through to 60-minutes, with a distinct change evident at 120-minutes. On the other hand, limited similarity was observed between the MDA-MB231 replicates (Figure 4.2B). Less transcriptional change was evident following SAHA treatment, with any changes occurring much more slowly. For example, more genes were represented in blue rather than yellow or orange at 30-minutes. In addition, the scales used for the heatmaps highlight the smaller changes occurring in MDA-MB231 cells within 2-hours; -1.5 compared with -0.5. It was important that the hierarchical clustering mostly grouped the replicates by timepoint, other than one 0-minute replicate which was closer in expression to 30-minutes. This highlighted that the timepoint replicates correlated, and that their gene expression patterns appeared similar because little change had been induced during this time. 0 and 30-minutes replicates were clustered together and kept distinct from those at 60 and 120-minutes. This indicated a slower response to HDAC inhibition in MDA-MB231 cells, associated with fewer overall treatment related changes in gene expression.

These plots can be broken down into sections based on gene response. Cluster 1 includes genes progressively downregulated with time. HAT complex genes were observed within this cluster in both cell-lines. Enhancer of Polycomb Homolog 1 and 2 (*EPC1* and *EPC2)* genes were evident in both cell-lines, with *KAT6B* and JADE Family PHD Finger 2 and

(*JADE2)* also observed in MCF7 cells (Figure 4.2). This confirms the association between SAHA treatment and the downregulation of acetyltransferase related genes in our solid tumour cell-lines. These HAT related genes were all downregulated by 120-minutes – with this downregulation occurring after an initial 30-minute delay. Cluster 2 shows genes progressively upregulated in MCF7 cells. These genes, including *TUFT1* and *CPEB4* exhibited higher expression by 120-minutes. In MDA-MB231 cells changes occurred much more slowly in this cluster, with upregulation not observed until 60-minutes. However, it was interesting that common genes, such as *DLL4* and *TENT5C*, were identified in this cluster in both cell-lines. Cluster 3 identified genes in MCF7 cells that exhibit a peak in their expression at 30-minutes, followed by downregulation. This cluster consists mostly of TF genes, including those from the Early Growth Response Protein (EGR) and Nuclear Receptor Subfamily Group 4 Group A (NR4A) families – such as *EGR1* and *NR4A1* (Figure 4.2). Similar TF family genes were evident in this cluster in MDA-MB231 cells, though they exhibited a different pattern of expression. Their expression increased initially, but then remained consistent through to 120-minutes. The genes grouped in the two Cluster 4 sections in MDA-MB231 cells exhibit inconsistent patterns of expression across the replicates and timepoints. This expression pattern was believed to correlate with the idea that the transcriptional response occurring in this cell-line was less regulated.

The heatmaps shown in Figure 4.2 suggested that the MDA-MB231 cells mount a smaller transcriptional response following SAHA treatment. There is, however, no obvious disruption to their transcription or evidence of a loss in transcriptional control in these cells. This analysis suggests that being slower to induce these gene expression changes leaves MDA-MB231 cells sensitive to HDACi treatment. This correlates with the

hypothesis that it is the early transcriptional change of a small, specific number of genes that enabled MCF7 cells to survive in the presence of an HDACi. Interestingly, cluster 3 highlights the rapid upregulation of *TF* genes in MCF7 cells. Are these the early responding genes helping cells cope with the stress induced following HDACi treatment?

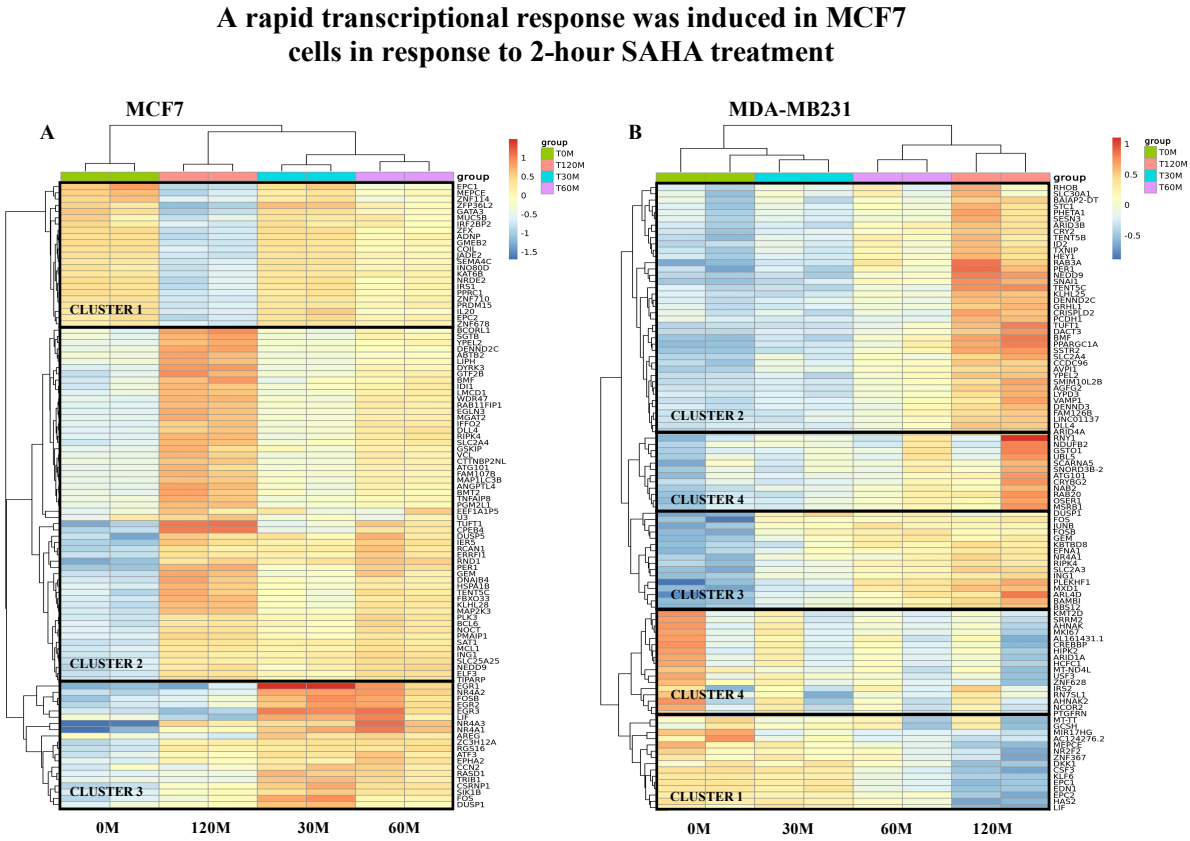


Figure 4.2: SAHA treatment induced greater transcriptional change in MCF7 cells. *The Log2value of the fold change in expression of the top 100 genes with the highest variance against their mean expression levels among all samples were plotted across the SAHA treatment time-course in A. MCF7 and B.MDA-MB231 cells. Indicated within the boxes are genes clustered based on their response to SAHA treatment (Cluster 1-4). Heatmaps created at Zymo Research.*

The suggestion that a larger transcriptional response was induced in MCF7 cells led to an analysis of the number of significantly differentially expressed genes (DEG) identified at each timepoint. The number of DEGs identified between timepoints in each cell-line were identified using DESeq2, with $p<0.05$ set as the cut-off. A greater number of genes showed a significant difference in their expression following SAHA treatment in MCF7 cells

(Figure 4.3). Interestingly, very few genes in MDA-MB231 cells exhibited significant changes in their expression in response to SAHA treatment. At 120-minutes, 759 genes in MDA-MB231 cells and 4675 genes in MCF7 cells were significantly differentially expressed. The greatest gene expression differences were observed comparing 0 with 120-minutes. However, even this comparison displayed only 534 DEGs – which was around four times fewer than the 2674 observed during the same comparison in MCF7 cells. This, along with the initial sample comparisons, indicated that SAHA had little effect on the gene expression patterns of MDA-MB231 cells within 120-minutes.

Differential gene expression analysis also suggested an early bias towards gene upregulation at 30 and 60-minutes. 912 genes were significantly up-regulated in MCF7 cells while only 325 genes were significantly down-regulated after 60-minute SAHA treatment (Figure 4.3). This pattern was also observed in MDA-MB231 cells at both timepoints, though more obvious at 60-minutes with the presence of a greater number of DEGs. This early upregulation was thought to relate to an acetylation driven increase in transcription, which had not been observed in previous Microarray analysis (Halsall *et al*., 2015). However, this finding agrees with work by Peart *et al*. in 2005 in which they showed most early responding genes (between 1-4 hours) were transcriptionally activated following SAHA or Depsipeptide treatment. At 2-hours, the gene expression pattern in MCF7 cells matched that observed by Halsall *et al*. in 2012 – with a similar number of genes up and downregulated after 120-minute HDACi treatment (Figure 4.3). At this timepoint, 2674 genes were upregulated and 2001 were downregulated. This pattern, however, was less clearly observed in MDA-MB231 cells. A greater number of genes were up-regulated at 120-minutes; 534 were upregulated compared with only 225 downregulated.

This analysis concluded that a larger transcriptional response was mounted by MCF7 cells in response to 120-minute SAHA treatment. Gene expression progressively changed with time in MCF7 cells, while far fewer genes exhibited differential expression in response to SAHA treatment in MDA-MB231 cells. This correlated with the hypothesis that these gene expression changes are what drives the ability of cells to survive an HDACi. MDA-MB231 cells are not able to mount such a response, leaving them more sensitive to HDAC inhibition.

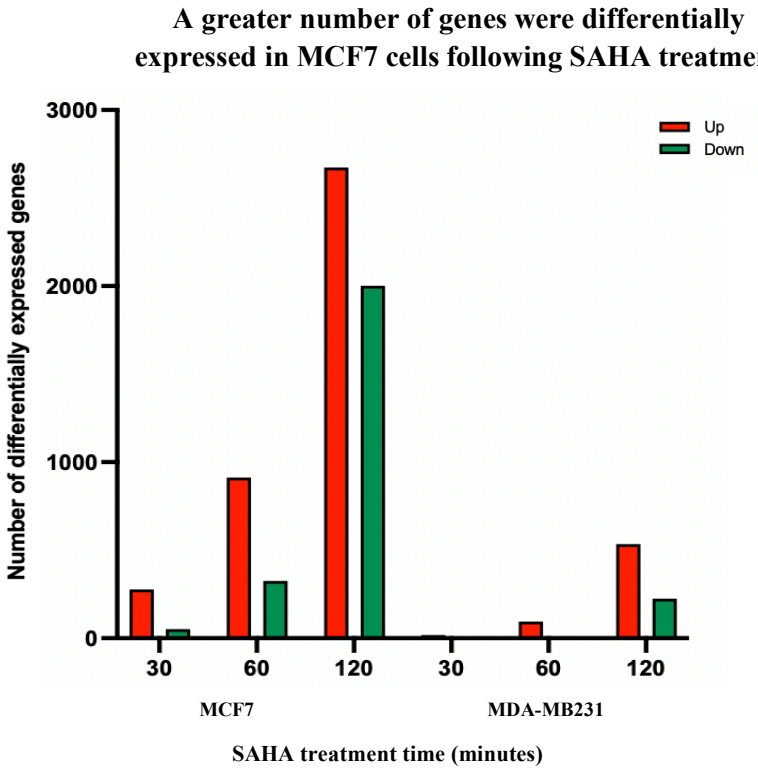


Figure 4.3: A greater number of genes in MCF7 cells were differentially expressed following SAHA treatment. *The number of genes exhibiting significantly increased (red) or decreased (green) expression following 30, 60 or 120-minute SAHA treatment compared with expression at 0-minutes identified from DESeq2 (with significance set as $p<0.05$) in MCF7 and MDA-MB231 cells.*

4.2 Ontology suggested a common response, occurring earlier in MCF7 cells

Our next step involved analysis of the differential expression of genes among timepoints using the likelihood ratio test (LRT) (Fang *et al.,* 2012). An alternative to pair-wise comparison, operating like an ANOVA, this test analyses all levels of a factor at once (hbctraining, 2023). LRT identifies genes that exhibit the greatest change in expression

across the different timepoints, without focussing on when these changes occur. The genes identified by LRT in both cell-lines were analysed using Venny 2.0, with Figure 4.4 showing the genes common to both. As expected, many more genes were significantly differentially expressed in MCF7 cells. This was observed with the size of transcriptional change; 2177 genes versus only 209 in the MDA-MB231 cells. However, 155 genes were common to both. Ontology identified terms relating to transcription, DNA binding and regulation of biosynthetic processes among these shared genes. To conclude, LRT analysis indicated that a common set of genes were induced in both of our cell-lines in response to SAHA treatment. However, this analysis further highlighted the sheer difference in the size of transcriptional response induced between the two cell-lines.

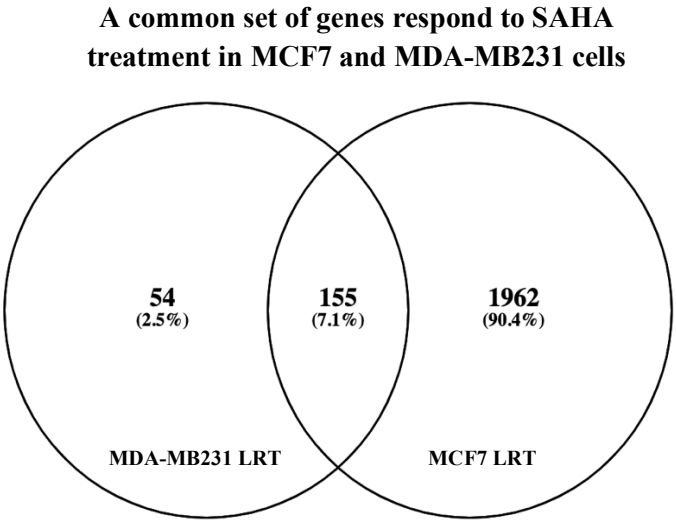


Figure 4.4: A common set of SAHA-responsive genes were identified in MCF7 and MDA-MB231 cells. *LRT analysis identified genes displaying the greatest change in their expression across the 2-hour SAHA treatment time-course in each cell-line. Venny 2.0 was then used to compare these two lists, producing a Venn Diagram showing the 155 genes commonly differentially regulated in both cell-lines.*

Interest then turned to looking at the processes enriched in each cell-line following SAHA treatment. g:Profiler was used at Zymo Research. This programme derives its data from Ensembl and identifies biological categories enriched in gene lists (Raudvere *et al.,* 2019). Our analysis used DAVID to analyse the ontology of genes more highly expressed at each treatment time-point (Huang *et al.,* 2009a; Huang *et al.,* 2009b). Analysis of terms

upregulated after 30, 60 or 120-minute treatment was used to visualise the early response of MCF7 and MDA-MB231 cells to HDACi treatment and identify any differences.

In MCF7 cells, terms relating to the nucleus and transcription were elevated at 30-minutes. By 60-minutes, protein binding and the nucleoplasm were suggested alongside an elevation of terms relating to transcription from RNA Polymerase II. At 120-minutes terms relating to cell-cell adhesion, cytoplasm and the membrane were elevated alongside protein binding (Figure 4.5). g:Profiler highlighted that deacetylation by HDAC enzymes was downregulated after 30 and 60-minute SAHA treatment, as was acetylation by HAT enzymes. Transcription related terms were downregulated at 120-minutes alongside an upregulation of cellular protein localization and intracellular protein transport processes. These final terms suggested the initiation of cellular processes in this cell-line as it continues to survive in the presence of SAHA. This correlated to what was reported by Andrews *et al*. in 2019, with the expression of high levels of chemotaxis and migration related ontology terms.

Fewer terms were significantly enriched in the MDA-MB231 cells following 2-hour SAHA treatment (Figure 4.5). Terms relating to transcriptional activator activity, response to cAMP and DNA binding were upregulated at 30-minutes. Terms relating to the nucleus, circadian rhythms and the positive regulation of transcription emerged at 60-minutes. The nucleus, and regulation of transcription were still observed at 120-minutes. g:Profiler highlighted transcription regulation at all SAHA treatment timepoints in this cell-line.

Analysis of the gene terms enriched indicated that similar responses were being induced in both cell-lines. For example, terms relating to transcription were observed at 30-minutes

and terms relating to protein binding at 60-minutes. This correlated with this idea of our cell-lines exhibiting a common set of HDACi responsive genes, as had been suggested in the LRT analysis.

What was interesting was that only nuclear processes were enriched at 30-minutes; with terms relating to transcription evident in both cell-lines. This response then appeared to broaden in our resistant cells by 120-minutes, with terms moving beyond the nucleus and relating instead to the cytoplasm and the membrane. However, terms at this timepoint in our sensitive cell-line still related to nuclear processes. Additionally, far fewer terms reached significance at these early treatment timepoints in our sensitive cell-line, with a low gene count associated even with those deemed significant. For example, at 30-minutes – no term was associated with greater than 8 genes in this cell-lines (Figure 4.5). Additionally, the scale of their $-\log_{10}$*p-value* was vastly different – with the scale spanning to 55 in our more resistant cell-lines, but only 8 in the more sensitive cells. This indicated that a common response was being observed albeit more slowly in our more HDACi sensitive cell-line.

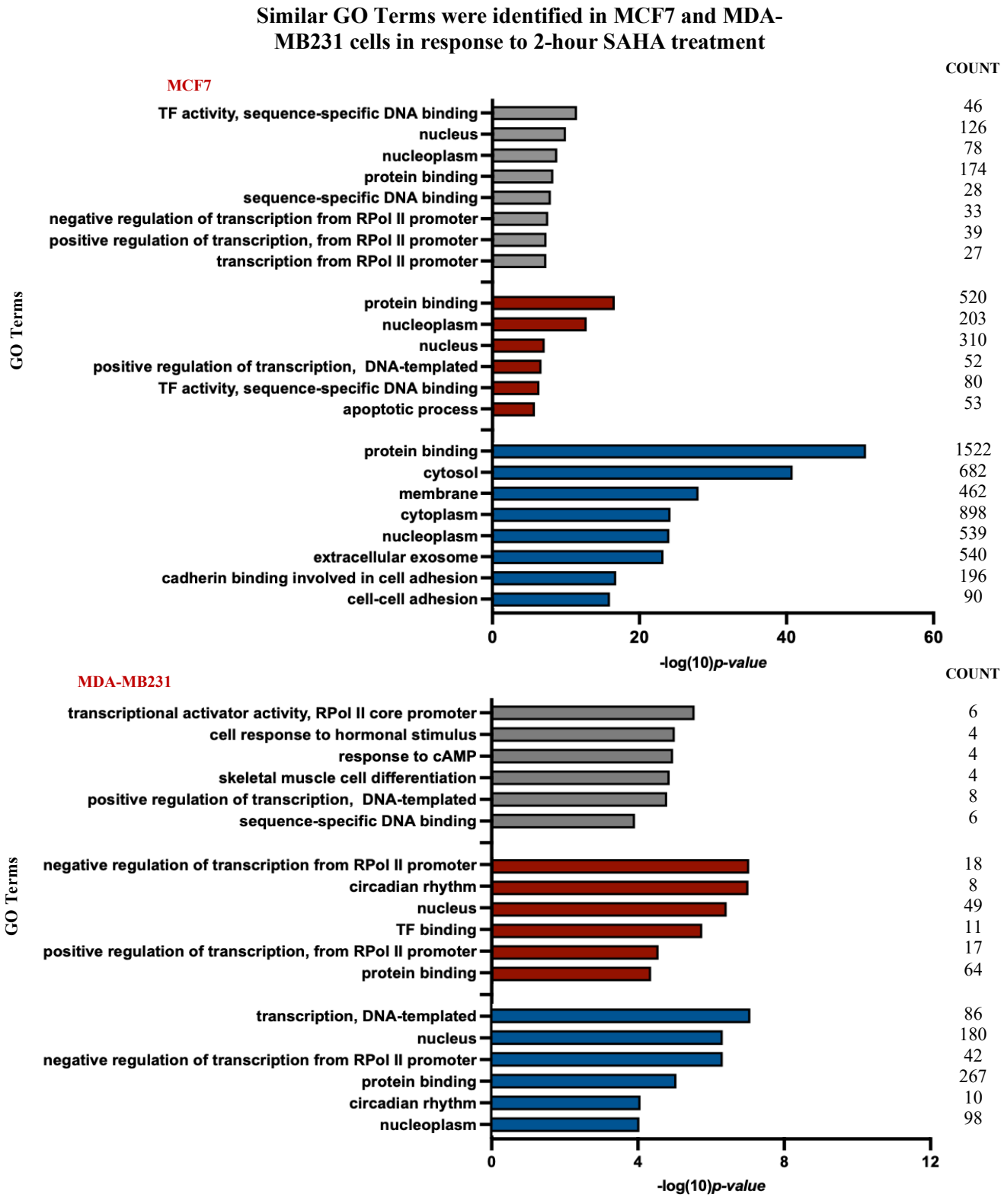


Figure 4.5: Ontology Analysis identified similar terms in MCF7 and MDA-MB231 cells. *DAVID ontology GO Terms identified considering all significantly differentially expressed genes ($p<0.05$) after 30, 60 or 120-minute SAHA treatment in MCF7 and MDA-M231 cells Depicted is the -log10(p-value) for each term identified in the Annotation Chart.*

4.3 Specific patterns of gene expression were induced in response to SAHA treatment

The next step involved assessing the RNA-Sequencing data to identify patterns of gene expression induced in response to SAHA. The initial focus was on *HAT* downregulation, which was recognised as a characteristic of the HDACi survival response (Halsall *et al.,* 2015). Closer examination of the RNA-Sequencing data using terms identified from the ontology analysis highlighted an upregulation in the expression of *HDAC, HSP* and *TF* genes. These gene expression changes were followed up by qPCR, to validate their occurrence in MCF7 and MDA-MB231 cells following 30, 60 or 120-minute SAHA treatment.

4.3.1 HAT gene expression was downregulated in response to HDACi treatment

Considering that HAT gene downregulation is a hallmark of the response to HDACi exposure, interest turned to assessing whether SAHA treatment affected the expression of acetylation related genes in our cell-lines. This followed up on Microarray data from our lab showing the rapid downregulation of HAT complex component genes in LCL cell-lines treated with an HDACi (Halsall *et al.,* 2015). The important question asked was whether this characteristic response was also observed in these solid tumour cell-lines. The RNA-Sequencing data showed HAT complex genes were downregulated in MDA-MB231 and MCF7 cells within 2-hours (Figure 4.6). Analysis of the acetylation related ontology terms in DAVID identified 24 HAT complex component genes. All 24 genes were downregulated in both cell-lines following SAHA treatment. 23 of these

were significantly downregulated in MCF7 cells, while only 4 were significantly downregulated in MDA-MB231 cells. Figure 4.6 depicts the fold change in expression of the six HAT genes, selected for qPCR validation, versus their expression in untreated cells. Interestingly, HAT complex component genes were not immediately downregulated following SAHA exposure. In both cell-lines, they were instead downregulated following an initial delay. Their expression between 0 and 30-minutes, did not change significantly – and in some cases slightly increased. This suggested that an initial response or recognition of the change in acetylation dynamics occurred first. Overall, MCF7 cells induced a larger and more rapid downregulation in HAT gene expression compared with MDA-MB231 cells.

This observation was then validated by qPCR. Six primers were designed to the HAT complex genes identified as significantly downregulated in the RNA Sequencing analysis. Selected were *EPC1, EPC2, KAT7, KAT6B* and *ING5* (Inhibitor of Growth Family 5). An additional primer was designed for *JADE1*, the only other HAT gene significantly downregulated in MDA-MB231 cells. The downregulation of HAT complex components following SAHA treatment was confirmed by qPCR in both cell-lines (Figure 4.7). *EPC1* and *KAT7* were significantly downregulated after 120-minute SAHA treatment in MCF7 cells while *EPC1* and *EPC2* were in MDA-MB231 cells. Though the pattern was similar, with all genes downregulated by 120-minutes, this analysis more clearly showed the initial upregulation. The red-line, which depicts a fold-change of 1, shows that HAT genes were upregulated at 30 and 60-minutes - prior to their downregulation by 120-minutes (Figure 4.7). However, only *JADE1* in MCF7 cells and *EPC1* in MDA-MB231 cells were significantly up-regulated at 30-minutes ($p<0.05$; Figure 4.7).

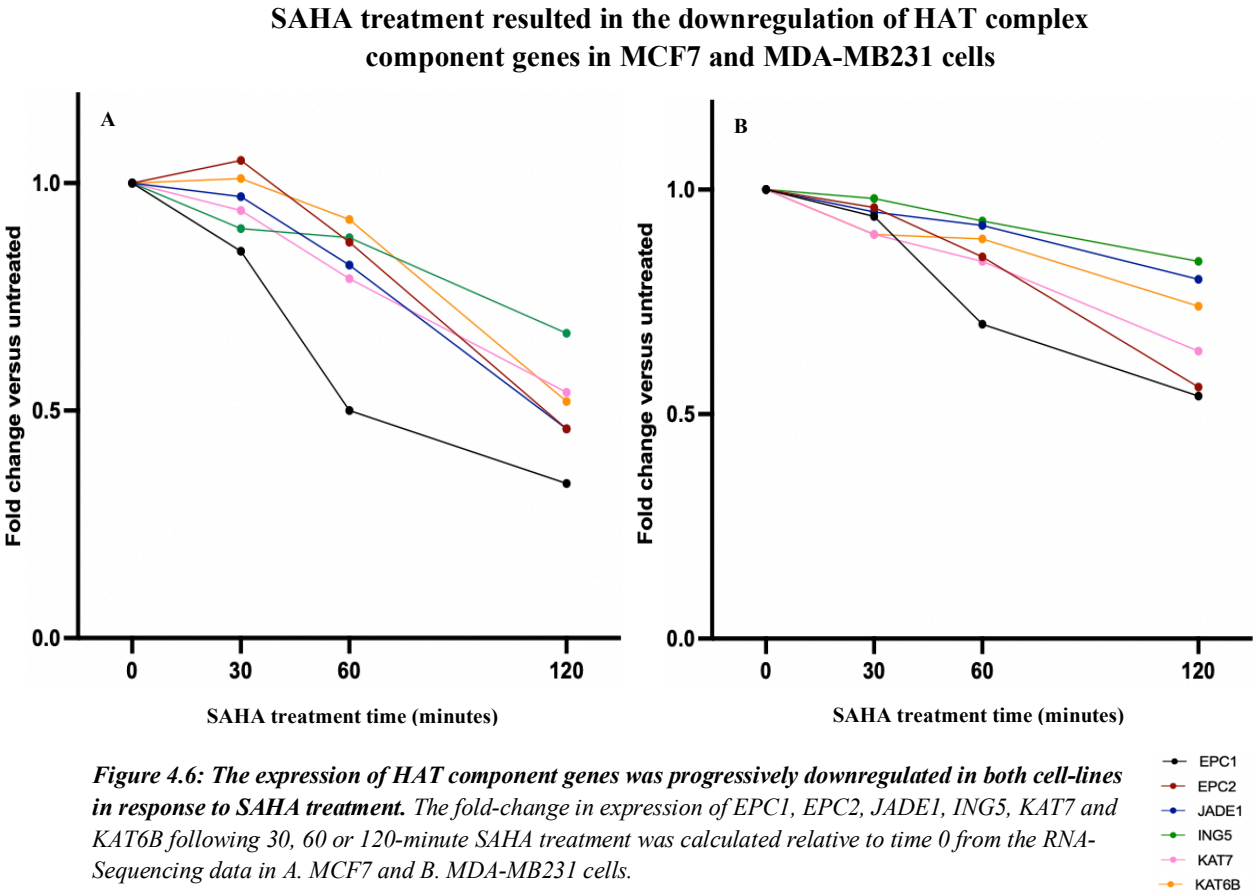


Figure 4.6: The expression of HAT component genes was progressively downregulated in both cell-lines in response to SAHA treatment. *The fold-change in expression of EPC1, EPC2, JADE1, ING5, KAT7 and KAT6B following 30, 60 or 120-minute SAHA treatment was calculated relative to time 0 from the RNA-Sequencing data in A. MCF7 and B. MDA-MB231 cells.*

This initial up-regulation was thought to relate to an early general acetylation driven increase in transcription. It could be considered an initial response to shock, followed by the cell reacting to correct the change. This had not been observed in previous Microarray experiments in the lab and was only hinted at in our RNA-Sequencing (Figure 4.6). As will be discussed, qPCR is normalised using the expression of housekeeper genes while RNA-sequencing considers all transcripts. Thus, an early increase in expression relative to housekeepers may be more easily detected.

There was a degree of inconsistency evident between MCF7 replicates. As the HDACi survival response is thought to be mounted to a greater extent in these cells, this may relate to how stressed the tested cell population was. This would be less evident in MDA-MB231 cells, which mount a smaller response. To conclude, this analysis showed

that an initial acetylation driven increase in HAT gene expression was followed by the downregulation of all HAT related genes after 2-hour SAHA treatment in both cell-lines.

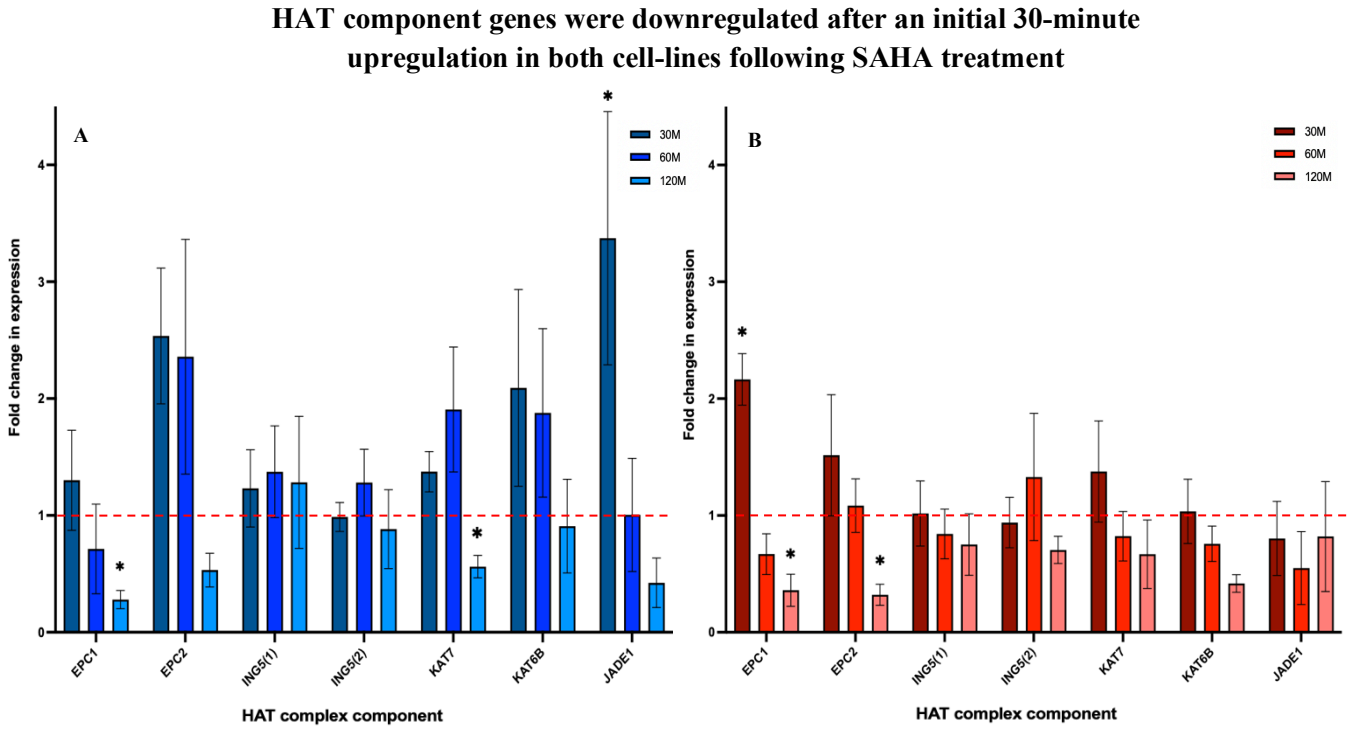


Figure 4.7: In response to SAHA treatment HAT complex genes exhibited an initial upregulation followed by a downregulation in their expression by 120-minutes. *Fold changes in expression of HAT complex genes 30, 60 or 120-minutes after SAHA treatment were assessed by qPCR relative to pre-treatment expression in A. MCF7 and B. MDA-MB231 cells following normalization to housekeeper genes. Paired, one-tailed T-test comparing normalized expression at 0-minutes with 30 or 120-minutes *p<0.05. Error bars show SEM of independent experiments (N=5). The red line depicts a fold-change of 1.*

In that acetylation related genes were downregulated, and considering that the survival response may be homeostatic, the effect of SAHA on the expression of *HDACs* was then assessed. The RNA-Sequencing data suggested that *HDACs* were upregulated in response to HDAC inhibition (Figure 4.8). This finding agrees with Dangond and Gullans who showed in 1998 that HDAC mRNA expression was upregulated in peripheral blood mononuclear cells following HDACi treatment. Expression of the individual HDAC genes was analysed. Five were upregulated and five downregulated in MCF7 cells. In MDA-MB231 cells, four were upregulated and four downregulated –

with the remaining HDAC genes exhibiting little change in their expression by 120-minutes (data not shown). The expression of *HDAC2,3* and *5* was shown to be upregulated following HDACi treatment in both cell-lines though significance was only reached in MCF7 cells (Figure 4.8). *HDAC2, 3* and *5* were significantly upregulated and *HDAC7* significantly downregulated in MCF7 cells. In MDA-MB231 cells only *HDAC5* was significantly upregulated. Though only small fold-changes were observed, this suggested that cells were attempting to compensate for the loss of HDAC activity. This may occur in a similar manner to HAT gene downregulation, as cells recognise the occurrence of unchecked acetylation.

These results were then followed up by qPCR, with primers designed to the four HDAC genes significantly differentially regulated in MCF7 cells; *HDAC2, 3, 5* and 7. This analysis showed that SAHA had little effect on the expression of these *HDACs* in either cell-line (Figure 4.9). Due to the inconsistency between replicates, only a pattern of change could be discerned. *HDAC2* and *HDAC3* were upregulated in the MCF7 line, however, SAHA did not affect the expression of *HDAC5* and *HDAC7. HDAC2, 3* and *5* were upregulated in MDA-MB231 cells. Interestingly, the downregulation of *HDAC7* in MDA-MB231 was the only significant difference that matched what was suggested from the RNA-Sequencing. It was therefore concluded that SAHA treatment did not significantly affect the expression of *HDACs* in either cell-line by 120-minutes. The expression of *HDACs* in our two cell-lines was variable – as was discussed in the introduction.

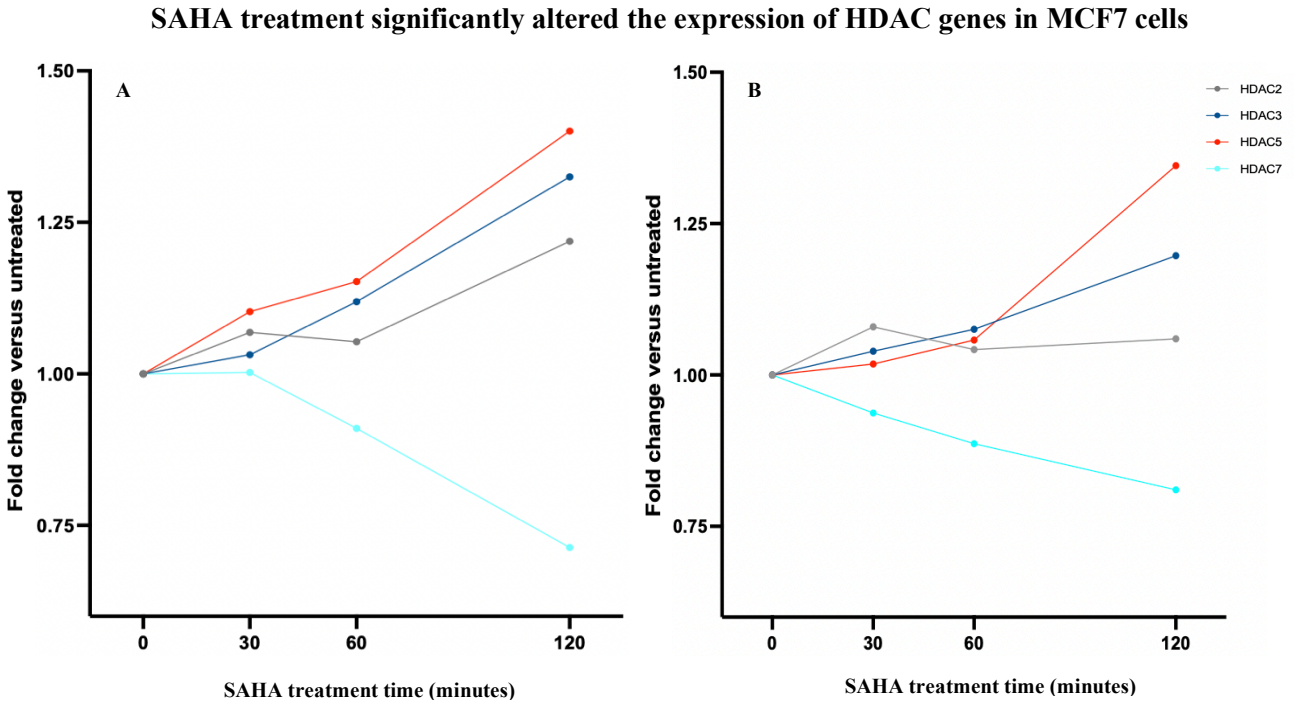


Figure 4.8: HDAC genes were differentially expressed in MCF7 cells in response to SAHA treatment. *The fold-change in expression of HDAC2, HDAC3, HDAC5 and HDAC7 was calculated after 30, 60 or 120-minutes SAHA treatment from the RNA Sequencing relative to basal expression in A. MCF7 and B. MDA-MB231 cells.*

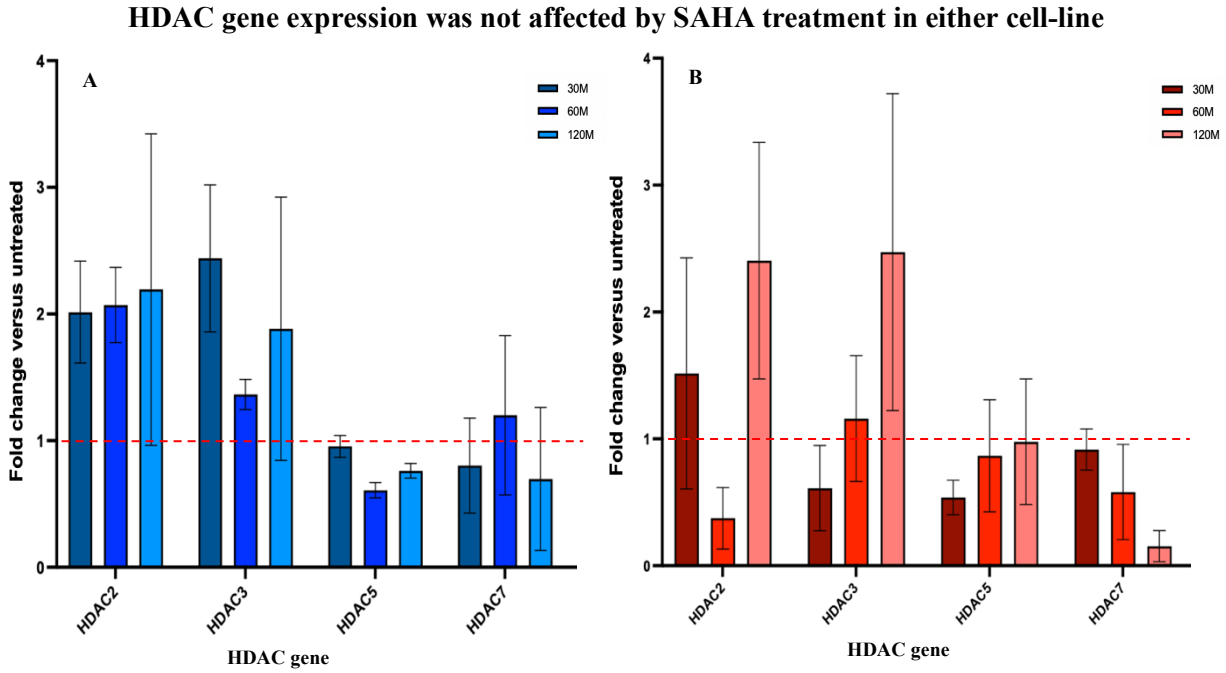


Figure 4.9: The expression of HDAC genes was not affected by SAHA treatment. *Fold changes in expression of HDAC2, HDAC3, HDAC5 and HDAC7 30, 60 or 120-minutes following SAHA treatment was assessed by qPCR relative to pre-treatment expression in A. MCF7 and B. MDA-MB231 cells after normalization to housekeepers. Error bars show SEM of independent experiments (N=4). The red line depicts a fold-change of 1.*

4.3.2 The identified SAHA-responsive transcription factor genes were upregulated in MCF7 cells

We were then interested in identifying the initial responding genes in our resistant cell-line. For this, we considered genes identified by DESeq2 as significantly upregulated in MCF7 cells following 30-minute SAHA treatment. Several *TFs* were identified among the early responding genes. As transcription had been mentioned in the ontology, interest turned to assessing how SAHA affected *TF* expression in both cell-lines. Shown in Figure 4.10 are genes displaying a twofold-change in expression or greater at 30-minutes in MCF7 cells, and their comparative expression in MDA-MB231 cells. This highlights the rapid upregulation of *TFs* - specifically *EGR1, NR4A1* and *NR4A3* - in MCF7 cells (Figure 4.10A). Interestingly, *TF* expression in MCF7 cells appeared to return almost to basal level by 120-minutes. This suggested that their expression rose quickly to initiate the survival response, with their expression then returning to pre-treatment levels once it had been initiated. This rapid upregulation did not occur in MDA-MB231 cells - with *TF* expression remaining similar across the time-course (Figure 4.10B).

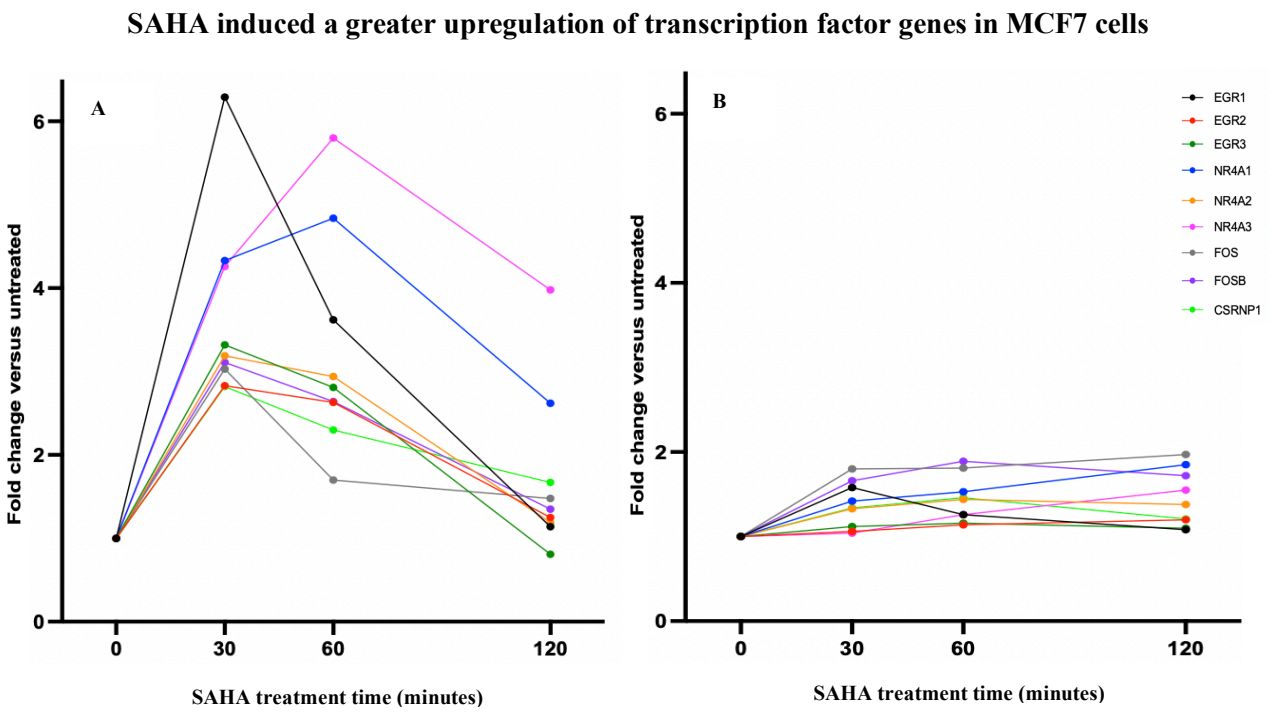


Figure 4.10: Transcription factor genes were rapidly upregulated by 30-minutes in MCF7 cells. *The fold-change in expression of transcription factor genes identified as displaying a greater than two-fold change in expression at 30-minutes in MCF7 cells. Shown are fold-changes in expression at 30, 60 or 120-minutes compared with pre-treatment expression levels from the RNA-Sequencing data in A. MCF7 and B. MDA-MB231 cells.*

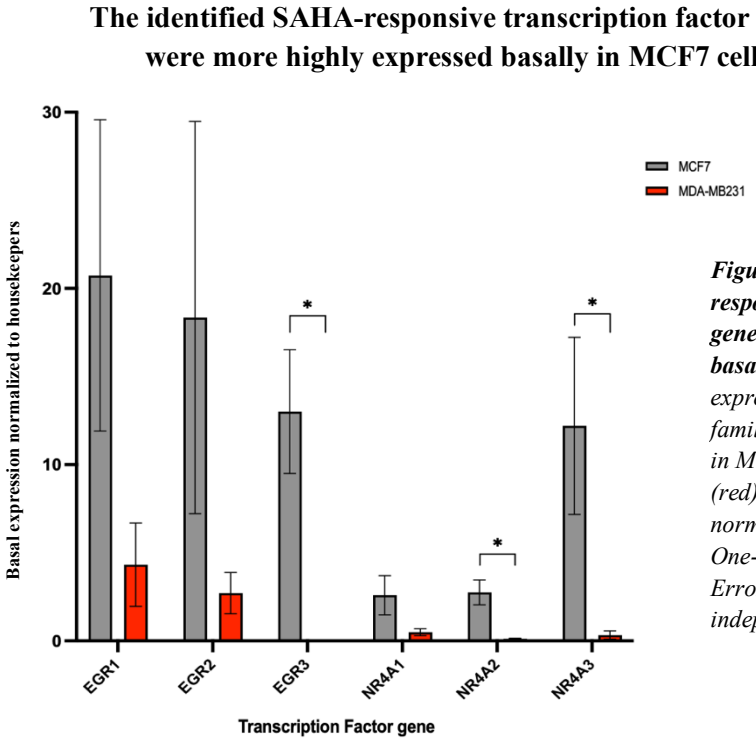


Figure 4.11: The selected SAHA-responsive transcription factor genes were more highly expressed basally in MCF7 cells. *The basal expression of the EGR and NR4A family member genes was assessed in MCF7 (grey) and MDA-MB231 (red) cells. All qPCR data was normalized to housekeeper genes. One-tailed, unpaired T-test *p<0.05. Error bars depict SEM of independent experiments (N=3).*

TF expression following SAHA treatment was then validated by qPCR, with primers designed to *NR4A1, NR4A2* and *EGR1-3*. These genes were selected from the RNA-Sequencing, which had identified members of both TF families as rapidly upregulated following SAHA treatment in MCF7 cells (Figure 4.10A). All the selected *TF* genes were more highly expressed basally in MCF7 cells, with *EGR3* as well as *NR4A2* and *NR4A3* significantly more highly expressed (Figure 4.11). This suggested that MCF7 cells are ready to respond as they express the necessary TFs to a greater extent than MDA-MB231 cells. However, the expression differences suggested in the RNA-Sequencing were not observed by qPCR. A greater expression of *TFs* was observed in MCF7 cells, as expected, however there was no 30-minute peak and subsequent downregulation. Instead, *NR4A1, NR4A2* and *EGR2* were not significantly upregulated in the presence of SAHA in MCF7 cells while the expression of *EGR1* and *EGR3* did not change (Figure 4.12). The five *TF* genes selected were upregulated in MDA-MB231 cells, with *NR4A2* and *EGR2* significantly upregulated at 120-minutes ($p<0.05$). The fold-changes in expression appear greater in this cell-line, likely influenced by their lower basal expression. Interestingly, this analysis suggested that a number of immediate early response (IER) genes were expressed to a greater extent basally in the resistant cell-line and then upregulated following HDACi treatment. This led us to consider whether the IER is involved in the HDACi survival response?

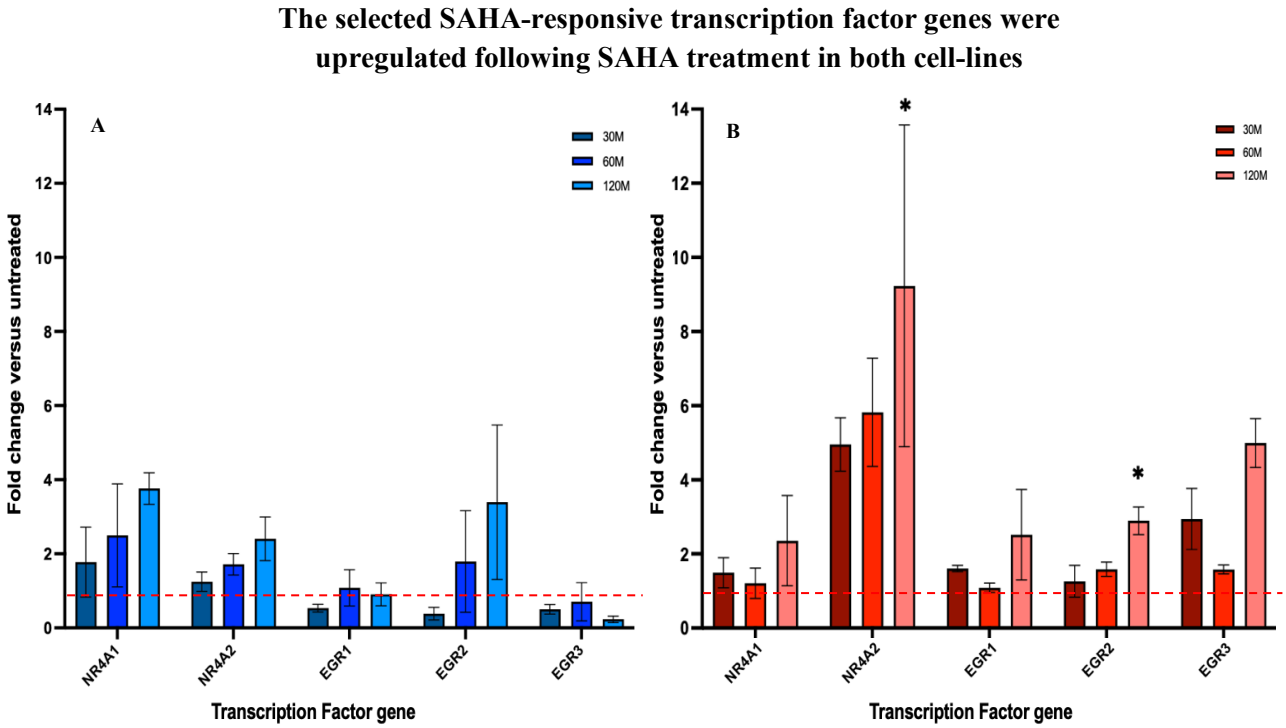


Figure 4.12: The expression of selected transcription factor genes was upregulated in both cell-lines following SAHA treatment. *Fold change in expression of NR4A1, NR4A2, EGR1, EGR2 and EGR3 following 30, 60 or 120-minute SAHA treatment assessed by qPCR relative to pre-treatment expression in A. MCF7 and B. MDA-MB231 cells after normalization to housekeepers. Paired, one-tailed T-test comparing normalized 0-minute and 120-minute expression *p<0.05. The red line depicts a fold-change of 1. Error bars depict SEM of independent experiments (N=3).*

4.3.3 Heat shock protein genes were variably expressed basally

Responses to stress were mentioned in the MCF7 ontology. This, coupled with the suggestion of crossover between the HDACi survival response and Heat Shock Response (HSR), led to a consideration of *HSP* expression. 70 *HSP* genes were identified from the overall list of DEGs. Many, particularly from Family A, were upregulated in response to SAHA treatment. The RNA-Sequencing data suggested that the expression of a greater number of *HSPs* increased in MCF7 cells in response to SAHA treatment (Figure 4.13). 2 *HSP* genes were significantly up-regulated in MDA-MB231 cells, while 12 were significantly up-regulated and 2 significantly down-regulated in MCF7 cells.

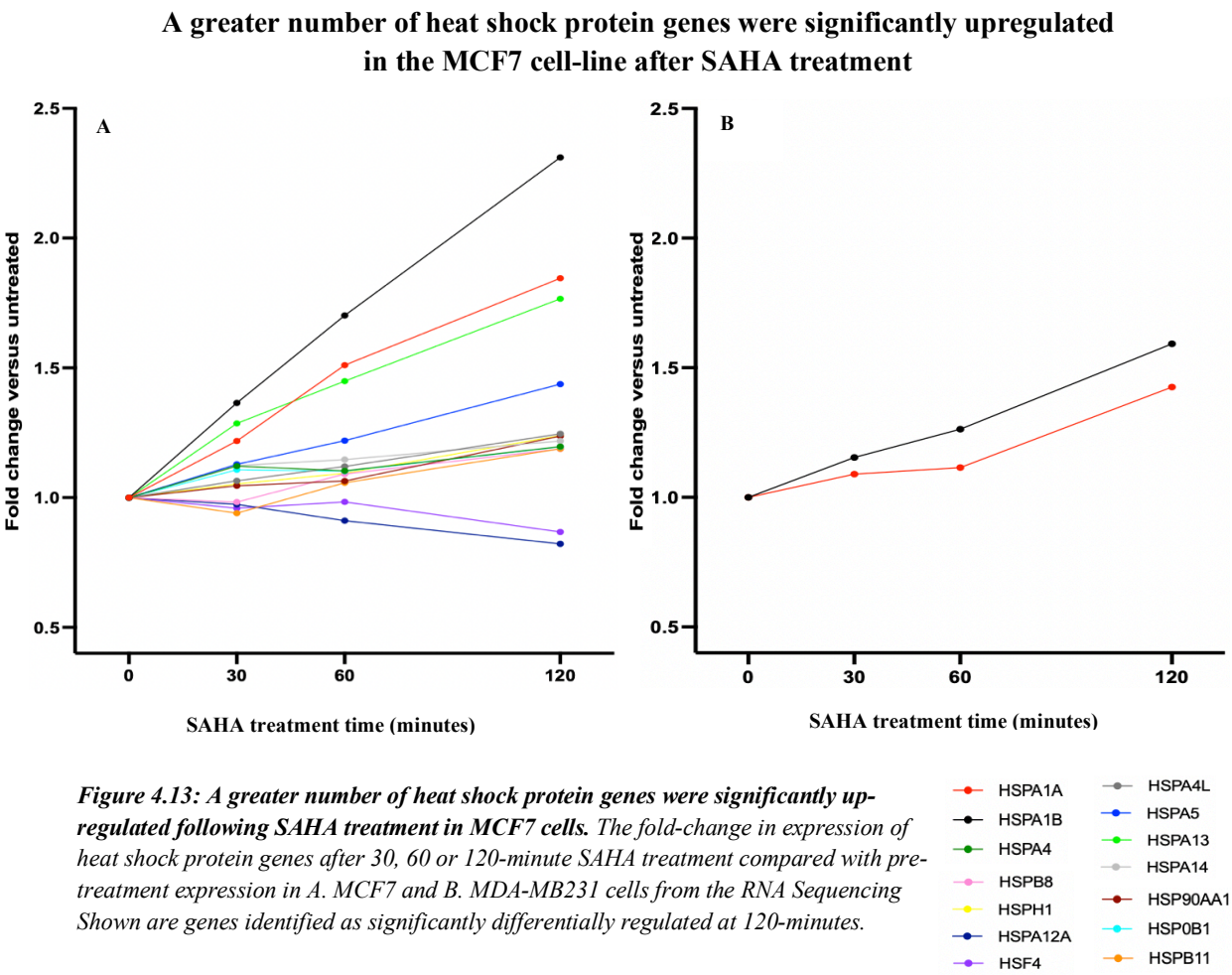


Figure 4.13: A greater number of heat shock protein genes were significantly up-regulated following SAHA treatment in MCF7 cells. *The fold-change in expression of heat shock protein genes after 30, 60 or 120-minute SAHA treatment compared with pre-treatment expression in A. MCF7 and B. MDA-MB231 cells from the RNA Sequencing Shown are genes identified as significantly differentially regulated at 120-minutes.*

This response was validated by qPCR, with primers designed to Heat Shock Protein Family A members; *HSPA1A*, *HSPA1B*, *HSPA5, HSPA13* and *HSPA14*. The first two genes were selected as they were significantly upregulated in both cell-lines, with the subsequent three displaying the greatest fold-change in expression in MCF7 cells at 120-minutes. The up-regulation of *HSP* genes following SAHA treatment was not as significant as suggested from the RNA-Sequencing (Figure 4.14). Their expression was then considered in relation to the red line depicting a fold-change of 1. This showed that a greater number in MCF7 cells were expressed above this line, while most in MDA-MB231 cells were below. This indicated that overall, there was a greater upregulation of *HSP* genes in MCF7 cells in response to SAHA treatment. The only gene displaying

significant upregulation in the presence of SAHA in MCF7 cells was *HSPA1B* (Figure 4.14). On the other hand, *HSPA13* and *HSPA1A* were more highly expressed at 60-minutes - with their expression returning to pre-treatment level by 120-minutes. *HSPA5* and *HSPA14* exhibited only a peak in their expression at 30-minutes, with their expression unchanged comparing 120-minutes with 0-minutes. In agreement with the RNA-Sequencing, no significant difference was exhibited in the expression of *HSPA5, HSPA14* or *HSPA13* in MDA-MB231 cells. *HSPA1B* displayed a progressive up-regulation with increasing treatment time, while *HSPA1A* was upregulated only at 120-minutes.

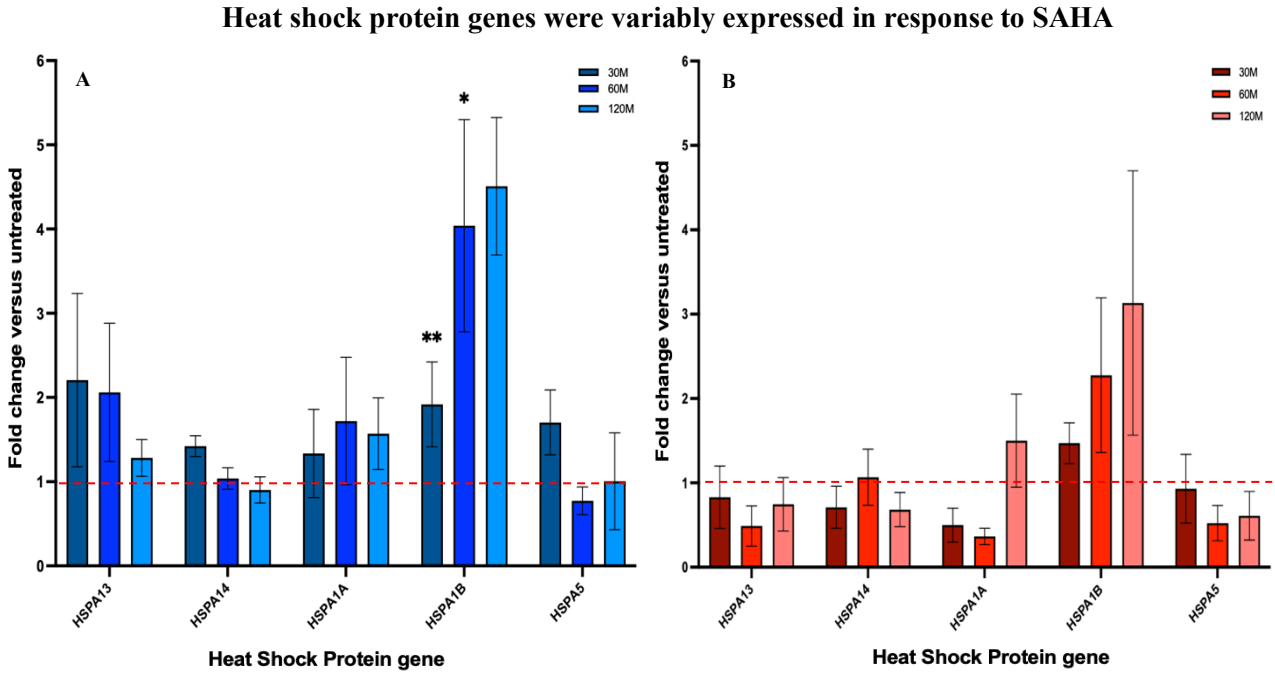


Figure 4.14: Heat shock protein gene expression varied in response to SAHA treatment. *Fold change in expression of HSPA13, HSPA14, HSPA1A, HSPA1B and HSPA5 following 30, 60 or 120-minute SAHA treatment assessed by qPCR relative to pre-treatment expression in A. MCF7 and B. MDA-MB231 cells after normalization to housekeepers. Paired, two-tailed T-test comparing normalized expression at 0-minutes with 30, 60 or 120-minutes **p<0.01, *p<0.05. The red-line depicts a fold-change of 1. Error bars show SEM of independent experiments (N=3).*

The selected HSP genes were more variably expressed basally in MDA-MB231 cells (Figure 4.15). The resounding message that arises when considering their basal and SAHA induced transcriptional expression is variation. These are stress responsive

genes, employed by cells to survive environmental insults. Therefore, their job is to respond within the context of the cell. Despite this variability – they did appear to be more highly expressed basally in MDA-MB231 cells. This raised the question of whether this cell-line was inherently more stressed, something that will be followed up on later.

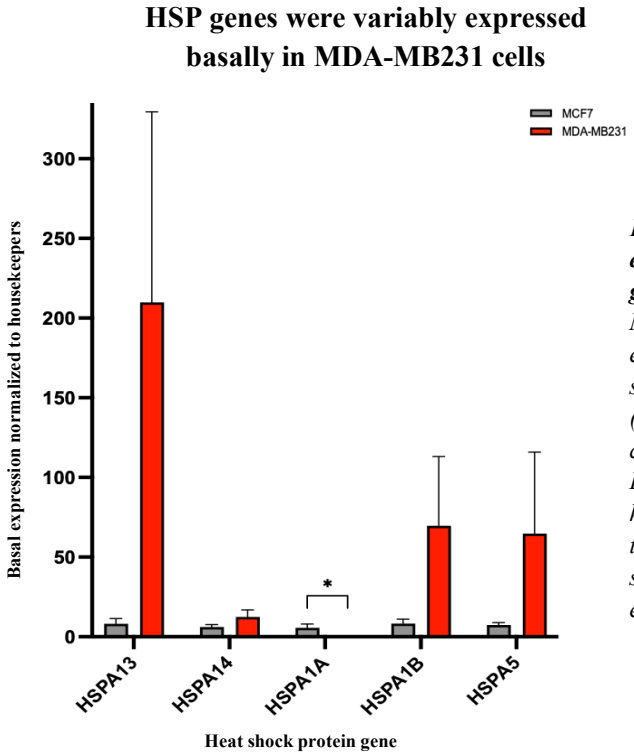


Figure 4.15: The basal expression of heat shock protein genes was more variable in MDA-MB231 cells. *The basal expression of the selected heat shock protein genes in MCF7 (grey) and MDA-MB231 (red) cells was determined by qPCR. Expression was normalized to housekeepers. Unpaired, one-tailed T-test *p<0.05. Error bars show SEM of independent experiments (N=3)*

Gene expression differences depend on the state of the cells at the time. This is unlikely to be easily replicated in different cell populations. The changes induced in the individual *HAT, TF* and *HDAC* replicates varied. This was more clearly observed in MCF7 cells, perhaps suggesting that they induce a large transcriptional response – which would result in variation across the replicates.

qPCR and RNA-Sequencing use different normalisation methods, so the fold changes identified would not necessarily be identical. qPCR is normalised against the expression

of selected housekeeper genes, which are expected to be consistent across samples and in response to treatment (Kozera and Rapacz, 2013). RNA-sequencing assumes that each sample expresses the same total mRNA. This method detects more subtle changes as it considers absolute and not relative expression. Both would detect significant differences in expression; however, RNA-Sequencing is not as sensitive at detecting changes in low abundance transcripts (Ayturk *et al.,* 2013).

4.4 Motif analysis identified factors driving early gene expression change

To understand the initiation of the HDACi survival response, interest turned to defining which TFs were mediating early gene expression changes. It was hypothesised that identifying factors involved at this early stage could point to the TFs driving the survival response. Motif enrichment analysis was used to assess the consensus sequences present in genes differentially expressed after 30, 60 and 120-minute SAHA treatment. Genes differentially expressed at each timepoint in MCF7 and MDA-MB231 cells were analysed using HOMER software. HOMER identifies common motifs at promoter regions (+/-500bp) of genes and indicates the number of target genes containing these sequences compared to the background. Matches to predicted TF binding sites are then assigned to the identified motifs.

4.4.1 Predicted binding sites for ATF1, SRF and OCT6 were found in genes differentially expressed by 30-minutes in MCF7 cells

The initial focus was on changes at 30-minutes, which would identify the earliest responding genes. The 277 genes significantly differentially expressed at 30- versus 0-

minutes in MCF7 cells were analysed by HOMER. Two motifs of interest were matched to the predicted binding sites of SRF (Serum Response Factor) and ATF1 (Activating Transcription Factor 1). The top match, ATF1, is depicted in Figure 4.16A. Due to the number of genes input for this analysis, the targets were not highly enriched against the background. To narrow this down, genes from the initial 30-minute list displaying a fold-change>2 were then analysed. Consensus sequences in these 56 genes again matched the suggested ATF1 and SRF binding sites (Figure 4.16B/C). Both alignments displayed high match scores and a good degree of overlap. The inclusion of a more refined number of genes resulted in a greater percentage of the total targets matching the motifs. The predominance of IER genes among those rapidly upregulated at 30-minutes lends confidence to the enrichment of SRF, suggesting this as our initial target for knockdown.

Predicted SRF and ATF1 binding sites were enriched in genes upregulated at 30-minutes in MCF7 cells

	Motif Logo	p-value	%Target/%Background	Best Match
A		1e-14	17.6/4.6	ATF1
B		1e-14	22.45/0.55	CArG(MADS – Srf)
C		1e-12	44.9/7.4	ATF1

Figure 4.16: Binding sites for ATF1 and SRF motifs were identified among genes upregulated at 30-minutes in MCF7 cells. *A. ATF1 was the top motif identified by HOMER analysis when all significantly upregulated genes ($p<0.05$) at 30-minutes in MCF7 were input. Refining this list to include those displaying a fold-change>2 identified B. SRF and C. ATF1 binding sites.*

Analysis of the 52 significantly downregulated genes ($p<0.05$) at 30-minutes identified predicted OCT6 (Octamer Binding Transcription Factor 6) and SMAD3 (SMAD Family

Member 3) binding sites (Figure 4.17A/B). Interestingly, the percentage of the background containing these motifs was much lower than had been observed with motifs identified from the upregulated genes. This suggested that the HDACi survival response could be characterised by a broad, general upregulation and a more specific gene downregulation. These two TF families were selected as potential targets for knockdown.

An OCT6 predicted site was identified among MCF7 genes downregulated at 30-minutes

	Motif Logo	p-value	%Target/%Background	Best Match
A		1e-19	26.19/0.2	Oct6
B		1e-19	21.43/0.07	Smad3

Figure 4.17: OCT6 and SMAD3 binding sites were found among genes downregulated at 30-minutes in MCF7 cells. *HOMER identified the A. OCT6 and B. SMAD3 binding sites in all significantly downregulated genes ($p<0.05$) at 30-minutes in MCF7 cells.*

4.4.2 The predicted binding site for NFY was enriched among genes upregulated at 60-minutes in MCF7 cells

NFY (Nuclear Transcription Factor Y), the GC-box and ATF1 binding sites were identified from the 912 significantly up-regulated genes ($p<0.05$) in MCF7 cells after 60-minute SAHA treatment. The NFY binding site is depicted in Figure 4.18. The predicted OCT6 binding site was also identified from the 325 significantly downregulated genes, as had been observed at 30-minutes.

The NFY binding site was identified in genes upregulated at 60-minutes in MCF7 cells

Motif Logo	p-value	%Target/%Background	Best Match
	1e-23	29.57/15.71	NFY

Figure 4.18: The predicted binding site for NFY was identified among genes significantly upregulated at 60-minutes in MCF7 cells. *HOMER identified the NFY binding site among all genes significantly upregulated ($p<0.05$) following 60-minute SAHA treatment.*

4.4.3 Sp1, NFY and ATF binding sites were enriched among MCF7 genes upregulated at 120-minutes

Analysis of the 2674 significantly up-regulated genes in MCF7 cells identified the predicted binding sites of Sp1 (Sp1 Transcription Factor), NFYC (Nuclear Transcription Factor Y Subunit Gamma) and ATF1 (Figure 4.19A-C). The YY1 binding site was identified among the 2001 significantly down-regulated genes ($p<0.05$). Due to the number of genes included in the analysis, these were not enriched to such an extent over the background as those at earlier points. This list was then refined to include only the 395 genes also displaying a fold-change>2. This identified the potential binding site of Six4 (Six Homeobox 4) motif (Figure 4.19D).

Sp1, NFY and ATF binding sites were identified in genes upregulated at 120-minutes in MCF7 cells

	Motif Logo	p-value	%Target/%Background	Best Match
A		1e-46	44.98/30.91	Sp1
B		1e-26	32.61/22.91	NFYC
C		1e-22	29.59/20.93	ATF1
D		1e-12	3.06/0.09	Six4

Figure 4.19: Binding sites for Sp1, NFYC, ATF1 and Six4 were identified among genes significantly upregulated after 120-minute SAHA treatment. *A. Sp1, B. NFYC and C. ATF1 binding sites were identified by HOMER among all significantly upregulated genes ($p<0.05$) in MCF7 cells at 120-minutes. D. The Six4 binding site was identified when this list was refined to include those displaying a fold-change>2.*

4.4.4 Significantly enriched motifs were only identified among genes upregulated at 120-minutes in MDA-MB231 cells

The DEGs identified at each time-point were then assessed in MDA-MB231 cells. Far fewer genes were considered in this analysis, as a limited number of genes displayed differential expression between treatment timepoints. Significant matches to the predicted binding sites of NFY and Sp1 were only observed considering the 534 genes significantly up-regulated at 120-minutes – sites which had also been enriched in MCF7 cells at this timepoint (Figure 4.20). This analysis, and the fact that significant motifs were only identified at 120-minutes in this cell-line, suggests that they are slower to respond to SAHA treatment.

Binding sites for NFY and Sp1 were found among MDA-MB231 genes upregulated at 120-minutes

	Motif Logo	p-value	%Target/%Background	Best Match
A		1e-25	24.9/8.78	NFY
B		1e-12	42.65/27.6	Sp1

Figure 4.20: NFY and Sp1 binding sites were identified among MDA-MB231 genes significant upregulated following 120-minute SAHA treatment. *HOMER identified A. NFY and B. Sp1 binding sites from all significantly upregulated genes (p<0.05) in MDA-MB231 cells at 120-minutes.*

4.4.5 No common binding sites were identified among downregulated HAT genes

Considering the uniform downregulation of HAT complex genes following HDACi treatment, motif analysis was used to investigate whether these genes had a common regulator. However, analysis of the promoter sequences of the 24 HAT complex genes did not identify any significant motifs. Based on the suggested crossover between the HDACi survival response and HSR, it was interesting that the known Heat Shock Response Element (HRE) was enriched from HAT genes (Figure 4.21).

No significant binding site was identified among the downregulated HAT genes

Motif Logo	p-value	%Target/%Background	Best Match
	1e-2	14.29/1.56	HRE(HSF)

Figure 4.21: The HRE motif was identified among HAT genes downregulated following SAHA treatment. *HOMER identified the known Heat Shock Response Element binding site among HAT complex genes downregulated in response to SAHA treatment.*

4.4.6 Chapter Conclusions

This chapter analysed the results of an RNA-Sequencing experiment comparing the response of MCF7 and MDA-MB231 cells to treatment with SAHA for 30, 60 or 120-minutes. An analysis of the number of genes differentially expressed across the time-course highlighted that a greater transcriptional response was induced in MCF7 cells. This was further investigated through Top Gene Expression Analysis and assessing the RNA-Sequencing replicates in Sample Similarity Matrices and MDS Plots. Interesting patterns of gene expression arising from the RNA-Sequencing were investigated. These included the downregulation of all *HAT* complex genes following an initial delay and the upregulation of *TF* and *HSP* genes in both cell-lines. Ontology analysis suggested that common genes were induced in both cell-lines following SAHA treatment. Motif analysis was then used to investigate the TFs driving early gene expression change in our resistant MCF7 cell-line. This identified potential target genes for knockdown analysis, including SRF as well as the ATF/CREB, SMAD and POU TF families.

5. DOES DNA METHYLATION LOCK IN THE LONG-TERM SURVIVAL RESPONSE TO AN HDACi?

Reduced Representation Bisulfite Sequencing (RRBS) was carried out on cells treated with SAHA for 0, 24 or 48-hours. RRBS is a variation on whole genome bisulfite conversion using restriction enzyme digestion and DNA size selection to focus on CpG dinucleotides, where most DNA methylation occurs (Nagarajan *et al.,* 2014). This type of analysis cannot distinguish between 5' methyl or 5' hydroxy methyl groups, only indicating whether CpG sites gain or lose methylation in response to SAHA treatment (Sun, 2019). This experiment was carried out based on the crosstalk identified between histone acetylation and DNA methylation (Kondo, 2009; Vaissière *et al.,* 2008; Milutinovic *et al.,* 2007). Unpublished data from our lab showed that cells sensitive to HDAC inhibition were also sensitive to DNMT inhibition, indicative of possible crossover in the pathways used. Analysis of the DNA methylation induced in MCF7 and MDA-MB231 cells following 24 or 48-hour SAHA treatment investigated whether methylation locked in the long-term survival response to an HDACi.

This work assessed a different timescale to the RNA-Sequencing, treating cells for 24 or 48-hours rather than 2-hours. This was the case as it had not been known whether any HDACi-induced methylation changes would be observed within 2-hours, as methylation changes are believed to take longer to be established. The original planned treatment schedule included additional timepoints at 12 and 36-hours. However, due to time constraints and the disruption caused by the Covid pandemic – only two timepoints were followed up for sequencing. 24 and 48-hours were selected to be certain that changes would be observed in both cell-lines.

5.1 A greater number of differentially methylated CpG sites were identified in MDA-MB231 cells

The first step involved analysing how SAHA treatment affected the methylation of individual CpG sites. A DMS represents an individual CpG site exhibiting a change in methylation between treatment timepoints. The benefit of RRBS is that less 5% of the genome is sequenced, but this incorporates 10-15% of CpG sites and around 84% of CpG islands irrespective of methylation status (Smith *et al*., 2009; Gu *et al.,* 2011). Figure 5.1 shows heatmaps generated at Zymo depicting the individual CpG sites displaying the greatest change in methylation across the 48-hour SAHA treatment time-course. It was important to see that the replicates clustered by timepoint. This indicated that downstream methylation changes were induced in both cell-lines in response to HDACi treatment. Interestingly, a distinct methylation signature was observed at each timepoint – with a similar pattern observed in MCF7 and MDA-MB231 cells. Hierarchical clustering grouped 0 and 48-hours closest, keeping them separate from 24-hours. The induced methylation changes were, therefore, more dynamic than had been expected. The heatmaps showed a progressive change in methylation state in response to SAHA treatment, with a distinct change occurring at 24-hours. The responding CpG sites could be separated based on their response. CpG sites in Cluster A exhibited a loss in methylation between 0 and 24-hours, followed by a gain in methylation from 24 to 48-hours (Figure 5.1). CpG sites in Cluster B exhibited the opposite effect, gaining methylation between 0 and 24-hours followed by a loss from then until 48-hours. Two interesting discoveries arose from this analysis, firstly that CpG sites exhibited such a reversal in their methylation state within 48-hours and secondly that the pattern of response was similar in both cell-lines.

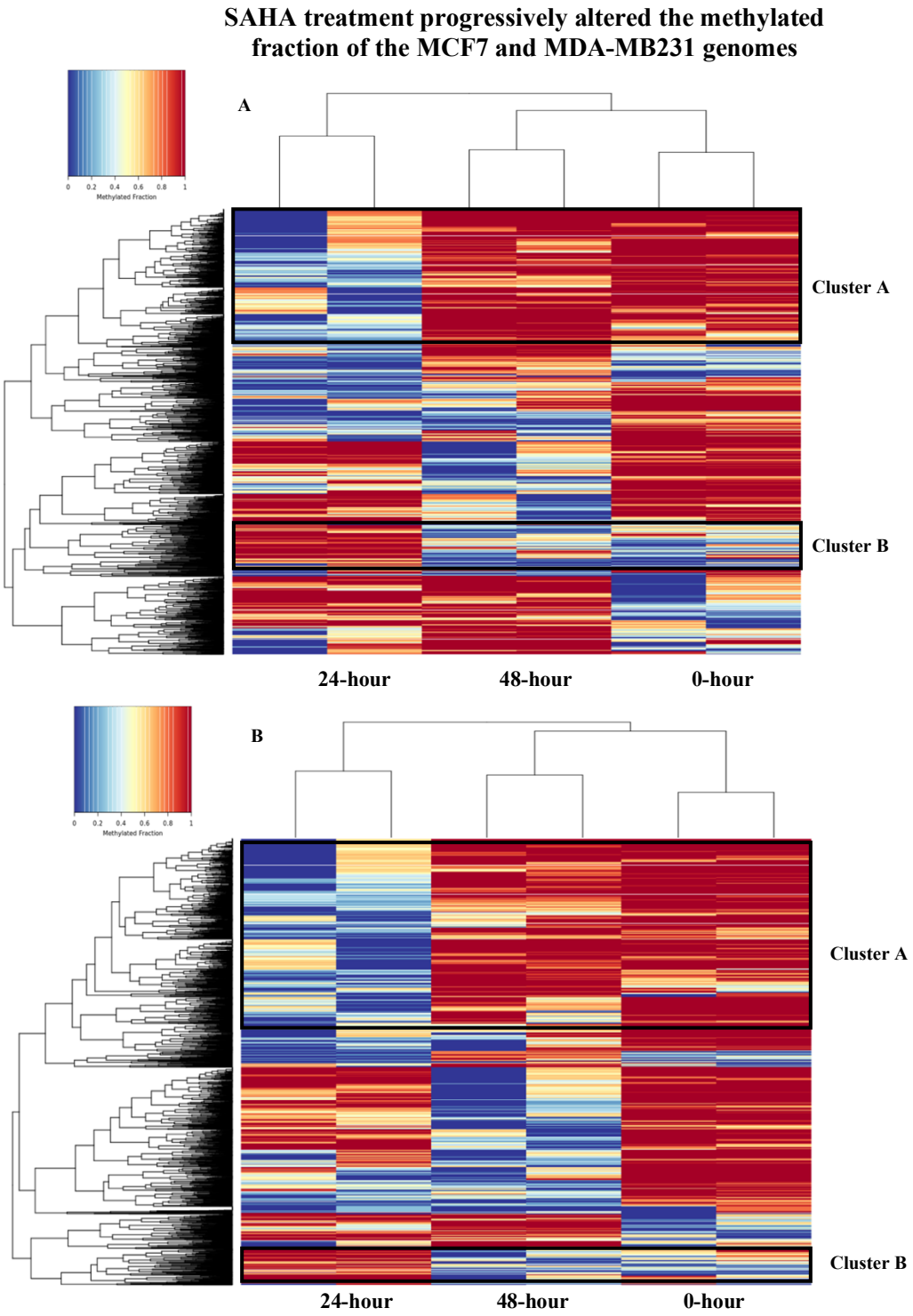


Figure 5.1: SAHA treatment progressively altered the methylated fraction of the MCF7 and MDA-MB231 genomes. *CpG sites differentially methylated in the A. MCF7 and B. MDA-MB231 genomes following 24 or 48-hour SAHA treatment. Blue depicts unmethylated regions and red methylated regions. Indicated in Cluster A/B are those sites exhibiting the largest change in methylation across the 48-hours. Heatmap generated by Zymo Research.*

This led to a consideration of the number of DMS present in each timepoint comparison - as an indication of the size of the methylation response induced. Figure 5.2 shows the number of individual CpG sites exhibiting differential methylation during the three timepoint comparisons in both cell-lines. A greater number of CpG sites exhibited differential methylation following SAHA treatment in MDA-MB231 cells across all timepoints. This was the initial suggestion of a larger methylation response being induced in the HDACi-sensitive cell-line following SAHA treatment.

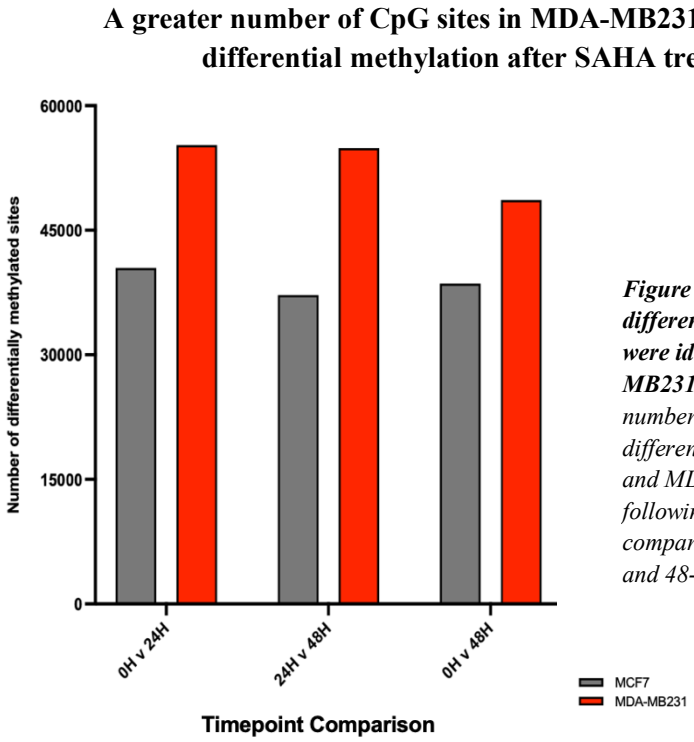


Figure 5.2: A greater number of differentially methylated sites were identified in the MDA-MB231 genome. *The total number of CpG sites exhibiting differential methylation in MCF7 and MDA-MB231 genomes following SAHA treatment comparing 0 and 24-hours, 24 and 48-hours and 0 and 48-hours.*

The location of these CpG sites was then considered, selecting those which may be involved in gene regulation following SAHA treatment. The percentage of the total number of DMS identified that were located at promoters was first considered. Similar percentages were located at promoter regions at all timepoints in both cell-lines. Around 10-13% of DMS were located at gene promoters in MCF7 cells and around 9-11% in MDA-MB231 cells. A greater number of CpG sites were identified in MDA-MB231 cells,

suggesting that a larger methylation response occurred in the sensitive, compared with the resistant cell-line. Despite inducing methylation change at a larger number of CpG sites, a greater number were not located at promoter regions.

The next consideration was whether these sites gained or lost methylation in response to SAHA treatment. To answer this question, the list of DMS located at promoters was filtered to select only those exhibiting a difference in methylation >0.5 (increase in methylation) or <-0.5 (loss of methylation) in response to SAHA (Figure 5.3). It was thought that this cut-off would select sites at which SAHA induced meaningful changes in methylation. A similar pattern of response was observed in both cell-lines. SAHA induced an initial loss in methylation by 24-hours. A correction then occurred, with a gain in methylation at individual CpG sites more prevalent between 24 and 48-hours. Though their pattern of response was similar, a greater overall number of sites exhibited differential methylation in MDA-MB231 cells. For example, 212 sites gained methylation and 142 lost methylation in MCF7 cells, while 313 gained methylation and 200 lost methylation in MDA-MB231 cells between 24 and 48-hours. From 24- through to 48-hours, most CpG sites exhibited a loss in their methylation. This was the timepoint at which their response diverged. By 48-hours, MCF7 cells appeared to have corrected for the induced methylation changes. This was highlighted by the similar number of CpG sites exhibiting a gain and loss in methylation (Figure 5.3). On the other hand, a greater number of CpG sites in MDA-MB231 cells still exhibited a loss in methylation during this final timepoint comparison. This suggested that the regulation of SAHA-induced methylation occurred more slowly in MDA-MB231 cells.

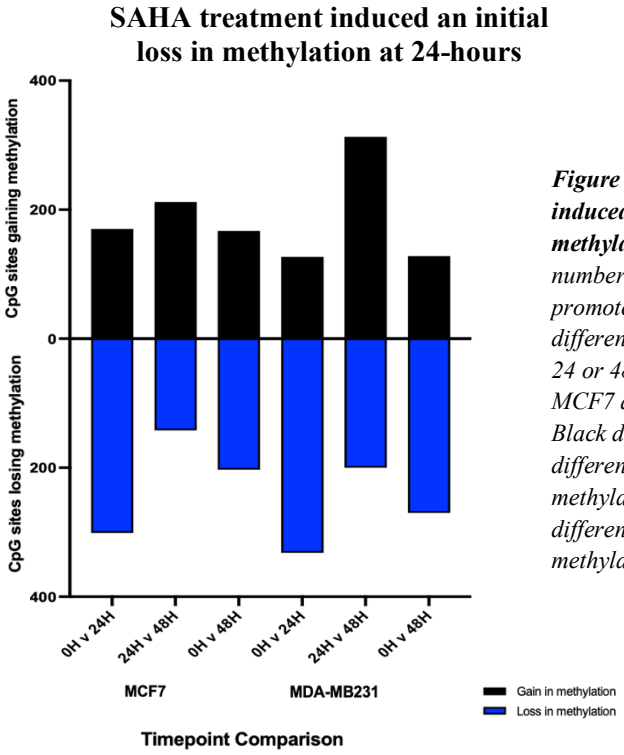


Figure 5.3: SAHA treatment induced an initial loss in methylation by 24-hours. *The number of CpG sites located at promoter regions exhibiting a difference in methylation following 24 or 48-hour SAHA treatment in MCF7 and MDA-MB231 cells. Black depicts those exhibiting a difference >0.5 (gain in methylation), while blue depicts a difference <0.5 (loss in methylation).*

5.2 A greater number of regions were differentially methylated in MDA-MB231 cells in response to SAHA treatment

Following on from the analysis of individual CpG sites, DMRs were then investigated. These are regions in which several CpG sites exhibit a similar significant difference in methylation following SAHA treatment (Rakyan *et al.,* 2011). Due to their size, and the presence of several CpG sites, these regions are considered more biologically relevant. A greater number of DMRs were identified in MDA-MB231 cells across all the timepoint comparisons (Figure 5.4). For example, four times as many were recognised in MDA-MB231 cells between 0 and 24-hours and twice as many between 24 and 48-hours. Interestingly, a similar number of DMRs were identified in the MCF7 cell-line across all

the timepoint comparisons. The greater number of DMRs identified in the 0 to 24-hour comparison suggested that this is a rapid response.

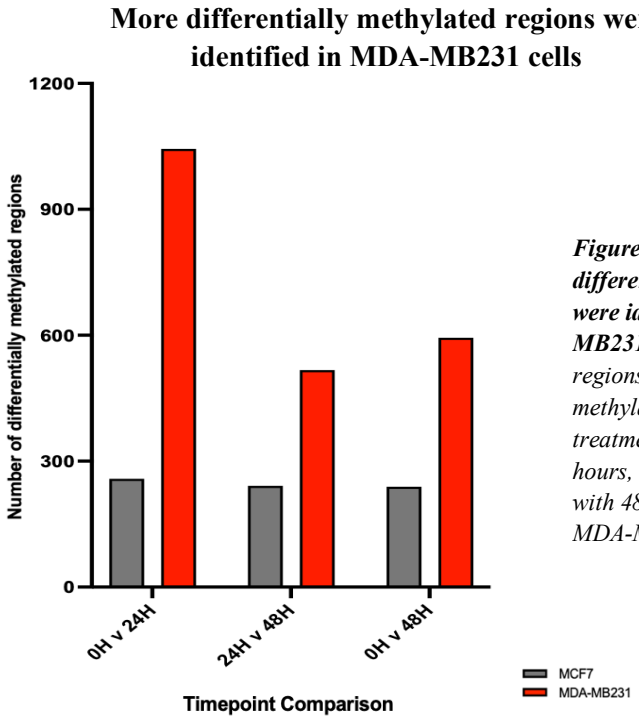


Figure 5.4: A greater number of differentially methylated regions were identified in the MDA-MB231 genome. *The number of regions identified as differentially methylated following SAHA treatment comparing 0 with 24-hours, 24 with 48-hours and 0 with 48-hours in MCF7 (grey) and MDA-MB231 (red) cells.*

The DMRs were then analysed to confirm how many regions gained methylation and how many lost methylation following SAHA treatment. The list of DMRs was filtered, selecting those with an areaStat>10 or <-10. AreaStat provides a way to rank DMRs, with larger values more likely to represent DMRs. The bsseq package defined areaStat as the sum of the test statistics of the CpG sites contained in the DMR (Feng and Wu, 2019). AreaStat combines the length (number of CpGs) and height (methylation difference between groups) – as both are important when ranking DMRs. The methylation pattern observed in both cell-lines was similar to previous analysis (Figure 5.3).

As shown in Figure 5.5, SAHA treatment induced an initial loss in methylation by 24-hours. Three times as many regions lost as gained methylation in MCF7 cells during 0 and

24-hours, while ten times as many did in MDA-MB231 cells. A greater number of DMRs then exhibited a gain in methylation between 24 and 48-hours. The greatest difference in their response was evident comparing 0 with 48-hours. A similar number of regions in MCF7 cells lost and gained methylation in this comparison, while four times as many MDA-MB231 regions exhibited a loss in methylation. Far fewer regions exhibited a significant change in methylation in MCF7 cells, suggesting that a more regulated response occurred in these cells. MDA-MB231 cells exhibit a greater change in methylation in response to SAHA treatment and appear slower in regulating this SAHA-induced methylation.

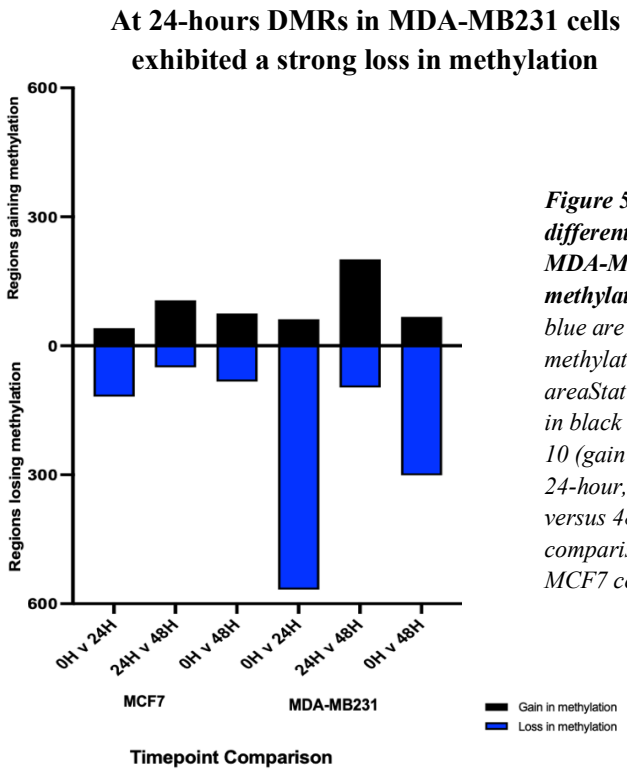


Figure 5.5: A greater number of differentially methylated regions in MDA-MB231 cells exhibited a loss in methylation at 24 hours. *Depicted in blue are the number of differentially methylated regions exhibiting an areaStat>10 (loss of methylation) and in black are those with an areaStat <-10 (gain in methylation) in the 0 versus 24-hour, 24 versus 48-hours and 0 versus 48-hour SAHA treatment comparisons in MDA-MB231 and MCF7 cells.*

The DMRs were then considered based on their location, selecting only those found at gene promoters (Figure 5.6). A similar number of DMRs were located at gene promoters across all the MCF7 timepoint comparisons. However, in MDA-MB231 cells a greater

number of DMRs were located at promoters in the 0 and 24-hour comparison. Twice as many DMRs were identified at this timepoint comparison compared with the number identified in MCF7 cells. Filtering the DMRs located at promoters to show only those with an areaStat >10 or <-10 was used to indicate whether these regions gained or lost methylation following SAHA treatment (Figure 5.7). A greater number of DMRs in MCF7 cells exhibited a loss in methylation at 24-hours, more gained methylation between 24 and 48-hours while a similar number of regions gained and lost methylation at 48-hours. In MDA-MB231 cells, at both 24 and 48-hours a greater proportion of the DMRs exhibited a loss in methylation in response to SAHA treatment. This analysis confirmed that the size and genomic location of a CpG site dictated its speed of change. Methylation at single CpG sites occurred remarkably quickly. This could explain the larger number of DMSs compared with DMRs identified in both cell-lines and how the CpG sites in Figure 5.1 exhibit such dramatic changes across 48-hours. This was also confirmed by the limited change in mean methylation observed at the DMRs within promoters.

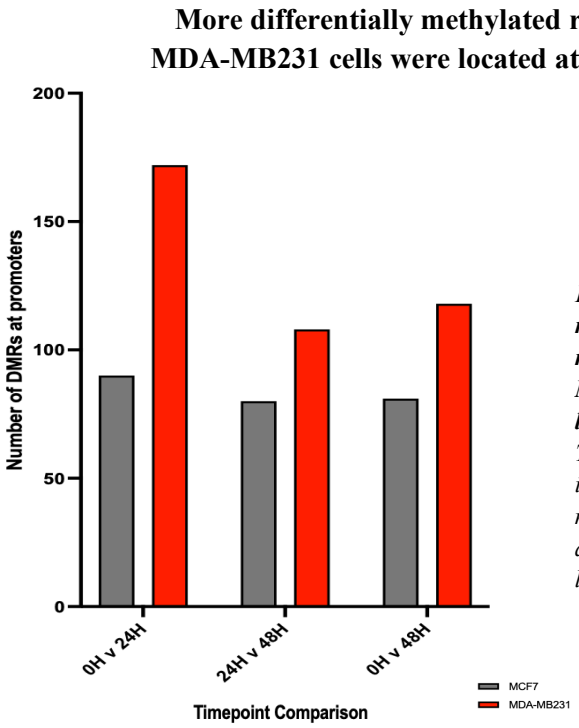


Figure 5.6: A greater number of differentially methylated regions in MDA-MB231 cells were located at gene promoters. *The number of regions identified as differentially methylated in MCF7 (grey) and MDA-MB231 (red) located at gene promoters.*

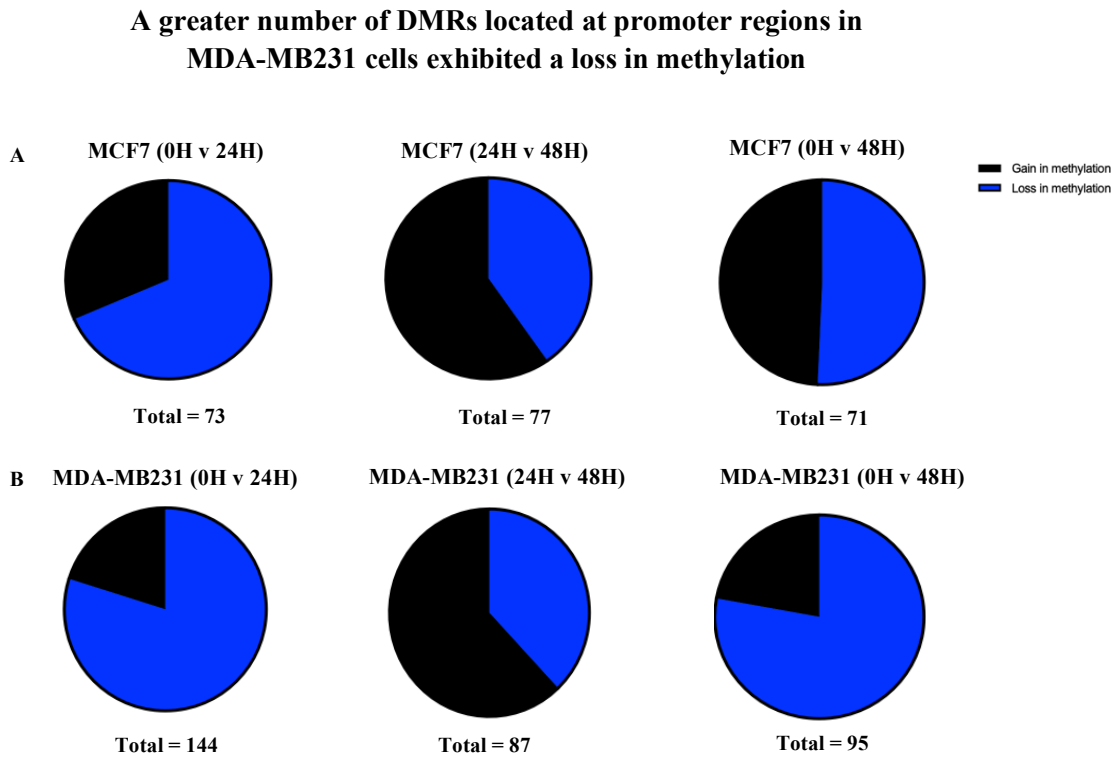


Figure 5.7: A greater number of DMRs located at promoter regions in MDA-MB231 cells exhibited a loss in methylation in response to SAHA treatment. *The number of DMRs found at promoters at 0 versus 24-hours, 24 versus 48-hours and 0 versus 48-hours in A. MCF7 and B. MDA-MB231 cells. Depicted in blue are those exhibiting an areaStat>10 (loss in methylation) and in black an areaStat <-10 (gain in methylation).*

This analysis suggests that this may be a homeostatic methylation response. Are we observing cells trying to return to their pre-treatment methylation state? The initial loss in methylation observed following 24-hour SAHA treatment was corrected, with CpG regions gaining methylation between 24 and 48-hours. By 48-hours, a similar number of sites and regions in MCF7 cells gained and lost methylation. This indicated that this cell-line was more stable, with fewer methylation changes induced in response to SAHA treatment. It also suggested that MCF7 cells can regulate their methylation levels more quickly. On the other hand, MDA-MB231 cells appeared to act more dynamically and exhibited a greater overall change in methylation state across the 48-hours.

A loss in methylation at 24-hours could be explained by the fact that HDACs regulate the stability of DNMT1. DNMT1 is regulated through acetylation, with deacetylation activating it and acetylation targeting it for proteasomal degradation (Peng *et al.,* 2011; Zhou *et al.,* 2008). Treatment of cells with an HDACi results in an increase in cellular acetylation which leaves DNMT1 no longer protected by HDACs and, therefore, targeted for ubiquitination. On the other hand, TF binding also alters DNA methylation patterns. It has been shown that CTCF and OCT4 can bind at methylated regions and recruit TET enzymes, inducing demethylation and keeping these regions unmethylated (Héberle and Bardet, 2019). Luo *et al.* also showed in 2021 that methylation was reduced near CTCF binding sites, again suggesting that this TF may play a role in promoting DNA demethylation.

5.3 Ontology confirmed that methylation was not related to coordinated gene expression changes

Ontology analysis was carried out to determine which cell processes were upregulated in response to 24 or 48-hour SAHA treatment. As these timepoints differed from the 2-hour time course used for the RNA-Sequencing, we did not expect any crossover in the identified gene processes. To determine which processes were enriched at promoters identified within DMRs, regions exhibiting an areaStat>10 or <-10 were assessed using DAVID. No significant outputs were identified, which indicated that the identified methylation changes were not related to coordinated gene expression changes. No crossover existed when considering the DMRs at gene promoters in both cell-lines, indicating that their responses were unique. This confirmed that though the pattern of CpG

change observed was similar, no common methylation response was employed in our cell-lines in response to SAHA treatment. However, this was limited in only being able to include DMRs located at the promoters of named genes.

5.4 Motif analysis indicated that the methylation response was not TF specific

The interest in downstream methylation stemmed from the question of whether long term changes following SAHA treatment were induced through methylation. The identified DMRs were analysed using HOMER. The aim of this was to look for TFs bound at regions that exhibit a change in methylation 24 or 48-hour following SAHA treatment. As the SAHA treatment time differed, these results could not be correlated with those identified from the RNA-Sequencing.

All the DMRs identified following 24 or 48-hour SAHA treatment time with an areaStat>10 or <-10 were initially assessed. Only analysis of the 368 regions identified in MDA-MB231 cells at 48 versus 0-hours identified significant motif matches. The predicted binding sites for OSR1 (Odd-Skipped Related Transcription Factor) and SOX2 (SRY-Box Transcription Factor 2) were identified, though these matches arose from only around 1% of the target genes (Figure 5.8).

OSR1 and SOX2 binding sites were enriched among the 48-hour DMRs in MDA-MB231 cells

	Motif Logo	p-value	%Target/%Background	Best Match
A		1e-10	1.68/0.02	OSR1
B		1e-9	1.12/0.00	SOX2

Figure 5.8: OSR1 and SOX2 binding sites were enriched in DMRs at 48-hours in MDA-MB231 cells. *HOMER identified the A. OSR1 and B. SOX2 binding sites from the differentially methylated regions at 48 versus 0-hours in MDA-MB231 cells.*

This was followed by a consideration of those exhibiting the greatest difference in their methylation between time-points. Analysis of all DMRs showing a difference in methylation >0.4 or <-0.4 between 0 and 24-hours or 0 and 48-hours identified only probable false positive matches. We then considered DMRs located at gene promoters. A significant match was only evident analysing the 0 v 24-hour comparison in MCF7 cells, which identified the predicted LIN54 (Lin-54 DREAM MuyB Core Complex Component) binding site (Figure 5.9A). The ZNF341 (Zinc Finger 341) binding site was identified from DMRs at promoters at 24-hours, and the NFAT (Nuclear factor of activated T-cells) binding site from DMRs identified at promoters at 48-hours in MDA-MB231 cells (Figure 5.9B/C).

DMRs located at promoters were enriched for LIN54, ZNF341 and NFAT binding sites

	Motif Logo	p-value	%Target/%Background	Best Match
A		1e-12	10/0.26	LIN54
B		1e-15	4.84/0.04	ZNF341
C		1e-16	4.58/0.01	NFAT

Figure 5.9: LIN54, ZNF341 and NFAT binding sites were enriched among DMRs in gene promoter regions. *A. The LIN54 binding site was identified among all differentially methylated regions at promoters in MCF7 cells in the 0 versus 24-hour comparison. In MDA-MB231 cells, B. the ZNF431 binding site was identified in the 0 versus 24-hour and B. the NFAT binding site in the 0 versus 48-hour comparison when considering all differentially methylated regions at gene promoters.*

5.5 Are MCF7 cells inherently better at regulating methylation changes?

An important question emerging from this analysis was whether MCF7 cells were better at regulating SAHA-induced methylation changes. The greatest difference between the cell lines seemed to result from MDA-MB231 cells being slower to balance the HDACi-induced methylation. The involvement of *DNMT* and ten-eleven translocation (*TET)* genes was therefore considered. As previously discussed, DNMTs facilitate DNA methylation – either *de novo* or maintenance methylation (Okano *et al.,* 1999). On the other hand, TETs oxidise 5-methylcytosine to 5-hydroxymethylcytosine and promote DNA demethylation (Ito *et al.,* 2010).

The basal expression of *DNMT* and *TET* genes was therefore assessed. *DNMT1* was similarly expressed in MCF7 and MDA-MB231 cells, while *DNMT3A* and *DNMT3B* were more highly expressed in MCF7 cells. Little difference was observed in the expression of *TET1* but *TET2* and *TET3* were more highly expressed basally in MCF7 cells (Figure 5.10). Interestingly, their expression was not affected by SAHA treatment. The difference in their basal expression could perhaps explain the more controlled response observed in MCF7 cells.

This was then investigated in the literature. *TET* gene depletion or mutation occurs in cancer. *TET* gene expression was significantly reduced in breast and liver tumour cells versus matched normal tissue (Yang *et al.,* 2013). TET1, 2 and 3 are all acetylated. Thus, we next researched whether acetylation regulates TET activity. The acetylation of the K110 residue on TET2 increases its enzymatic activity, protein stability and interaction with DNMT1 (Zhang *et al.,* 2017). TET2 is recruited to chromatin to remove the aberrant methylation induced in tumour cells during oxidative stress – protecting them from

abnormal DNA methylation (Zhang *et al.,* 2017). This raises the question of whether TET protein acetylation explains the improved survival of MCF7 cells? To address this, the acetylation of TET2 and TET3 following HDACi treatment in these cell-lines could be assessed.

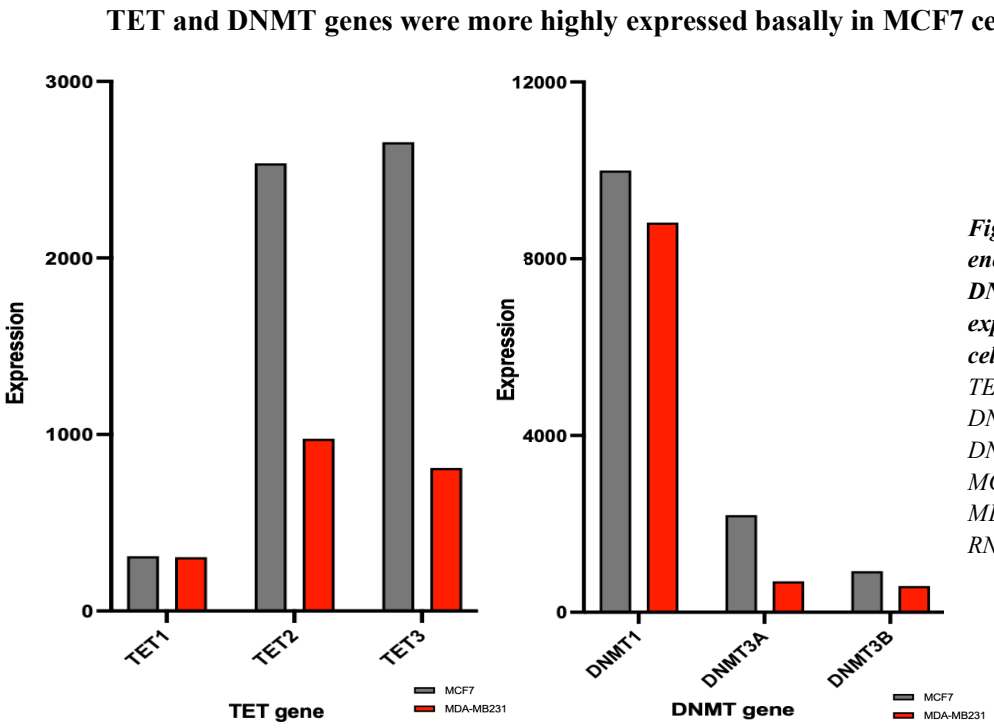


Figure 5.10: The genes encoding Tet2, Tet3 and DNMT were more highly expressed basally in MCF7 cells*. The expression of A. TET1, TET2 and TET3 and B. DNMT1, DNMT3A and DNMT3B in pre-treatment MCF7 (grey) and MDA-MB231 (red) cells from the RNA-Sequencing data.*

5.6 Chapter conclusions

This work was carried out to investigate whether DNA methylation was involved in the early transcriptional response following HDACi treatment. Though there was no evidence that this was the case, this analysis highlighted that dynamic methylation changes were induced in both cell-lines in response to 24 and 48-hour SAHA treatment. Similar methylation patterns were observed in both cell-lines. No overlap was evident when considering their DMRs, indicating that though their response was similar in nature, it did not involve a common set of genes. This may contribute to the difference in their HDACi

sensitivity. This response was characterised by an initial loss in methylation at 24-hours, balanced by a gain in methylation from then until 48-hours. This emphasised the importance of looking at the dynamics of change, with the chosen timepoint comparisons effectively capturing overall change. SAHA-treatment induced a greater overall change in methylation in MDA-MB231 cells. These cells were also less able to balance these changes by 48-hours.

Basal methylation levels can be compared using RRBS. However, the RRBS analysis in this project focussed on differences in methylation at CpG sites in the MCF7 and MDA-MB231 cells in response to 24 or 48-hour SAHA treatment. Without considering basal methylation, we do not understand the context within which these changes occur and whether MCF7 cells are better at regulating methylation.

We do not yet understand how gene expression changes induced in response to SAHA relate to histone modifications. ChIP samples were generated to H3K27ac and H3K27me3 in MCF7 and MDA-MB231 cells following 30, 60 or 120-minute SAHA treatment. These marks were selected as H3K27ac would identify active genes, and H3K27me3 repressed genes. This would enable the histone modifications occurring at regions which then go on to exhibit differential methylation at 24 or 48-hours to be examined. This would address whether early gene expression changes were tied to later DNA methylation changes and whether transcription or methylation changes occurred independently of histone PTMs. These samples were generated but have not yet been sequenced.

6. DOES POU2F2 PLAY A ROLE IN THE HDACi SURVIVAL RESPONSE?

A set of TFs potentially involved in the HDACi survival response were identified from the RNA-Sequencing and subsequent motif analysis. Their importance in mediating the response of our HDACi sensitive and more HDACi resistant cell-lines to SAHA treatment was then tested through knockdown analysis. Factors were knocked down individually, or in combination, and the effect of knockdown determined by investigating the loss in viability observed in Annexin V Assays following 48-hour SAHA treatment. Those significantly affecting cell viability were followed up by qPCR, assessing whether the initial transcriptional response was perturbed following knockdown.

6.1 Identification and verification of targets for knockdown

It was hypothesised that knocking down TFs involved in mediating early gene expression changes in response to SAHA would prevent this specific transcriptional response and enhance the HDACi sensitivity of MCF7 cells. This work followed on from HOMER analysis, identifying consensus motifs within the promoters of genes differentially expressed in MCF7 cells following 30, 60 or 120-minute SAHA treatment. This analysis identified POU(OCT), ATF/CREB, SRF and SMAD binding sites. The next step in identifying potential driver genes in the HDACi survival response involved investigating the expression of the individual family members from the RNA-Sequencing data. Selected for knockdown analysis were factors more highly expressed in our resistant cell-lines or those regulated by acetylation.

6.1.1 SRF was identified among genes upregulated by 30-minutes in MCF7 cells

SRF was the first motif identified among genes significantly upregulated after 30-minute SAHA treatment displaying a fold-change>2. This is a member of the MADS (MCM1, AG, DEFA and SRF) box TF family (Shore and Sharrocks, 1995). This factor was characterised as the gene regulator induced upon treatment of starved cells with serum (Miano *et al.,* 2007). It was named SRF as it was discovered binding to the serum response element (SRE) in the promoter of the *c-fos* gene (Norman *et al.,* 1988). SRF binds the CArG box, which is the region of the SRE that regulates promoter inducibility in response to growth factors (Treisman *et al.,* 1992). It binds to DNA as a homodimer, promoting the transcription of genes encoding growth factor and cell cycle proteins (Treisman *et al.,* 1992; Khachigian and Collins, 1997). SRF regulates the expression of IER, muscle and neuronal genes (Treisman, 1987; Chai and Tarnawski, 2002).

The number of IER genes identified as upregulated by 30-minutes in our resistant cell-line lends confidence to this as a potential target for knockdown. It was hypothesised that SRF knockdown and loss of the IER, would leave MCF7 cells more sensitive to HDAC inhibition. Knockdown work began with this factor.

6.1.2 SMAD Family Member were similarly expressed in both cell-lines

The second motif identified by HOMER from the 30-minute downregulated genes (p<0.05) was SMAD Family Member 3 (SMAD3). The SMAD family got their name due to their similarity to the *C.elegans* Sma proteins and Mad proteins in Drosophila

(Liu *et al.,* 1996). These proteins recognise the Smad-binding element (SBE) on DNA (Massagué *et al*., 2005). They are involved in cytokine signalling and play a central role in the transforming growth factor β (TGF-β) pathway. SMAD2 and SMAD3 control TGF-β target genes through interactions with coactivators or repressors such as p300 (Simonsson *et al.,* 2006). SMAD proteins are made up of two domains, attached by a linker region (Shi and Massagué, 2003). The N-terminal region, referred to as the Mad-homology 1 domain binds DNA. The Mad-homology 2 domain is where TGF-β phosphorylation and the interactions with p300 or CBP occur (Kamato *et al.,* 2020; Pouponnot *et al.,* 1998). It has been suggested that SMADs may influence chromatin structure, with HDACs evident in SMAD complexes (Kang *et al.*, 2005). Though primarily regulated by phosphorylation, SMAD7 was the first family member identified as acetylated (Simonsson *et al*., 2005). SMAD2/3 have now been shown to be acetylated by p300 and CBP, with SMAD2 additionally acetylated by P/CAF. Their transcriptional ability is improved through this PTM (Simonsson *et al*., 2006; Inoue *et al.,* 2007; Tu and Luo, 2007).

The motif enrichments identified SMAD Family members 2-5. To discern which family member was the best match in this instance, their expression from the RNA-Sequencing was considered. Expression of the family members was similar across both cell-lines (Figure 6.1). *SMAD3* and *SMAD5* were most highly expressed and expressed to a similar extent in both. Their expression did not change in response to SAHA treatment. The initial criterion for a knockdown target was a TF differentially expressed between the sensitive and resistant line. As their expression patterns were similar in both cell-lines, this gene family was not considered a potential target for knockdown.

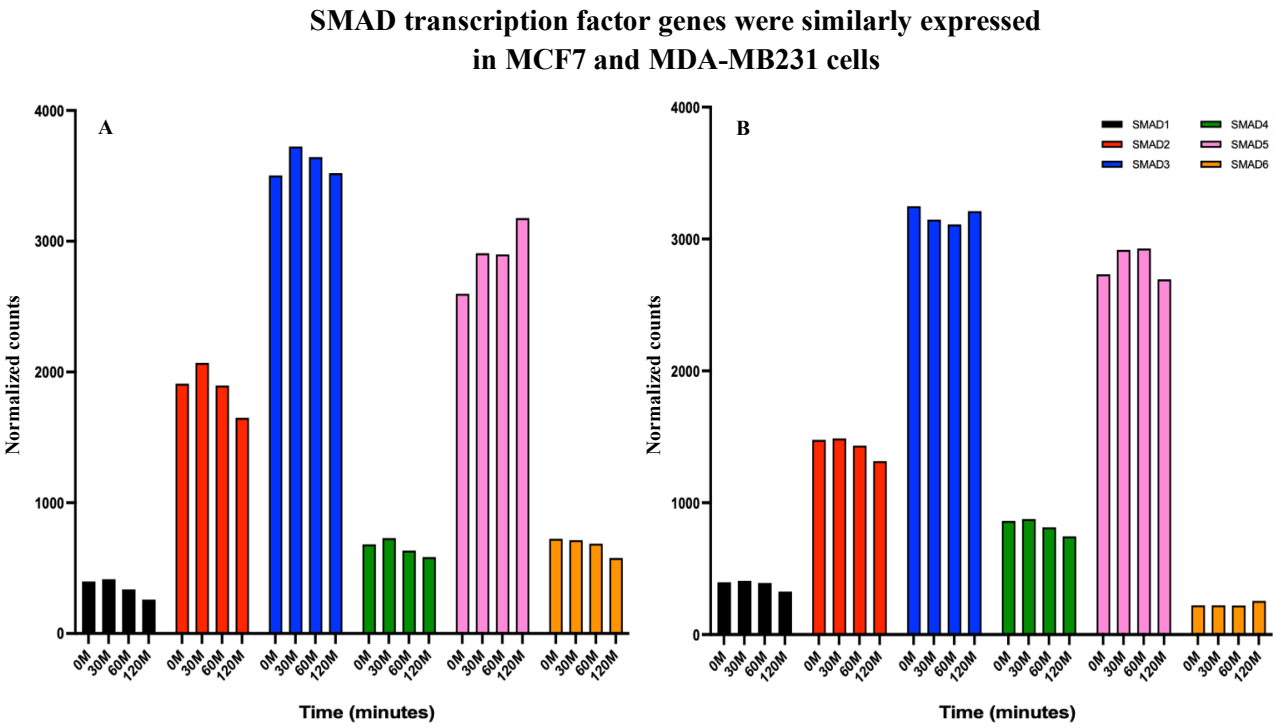


Figure 6.1: SMAD transcription factor genes were similarly expressed in the MCF7 and MDA-MB231 cells. *Normalized counts values for the SMAD protein genes after treatment with 2.5 μM SAHA for 30, 60 or 120-minutes relative to pre-treatment expression in A. MCF7 and B. MDA-MB231 cells from DESeq2 analysis.*

6.1.3 The expression of POU2F2 differed between our cell-lines

The binding site for OCT6, also known as POU3F1, was identified among genes significantly downregulated in MCF7 cells following 30- and 60-minute SAHA treatment. The POU domain family were identified based on the sequence homology of the mammalian Pit-1, Oct-1, and Oct-2 factors (POU) and the nematode Unc-86 protein (Herr *et al.,* 1988). They contain two transcriptional activating domains, attached to a central DNA binding POU domain. This is formed of two distinct elements, the POU-homeodomain as well as the POU-specific domain - which is unique to these factors (Qin *et al.,* 1994). As the naming suggests, the POU specific domain mediates high-affinity DNA binding. These two subdomains are attached by a short linker (Latchman, 1999). Oct proteins are a highly conserved subclass of this family that recognise an 8 base-pair consensus DNA sequence, ATGC(A/T)AAT, known as the 'octamer motif'

(Tantin, 2013). This motif is identified in the promoters and enhancers of many ubiquitous as well as cell-type specific genes (Zhao *et al.,* 2004; Schöler *et al.,* 1989). The POU TFs positively or negatively regulate the expression of genes including histone H2B or immunoglobulins (Shakya *et al*., 2011; Schöler, 1991). Oct proteins were originally thought to function as monomers, however, there is now evidence that they form homo and heterodimers (Jacobson *et al.,* 1997). POU2F1 and possibly POU2F2 are ubiquitously expressed, while the other POU proteins exhibit tissue-specific expression patterns (Zhao *et al.,* 2004; Dong and Zhao, 2007; Veenstra *et al.,* 1997).

The motif matches identified members of this family including *POU2F2* and *POU5F1*. Expression of the individual POU family members was analysed from the RNA-Sequencing, to identify which family members could be driving gene expression change at this time. As shown in Figure 6.2A, *POU2F1* was most highly expressed in MCF7 cells with SAHA treatment having little effect on its expression. *POU2F1* was similarly expressed in MDA-MB231 cells, but alongside a similar expression of *POU2F2* (Figure 6.2B). This was the opposite expression pattern to that hypothesised. The hypothesis involved a TF expressed in the resistant, and not sensitive cells, which when knocked down would leave the resistant cells more sensitive to HDACi treatment. This alternative expression pattern produced a new hypothesis – based on the Bentrari *et al.,* 2015 publication. POU2F1 may be a key player in the HDACi survival response, with its action suppressed in some cells by POU2F2. This led to the hypothesis that knockdown of POU2F2 in our more sensitive cells would enable them to mount the HDACi survival response.

Primers were designed to validate the expression of the POU family members in both cell-lines by qPCR. POU2F2 mRNA was not expressed in MCF7 cells but was highly expressed in MDA-MB231 cells (Figure 6.3). *POU2F1, POU5F1*, and *POU3F1* were less highly expressed in both cell-lines though they exhibited around a ten-fold greater expression in MCF7 cells. This showed that *POU2F2* was differentially expressed between our cell-lines, highlighting POU2F1 and POU2F2 as our next targets for knockdown analysis.

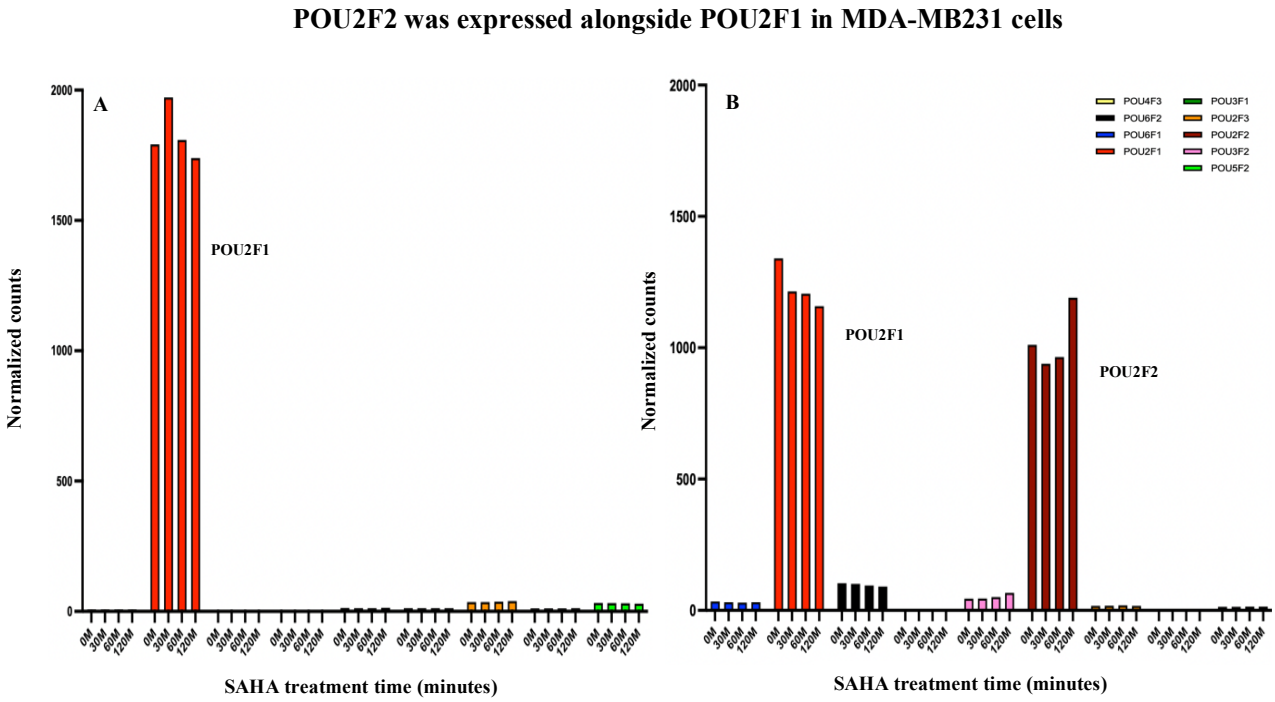


Figure 6.2: POU2F1 was expressed similarly in both cell-lines, while POU2F2 was expressed only in MDA-MB231 cells. *Normalized counts values of the POU domain family protein genes, common to both cell-lines, after 0, 30, 60 or 120-minute SAHA treatment in A. MCF7 and B. MDA-MB231 cells from DESeq2 analysis.*

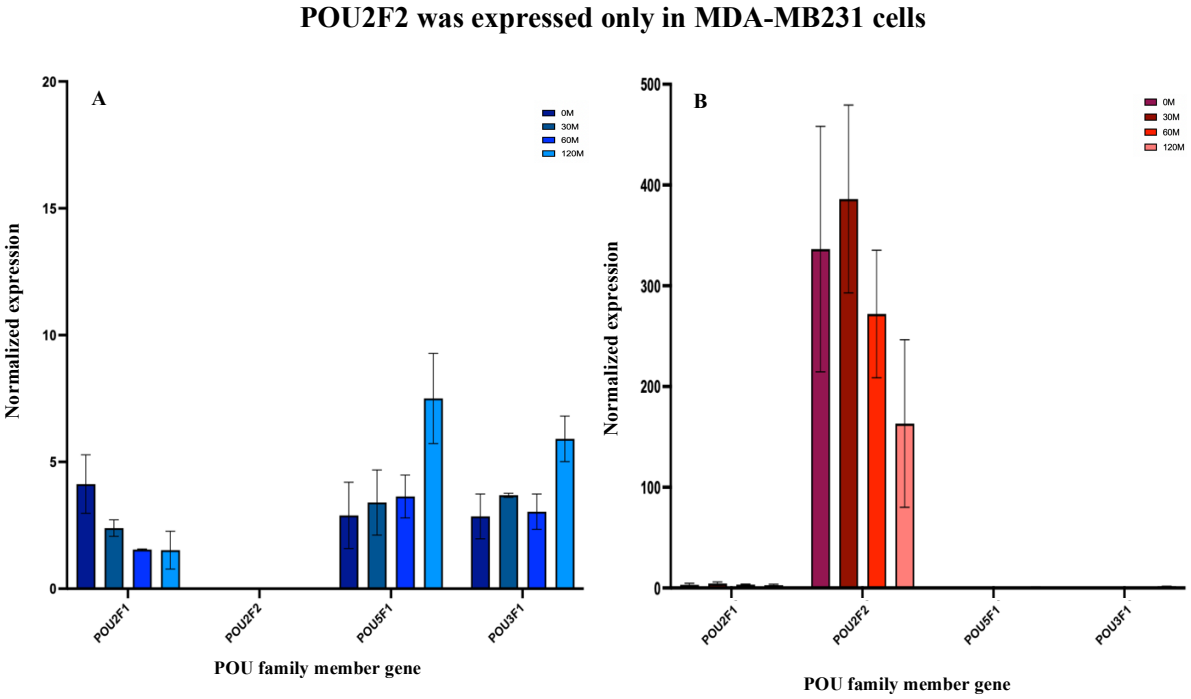


Figure 6.3: POU2F2 mRNA was expressed only in MDA-MB231 cells. *The expression of the POU domain family protein genes POU2F1, POU2F2, POU5F1 and POU3F1 after 30, 60 or 120-minute SAHA treatment normalized to housekeeper gene expression in A. MCF7 and B. MDA-MB231 cells was assessed by qPCR. Error bars show SEM of independent experiments (N=3).*

POU2F1 operates through Jmjd1a and NuRD, altering the repression or inducibility of genes (Shakya *et al.,* 2011). Its target genes are upregulated in several cancers, without POU2F1 itself being upregulated – suggesting its activity may be dysregulated in cancer **(**Shakya *et al.,* 2011). Interestingly, high levels of POU2F1 have been associated with resistance to stress (Tantin *et al.,* 2005). POU2F2 both activates and represses genes (Friedl and Matthias, 1995). This factor was initially considered a B-cell specific TF (Clerc *et al.,* 1988). POU2F2, however, is expressed in several solid tumours. Its expression provides the prognosis of gastric, pancreatic, and clear cell renal cell carcinoma patients (Katoh and Katoh, 2009; Marin-Muller *et al.,* 2013; Qin *et al.,* 2019). For example, POU2F2 is involved in cell networks promoting metastasis in gastric and triple-negative breast cancer cells (Wang *et al.,* 2016; Zhang *et al.,* 2019).

6.2 SRF knockdown did not affect the SAHA sensitivity of MCF7 cells

SRF was the initial target knocked down. The first step involved an optimisation of the Lipofectamine 3000 protocol in our cell-lines, as detailed in Appendix 10.6. This was followed by a time-course experiment designed to determine the optimum length of time for transfection. This was required as previous work in the lab had assessed plasmid incorporation at 48-hours, while this work involved siRNA. MCF7 cells were transfected with 10 nM SRF siRNA (ORIGENE), harvested on days 1-4 post transfection and *SRF* expression quantified by qPCR on each of these days. The ORIGENE transfection formulation includes three SRF siRNAs (A-C) alongside a scrambled, non-targeted negative control siRNA D. The greatest knockdown in *SRF* expression was observed after 24-hours (Figure 6.4). siRNA A was most effective - knocking down *SRF* expression by around 99% on Day 1. However, siRNA B and C appeared to lose effectiveness by Day 3 post-transfection. These results confirmed that cells would be treated with SAHA 24-hours after knockdown.

SRF knockdown was most efficient on Day 1 post-transfection

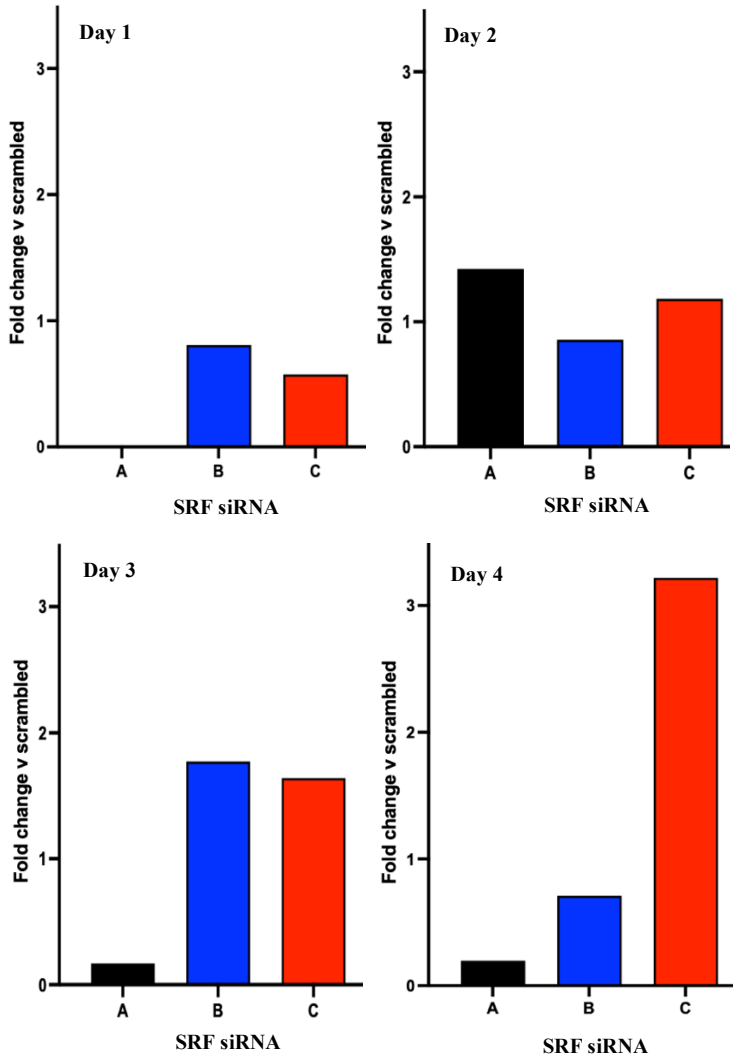


Figure 6.4: The most efficient SRF knockdown occurred on Day 1 using siRNA *A. Fold-change in SRF expression following treatment with siRNA A, B and C was calculated by qPCR compared with expression in MCF7 cells transfected with scrambled siRNA (D) on Day 1, Day 2, Day 3, and Day 4 post transfection. All data was initially normalized to housekeeper expression.*

An initial experiment was set up to knockdown *SRF* in MCF7 cells. The aim of this was to compare the apoptosis induced in cells transfected with scrambled and SRF siRNA and then treated with 2.5 μM SAHA for 48-hours. Plates were set up in triplicate. One set assessed the expression of *SRF* on Day 1 post-transfection. A second assessed *SRF* expression on Day 4 post-transfection in untreated, and SAHA treated cells to determine whether HDACi treatment affected *SRF* expression (data not shown). The final set was

used in the Annexin V Assay to assess whether SRF knockdown affected the sensitivity of MCF7 cells to SAHA treatment.

The extent of SRF knockdown, as calculated by qPCR, differed significantly between experiments (data not shown). No additional loss in viability was evident after knockdown and there was also little increase in the size of the apoptotic population (Figure 6.5). It was concluded from this work that SRF knockdown alone did not affect the sensitivity of MCF7 cells to HDACi treatment. However, a more consistent knockdown would be required to determine the role of SRF in the HDACi survival response.

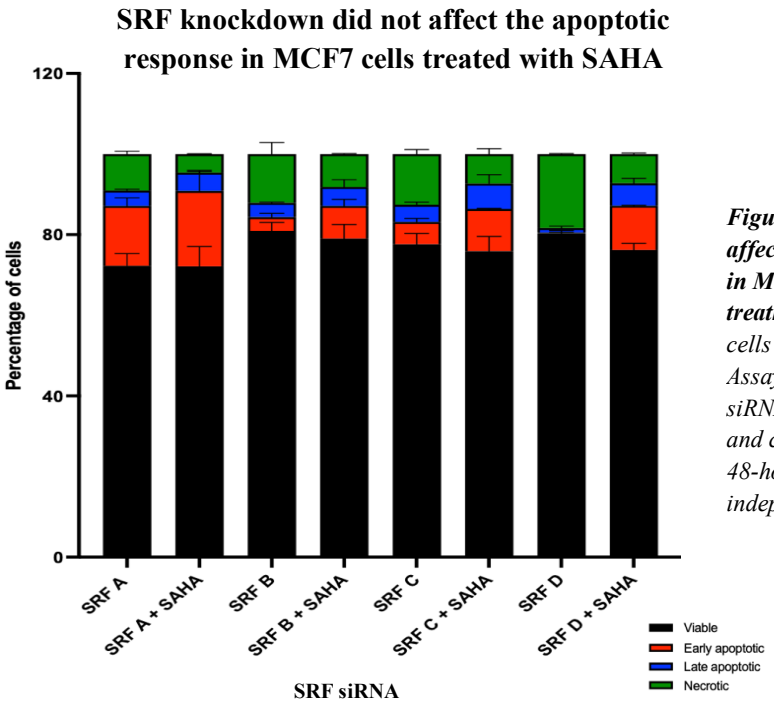


Figure 6.5: SRF knockdown did not affect the apoptotic response induced in MCF7 cells following SAHA treatment. *The proportion of MCF7 cells per quadrant of the Annexin V Assay following transfection with SRF siRNA A, B, C or D in untreated cells and cells treated with 2.5 µM SAHA for 48-hours. Error bars show SEM of independent experiments (N=2).*

6.3 POU2F2 transcript variant expression

Following the disappointing results with SRF, the POU family was then the next target for knockdown analysis. This work addressed the question of whether it is the expression of

POU2F2 that prevents POU2F1 being able to drive the HDACi survival response in MDA-MB231 cells. Before carrying out any knockdown experiments, the ten *POU2F2* transcript variants (TV) were analysed to confirm that POU2F2 mRNA was expressed only in MDA-MB231 cells. In addition, this analysis would ensure that the siRNA formulation used could knockdown all the expressed variants.

The initial primers were designed to amplify the *POU2F2* CDS, with a forward primer designed to amplify TV1-4, 6-10 and a second designed to the alternative TSS of TV5 (Table 2.1; Appendix 10.7). The TV1-10 primer was used with the Oct2 R reverse primer, located in an upstream exon shared by all the TVs. The size of the products amplified would differ based on the exons incorporated in each variant (Appendix 10.7). 40-cycle PCR reactions were carried out using ReddyMix at 60°C with the PCR products then run on a 2.5% Agarose gel alongside an 100 bp DNA ladder (New England Biosciences; Table 2.2). The outcome of these reactions was inconclusive with bands smaller than 100 bp evident in both cell-lines (data not shown). As these primers did not amplify product of the correct size, the cloning primers specified in the Bentrari *et al*., 2015 publication were amplified in the same manner. Again, no specific bands were observed. Considering the intended product size was around 1.5 kb, the Bentrari primers were amplified with Pfu DNA Polymerase (Table 2.3). It was thought that the proof-reading ability of this enzyme would enable the amplification of larger product sizes. However, this initial work confirmed that a polymerase more suited to this product size was required.

6.3.1 Dream Taq DNA Polymerase amplified the POU2F2 coding sequence

Validated up to 6 kb with genomic DNA, Dream Taq DNA Polymerase is considered more efficient with larger amplicons. A 35-cycle PCR reaction was set up using this enzyme and the Bentrari cloning primers. Increasing the annealing to 66°C and 68°C reduced the occurrence of non-specific binding, producing one distinct band around 1.2 kb only in MDA-MB231 cells (Figure 6.6).

The saturation of this band suggested that it may contain several variants of a similar molecular weight. To separate these molecular weight bands, the PCR products from the 68°C reaction were re-run on a 1.5% Agarose gel. Four products were identified within this band. These were identified as the bottom of the main band (1), the bulk of the main band (2) and the two faint bands above (3/4) (Figure 6.7A). A needle was used to select product from each of these regions for re-amplification. Following clean up, 5 µl of each DNA sample at 10 ng/µl was sent alongside 5 µl 3.2 pmol/µl Bentrari forward or reverse primer for sequencing. These results were analysed using Nucleotide Blast. Products 2-4 matched TV1 and 3, while product 1 matched TV2, 4 and 7. As shown in Figure 6.7B, when the four products were run on a 1.5% Agarose gel only product 4 appeared to be of a different molecular weight. It is likely, therefore, that the products sent for sequencing contained trace amounts of multiple variants.

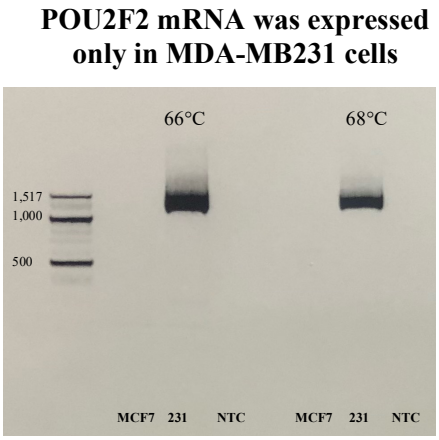


Figure 6.6: A 1.2 kb product was amplified only in MDA-MB231 cells. *Amplifications were carried out using Bentrari et al., 2015 POU2F2 primers with Dream Taq Polymerase at 66°C and 68°C in MCF7 and MDA-MB231 cDNA and the products run on a 2.5% Agarose gel alongside a non-template control. Product size was determined using a 100bp DNA ladder.*

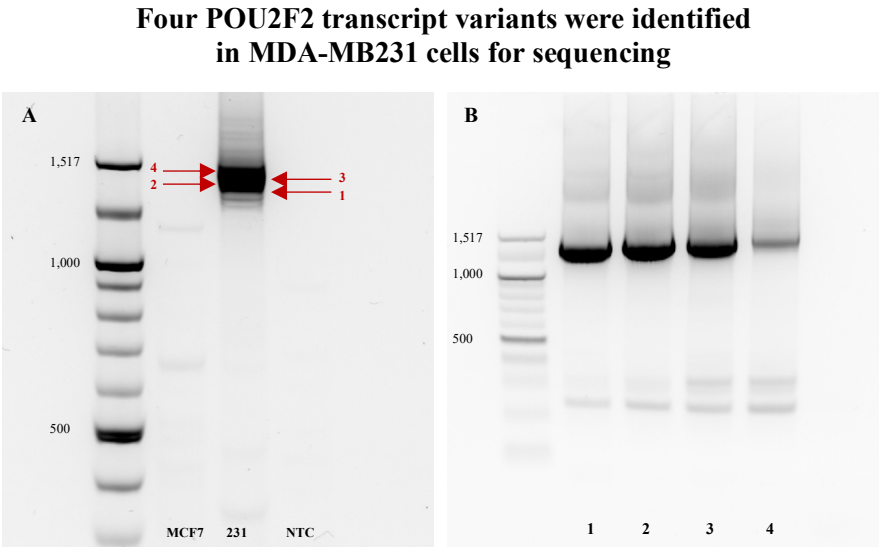


Figure 6.7: Four POU2F2 transcript variants were selected from MDA-MB231 cells. *A. An amplification was carried out using the POU2F2 coding sequence primers from Bentrari et al., 2015 with Dream Taq Polymerase at 68°C in MCF7 and MDA-MB231 cDNA and the products run on a 1.5% Agarose gel. Depicted in red are the four regions selected for sequencing. B. The four regions were re-amplified at 66°C, following DNA clean up, and run on a 1.5% Agarose gel. Product sizes were determined using a 100 bp DNA ladder.*

6.3.2 TV5 was not expressed in MDA-MB231 cells

The Bentrari primers do not amplify TV5, as they use an exon not included in this variant. Thus, TV5 specific primers were designed. Amplification of Oct2 TV5 forward and the Bentrari reverse primer did not produce a band of the expected size, suggesting that TV5 was not expressed. However, as *POU2F2* expression was the distinction

between our cell-lines this was confirmed using additional primers. The TV5 154F/R primers were designed to amplify the initial exons of TV5, while pairing 154F with the Bentrari reverse would amplify the TV5 CDS (Appendix 10.7). No band of the correct molecular weight was observed using either primer set, leading to the conclusion that TV5 was not expressed in either cell-line.

6.3.3 MDA-MB231 cells express four POU2F2 transcript variants

Based on the suggestion that multiple variants were expressed, the PCR reactions were repeated using the Bentrari forward and new Oct2 CDSb R primer. This primer was designed to improve on the mispriming with the original Bentrari R primer. A 35-cycle reaction, carried out with 64°C annealing, produced multiple faint bands around 1.2 -1.5 kb. The presence of four distinct molecular weight bands indicated that MDA-MB231 cells express four variants of the *POU2F2* gene (Figure 6.8A). These, however, could not be easily distinguished as individual variants. It was thought that the 1261 bp band represented TV4, 1396 bp represented TV2, 1445 bp TV1 and that the 1471 bp band was TV7. A needle was used to select products 5-8 to be sequenced using the Bentrari F and Oct2 CDSb R primer (Figure 6.8A). Nucleotide Blast matched products 5/6 to variants containing an 117bp exon 5 and 114bp exon 8 – suggestive of TV2, 4 or 7. Products 7 and 8 matched variants containing either an 114 bp or 162 bp exon 8 – indicative of a several variants. These inconclusive results can be explained by the presence of two distinct molecular weight bands in products 5/6 (Figure 6.8B).

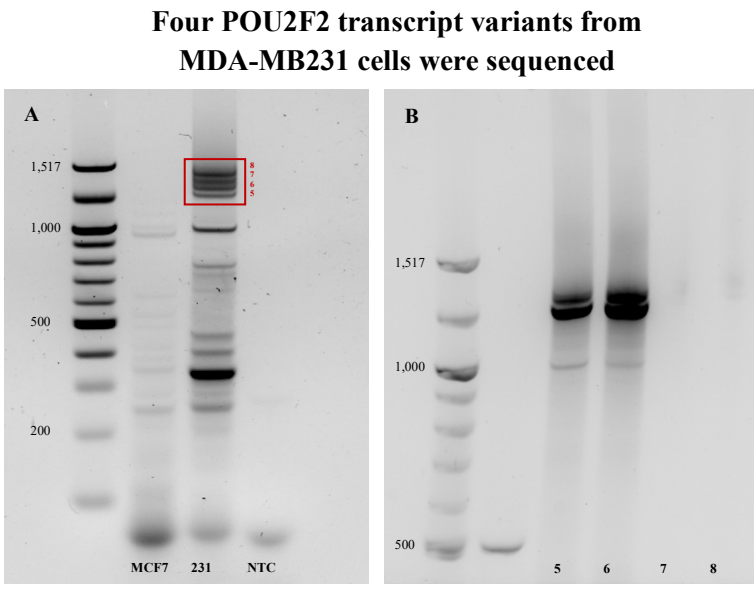


Figure 6.8: Four transcript variants identified in MDA-MB231 cells were sequenced. *A. An amplification was carried out using Bentrari F and Oct2 CDS R primer with Dream Taq DNA Polymerase in MCF7 and MDA-MB231 cDNA at 64°C annealing for 40-cycles. Indicated in red are the four bands from which sequencing products were selected. B. The four regions were re-amplified at 64°C with only two evident in a 2% Agarose gel. Product size was determined using a 100 bp DNA ladder.*

6.3.4 MDA-MB231 cells express TV1, 2, 4 and 7

The *POU2F2* variants differ most at the 3' end – which so far, sequencing and PCR amplification have provided little information on. Thus, exon inclusion was used to separate variants. The variants identified from the sequencing differ in the size of exon 8 incorporated. TV1 and 3 contain a 162 bp exon, while TV2, 4 and 7 incorporate a smaller 114 bp exon. Primers were designed across this exon boundary, with one set designed to the 92/162 boundary expressed in TV1/3 [TV1xx F/R] and a second forward primer designed to the 92/114 boundary of TV2,4,7 [TV2xx F]. The unique 66 bp exon of TV4 [TV4 66F] was also amplified as this would separate variants by their 3' structure. The TV4 66F and TV2xx forward primers were paired with the same POU2F2xx R primer. One product, matching the expected size of TV1, was observed in MDA-MB231 cells using TV1xx F/R (Figure 6.9). TV2xx F identified products matching the expected sizes of TV2, 4 and 7 - suggesting that TV4 was not as highly

expressed. The TV4 66F primer confirmed expression of all four variants in MDA-MB231 cells (Figure 6.9).

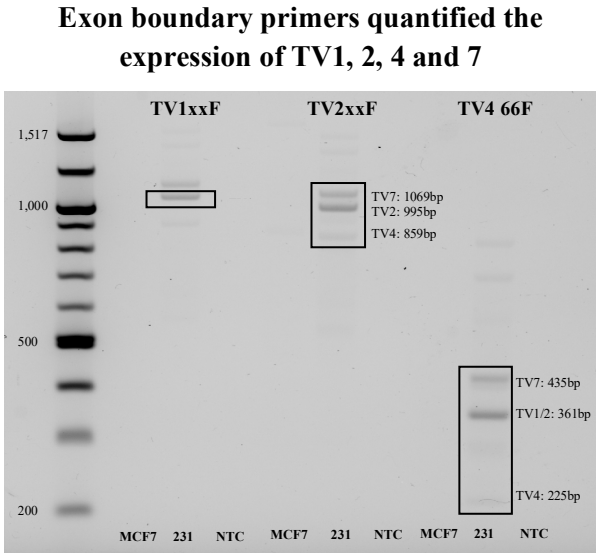


Figure 6.9: POU2F2 transcript variants 1,2, 4 and 7 were expressed in MDA-MB231 cells. *Amplifications were carried out using TV1xxF/R and the TV2xxF and TV4 66F primers with the POU2F2xx R primer using Dream Taq DNA Polymerase at 66°C for 35-cycles in MCF7 and MDA-MB231 cDNA. Products were run on a 2% Agarose gel with a 100 bp DNA ladder. Indicated are bands matching the expected size of the transcript variants.*

Primers designed around exon 8 (162F/R) were then used to determine whether there was a dominant *POU2F2* variant. These produced a product of either 162 bp or 114 bp based on the size of exon 8 incorporated. An approximately equal ratio of each variant size was expressed using an annealing temperature of 66°C (Figure 6.10A). This suggested that there was an equal ratio in expression of variants incorporating the 162 bp exon (TV1 or 3) to those incorporating the 114 bp exon (TV2,4 or 7). As this was observed following 35-cycles, an additional 30-cycle reaction was set up for a more quantitiative assessment. This showed that there was an equal ratio of the two exon 8 sizes observed (Figure 6.10B). As no TV3 sized product had been observed, this suggested that TV1 was the dominant *POU2F2* variant.

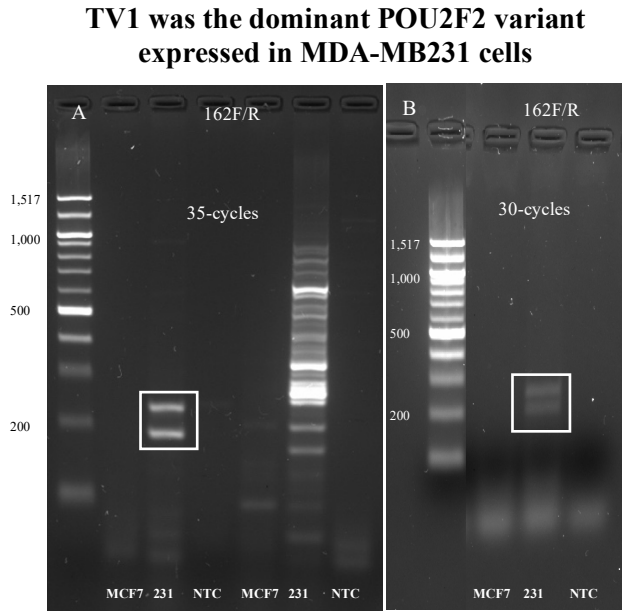


Figure 6.10: An equal ratio of the two exon 8 variants was expressed in MDA-MB231 cells. *A. 35-cycle amplifications were carried out using 162F/R primers with Dream Taq DNA Polymerase at 66°C in MCF7 and MDA-MB231 cDNA. B. 30-cycle amplifications were carried out using 162F/R primers with Dream Taq DNA Polymerase at 64°C in MCF7 and MDA-MB231 cDNA. The white boxes show the two exon 8 variant sizes – 162 bp or 114 bp.*

6.4 MCF7 and MDA-MB231 cells express distinct POU2F1 transcript variants

POU2F1 transcript variant expression was then analysed in both cell-lines. *POU2F1* is expressed in both cell-lines, however it is not known whether they express the same TVs. There are six *POU2F1* gene variants, with only five coding for protein as shown in Appendix 10.8. Exon boundary primers were designed to identify the unique exon structure of each variant. The TV2xx F/R primer set was designed across the exon boundary of the first two exons of TV2. The TV136xx F/R primer set was designed to the unique 73/65 exon boundary present in TV1,3 and 6 and paired with an upstream reverse to produce bands of differing molecular sizes based on their 3' structure. The TV5xx F/R set amplified the unique 73/203 exon boundary of TV5. The primer sets were amplified using DreamTaq DNA Polymerase at annealing temperatures of 64°C and 66°C. A 237 bp product, matching the expected size of the TV2 fragment, was observed only in the MDA-MB231 cells (Figure 6.11A). A 1060 bp product, matching the size of TV5, was expressed

only in MCF7 cells. Both cell-lines expressed TV1 and TV3, while neither expressed TV6 (Figure 6.11B).

MCF7 and MDA-MB231 cells express different POU2F1 transcript variants

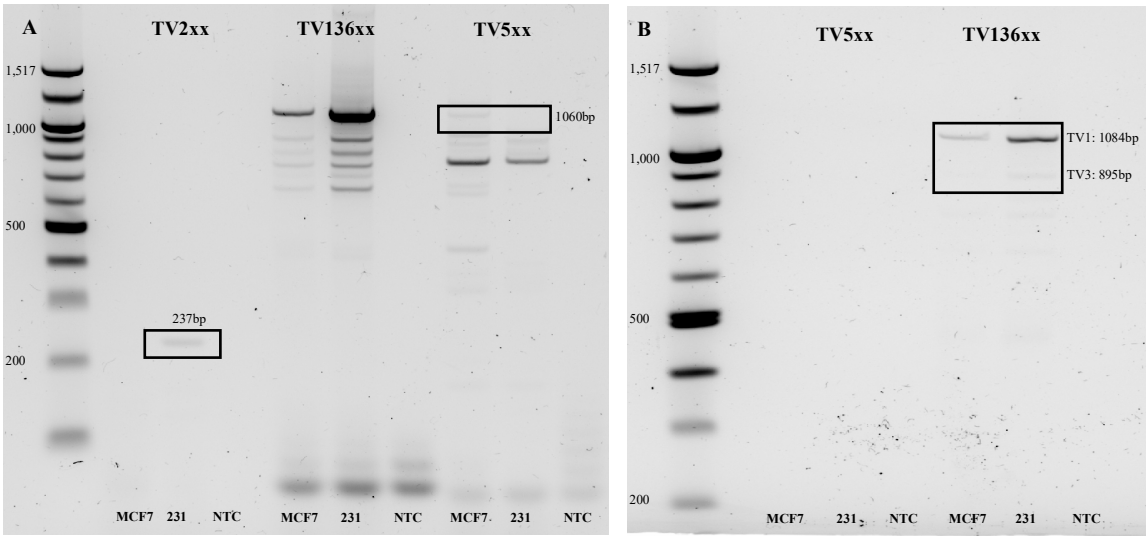


Figure 6.11: MCF7 and MDA-MB231 cells express different POU2F1 transcript variants. *A. Amplifications were carried out using TV2xx, TV136xx and TV5xx exon boundary primers at 64°C annealing with Dream Taq DNA Polymerase in MCF7 and MDA-MB231 cDNA and products run on a 2% Agarose gel for 2-hours. Indicated is the expression of TV2 in MDA-MB231, and TV5 in MCF7 cells. B. An amplification using TV136xx exon boundary primers was carried out at 66°C annealing with Dream Taq DNA Polymerase and the products run on a 2% Agarose gel for 3-hours. Indicated is the expression of TV1 and TV3 in both cell-lines.*

The *POU2F1* and *POU2F2* transcript variant analysis confirmed that *POU2F2* was expressed only in MDA-MB231 cells, with PCR bands corresponding to the expected molecular sizes of TV1, 2, 4 and 7 observed in this cell-line. TV1 appeared to be the dominantly expressed variant, with TV2 and 7 expressed more highly than TV4. No *POU2F2* transcript variant was evident in MCF7 cells. The analysis also confirmed that MCF7 and MDA-MB231 cells express different *POU2F1* transcript variants. TV2 was expressed only in MDA-MB231 and TV5 in MCF7 cells, while TV1 and TV3 were expressed in both cell-lines.

6.5 POU family member knockdown

Our hypothesis was that POU2F1 was important in driving the survival response, with the additional expression of POU2F2 preventing this occurring in the MDA-MB231 cells. Thus, having verified that *POU2F2* was expressed only in MDA-MB231 cells we then continued with an assessment of how knockdown of these two POU TFs affected the HDACi resistance of our MCF7 and MDA-MB231 cells. This work involved two steps. The first of which was the knockdown of POU2F2 in MDA-MB231 cells, creating cells with an expression profile more closely resembling MCF7 cells. This investigated whether POU2F2 knockdown would make the MDA-MB231 cells more resistant to HDACi treatment. Alongside this, POU2F1 was knocked down in MCF7 cells – with the aim of determining whether this created cells more sensitive to HDAC inhibition. Together, these experiments would explore the role of POU2F1 in mediating the survival response.

The experimental protocol involved comparing HDACi-induced apoptosis in cells transfected with POU2F2 or POU2F1 siRNA, cells transfected with scrambled siRNA, and untransfected cells. Untreated cells were compared with those treated with 2.5 μM SAHA for 48-hours. A duplicate plate was set up to quantify knockdown on the day that the Annexin V Assay was carried out.

6.5.1 POU2F2 knockdown resulted in MDA-MB231 cells more sensitive to HDAC inhibition

A new siRNA formulation was used in this work. Thus, an initial transfection was carried out to determine the extent of knockdown achieved using 25 nM POU2F2 siRNA (SMARTpool, Dharmacon), alongside 25 nM of the non-targeted scrambled

siRNA. Plates were harvested on Days 1, 2 and 3 post transfection and *POU2F2* expression assessed by qPCR to indicate the transfection efficiency. A 71% knockdown in *POU2F2* expression was observed on Day 1 – with knockdown maintained through to Day 3 when a 78.7% knockdown was observed (Figure 6.12A).

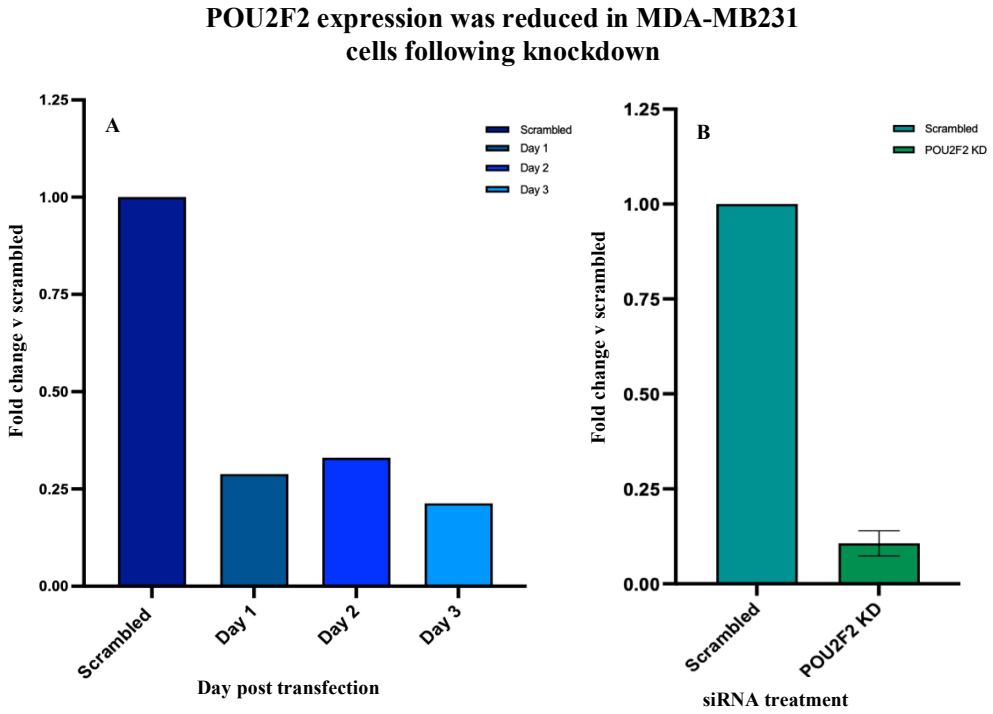


Figure 6.12: POU2F2 expression was reduced in MDA-MB231 cells following knockdown. *A. The fold change in POU2F2 expression in comparison to expression in scrambled siRNA treated cells on Days 1-3 post transfection was assessed by qPCR. B. Fold-change in expression of POU2F2 96-hours following knockdown compared with expression in cells transfected with scrambled siRNA. Error bars show SEM of independent experiments (N=5).*

Quantification by qPCR showed that *POU2F2* expression was depleted by 89.3% compared with expression in scrambled siRNA treated cells after 96-hours (Figure 6.12B). Analysis of the resulting viable populations from the annexin V/PI apoptosis assay indicated that POU2F2 knockdown enhanced the sensitivity of MDA-MB231 cells to HDACi treatment (Figure 6.13). SAHA induced a 38.9% loss in viability in untransfected cells, while cells transfected with scrambled siRNA exhibited a 36.8% loss in viability and those transfected with POU2F2 siRNA exhibited a 47.4% loss.

Interestingly, POU2F2 knockdown resulted in an accumulation of late apoptotic cells (Figure 6.13). The loss of around 10% in viability was observed with an increase in the number of cells in late apoptosis. This suggested that cells were progressing more quickly through apoptosis and that POU2F2 may be involved in mediating cell progression through this pathway.

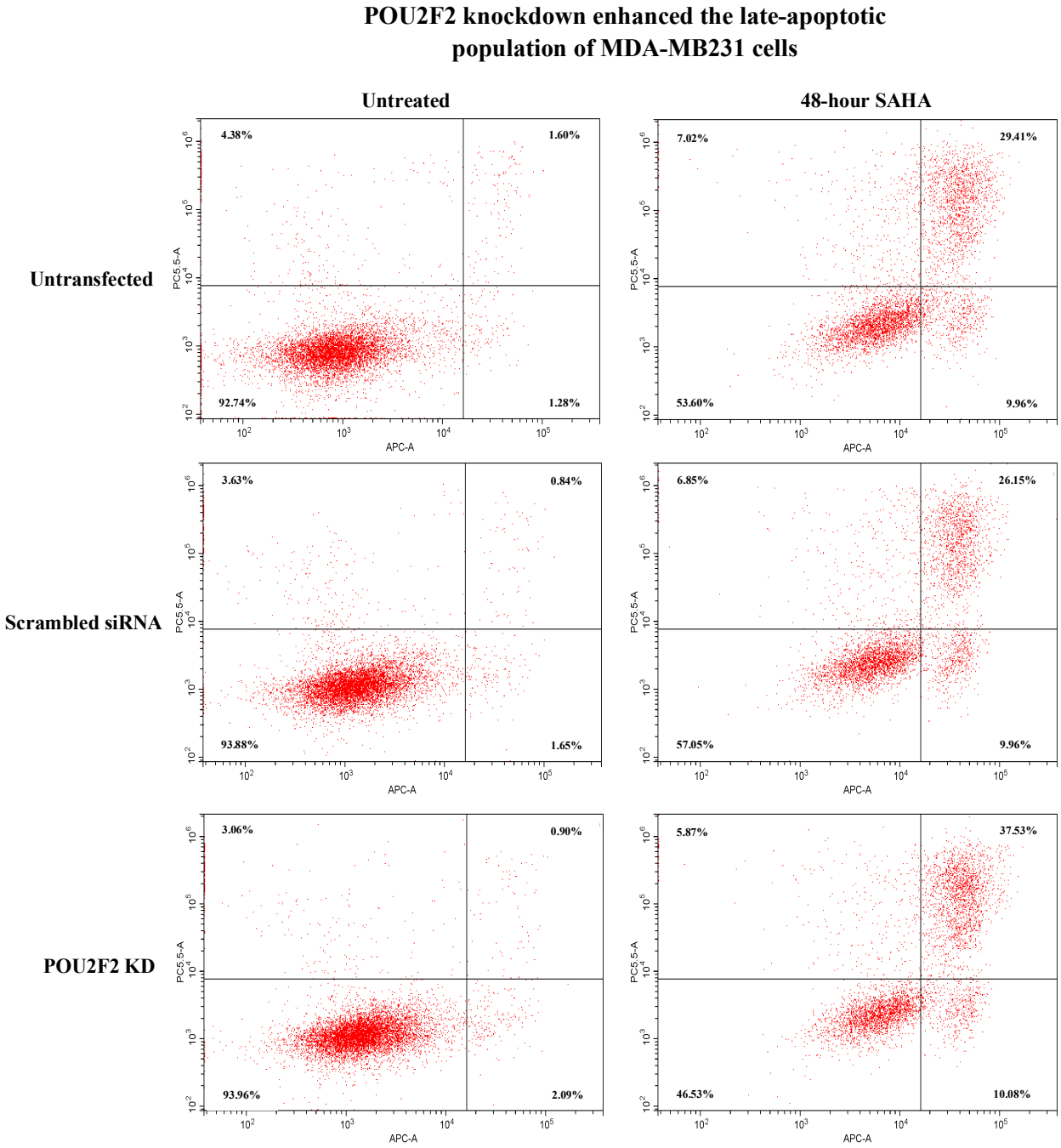


Figure 6.13: POU2F2 knockdown enhanced the apoptosis observed in MDA-MB231 cells following 48-hour SAHA treatment. *Apoptosis was assayed by the Annexin V/Propidium Iodide assay in untransfected cells, cells transfected with 25 nM scrambled or POU2F2 siRNA following treatment with 2.5 μM SAHA for 48-hours. Images generated using CytExpert 3.4 Software.*

POU2F2 knockdown did not affect untreated cells – indicating that loss of this factor did not affect the health of the cells in the absence of SAHA treatment (Figure 6.14A). Looking more closely, a significant increase in the late apoptotic population was evident comparing SAHA treated POU2F2 knockdown cells with the scrambled siRNA transfected control cells (Figure 6.14B; p=0.006). This suggested a role for POU2F2 in the induction of apoptosis in response to an HDACi. These results indicate that, when expressed, POU2F2 may protect breast cancer cells from HDACi-induced apoptosis. Identifying a TF that altered the apoptotic response of a cell to an HDACi was a novel finding. This led to the question of whether POU2F2 was an inhibitor of the HDACi survival response – with its knockdown resulting in cells more sensitive to HDAC inhibition? This finding differed significantly from the initial hypothesis - instead suggesting that POU2F2 knockdown created MDA-MB231 cells even more sensitive to HDACi treatment.

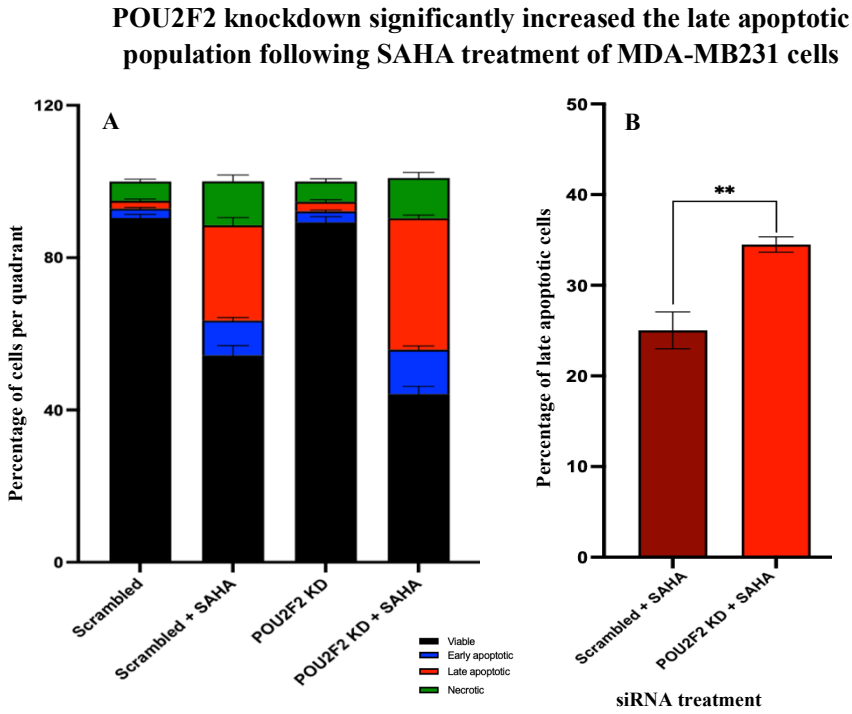


Figure 6.14: POU2F2 knockdown in MDA-MB231 cells resulted in a significantly greater number of cells in late apoptosis. *A. The percentage of cells in each quadrant of the Annexin V Assay in scrambled and POU2F2 knockdown untreated cells and cells treated with 2.5 μM SAHA for 48-hours. B. A significantly greater number of late apoptotic cells were observed comparing SAHA treated POU2F2 knockdown and scrambled cells. Paired, one-tailed T-test, *p<0.05. Error bars show SEM of independent experiments (N=5).*

6.5.2 POU2F1 knockdown did not affect the SAHA sensitivity of MCF7 cells

Alongside this, POU2F1 was knocked down in MCF7 cells. This investigated whether POU2F1 knockdown enhanced the sensitivity of MCF7 cells to HDACi treatment, with the aim of exploring whether POU2F1 was involved in the HDACi survival response. An initial experiment was carried out to confirm the extent of knockdown achieved using 25 nM POU2F1 siRNA (SMARTpool, Dharmacon), alongside a non-targeted scrambled control. Plates were harvested on Days 1, 2 and 3-post transfection and knockdown efficiency assessed by qPCR examination of *POU2F1* expression. An 83% knockdown in *POU2F1* expression versus the scrambled control was observed on Day 1 post-transfection (Figure 6.15A). This efficiency was maintained – with a 75% knockdown observed on Day 3. Thus, as with POU2F2 siRNA, cells would be treated with SAHA 24-hours post transfection.

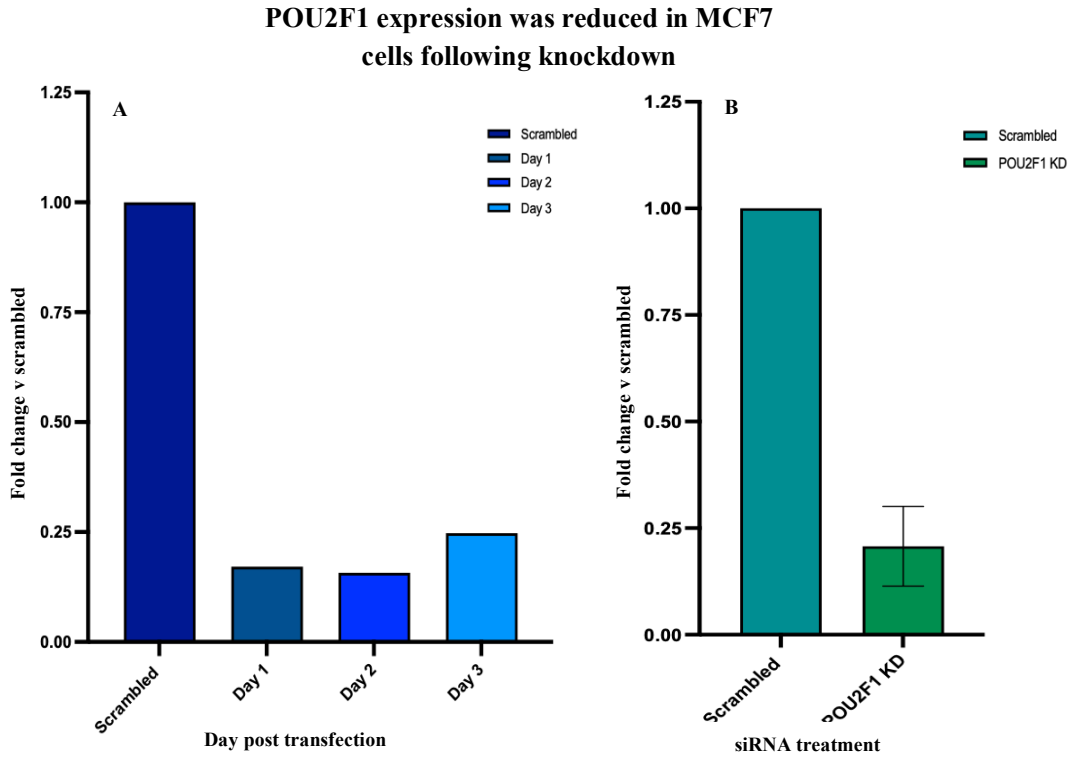


Figure 6.15: POU2F1 expression was reduced in MCF7 cells following knockdown. *A. Fold-change in POU2F1 expression compared with expression in scrambled siRNA treated cells on Days 1-3 post transfection assessed by qPCR. B. Fold-change in expression of POU2F1 96-hours following knockdown compared with expression in scrambled siRNA transfected cells. Error bars show SEM of independent experiments (N=3).*

Quantification by qPCR showed that *POU2F1* expression was depleted by 79% compared with expression in scrambled siRNA treated cells after 96-hours (Figure 6.15B). HDACi-induced apoptosis in MCF7 cells transfected with POU2F1 or scrambled siRNA was assessed using Annexin V/PI apoptosis alongside an untransfected control. POU2F1 knockdown did not affect the response of MCF7 cells to HDACi treatment (Figure 6.16). SAHA treatment of untransfected or scrambled siRNA treated cells resulted in a 4% loss in viability, with this loss only increased by approximately 2% following POU2F1 knockdown. No difference was evident in either the size of the viable or apoptotic population following SAHA treatment of cells transfected with scrambled or POU2F1 siRNA (Figure 6.16). This confirmed that POU2F1 knockdown did not increase the sensitivity of MCF7 cells to SAHA treatment, indicating that POU2F1 was not involved in driving the HDACi survival response.

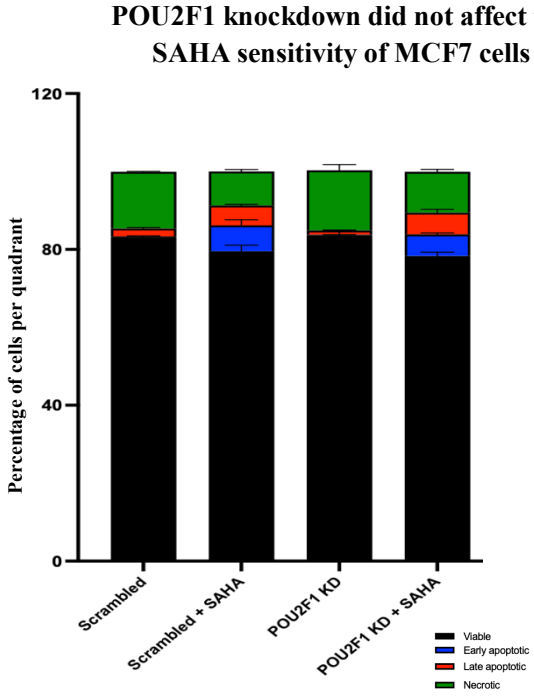


Figure 6.16: POU2F1 knockdown did not increase the SAHA sensitivity of MCF7 cells. *A. The percentage of cells in each quadrant of the Annexin V assay in scrambled and POU2F1 knockdown untreated cells and cells treated with 2.5 μM SAHA for 48-hours. Error bars show SEM of independent experiments (N=3).*

6.5.3 POU2F1 knockdown did not affect the SAHA sensitivity of MDA-MB231 cells

Following on from POU2F2 knockdown, POU2F1 was next knocked down in the more HDACi sensitive MDA-MB231 cell-line. POU2F1 knockdown alone had not increased the sensitivity of MCF7 cells to SAHA – suggesting it did not play a role in mediating their HDACi resistance. However, considering how significantly POU2F2 knockdown had affected their apoptotic response it was believed that perhaps the loss of POU2F1 would affect their HDACi sensitivity. An initial transfection experiment was carried out to confirm the extent of knockdown achieved using 25 nM POU2F1 siRNA (SMARTpool, Dharmacon), alongside a non-targeted scrambled siRNA. Plates were harvested on Days 1, 2 and 3-post transfection and *POU2F1* expression quantified by qPCR. An 81% knockdown was achieved on Day 1, with a knockdown of 72.1% then observed on Day 3 (Figure 6.17A).

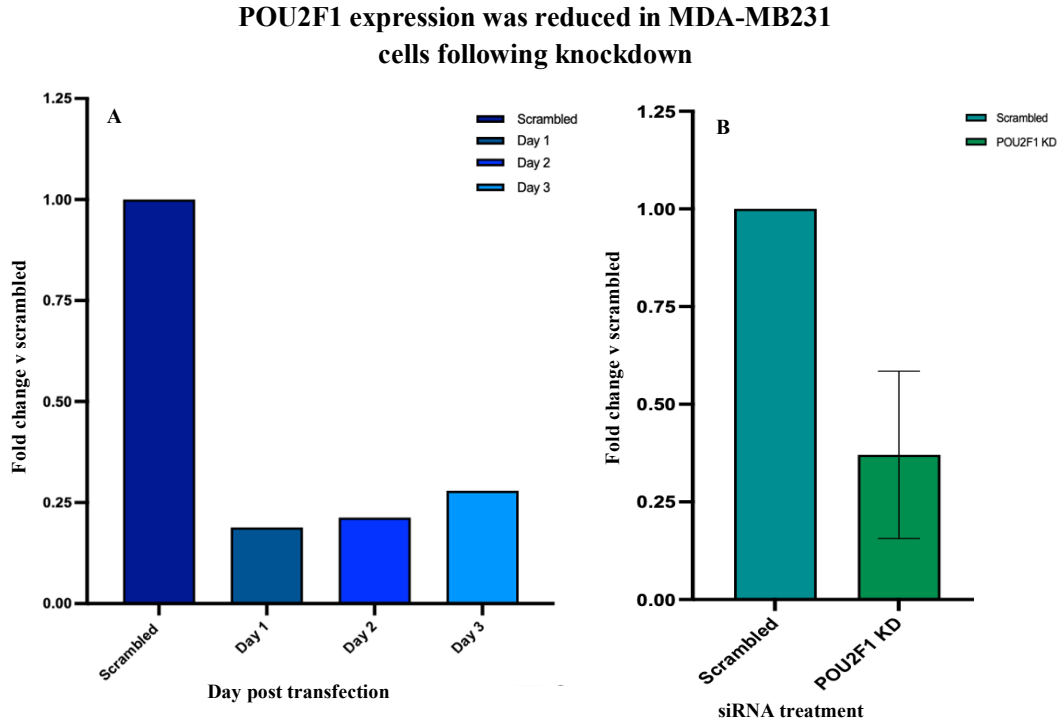


Figure 6.17: POU2F1 expression was reduced in MDA-MB231 cells following knockdown. *A. Fold-change in POU2F1 expression compared to expression in scrambled siRNA treated cells on Days 1-3 post transfection was assessed by qPCR. B. Fold-change in expression of POU2F1 following knockdown compared with expression in cells transfected with scrambled siRNA. Error bars show SEM of independent experiments (N=3).*

Quantification by qPCR showed that *POU2F1* expression was depleted by 63% compared with expression in scrambled siRNA treated cells after 96-hours (Figure 6.17B). The annexin V assay confirmed that POU2F1 knockdown alone did not affect the apoptotic response induced in MDA-MB231 cells treated with SAHA. Little difference was observed between treated scrambled and POU2F1 knockdown cells. The viable population remaining following SAHA treatment was similar, and there was no significant difference in the number of late apoptotic cells observed (Figure 6.18). It was, therefore, concluded that POU2F1 knockdown did not affect the sensitivity of MDA-MB231 cells to HDACi treatment.

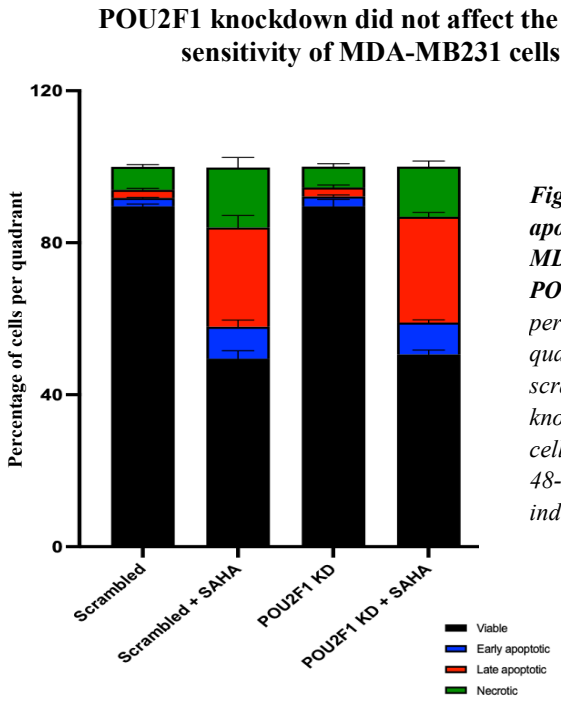


Figure 6.18: HDACi induced apoptosis was not increased in MDA-MB231 cells following POU2F1 knockdown. *A. The percentage of cells in each quadrant of the Annexin V Assay in scrambled and POU2F1 knockdown untreated cells and cells treated with 2.5 μM SAHA for 48-hours. Error bars show SEM of independent experiments (N=3).*

6.5.4 Double knockdown did not additionally increase the SAHA sensitivity of MDA-MB231 cells

Initial experiments knocked down only one member of the POU family at a time. A double POU2F1 and POU2F2 knockdown was next carried out to investigate the interaction between these two factors. This questioned whether the addition of POU2F1 would enhance or diminish the apoptotic response induced following POU2F2 knockdown in the HDACi sensitive MDA-MB231 cells.

Double knockdown was initially carried out in MDA-MB231 cells. Based on previous work, cells were treated with 25 nM POU2F1 and 25 nM POU2F2 siRNA or 25 nM of the non-targeted scrambled siRNA and treated with 2.5 μM SAHA 24-hours later. Double (POU2F1 and POU2F2) or scrambled siRNA treated MDA-MB231 cells were then compared to an untransfected control using the annexin V/PI apoptosis assay. An average *POU2F2* knockdown of 84%, and *POU2F1* knockdown of 83% was achieved after 96-hours (Figure 6.19).

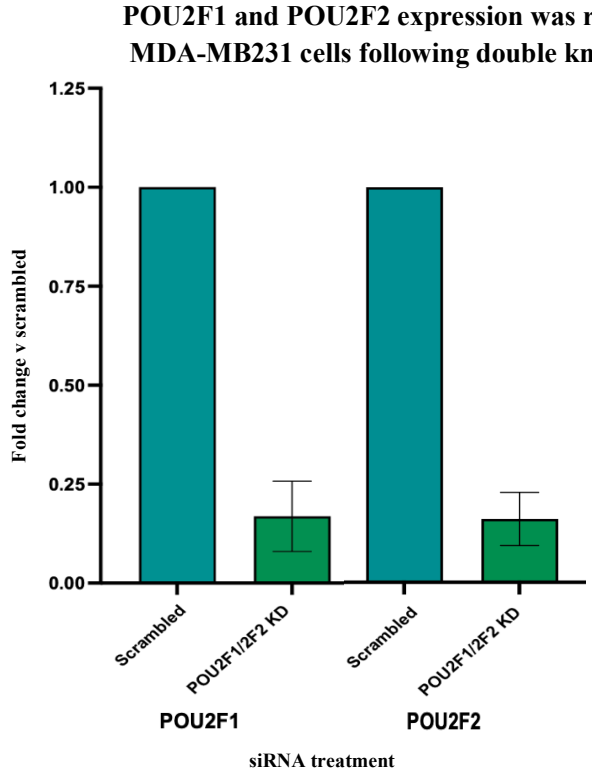


Figure 6.19: The expression of POU2F1 and POU2F2 was reduced in MDA-MB231 cells following double knockdown. *The fold-change in expression of POU2F1 and POU2F2 following double knockdown in MDA-MB231 cells was compared with their expression in cells transfected with scrambled siRNA. Error bars show SEM of independent experiments (N=2).*

Analysis of the resulting viable populations from the Annexin V Assay indicated that double knockdown increased the sensitivity of MDA-MB231 cells to HDACi treatment, compared with the scrambled control cells (Figure 6.20A). As observed with POU2F2 knockdown, double knockdown resulted in an increase in the percentage of late apoptotic cells (Figure 6.20B). The late apoptotic population was then compared to that observed following individual POU2F1 or POU2F2 knockdown in this cell-line (Figure 6.20B). This highlighted that the apoptotic response was not enhanced in the double knockdown over that observed with POU2F2 knockdown alone. The lack of additive effect suggested that both factors may operate in the same pathways.

It was concluded from this work that POU2F1 did not increase the apoptotic response when knocked down alongside POU2F2 – instead producing results similar to those observed following POU2F2 knockdown alone. This suggested that POU2F1 was not involved in mediating the response of MDA-MB231 cells to HDACi treatment.

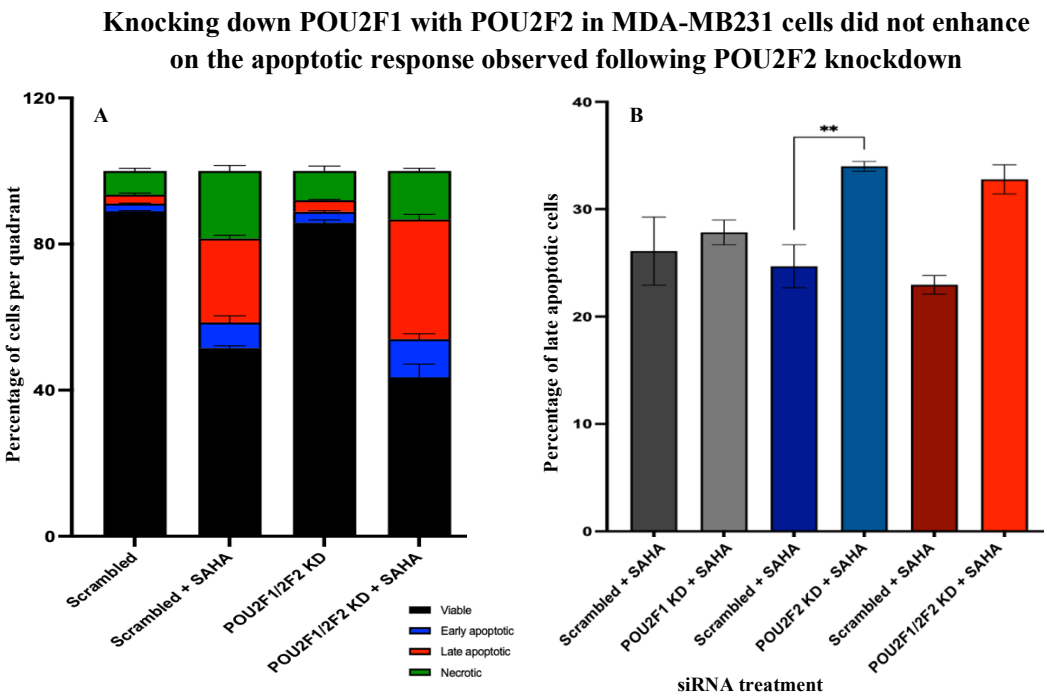


Figure 6.20: Knockdown of POU2F1 and POU2F2 in MDA-MB231 cells did not increase on the apoptotic response induced following POU2F2 knockdown alone. *A. The percentage of cells in each quadrant of the Annexin V Assay in scrambled and POU2F1/POU2F2 knockdown untreated cells and cells treated with 2.5 μM SAHA for 48-hours. B. The late apoptotic population of 48-hour SAHA treated individual POU2F1, POU2F2 or double POU2F1 and POU2F2 knockdown cells alongside their respective scrambled control population. Paired, one-tailed T-test **p<0.01. Error bars show SEM of independent experiments (N=2 (double), N=3 (POU2F1), N=5 (POU2F2)).*

The RNA-Sequencing, and subsequent qPCR analysis confirmed that *POU2F2* was not expressed in the MCF7 cells. However, POU2F2 knockdown as well as the double POU2F1 and POU2F2 knockdown were carried out in MCF7 cells to be compared with the response observed in MDA-MB231 cells. Neither had any effect on the HDACi-sensitivity of MCF7 cells (data not shown).

It is important to consider that an siRNA targeting either *POU2F1* or *POU2F2,* which are from the same POU domain family, would likely affect the expression of the other. This work did not assess the expression of both genes following each individual knockdown. This is something that could be assessed in future work and should be considered alongside these results. In addition, gene redundancy has been observed

with POU Class III proteins (Schreiber *et al.,* 1997). This suggests that *POU2F1* or *POU2F2* could compensate for the loss of the other and prevent the effect of an individual knockdown being observed.

6.6 Was a transcriptional response induced through POU2F2?

POU2F2 was identified as a TF which when knocked down altered the apoptotic response induced in MDA-MB231 cells treated with SAHA. The important question to follow this was whether a transcriptional response was regulated through POU2F2? We were interested in determining whether POU2F2 acted transcriptionally in mediating the response of these cells to SAHA, or whether a transcription independent mechanism was involved. This was explored by considering HAT complex gene downregulation observed in response to HDACi treatment. In that POU family members negatively regulate gene expression, we asked whether POU2F2 or POU2F1 were involved in the regulation of HAT genes post SAHA treatment.

Loss of the characteristic HAT gene downregulation following knockdown would indicate that the POU TFs regulate this response, while persistence of this downregulation would indicate that they were not alone in regulating HAT gene expression. This work assessed the expression of HAT complex genes (*EPC1, EPC2* and *KAT7*) in POU2F1 knockdown MCF7 cells and POU2F2 knockdown MDA-MB231 cells treated with SAHA for 48-hours. Comparing this expression to that in scrambled control cells indicated whether POU knockdown perturbed the downregulation of HAT genes.

6.6.1 HAT gene downregulation following HDACi treatment was maintained until 48-hours

HAT gene expression was assessed in MDA-MB231 cells following POU2F2 knockdown. *EPC2* and *KAT7* expression was significantly downregulated following SAHA treatment of cells transfected with scrambled or POU2F2 siRNA – while *EPC1* was only significantly downregulated in scrambled cells (Figure 6.21). The expression of all the tested HAT genes remained at a fold-change of around 1 following knockdown alone, indicating that POU2F2 did not regulate their expression. To conclude, the persistence of this downregulation following POU2F2 knockdown in MDA-MB231 cells confirmed that POU2F2 was not involved in regulating HAT gene downregulation in response to 48-hour SAHA treatment.

HAT gene downregulation was then assessed in MCF7 cells following POU2F1 knockdown. *EPC1, EPC2* and *KAT7* were significantly downregulated in response to SAHA in scrambled cells while *EPC1* and *EPC2* were following knockdown (Figure 6.22). Thus, POU2F1 knockdown did not prevent the SAHA induced downregulation of HAT complex genes. These results did, importantly, show that this response persisted until 48-hours. The downregulation of HAT genes had been clearly observed following 2-hour SAHA treatment, however, this data adds to this - showing HAT complex genes were still downregulated at this later timepoint. This suggested that a longer-term HAT downregulation response follows this initial characterised short-term response. In addition, this showed that the effect of SAHA treatment was maintained until this time – with the response still evident at 48-hours.

POU2F2 knockdown did not prevent SAHA induced HAT gene downregulation in MDA-MB231 cells at 48-hours

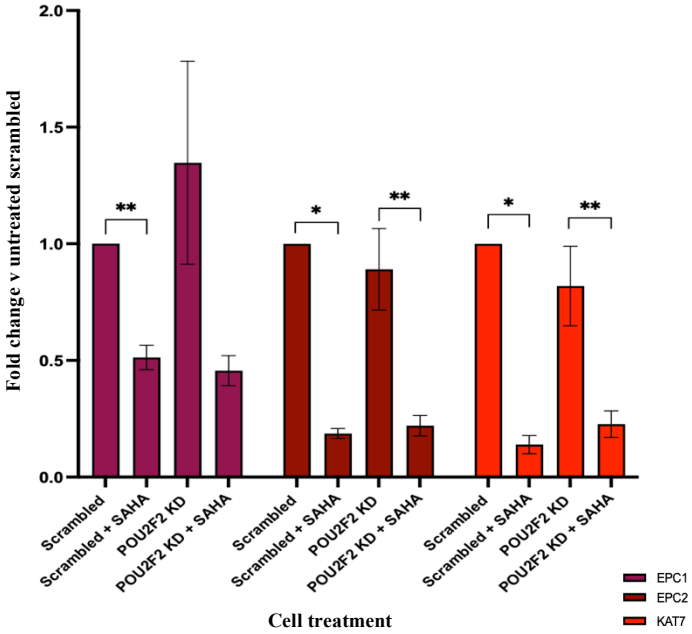


Figure 6.21: POU2F2 knockdown in MDA-MB231 cells did not prevent HAT gene downregulation after SAHA treatment. *EPC1, EPC2 and KAT7 expression was assessed in cells transfected with scrambled or POU2F2 siRNA – both untreated and following 48-hour treatment with 2.5 μM SAHA. Presented are fold changes compared with expression in untreated scrambled siRNA transfected cells. Paired, one-tailed T-test comparing normalized treated and untreated for each condition **p<0.01, *p<0.05. Error bars show SEM of independent experiments (N=3).*

POU2F1 knockdown did not prevent SAHA induced HAT gene downregulation in MCF7 cells at 48-hours

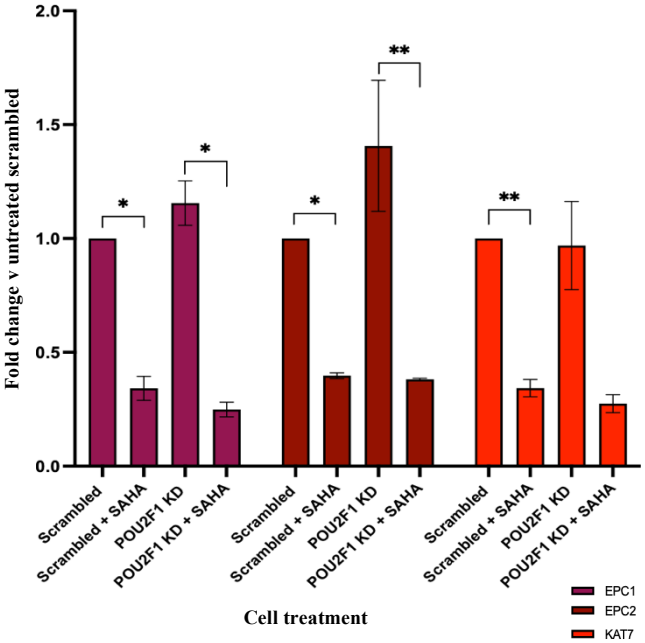


Figure 6.22: POU2F1 knockdown in MCF7 cells did not prevent SAHA-induced HAT gene downregulation. *EPC1, EPC2 and KAT7 expression was assessed in cells transfected with scrambled or POU2F1 siRNA – both untreated and following 48-hour treatment with 2.5 μM SAHA. Presented are fold changes compared with the expression in untreated scrambled siRNA transfected cells. Paired, one-tailed T-test comparing normalized treated and untreated for each condition **p<0.01, *p<0.05. Error bars show SEM of independent experiments (N=3).*

6.6.2 POU2F2 knockdown did not affect the SAHA-induced HAT gene downregulation at 2-hours in either cell-line

This project focused on the genes differentially expressed 30, 60 and 120-minutes after SAHA treatment. Assessment of gene expression changes after 48-hour SAHA treatment is at a different timescale to the early 2-hour gene expression changes identified from RNA-Sequencing. Thus, the next step in answering the question of whether POU2F2 played a role in HAT regulation was to assess HAT expression in response to 2-hour SAHA treatment. MDA-MB231 cells were transfected with scrambled or POU2F2 siRNA and treated 24-hours later with SAHA for 30, 60 or 120-minutes. SAHA treatment increased the expression of *POU2F2*, though not significantly (Figure 6.23). This was something that had not been observed in the RNA-Sequencing data. *POU2F2* expression was knocked down by around 80-90% across all treatment timepoints. The SAHA induced upregulation of *POU2F2* was no longer observed following knockdown.

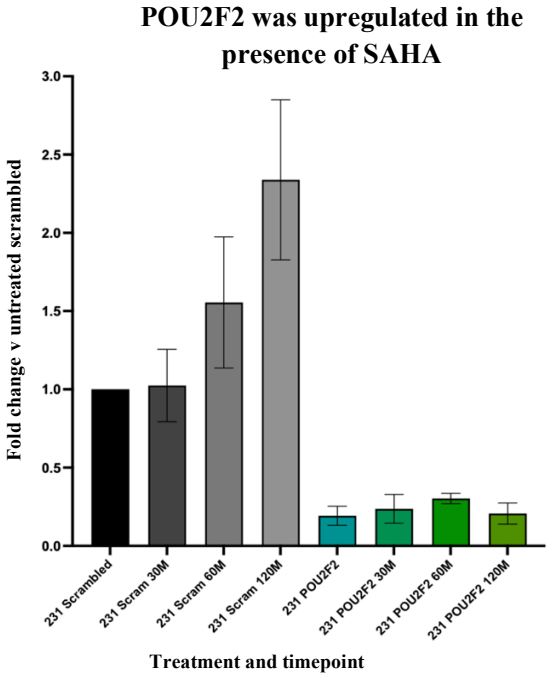


Figure 6.23: POU2F2 was upregulated following SAHA treatment with knockdown reducing POU2F2 expression and preventing this response. *Fold-change in POU2F2 expression assessed in cells transfected with scrambled or POU2F2 siRNA – either untreated or following treatment with 2.5 μM SAHA for 48-hours. Presented is fold-change compared with expression in untreated MDA-MB231 cells transfected with scrambled siRNA after data was normalized to housekeepers. Paired, one-tailed T-test comparing expression at 0 and 120-minutes showed no significant difference. Error bars show SEM of independent experiments (N=3).*

The fold-change in expression of the HAT genes was then assessed compared with their expression in untreated scrambled siRNA transfected cells. Four of the HAT genes were significantly downregulated following SAHA treatment in scrambled cells, while all five genes were following *POU2F2* knockdown (Figure 6.24). The HAT genes were not downregulated following POU2F2 knockdown alone (Figure 6.24). The expression of *EPC1* was upregulated, though not significantly, following knockdown – while expression remained similar in the other HAT genes. This indicated that POU2F2 may play a role in the regulation of *EPC1*. Their response following SAHA treatment differed across the HAT genes studied. For example, though POU2F2 knockdown increased the initial expression of *EPC1* it had no effect on its subsequent downregulation after SAHA treatment. Interestingly, the downregulation of *KAT6B* was more clearly observed following knockdown. Comparing expression at 120-minutes, *EPC2* and *ING5(1)* expression was significantly lower following POU2F2 knockdown (Figure 6.24). The more pronounced downregulation following knockdown suggested that POU2F2 may be involved in inhibiting HAT gene downregulation in response to HDACi treatment.

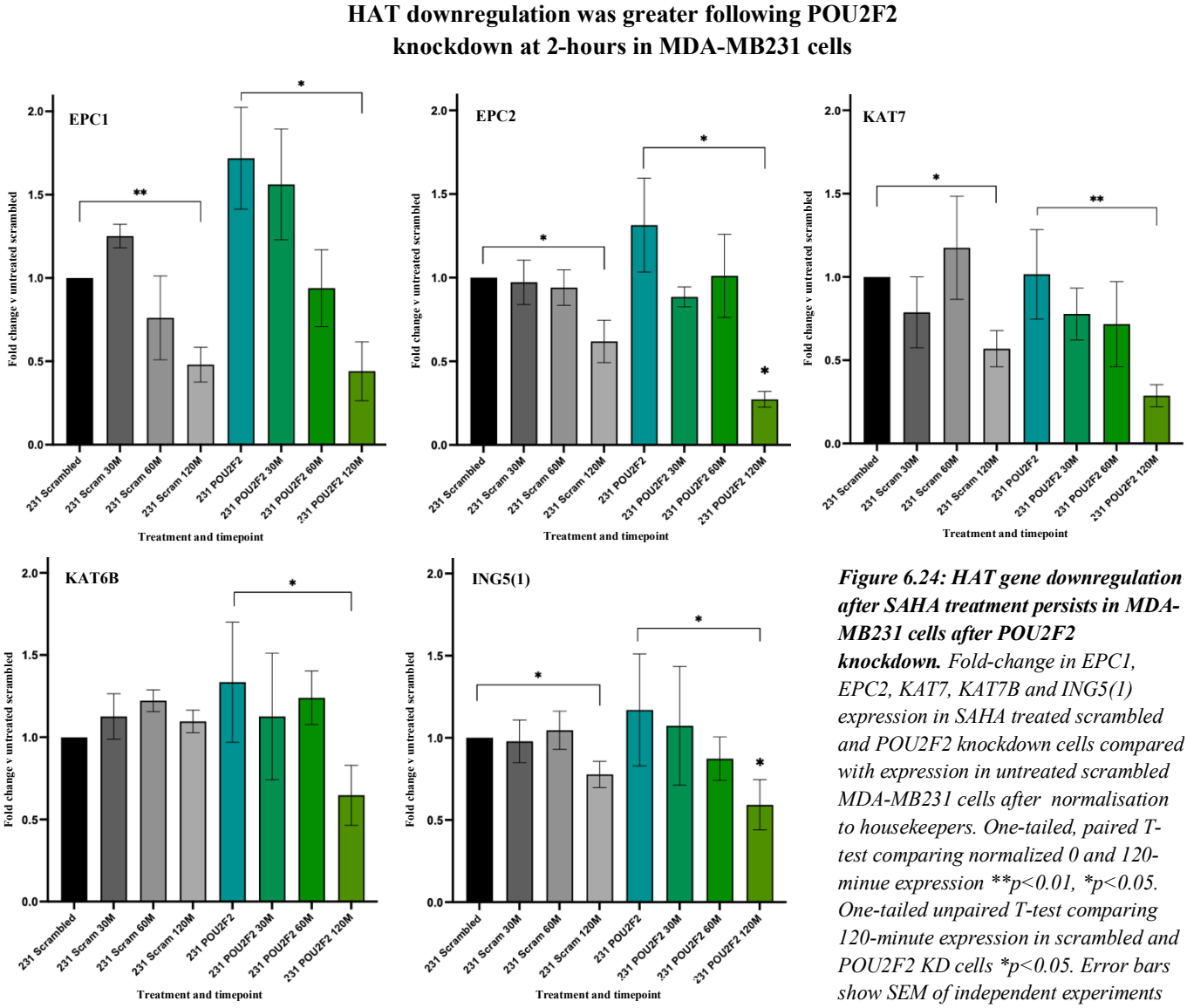


Figure 6.24: HAT gene downregulation after SAHA treatment persists in MDA-MB231 cells after POU2F2 knockdown. *Fold-change in EPC1, EPC2, KAT7, KAT7B and ING5(1) expression in SAHA treated scrambled and POU2F2 knockdown cells compared with expression in untreated scrambled MDA-MB231 cells after normalisation to housekeepers. One-tailed, paired T-test comparing normalized 0 and 120-minue expression **p<0.01, *p<0.05. One-tailed unpaired T-test comparing 120-minute expression in scrambled and POU2F2 KD cells *p<0.05. Error bars show SEM of independent experiments (N=3).*

6.6.3 The expression of POU2F2 regulated genes was affected by SAHA following knockdown

To further explore whether there was a transcription response induced through POU2F2, the regulation of identified POU2F2 target genes was assessed following knockdown. POU2F2 regulated genes were initially identified using the list of 30 and 60-minute downregulated genes in MCF7 cells, from which the POU motif was

matched. These lists were analysed by Venny 2.0 to identify genes common to both timepoints (data not shown). HARMONIZOME was then used to determine which genes were known POU2F2 TF interactors. This contains target genes of POU2F2 in ChIP-Seq datasets from the ENCODE transcription Factor Targets dataset. Primers were designed to ten of the suggested POU2F2 target genes and their expression assessed in cells transfected with scrambled or POU2F2 siRNA and treated with SAHA for 30, 60 or 120-minutes. The genes selected were *ATXN7L2, INO80E, JMJD8, MATR3, MED10, MEPCE, MIF, MIR17HG2, PPP1R14B* and *RPL36* (Table 2.1).

Only *ATXN7L2* and *JMJD8* appeared to be regulated by POU2F2. In scrambled cells, *ATXN7L2* expression did not significantly differ across the 120-minutes (Figure 6.25). Upon POU2F2 knockdown, the expression of this gene appeared dysregulated as shown by the size of the error bars. *JMJD8* expression was significantly upregulated by SAHA treatment in scrambled cells ($p<0.05$). However, its expression was significantly downregulated with increasing SAHA treatment time following POU2F2 knockdown (Figure 6.25; $p<0.05$). This suggested that these genes were being regulated by POU2F2, and that following knockdown their expression could then be influenced by SAHA.

A second set of genes were identified as SAHA responsive (Figure 6.26). *MEPCE* and *MIR17HG* expression was significantly downregulated with increasing SAHA treatment time. No difference was observed in their response to SAHA following POU2F2 knockdown, suggesting that these they were SAHA responsive but not via POU2F2. These genes are relatively insensitive to POU2F2 levels – but majorly downregulated by SAHA.

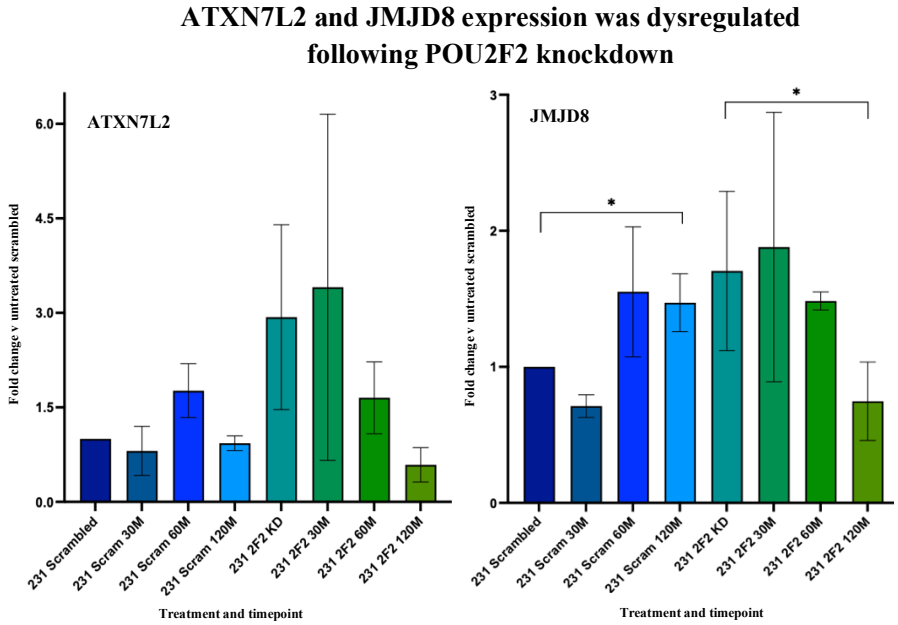


Figure 6.25: ATXN7L2 and JMJD8 expression was dysregulated following POU2F2 knockdown. *Fold-change in ATXN7L2 and JMJD8 expression in SAHA treated scrambled and POU2F2 knockdown MDA-MB231 cells assessed by qPCR versus expression in untreated scrambled cells after normalization to housekeepers. One-tailed paired T-test comparing 0 and 120-minute expression in each condition *p<0.05. Error bars show SEM of independent experiments (N=3).*

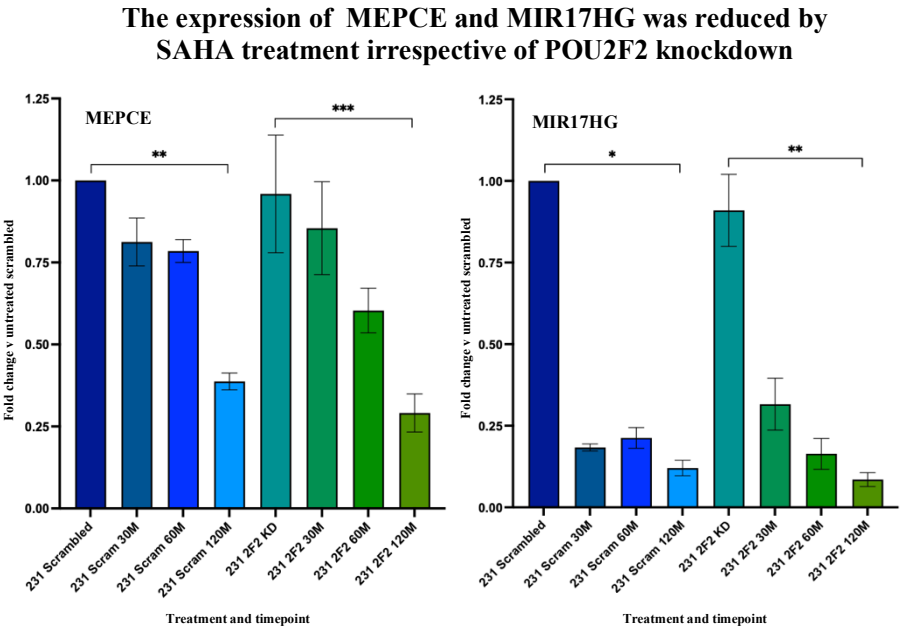


***Figure 6.26**: **MEPCE and MIR17HG expression was affected by SAHA treatment.** Fold-change in MEPCE and MIR17HG expression in SAHA treated scrambled and POU2F2 knockdown MDA-MB231 cells assessed by qPCR compared with expression in untreated scrambled cells after normalization to housekeepers. One-tailed, paired T-test comparing 0 and 120-minute expression in each condition ***p<0.001, **p<0.01, *p<0.05. Error bars show SEM of independent experiments (N=3).*

To conclude, analysis of the roles of the POU family members in mediating the response of our cell-lines to SAHA treatment showed that POU2F2 knockdown further enhanced the HDACi sensitivity of MDA-MB231 cells. However, POU2F2 did not play a transcriptional role during their early response to HDACi treatment – with the HAT gene downregulation not perturbed following knockdown. Though interesting, this

cannot explain the difference in sensitivity between our two cell-lines. This led us to investigate the next target identified from the motif analysis – the ATF/CREB family.

7. DO ATF FACTORS PLAY A ROLE IN THE HDACi SURVIVAL RESPONSE?

The differential expression of *POU2F2* between our cell-lines could not explain the difference in sensitivity between them. This led to an investigation of our next target identified through RNA-Sequencing and motif analysis– the ATF/CREB TF family. Knockdown analysis was used to test the importance of several family members in mediating the response of our HDACi sensitive and more HDACi resistant cell-line to SAHA treatment. Factors were knocked down individually, or in combination, and the loss in viability following 48-hour SAHA treatment observed using the Annexin V Assay. Those significantly affecting cell viability were followed up by qPCR, assessing whether the initial transcriptional response was perturbed following knockdown.

7.1 Activating Transcription Factors were differentially expressed in MCF7 and MDA-MB231 cell-lines

ATF1 was the top predicted binding site identified among genes significantly upregulated in MCF7 cells following 30-minute SAHA treatment. This site was also identified among genes upregulated after 60 and 120-minutes. ATFs exist within the basic leucine zipper domain (bZIP) family, a group of TFs recognised by their shared DNA binding region - the bZIP element. The basic region of this mediates DNA binding, while the attached leucine zipper enables homo or heterodimerization of bZIP factors (van Dam and Castellazzi, 2001). There are four subclasses of this family - AP-1, ATF/CREB, C/EBP and Maf (Chen *et al.,* 2022). The ATF/CREB subgroup functions as hetero or homodimers with members of the C/EBP or AP-1 families (Chen *et al.,* 2022). Their transcriptional activity and DNA

binding specificity is, therefore, regulated by the dimers they form. AP-1 factors, such as Jun, bind the AP-1 site. However, this differs by only one nucleotide from the cyclic AMP response element (CRE) site recognised by ATF/CREB factors (Hai *et al.,* 1989). Through responding to extracellular signals, these factors are believed to maintain homeostasis, in addition to regulating processes such as cell proliferation (Chen *et al.,* 2022). Interestingly, some ATF/CREB family members are more homologous to members of the AP-1 family than members of their own family (Hai, 2006).

The RNA-Sequencing data was analysed to observe how members of the ATF and CREB families, which share this binding site, were expressed in both cell-lines. This analysis identified three targets from this family. CREB3L4 was the initial factor identified. This gene was differentially expressed in our cell-lines, being more highly expressed in MCF7 cells (Figure 7.1A). This led to the hypothesis that it may be involved in mediating HDACi resistance. ATF5 was the second target identified. It was more highly expressed in MCF7 cells, and is known to be acetylated (Paerhati *et al.,* 2022). It was, thus, hypothesised that ATF5 may be involved in the early cellular response to an HDACi. ATF4 was the final target identified. This was the most highly expressed factor in both cell-lines (Figure 7.1). This factor was of interest as it can be acetylated and plays a role in regulating cell stress responses – including heat shock (Wortel *et al.,* 2017). Importantly, the expression of none of these TFs was affected by increasing SAHA treatment time. This follows the hypothesis that it is acetylation of TFs driving the transcriptional change, not an increase in their expression in response to HDACi treatment.

ATF4, ATF5 and CREB3L4 were selected as targets for knockdown

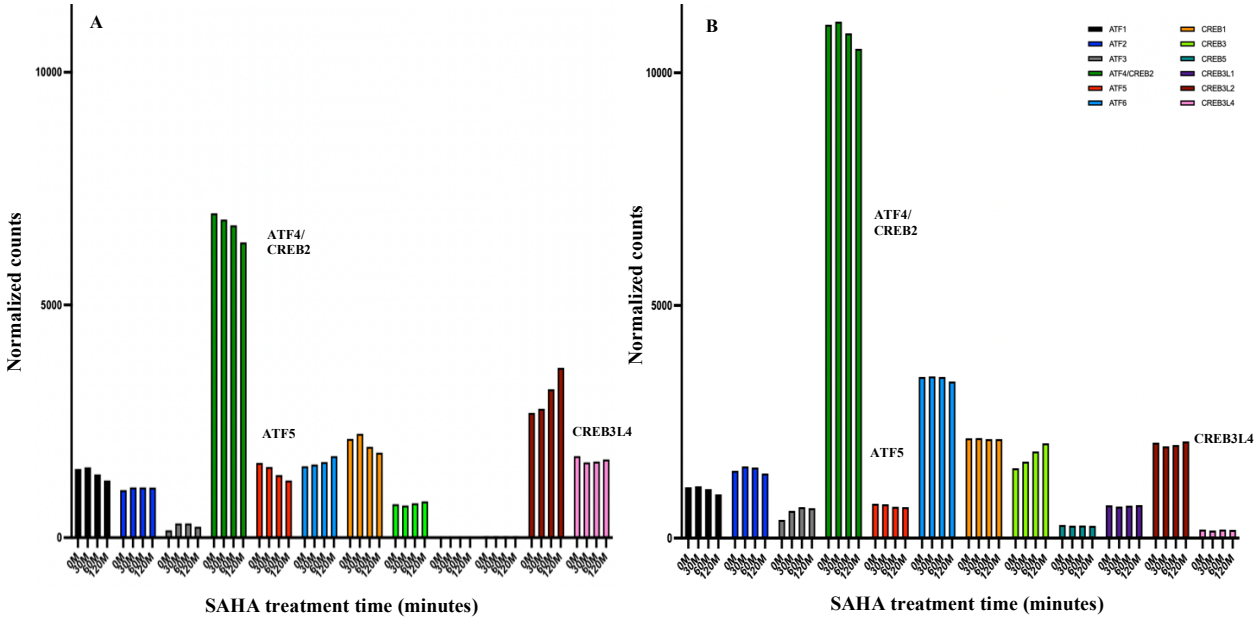


Figure 7.1: CREB3L4 and ATF5 were more highly expressed in resistant cells, while ATF4 was highly expressed in both cell-lines. *Normalized counts values of ATF and CREB domain family protein genes following treatment with 2.5 μM SAHA for 0, 30, 60 or 120-minutes in A. MCF7 and B. MDA-MB231 cell-lines from DESeq2 analysis.*

Primers were designed to validate the expression of these three ATF/CREB genes by qPCR. As observed in the RNA-Sequencing data, *ATF4* was the most highly expressed factor in both lines (Figure 7.2). *CREB3L4* and *ATF5* were more highly expressed in the MCF7 cells. This analysis confirmed the expected expression in each cell-line and showed that their expression was not upregulated in response to SAHA treatment in MCF7 cells.

The expression of ATF4, ATF5 and CREB3L4 differed in our cell-lines

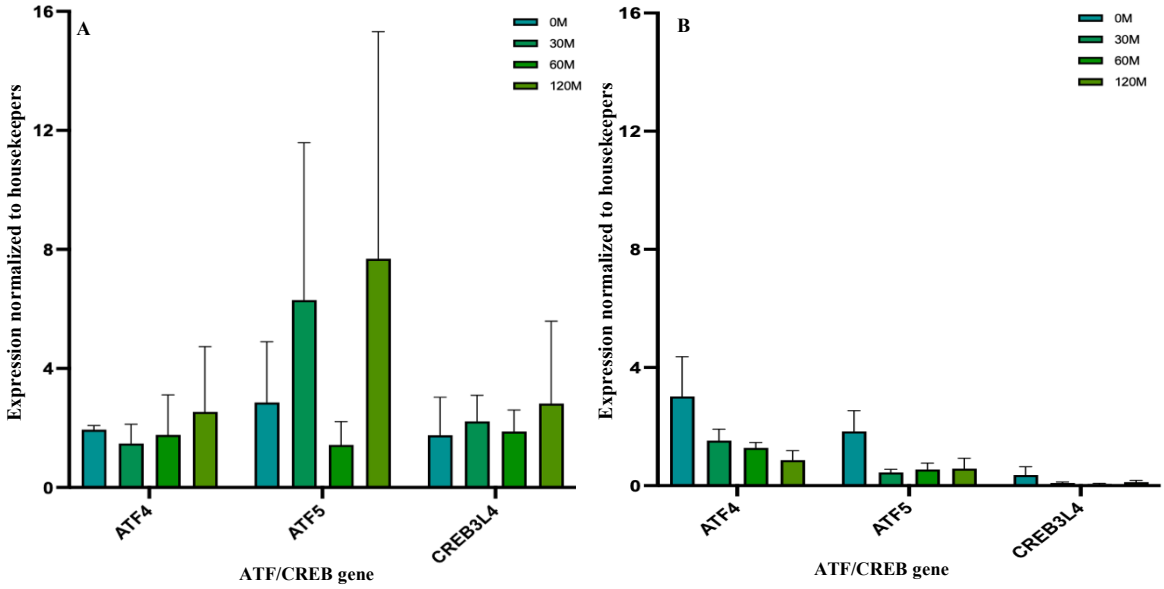


Figure 7.2: ATF5 and CREB3L4 were more highly expressed in MCF7 cells. *The expression of ATF4, ATF5 and CREB3L4 genes after 30, 60 or 120-minute treatment with 2.5 μM SAHA normalized to housekeeper gene expression in A. MCF7 and B. MDA-MB231 cells was assessed by qPCR. Error bars represent SEM of independent experiments (N=3).*

ATF4 is an important regulator of cellular stress responses (Lassot *et al.,* 2005). ATF4 mRNA is expressed in a variety of tissues and tumour cell-lines, but its short half-life prevents the protein from being easily detected in cells (Ameri and Harris, 2008; Rzymski *et al.,* 2009). It is acetylated by p300/CBP, with this modification stabilising the protein and preventing it from ubiquitination and proteasomal degradation. Its transcriptional activity is mediated through the heterodimers it forms with additional members of the C/EBP and AP-1 families (Vallejo *et al*., 1993; Vinson *et al.,* 1993).

ATF5 is highly expressed in cancers, with its expression linked to cancer progression (Greene *et al.,* 2009). It was identified as a cancer-specific cell survival factor in glioblastoma and breast cancer cells (Dluzen *et al.,* 2011). ATF5 regulates Bcl-2, with the stimulation of Bcl-2 expression believed to mediate its pro-survival action in these cancers

(Dluzen *et al*., 2011). Its selectivity to the survival of cancer cells was also suggested in recent work indicating that ATF5 loss resulted in apoptosis only in neoplastic breast cell-lines (Monaco *et al.,* 2007). ATF5 is acetylated by p300 on Lysine-29 (Liu *et al.,* 2011). This modification improves the interaction between ATF5 and p300 as well as the ability of this complex to bind at the promoters of their target genes. ATF5 also interacts with the other cell stress pathways. For example, HSP70 interacts with the N-terminal domain of ATF5 to protect it from protein degradation (Li *et al*., 2011). In addition, ATF5 has also been shown interacting in the HIF1 pathway. ATF5 is believed to act as a co-activator of the HIF1 transcriptional complex (He *et al.,* 2021).

CREB3L4 is one of five Creb3 family members, located at the endoplasmic reticulum and playing a role in initiating the unfolded protein response (Pu *et al.,* 2020). This factor is highly expressed in cancers such as prostate and endometrial as well as hepatocellular carcinomas (Kim *et al.,* 2017; Cui *et al*., 2016; Inagaki *et al.,* 2008). CREB3L4, alongside CREB3L1 is upregulated in breast cancer tissues. CREB3L4 is believed to play a crucial role in breast cancer progression (Pu *et al.,* 2020).

7.2 Knockdown of ATF/CREB family members in the resistant line

The ATF/CREB binding site was recognised among genes rapidly upregulated in response to 30-minute SAHA treatment in MCF7 cells. Analysis of ATF and CREB family member expression led to the selection of three knockdown targets: ATF5, CREB3L4 and ATF4. This work was initially carried out in the resistant, MCF7 cells – following the hypothesis that their sensitivity to HDACi treatment would be improved following knockdown of these factors. The experimental set-up was as before and involved comparing HDACi-

induced apoptosis in cells transfected with 25 nM ATF4, ATF5 or CREB3L4 siRNA, cells transfected with 25 nM scrambled siRNA, and untransfected cells. Untreated cells were compared with those treated with 2.5 μM SAHA for 48-hours.

7.2.1 ATF5 knockdown did not affect the SAHA sensitivity of MCF7 cells

ATF5 was the initial factor from this family knocked down in MCF7 cells. It was hypothesised that knocking down this TF, which was more highly expressed in MCF7 cells, would enhance their sensitivity to HDACi treatment. Quantification by qPCR showed that *ATF5* expression was depleted by 55% compared with expression in scrambled siRNA treated cells (data not shown; Table 7.1). HDACi-induced apoptosis in MCF7 cells transfected with ATF5 or scrambled siRNA was assessed alongside an untransfected control using the Annexin V/PI apoptosis assay. The distribution of cells per quadrant of the apoptosis assay was similar comparing the treated scrambled and ATF5 knockdown cells – with no significant difference evident in the remaining viable population (Figure 7.3). This indicated that ATF5 knockdown did not affect the sensitivity of MCF7 cells to 48-hour SAHA treatment.

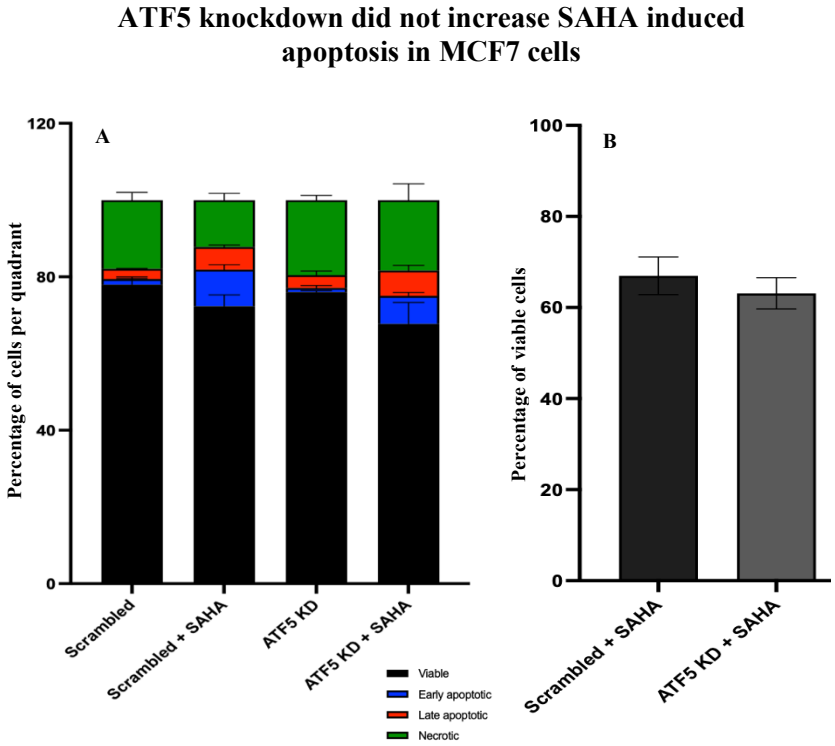


Figure 7.3: ATF5 knockdown did not increase the SAHA sensitivity of MCF7 cells. *A. The percentage of cells in each quadrant of the Annexin V Assay in scrambled and ATF5 knockdown untreated cells and cells treated with 2.5 μM SAHA for 48-hours. B. The viable population remaining in SAHA treated ATF5 knockdown cells and scrambled cells. Error bars show SEM of independent experiments (N=3).*

7.2.2 CREB3L4 knockdown enhanced the SAHA sensitivity of MCF7 cells

CREB3L4 was then knocked down to follow up on previous unpublished work from the lab suggesting that this enhanced SAHA-induced apoptosis in MCF7 cells. This had also been reported by Pu *et al*., in 2020. It was hypothesised that CREB3L4 was involved in regulating early gene expression changes in response to HDACi treatment and that its knockdown would enhance the sensitivity of MCF7 cells to SAHA treatment.

Quantification by qPCR showed that *CREB3L4* expression was depleted by 48.3% compared with expression in scrambled siRNA treated cells (data not shown; Table 7.1). CREB3L4 knockdown altered the distribution of cells per quadrant of the Annexin V Assay, with an increase evident in the apoptotic population and loss of viable population (Figure 7.4A). Knockdown resulted in a significant loss in the size of the viable population remaining after SAHA treatment (p=0.02; Figure 7.4B). It also resulted in a significant increase in the size of the late apoptotic population (p=0.03; Figure 7.4C). CREB3L4 knockdown significantly increased the sensitivity of MCF7 cells to 48-hour SAHA treatment. However, though this difference reached significance it related only to a small percentage of the total cells.

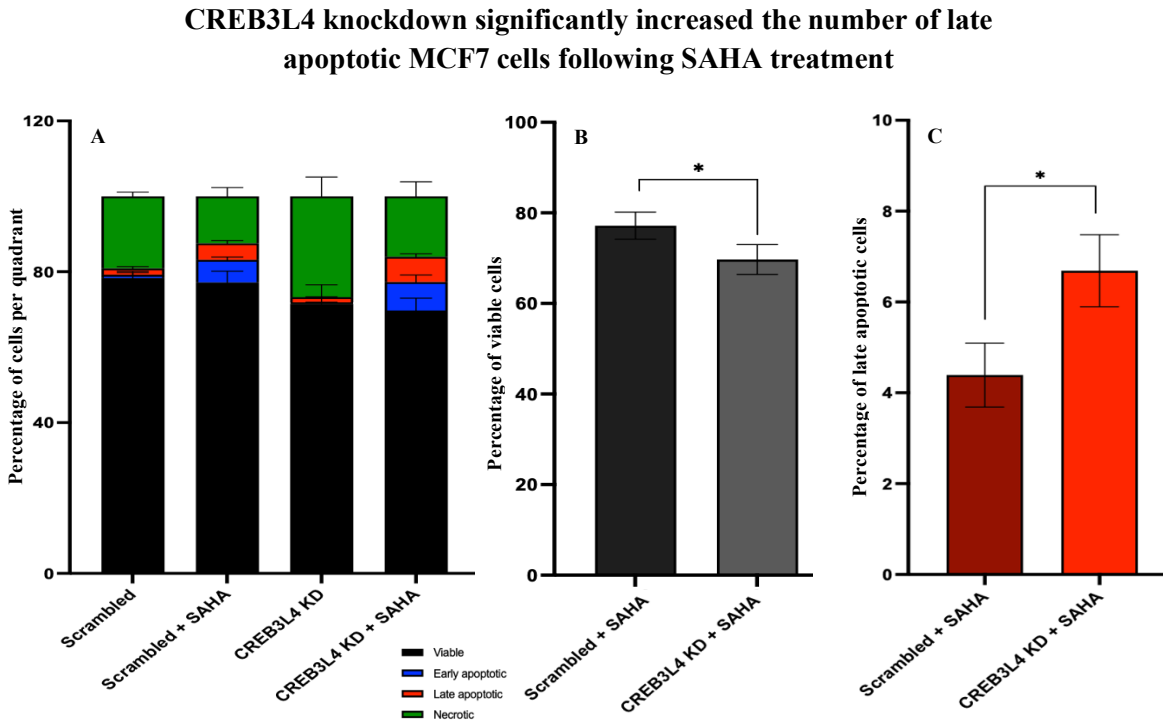


Figure 7.4: CREB3L4 knockdown in MCF7 cells increased the size of the late apoptotic population following HDACi treatment. *A. The percentage of cells in each quadrant of the Annexin V Assay in scrambled and CREB3L4 knockdown untreated cells or cells treated with 2.5 μM SAHA for 48-hours. B. The viable population remaining following SAHA treatment was significantly reduced following CREB3L4 knockdown. C. The late apoptotic population was significantly increased following CREB3L4 knockdown. Paired, one-tailed T-test *p<0.05. Error bars show SEM of independent experiments (N=3).*

7.2.3 ATF4 knockdown enhanced the SAHA sensitivity of MCF7 cells

ATF4 was the final family member knocked down in the more HDACi resistant MCF7 cells. This factor was selected due to its important role in regulating cellular stress responses. In addition, due to its high expression level it was thought that it may have to be knocked down to observe the effect of ATF/CREB family members which are not as highly expressed.

Quantification by qPCR showed that *ATF4* expression was depleted by 51.2% compared with expression in scrambled siRNA treated cells (data not shown; Table 7.1). The distribution of cells per quadrant of the Annexin V Assay showed that cell overcrowding affected the size of the resulting necrotic population (Figure 7.5A). Overgrowth of MCF7 cells in untreated wells resulted in death due to growth conditions and not HDACi-induced apoptosis in early replicates. Thus, SAHA treatment increased the apoptotic population by removing cells from the necrotic and not viable population. This meant that in scrambled cells the difference between treated and untreated cells was evident in the size of the apoptotic population only. Despite this, ATF4 knockdown alone resulted in a significant loss in viability following SAHA treatment (p=0.009; Figure 7.5B). This was accompanied by a significant increase in the number of late apoptotic cells (p=0.008; Figure 7.5C). These results indicated that ATF4 knockdown created MCF7 cells more sensitive to HDACi treatment.

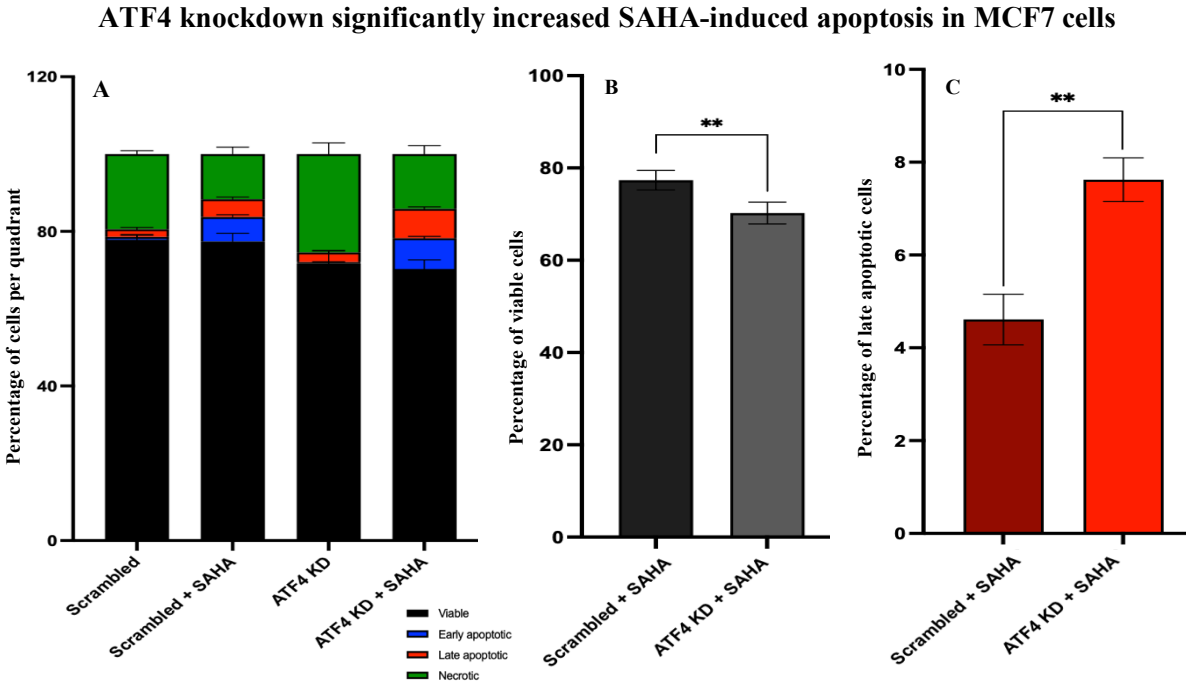


Figure 7.5: ATF4 knockdown in MCF7 cells significantly more sensitive to HDACi treatment. *A. The percentage of cells in each quadrant of the Annexin V Assay in untreated or 48-hour SAHA treated scrambled and ATF4 knockdown cells. B. The viable population remaining after SAHA treatment was significantly reduced following ATF4 knockdown. C. The late apoptotic population was significantly increased following ATF4 knockdown. Paired, one-tailed T-test. **p<0.01. Error bars show SEM of independent experiments (N=4).*

This work identified the first two TFs that, when knocked down, altered the apoptotic response in our more HDACi resistant cells. This was novel, as it had been expected that several TFs would have to be knocked down before this response was perturbed even slightly. Both CREB3L4 and ATF4 knockdown alone altered cell sensitivity to SAHA, suggesting that their respective pathways were important in mediating resistance. What was most surprising was that the TF most highly expressed across both cell-lines exhibited this effect. This led to a reconsideration of potential driver proteins, with less focus on the difference in their expression between the two cell-lines. As significant differences were observed following individual knockdowns, it was then questioned whether the knockdown of multiple members of the ATF/CREB family together would enhance the response.

7.2.4 Double ATF4 and CREB3L4 knockdown did not increase the SAHA sensitivity of MCF7 cells above individual knockdown

ATF4 and CREB3L4 were knocked down together in MCF7 cells. These factors were selected as they had both significantly increased the sensitivity of MCF7 cells to SAHA treatment, either reducing the remaining viable population or enhancing the apoptotic population (Figure 7.4; Figure 7.5). Considering that the HDACi survival response is an evolutionarily conserved response made up of multiple pathways – we questioned whether knocking down both factors would further increase MCF7 sensitivity above that observed in response to individual ATF4 or CREB3L4 knockdown. The experimental set-up was as before, comparing cells transfected with 25 nM ATF4 and 25 nM CREB3L4 siRNA to cells transfected with 25 nM scrambled siRNA or untransfected cells.

Quantification by qPCR showed that *CREB3L4* expression was depleted by 71.2% and ATF4 mRNA by 51.4% compared with expression in scrambled siRNA treated cells (data not shown; Table 7.1). An important initial observation was that knocking down both these TFs together did not affect the health of the cells (Figure 7.6A). Their combined knockdown resulted in an increase in the apoptotic population and a reduction in the viable population remaining following SAHA treatment (Figure 7.6A). The percentage of cells in late apoptosis was then compared to that observed following individual ATF4 or CREB3L4 knockdown. Though the late apoptotic population was greater following double knockdown, it was not significantly increased above that observed in scrambled siRNA treated cells (Figure 7.6B). This may relate to the inconsistent apoptosis induced in the double knockdown replicates. In conclusion,

knockdown of CREB3L4 and ATF4 did not increase on the apoptotic response observed with either knockdown alone. It had been believed that their combined knockdown would further enhance the sensitivity of the MCF7 cells. However, this result instead suggested that these two TFs may exist in the same pathway which would prevent this combination from having any additive effect.

Double ATF4 and CREB3L4 knockdown did not increase the SAHA sensitivity of MCF7 cells above individual knockdown

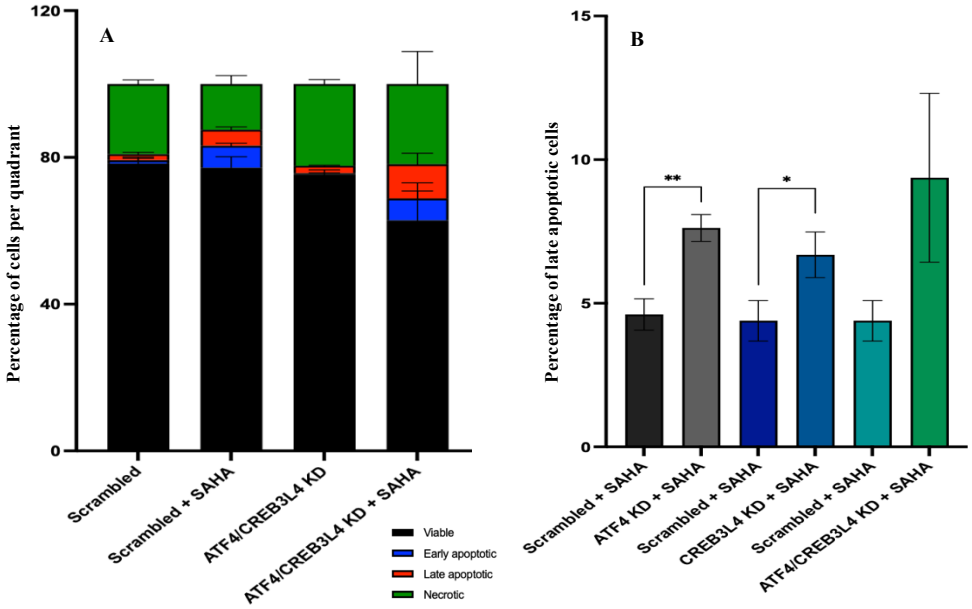


Figure 7.6:The knockdown of CREB3L4 with ATF4 did not increase on the apoptotic response observed following individual knockdown. *A. The percentage of cells in each quadrant of the Annexin V Assay in untreated and 48-hour SAHA treated scrambled and double CREB3L4 and ATF4 knockdown cells. B. The late apoptotic population of treated CREB3L4, ATF4, double ATF4 and CREB3L4 knockdown cells alongside their respective scrambled controls. Paired, one-tailed T-test *p<0.05, **p<0.01. Error bars show SEM of independent experiments (ATF4 N=4, CREB3L4 and ATF4/CREB3L4 N=3).*

7.2.5 The addition of ATF5 did not enhance on the response observed in MCF7 cells following ATF4 knockdown

ATF4 was then knocked down with ATF5 in MCF7 cells. The knockdown of ATF4 had significantly enhanced their sensitivity to SAHA treatment, while ATF5 did not affect

this response (Figure 7.3; Figure 7.5). This experiment was carried out to be compared with the response in MDA-MB231 cells. As will be shown, the knockdown of both ATF4 and ATF5 in the sensitive cell-line significantly enhanced their HDACi-sensitivity.

Quantification by qPCR showed that *ATF4* expression was depleted by 24.9% and *ATF5* by 46.4% compared with expression in scrambled siRNA treated cells (data not shown, Table 7.1). This experiment involved only two replicates, with *ATF4* expression not knocked down in the third replicate. Knockdown of ATF4 and ATF5 reduced the viable population remaining after SAHA treatment (Figure 7.7A). Analysis of the late apoptotic population remaining after individual ATF4, ATF5 or double ATF4/ATF5 knockdown showed that double knockdown resulted in an increase in the percentage of cells at late apoptosis despite the knockdown being less efficient (Figure 7.7B). However, this did not reach significance. The late apoptotic population after double knockdown was not significantly greater than that remaining after ATF4 knockdown, confirming that the knockdown of ATF5 with ATF4 did not enhance the sensitivity of MCF7 cells to SAHA treatment.

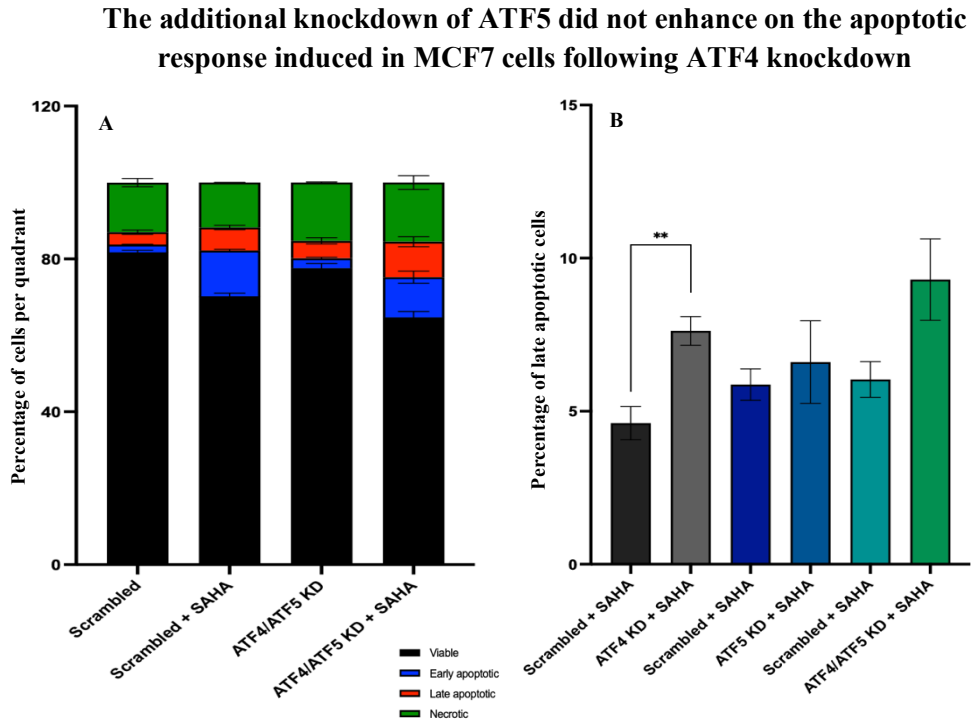


Figure 7.7: Double ATF4 and ATF5 knockdown resulted in a smaller apoptotic response than was observed following ATF4 knockdown. *A. The percentage of cells in each quadrant of the Annexin V Assay in untreated and 48-hour SAHA treated scrambled and double ATF4/ATF5 knockdown cells. B. The late apoptotic population of SAHA treated ATF4, ATF5 double ATF4/ATF5 with their respective scrambled controls. Paired, one-tailed T-test **p<0.01. Error bars show SEM of independent experiments (ATF4 N=4, ATF5 N=3, ATF4/ATF5 N=2).*

7.3 Knockdown of ATF/CREB family members in the sensitive line

The ATF/CREB TFs were identified from early gene expression changes in MCF7 cells, however, the next question asked was whether their knockdown affected the sensitivity of MDA-MB231 cells to HDACi treatment. ATF4, ATF5 and CREB3L4 were knocked down and the SAHA sensitivity of MDA-MB231 cells assessed using the Annexin V/PI apoptosis assay. This explored the idea that this cell-line contained fewer resistance pathways and therefore would be less protected by the HDACi survival response.

7.3.1 ATF5 knockdown enhanced the SAHA sensitivity of MDA-MB231 cells

ATF5 was the initial factor knocked down in MDA-MB231 cells. This knockdown alone had not affected the sensitivity of MCF7 cells to 48-hour SAHA treatment. However, it was believed that this knockdown may enhance the apoptotic response of MDA-MB231 cells – which are less protected by the HDACi survival response.

Quantification by qPCR showed that ATF5 expression was depleted by 93.9% compared with expression in scrambled siRNA treated cells (data not shown; Table 7.1). Despite the inconsistency observed between the replicates, ATF5 knockdown increased the sensitivity of the MDA-MB231 cells to SAHA treatment (Figure 7.8A). This was observed with a significant reduction in the number of viable cells remaining after SAHA treatment (p=0.016; Figure 7.8B) and a significant increase in the late apoptotic population (p=0.035; Figure 7.8C). It was, therefore, concluded that ATF5 knockdown resulted in MDA-MB231 cells more sensitive to HDACi treatment.

ATF5 knockdown significantly reduced the viable and increased the apoptotic MDA-MB231 population remaining after SAHA treatment

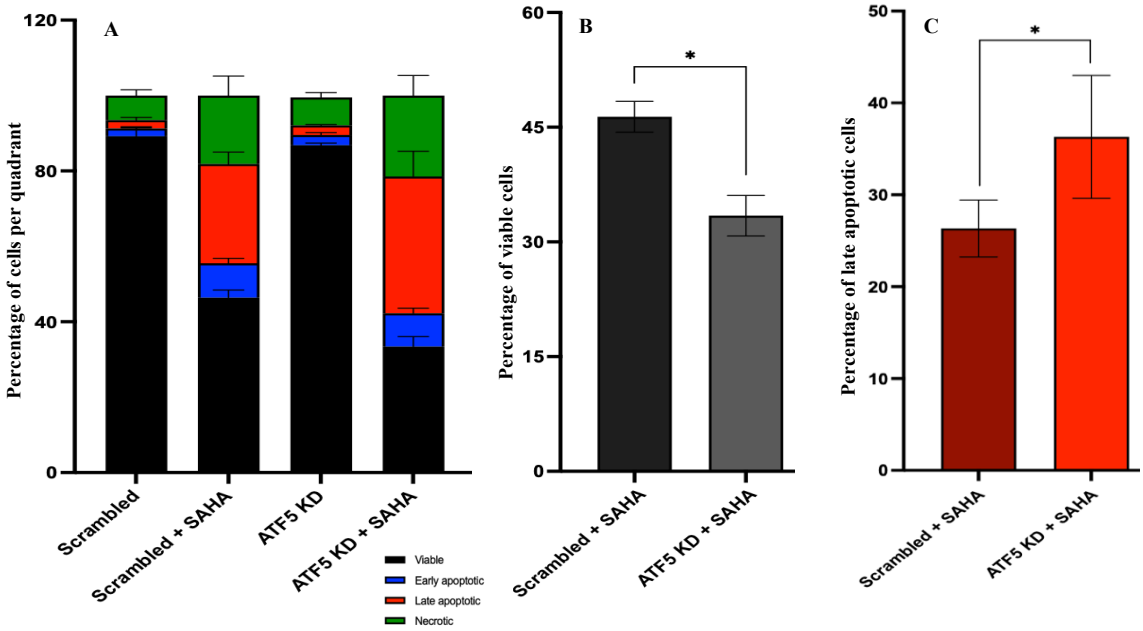


Figure 7.8: ATF5 knockdown significantly increased the sensitivity of MDA-MB231 cells to SAHA treatment. *A. The percentage of cells per quadrant of the Annexin V Assay in untreated and 48-hour SAHA treated scrambled and ATF5 knockdown cells. B. ATF5 knockdown resulted in a significant loss in the viable cells remaining post SAHA treatment. C. A significantly greater number of late apoptotic cells were observed in ATF5 knockdown versus scrambled cells. Paired, one-tailed T-test *p<0.05. Error bars show SEM of independent experiments (N=4).*

7.3.2 CREB3L4 knockdown did not enhance the sensitivity of MDA-MB231 cells to SAHA treatment

CREB3L4 was the next factor knocked down. As this knockdown had significantly increased the proportion of late apoptotic MCF7 cells, it was hypothesised that it would also enhance the SAHA-sensitivity of MDA-MB231 cells.

Quantification by qPCR showed that *CREB3L4* expression was depleted by 67% compared with expression in scrambled siRNA treated cells (data not shown; Table 7.1). CREB3L4 knockdown, however, had little effect on the apoptotic response

induced in MDA-MB231 cells following SAHA treatment. Little difference was observed comparing the distribution of cells per quadrant of the Annexin V assay – with the viable and apoptotic populations remaining similar following CREB3L4 knockdown (Figure 7.9). The late apoptotic population was not significantly increased in knockdown cells, compared with the scrambled control (Figure 7.9B). However, as demonstrated by the size of the error bars, the apoptotic response induced varied between replicates. In two replicates, around 30-35% of cells were in late apoptosis while in the third only 12% were. This led to the conclusion that CREB3L4 knockdown alone did not significantly increase the apoptotic response induced in MDA-MB231 cells in response to 48-hour SAHA treatment.

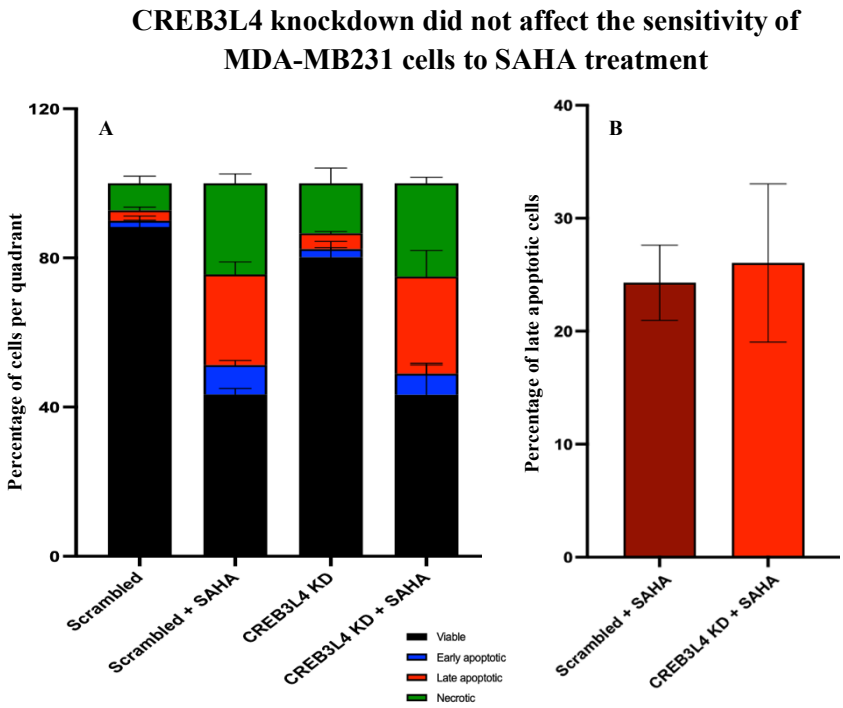


Figure 7.9: CREB3L4 knockdown did not affect the HDACi sensitivity of MDA-MB231 cells. *A. The percentage of cells per quadrant of the Annexin V assay in untreated and 48-hour SAHA treated scrambled and CREB3L4 knockdown cells. B. The late apoptotic population was not increased following CREB3L4 knockdown. Error bars show SEM of independent experiments (N=3).*

7.3.3 ATF4 knockdown enhanced the SAHA sensitivity of MDA-MB231 cells

ATF4 was then knocked down to complete the individual knockdown experiments in MDA-MB231 cells. Knockdown of ATF4 alone resulted in a significant loss in the viable population and significant increase in late apoptotic population of MCF7 cells. It was, therefore, hypothesised that ATF4 knockdown would enhance the sensitivity of MDA-MB231 cells to 48-hour SAHA treatment.

Quantification by qPCR showed that *ATF4* expression was depleted by 78.5% compared with expression in scrambled siRNA treated cells (data not shown; Table 7.1). Cells transfected with scrambled siRNA exhibited a 44.4% loss in viability, while ATF4 knockdown cells exhibited a 52.4% loss. As had been observed following POU2F2 knockdown in this cell-line, SAHA treatment of ATF4 knockdown cells resulted in an accumulation of cells at late-stage apoptosis. An increase of around 17% was observed specifically in this quadrant (Figure 7.10). ATF4 knockdown also resulted in a reduction in the remaining viable population (Figure 7.11A). The reduction in the number of viable cells remaining after HDACi treatment was significant (p=0.04; Figure 7.11B). Though ATF4 knockdown resulted in an increase in the late apoptotic population, this did not reach significance (Figure 7.11C). To conclude, ATF4 knockdown alone resulted in a significant increase in the sensitivity of MDA-MB231 cells to HDACi – observed clearly with a reduction in the viable population remaining following SAHA treatment. This represented the first TF enhancing the apoptotic response of the more HDACi resistant and HDACi sensitive cell-line to SAHA. This was an interesting finding, pointing to a potential role of ATF4 in mediating the early SAHA induced transcriptional response in cells.

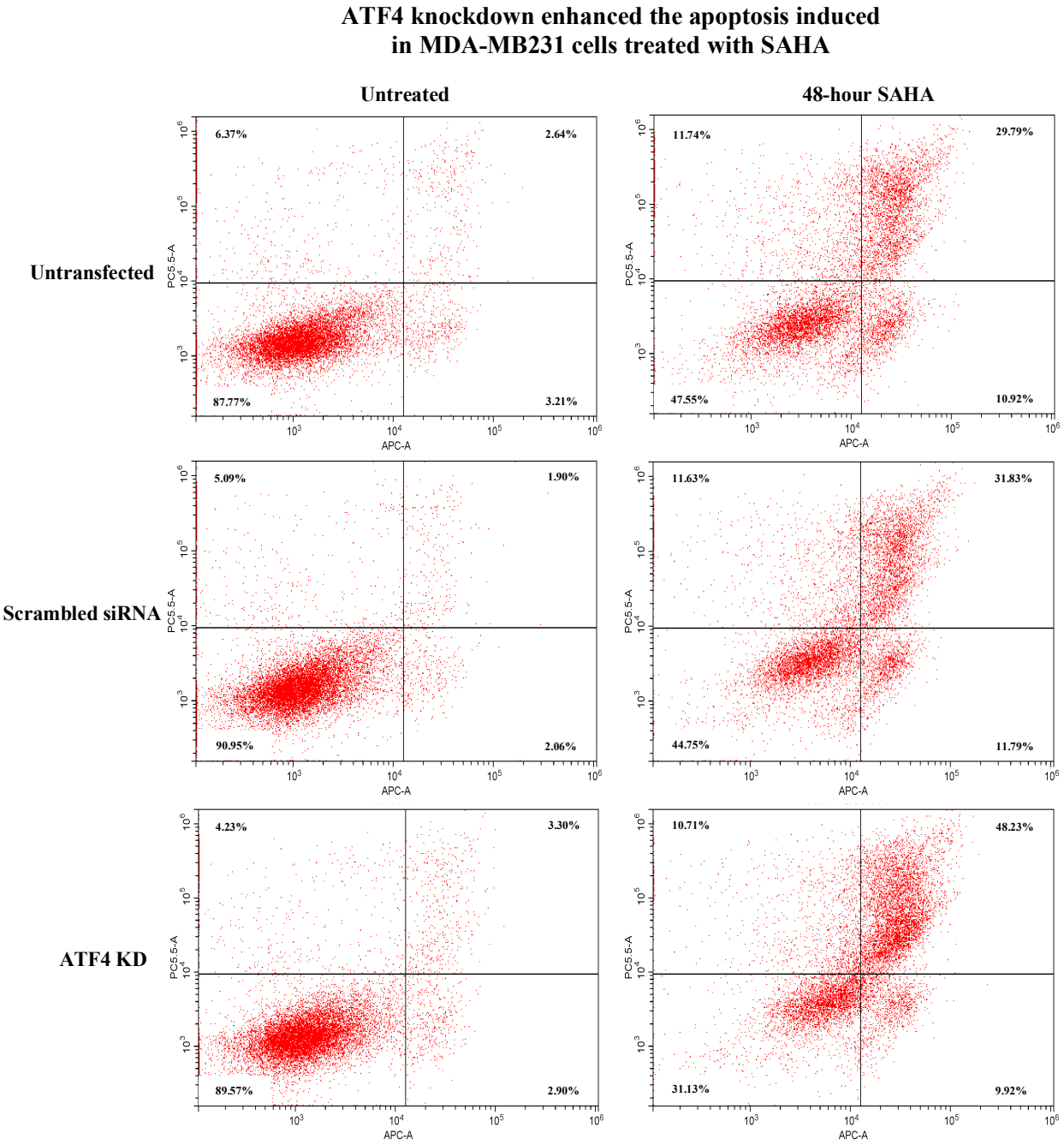


Figure 7.10: ATF4 knockdown reduced the viable population of MDA-MB231 cells following 48-hour SAHA treatment. *Apoptosis was assessed using the Annexin V/Propidium Iodide assay in untransfected cells, cells transfected with 25 nM scrambled or ATF4 siRNA following treatment with 2.5 μM SAHA for 48-hours. Images generated using CytExpert 3.4 Software.*

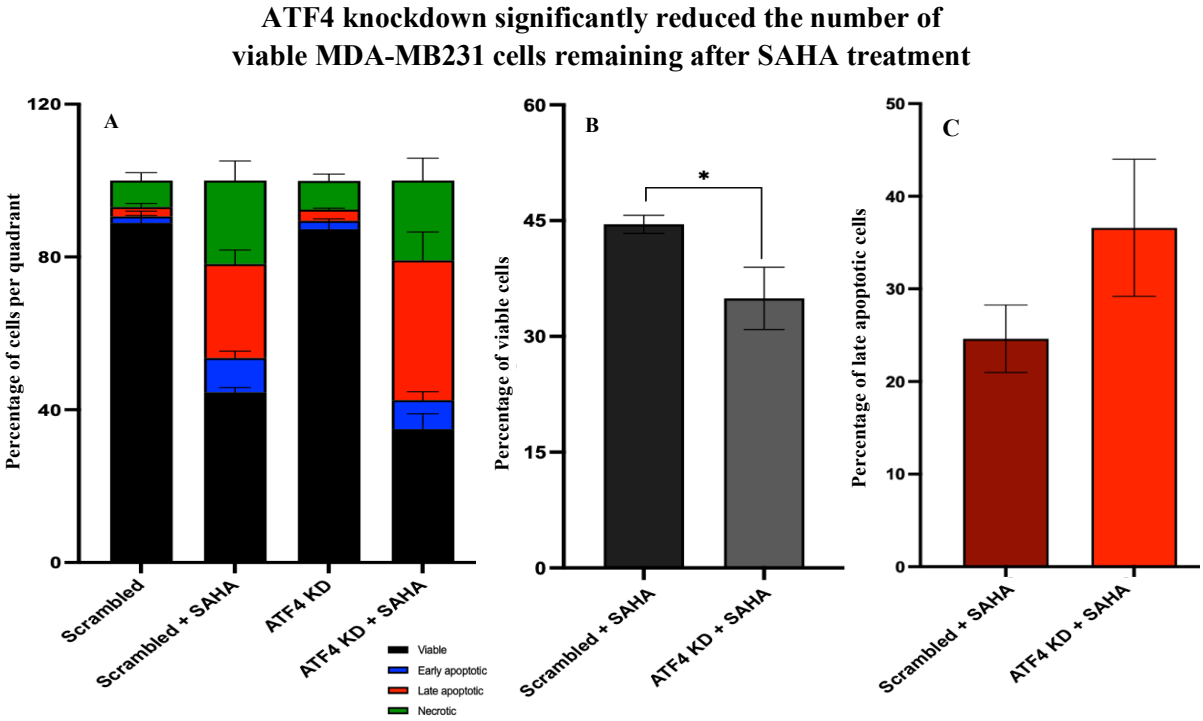


Figure 7.11: Knockdown of ATF4 in MDA-MB231 resulted in a significant loss in the viable population. *A. The percentage of cells in each quadrant of the Annexin V Assay in untreated and 48-hour SAHA treated scrambled and ATF4 knockdown cells. B. The viable population of cells was significantly reduced following ATF4 knockdown C. The increase in late apoptotic population comparing SAHA treated ATF4 knockdown and scrambled cells. Paired, one tailed T-test *p<0.05. Error bars show SEM of independent experiments (N=3).*

7.3.4 Double ATF4 and ATF5 knockdown was not additive in MDA-MB231 cells

ATF4 and ATF5 were next knocked down together in the more HDACi sensitive cell-line. The individual knockdown of both factors had enhanced the sensitivity of MDA-MB231 cells to HDACi treatment (Figure 7.8; Figure 7.11). Thus, this experiment aimed to investigate whether knocking them down together would further enhance the sensitivity of these cells to SAHA treatment.

Quantification by qPCR showed that *ATF4* expression was depleted by 78.6% and *ATF5* by 95% compared with expression in scrambled siRNA treated cells (data not

shown; Table 7.1). Knockdown of ATF4 with ATF5 resulted in a loss in the viable population remaining after SAHA treatment, alongside an increase in the apoptotic and necrotic populations (Figure 7.12A). Knockdown significantly reduced the number of viable MDA-MB231 cells remaining following SAHA treatment (p=0.0011; Figure 7.12B). However, no additive effect was observed from knocking down both together – with an increased loss of viability of around 5% compared with either ATF4 or ATF5 knockdown alone (Figure 7.12C). The average percentage of viable cells remaining after individual knockdowns was around 34%, while double knockdown reduced this to 29.6%. To conclude, knocking down ATF4 with ATF5 did not enhance on the apoptotic response observed with either knockdown alone. These factors are from the same TF family, so they may exist within the same signalling pathways – and therefore, their combined knockdown would not have an additive effect.

Knockdown of ATF4 with ATF5 did not significantly increase the SAHA induced loss in viability when compared with individual knockdown

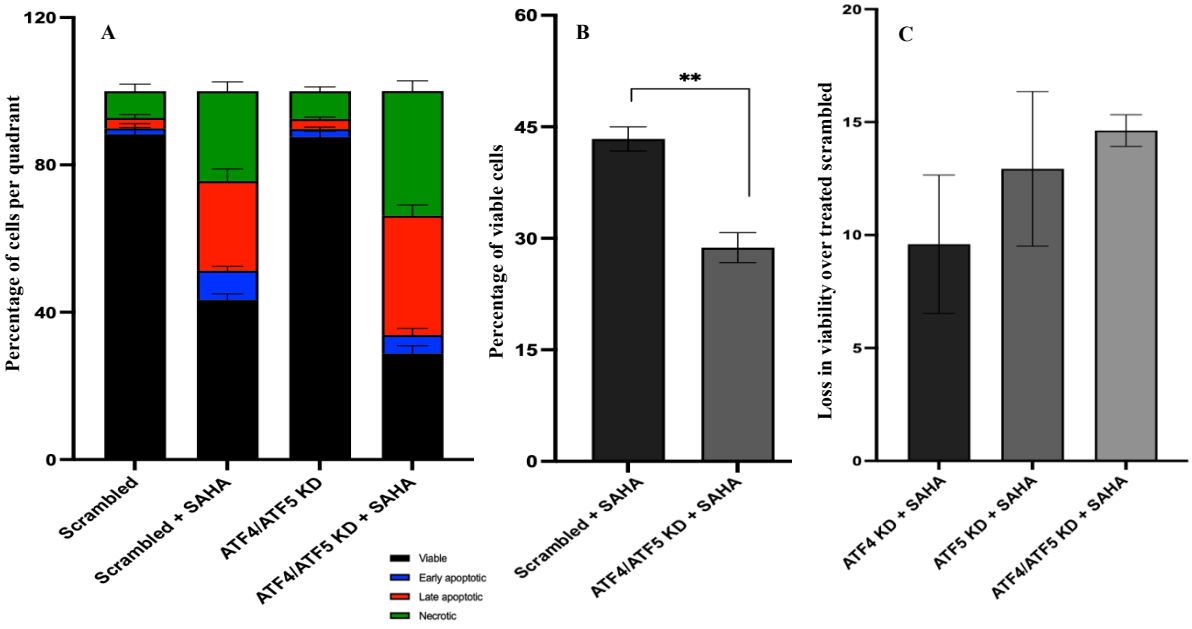


Figure 7.12: Double knockdown did not significantly increase the loss in viability compared with ATF4 or ATF5 knockdown alone. *A. The percentage of cells per quadrant of the Annexin V Assay in untreated and 48-hour SAHA treated scrambled and ATF4/ATF5 knockdown cells. B. A significant loss in the viable population was observed comparing SAHA treated double knockdown and scrambled cells. C. The loss in viability over the respective treated scrambled population in individual ATF4 or ATF5 knockdown and double ATF4/ATF5 knockdown cells. Paired, one-tailed T-test **p<0.01. Error bars show SEM of independent experiments (ATF4/5 and ATF4 N=3, ATF5 N=4).*

7.3.5 The additional knockdown of CREB3L4 did not increase the loss in viability over double ATF4 and ATF5 knockdown

A triple knockdown was then investigated in the MDA-MB231 cells. CREB3L4 was knocked down alongside ATF4 and ATF5, to determine how knocking down an additional member of this TF family affected their SAHA sensitivity.

Quantification by qPCR showed that *ATF4* expression was depleted by 75%, *ATF5* by 93.6% and *CREB3L4* by 75.3% compared with expression in scrambled siRNA treated cells (data not shown; Table 7.1). A significant reduction in the viable population was observed, accompanied by an increase in the late apoptotic and necrotic populations comparing the SAHA treated scrambled and triple knockdown cells (p=0.009; Figure 7.13A). However, the addition of CREB3L4 did not further enhance the sensitivity of the MDA-MB231 cells over the double knockdown – with a viable population of approximately 29% remaining following SAHA treatment of the double and triple knockdown cells (Figure 7.13B). This confirmed that triple ATF4, ATF5 and CREB3L4 knockdown did not enhance the SAHA-sensitivity of MDA-MB231 cells over double ATF4 and ATF5 knockdown.

The additional knockdown of CREB3L4 did not increase the loss in viability over double ATF4 and ATF5 knockdown

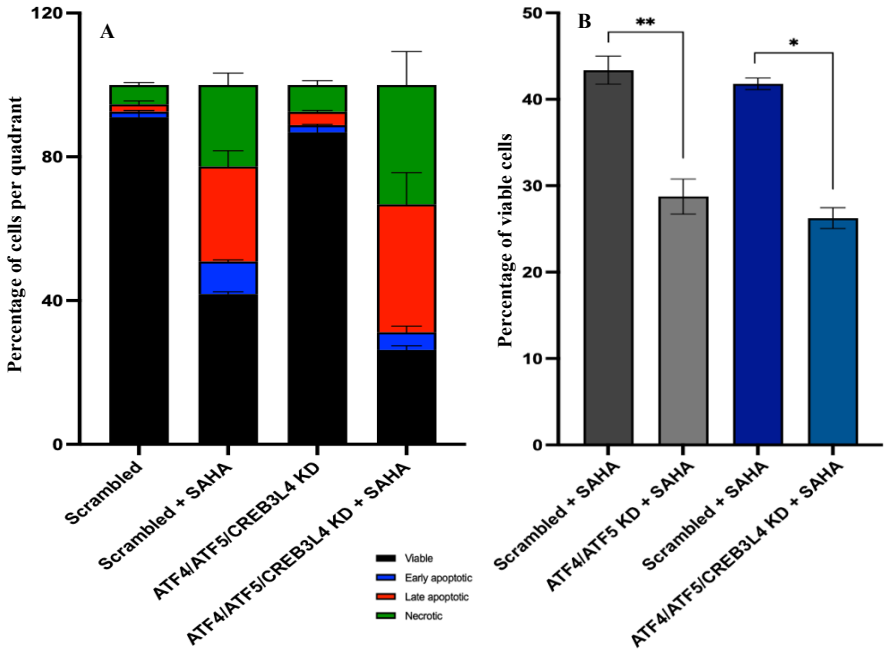


Figure 7.13: The addition of CREB3L4 did not increase the loss in viability over double ATF4/ATF5 knockdown. *A. The percentage of cells per quadrant of the Annexin V Assay in untreated and 48-hour SAHA treated scrambled and ATF4, ATF5 and CREB3L4 knockdown cells. B. The viable population remaining after SAHA treatment in double or triple knockdown cells compared to their respective scrambled control. Paired, one-tailed T-test *p<0.05 **p<0.01 Error bars show SEM of independent experiments (ATF4/ATF5 N=3, ATF4/ATF5/CREB3L4 N=2).*

Table 7.1: Knockdown efficiency observed with ATF/CREB factors

Transcription Factor	Percentage knockdown in MCF7 cells	Percentage knockdown in MDA-MB231 cells
ATF5	55%	93.9%
CREB3L4	48.3%	67%
ATF4	51.2%	78.5%
ATF4, ATF5	24.9%, 46.4%	78.6%, 95%
ATF4, CREB3L4	51.4%, 71.2%	-
ATF4, ATF5, CREB3L4	-	75%, 93.6%, 75.3%

7.4 Was a transcriptional response to SAHA induced through ATF?

ATF4 knockdown resulted in MCF7 cells more sensitive to SAHA treatment, while the knockdown of ATF4 and ATF5 enhanced the SAHA-sensitivity of MDA-MB231 cells. The novel identification of TFs altering the apoptotic response of cells to HDACi treatment led to the question of whether these factors were acting as TFs or whether this effect was mediated via a transcription independent mechanism? If ATF driven gene expression changes were enabling this resistance to SAHA, perhaps this response would be perturbed following ATF knockdown.

Genes, from the list of 30-minute MCF7 upregulated genes, containing ATF1 binding sites were identified by re-analysing the motif finding results. The 85 genes crossing over between these identified ATF1 target genes and the original list of genes upregulated at 30-minutes were considered target genes of interest. As coordinates were input, HOMER could identify genes at these sites which were ATF1 targets, but not included in the original list. The output list, therefore, contained a greater number of genes as it considered ATF1 binding sites not only in promoters (+/-500bp). It would identify genes in the vicinity of the TSS of matching genes and would identify ATF1 binding sites in exons and enhancers.

DUSP5, EGR1, HSPA1A, HSPA5 and *NR4A1* were selected as they were genes for which primers had been designed earlier in the project. Their expression was investigated by qPCR in scrambled cDNA samples, prior to treatment and following 48-hour SAHA treatment. Any difference between how scrambled and knockdown cells responded would indicate whether ATF was driving this transcriptional response.

7.4.1 An ATF regulated response was observed in MDA-MB231 cells following 48-hour SAHA treatment

Gene expression was initially assessed in MCF7 and MDA-MB231 cells following 48-hour SAHA treatment. A different response was observed in both cell-lines. For example, *HSPA5* was upregulated in SAHA treated MDA-MB231 cells transfected with scrambled siRNA (Figure 7.14B). This was not observed following ATF4 or ATF5 knockdown, with this gene instead displaying a very similar expression before and after SAHA treatment. Loss of this upregulation following knockdown suggested that an ATF driven transcriptional response occurred in these cells at 48-hours. This suggested that ATF4, ATF5, and their downstream genes were involved in regulating how MDA-MB231 cells responded to 48-hour SAHA treatment.

HSPA5 was downregulated following SAHA treatment of scrambled siRNA transfected MCF7 cells and remained so following ATF4 and ATF5 knockdown (Figure 7.14A). This suggested that there was no ATF driven transcriptional response occurring in MCF7 cells at 48-hours. This may relate to the expected timing of the response in this cell-line. MCF7 cells survive through rapid transcriptional change. In that these genes were selected as responding at 30-minutes in MCF7 cells, it was not surprising that their upregulation was not still observed at 48-hours. Seeing this response in MDA-MB231 cells, at this later timepoint, correlates with them not being able to mount the HDACi response as rapidly.

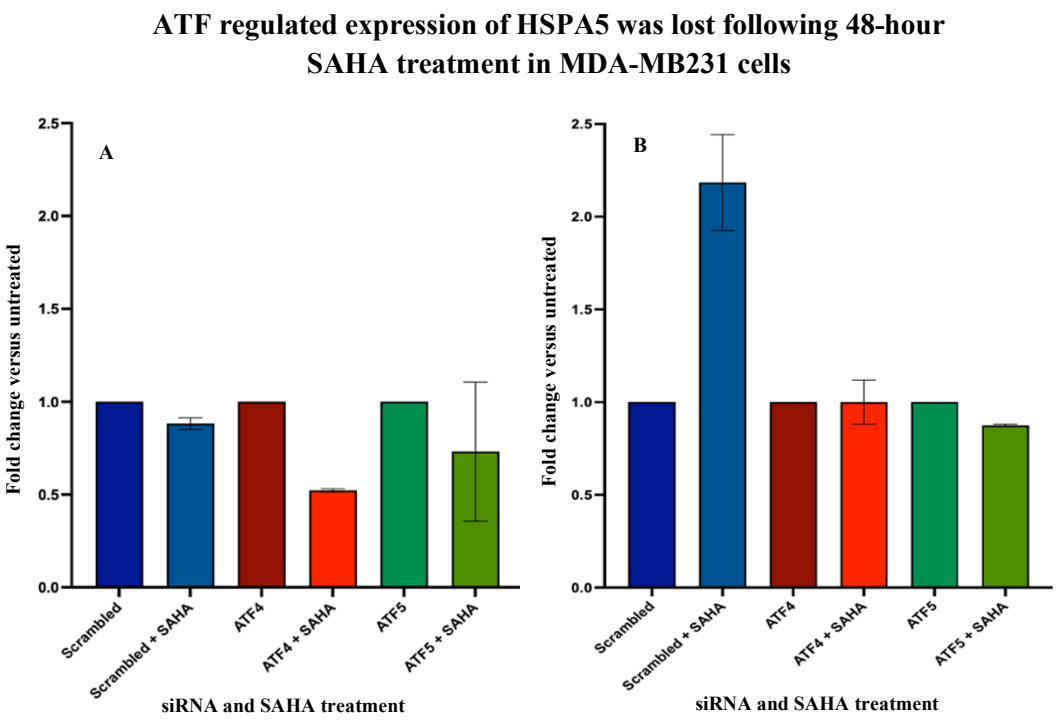


Figure 7.14: The SAHA induced change in HSPA5 expression is lost in MDA-MB231 cells only following knockdown of ATF4 or ATF5. *The fold-change in expression of HSPA5 in 48-hour SAHA treated cells incubated with scrambled, ATF4 or ATF5 siRNA was assessed by qPCR versus that in untreated A. MCF7 and B. MDA-MB231 cells. Error bars show SEM of independent experiments (N=2).*

7.4.2 An ATF driven transcriptional response was observed in MCF7 cells following 2-hour SAHA treatment

The target knockdown genes were selected from a list of genes up-regulated at 30-minutes. This led us to question whether analysis of the gene expression changes occurring at 48-hours was too late. To address whether ATF4 played a transcriptional role during the early HDACi survival response, ATF regulated gene expression was analysed following 2-hour SAHA treatment. ATF4 was knocked down in MCF7 and MDA-MB231 cells, as previously, with cells then treated with SAHA for 30, 60 or 120-minutes. Looking in MCF7 cells, the expression of ATF4 mRNA was significantly downregulated in the presence of increasing SAHA treatment time in scrambled siRNA

transfected cells (p=0.02; Figure 7.15). Considering knockdown efficiency, the expression of *ATF4* was knocked down by around 50% across all timepoints.

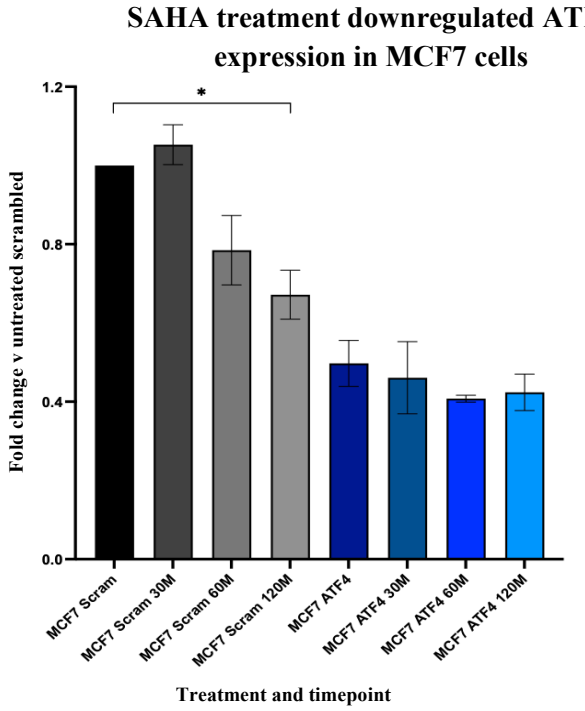


Figure 7.15: ATF4 expression was downregulated in MCF7 cells in response to SAHA treatment. *Fold-change in expression of ATF4 in SAHA treated scrambled and ATF4 knockdown cells compared with expression in untreated scrambled cells after data was normalized to housekeepers. One-tailed, paired T-test comparing normalized 0 and 120-minute expression *p<0.05. Error bars show SEM of independent experiments (N=3).*

The expression of *DUSP5, EGR1, HSPA5, HSPA1A* and *NR4A1* following SAHA treatment in MCF7 cells transfected with ATF4 or scrambled siRNA was assessed. A fold-change of around 0.5 was observed in all genes following knockdown (Figure 7.16). This downregulation in expression in response to knockdown alone indicated that these genes were positively regulated by ATF4. Though they were all regulated by ATF4, they each exhibited a distinct pattern of expression following SAHA treatment. *DUSP5* expression was upregulated by SAHA in scrambled siRNA transfected cells, though this did not reach significance. Though *DUSP5* expression was initially lower following ATF4 knockdown only, its expression was significantly upregulated following SAHA treatment (p=0.04). This indicated that the response of *DUSP5* to SAHA was not dependent on ATF4 alone. SAHA treatment did not affect the expression of *EGR1* or *HSPA5*. *HSPA1A* was upregulated and *NR4A1* was

significantly upregulated in the presence of SAHA. Following ATF4 knockdown both *NR4A1* and *HSPA1A* exhibited a significant upregulation (Figure 7.16). Though their expression was lower basally, they reached the same level of expression as scrambled siRNA transfected cells after 120-minute SAHA treatment.

All five genes responded similarly after knockdown, showing that ATF4 was not solely responsible for regulating their response to SAHA. Though their expression was lower basally, they all reached the expression level observed in scrambled siRNA transfected cells after 2-hour SAHA treatment. Thus, ATF4 may be involved in their homeostasis but not in their response to SAHA. This led to the question of whether the downregulation of ATF4 following SAHA treatment is part of the normal HDACi survival response.

ATF regulated genes responded similarly to SAHA treatment following ATF4 knockdown in MCF7 cells

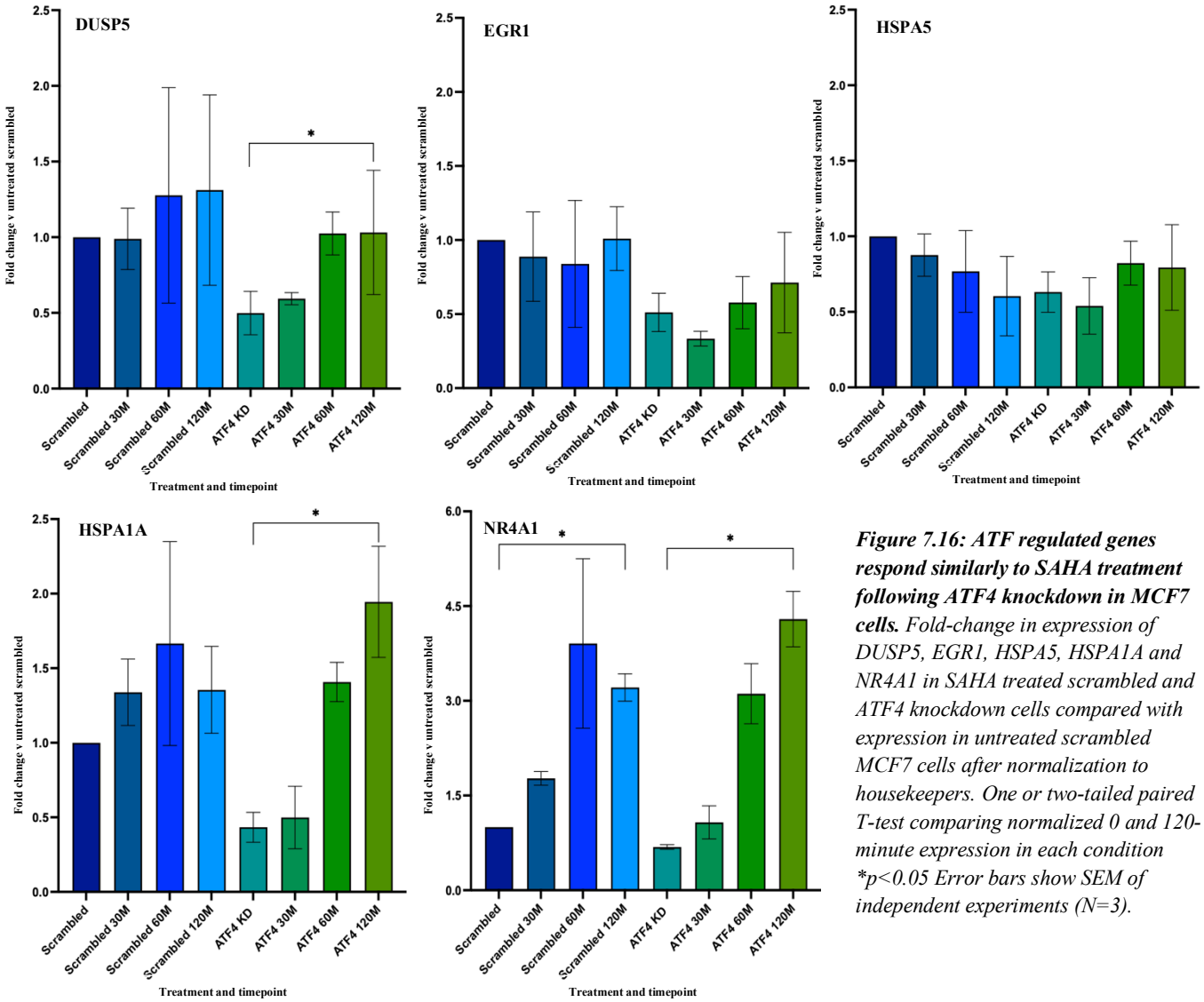


Figure 7.16: ATF regulated genes respond similarly to SAHA treatment following ATF4 knockdown in MCF7 cells. *Fold-change in expression of DUSP5, EGR1, HSPA5, HSPA1A and NR4A1 in SAHA treated scrambled and ATF4 knockdown cells compared with expression in untreated scrambled MCF7 cells after normalization to housekeepers. One or two-tailed paired T-test comparing normalized 0 and 120-minute expression in each condition *p<0.05 Error bars show SEM of independent experiments (N=3).*

DUSP5, EGR1, HSPA5, HSPA1A and *NR4A1* expression was then assessed in MDA-MB231 cells transfected with ATF4 or scrambled siRNA. SAHA treatment did not significantly affect *ATF4* expression in scrambled cells (Figure 7.17). *ATF4* expression was then reduced by 80-90% across all the knockdown timepoints.

These genes were not positively regulated by ATF4 in this cell-line, differing to what had been observed in the MCF7 cells. All the tested genes exhibited fold-change

differences of around 1.5 following ATF4 knockdown, indicating that the transcriptional regulation identified in MCF7 cells was not occurring in these cells (Figure 7.18). SAHA did not significantly affect the expression of *DUSP5, EGR1, HSPA5* and *HSPA1A*. *NR4A1* was the only gene significantly upregulated in the presence of SAHA, however, it was also significantly upregulated following ATF4 knockdown. These responses confirmed that these genes were not ATF4 dependent, responding similarly to SAHA treatment following knockdown. In addition, no ATF4 driven transcriptional response seemed to occur in MDA-MB231 cells following 2-hour SAHA treatment. To conclude, this suggested that an ATF4 driven transcriptional change occurred only in MCF7 cells. This correlates with the suggestion from the RNA-Sequencing that MDA-MB231 cells are more HDACi sensitive as they are slower to induce the necessary transcriptional changes.

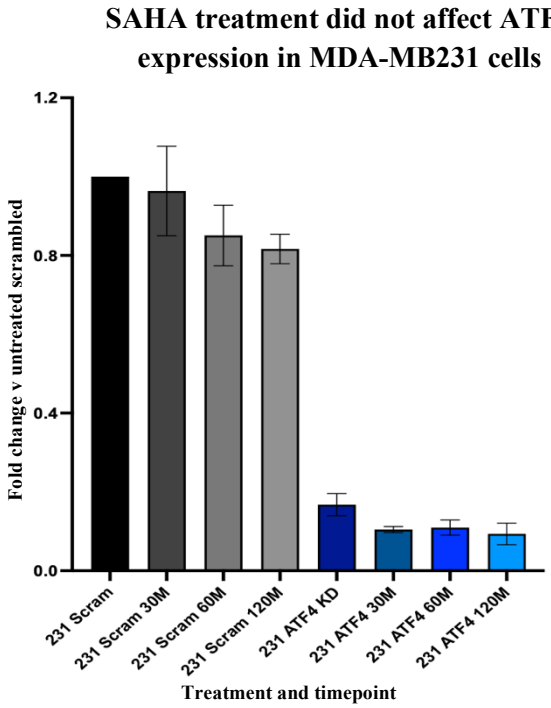


Figure 7.17: SAHA treatment did not affect ATF4 expression in MDA-MB231 cells. *Fold-change in ATF4 expression in SAHA treated scrambled and ATF4 knockdown cells compared to expression in untreated scrambled cells determined after normalization to housekeepers. Paired, two-tailed T-test showed no significant difference between normalized 0 and 120-minute expression. Error bars show SEM of independent experiments (N=3).*

No ATF4 dependent transcriptional regulation was observed in MDA-MB231 cells

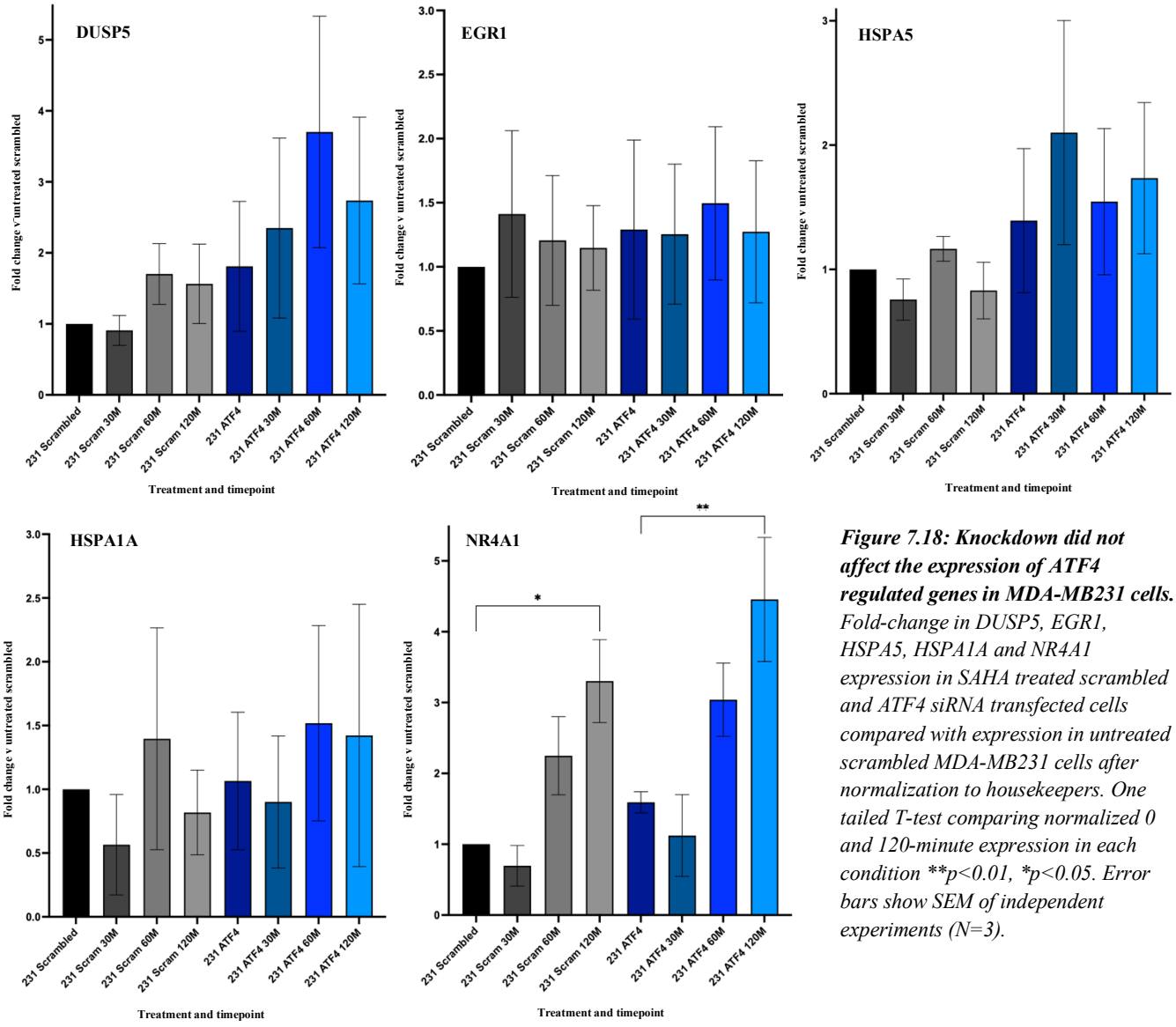


Figure 7.18: Knockdown did not affect the expression of ATF4 regulated genes in MDA-MB231 cells. *Fold-change in DUSP5, EGR1, HSPA5, HSPA1A and NR4A1 expression in SAHA treated scrambled and ATF4 siRNA transfected cells compared with expression in untreated scrambled MDA-MB231 cells after normalization to housekeepers. One tailed T-test comparing normalized 0 and 120-minute expression in each condition **p<0.01, *p<0.05. Error bars show SEM of independent experiments (N=3).*

7.4.3 ATF knockdown did not prevent SAHA-induced HAT gene downregulation

We next explored whether ATF4 was involved in regulating the characteristic downregulation of HAT complex genes in response to HDACi treatment. So far, the

involvement of POU2F1 or POU2F2 in regulating HAT regulation 48-hours post SAHA treatment had been investigated. The focus of this project is on the initial changes induced in response to SAHA. Thus, the expression of HAT genes in ATF4 knockdown MCF7 and MDA-MB231 cells was investigated following 30, 60 or 120-minute SAHA treatment. This investigated whether ATF4 knockdown prevented HAT gene downregulation within 2-hours.

There was no evidence of downregulation in the five acetyltransferase related genes (*EPC1, EPC2, KAT7, KAT6B* and *ING5*) following knockdown alone, with all HAT genes exhibiting a fold-change around 1 (Figure 7.19). This suggested the HAT genes were not positively or negatively regulated by ATF4. SAHA treatment resulted in the significant downregulation of *EPC1* and *EPC2* in scrambled siRNA treated cells. Both genes also exhibited a similar pattern of expression following ATF4 knockdown, though only *EPC2* was significantly downregulated. The expression of *ING5(1)* was downregulated following 120-minute SAHA treatment in scrambled and ATF4 knockdown cells, though only significantly in scrambled cells. The only differences were suggested in *KAT7* and *KAT6B*. *KAT7* was downregulated following SAHA treatment, with this response appearing delayed after ATF4 knockdown. *KAT6B* was significantly downregulated in scrambled cells, with this response perhaps dysregulated after knockdown. It was, thus, concluded that ATF4 was not regulating the SAHA-induced HAT gene downregulation observed in MCF7 cells.

HAT gene downregulation was still observed in MCF7 cells following ATF4 knockdown

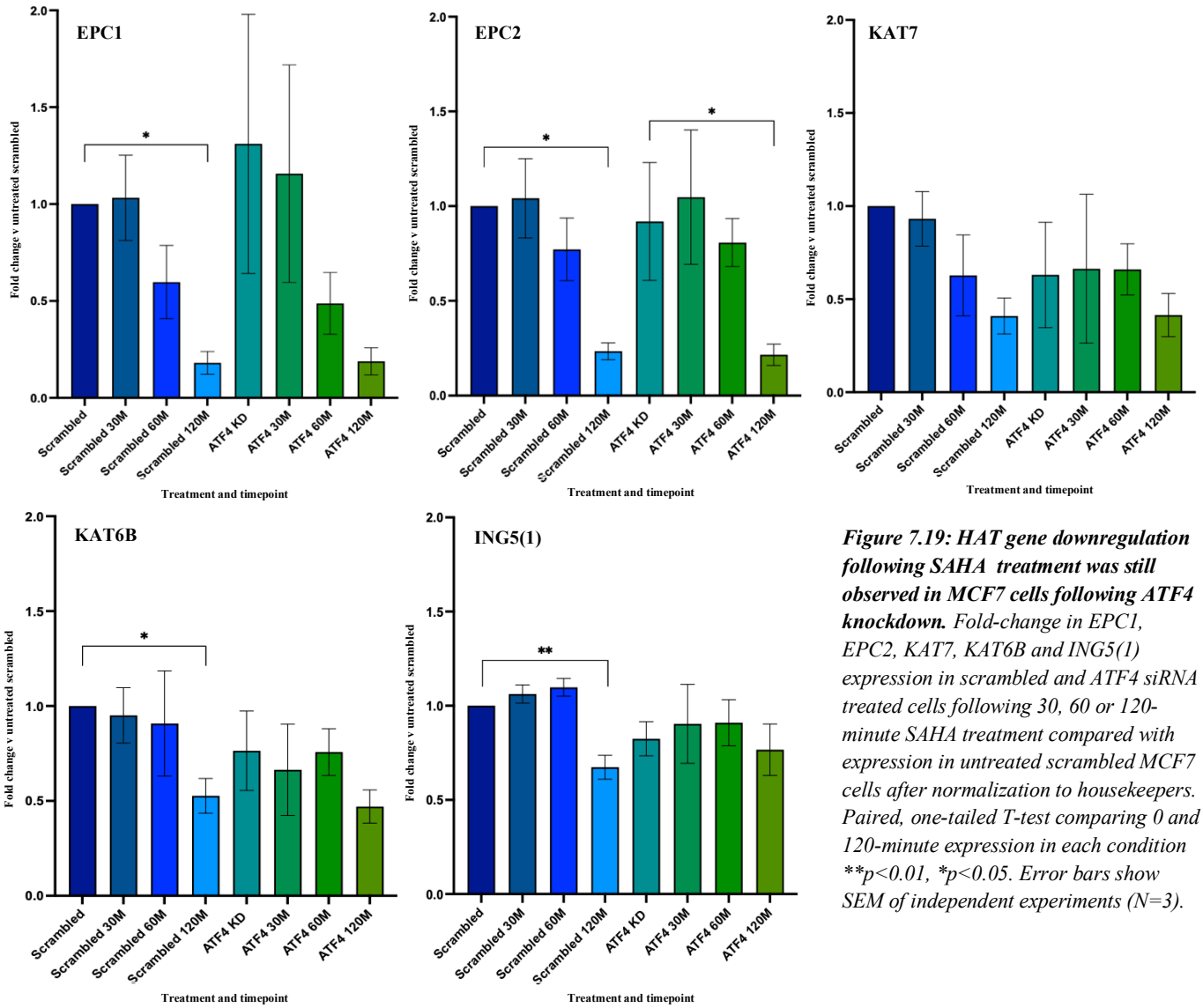


Figure 7.19: HAT gene downregulation following SAHA treatment was still observed in MCF7 cells following ATF4 knockdown. *Fold-change in EPC1, EPC2, KAT7, KAT6B and ING5(1) expression in scrambled and ATF4 siRNA treated cells following 30, 60 or 120-minute SAHA treatment compared with expression in untreated scrambled MCF7 cells after normalization to housekeepers. Paired, one-tailed T-test comparing 0 and 120-minute expression in each condition **p<0.01, *p<0.05. Error bars show SEM of independent experiments (N=3).*

The SAHA-induced HAT gene downregulation was then investigated in MDA-MB231 cells following ATF4 knockdown. *EPC2, KAT7* and *ING5(1)* expression were significantly reduced after SAHA treatment in scrambled and ATF4 siRNA transfected cells (Figure 7.20; $p<0.05$). *KAT6B* expression was not significantly downregulated, while *EPC1* expression was only significantly downregulated in scrambled cells. Their expression was not downregulated in response to knockdown

alone, indicating that none of these genes were solely dependent on ATF4. Interestingly, *KAT7* and *KAT6B* expression was upregulated following ATF4 knockdown alone – though not significantly (Figure 7.20). These results highlighted that ATF4 knockdown did not prevent the characteristic HAT gene downregulation observed in MDA-MB231 cells following SAHA treatment. This indicated that ATF4 was not involved in mediating their downregulation in response to HDACi.

To conclude, these knockdown experiments highlighted key differences between the cell-lines. Knockdown of ATF4 and ATF5 significantly increased the sensitivity of MDA-MB231 cells to SAHA, while knockdown of ATF4 and CREB3L4 significantly increased the SAHA sensitivity of MCF7 cells. ATF4 did not play a transcriptional role during their early response to HDACi treatment – with HAT gene downregulation and ATF gene expression not perturbed following knockdown. This led us to investigate knockdown across resistance pathways.

ATF4 knockdown did not prevent HAT gene downregulation in MDA-MB231 cells

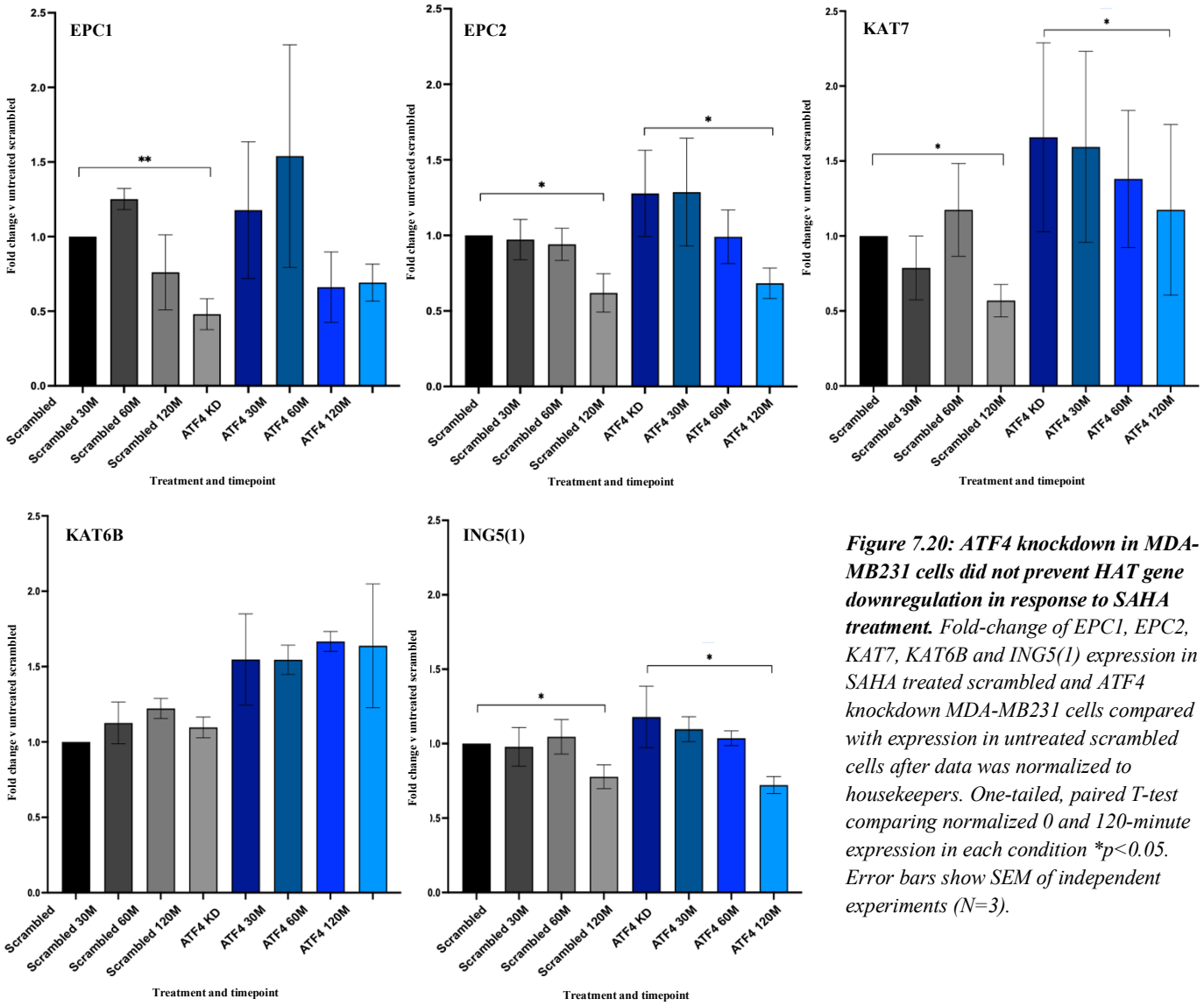


Figure 7.20: ATF4 knockdown in MDA-MB231 cells did not prevent HAT gene downregulation in response to SAHA treatment. *Fold-change of EPC1, EPC2, KAT7, KAT6B and ING5(1) expression in SAHA treated scrambled and ATF4 knockdown MDA-MB231 cells compared with expression in untreated scrambled cells after data was normalized to housekeepers. One-tailed, paired T-test comparing normalized 0 and 120-minute expression in each condition *p<0.05. Error bars show SEM of independent experiments (N=3).*

7.5 Knockdown across resistance pathways

The HDACi survival response is believed to involve several alternative resistance pathways. Thus, the knockdown of factors across multiple pathways was next investigated. The initial combination knockdowns in this project had involved TFs from the same family. ATF4, ATF5 and CREB3L4 were knocked down together. These factors are from the same family and identify a similar motif, so their combined knockdown investigated

only one resistance pathway. In addition, knocking down POU2F1 with POU2F2 considered two members of the same TF that recognise the same binding motif. Thus, an important step in understanding this early transcriptional response involved knocking down components of multiple resistance pathways to determine whether this enhanced the sensitivity of MCF7 and MDA-MB231 cells to HDACi treatment.

One factor was selected from each pathway for knockdown. ATF4 was selected as the only factor significantly affecting the sensitivity of MCF7 and MDA-MB231 cells; significantly increasing the apoptotic response in MCF7 cells and significantly increasing the loss in MDA-MB231 viability (Figure 7.5; Figure 7.11). ATF4 was knocked down alongside SRF, which exists in a distinct pathway and POU2F2 which when knocked down significantly enhanced the apoptotic response in MDA-MB231 cells (Figure 6.14). It was hypothesised that this triple pathway knockdown would enhance cell sensitivity to SAHA treatment – compared with individual knockdown. HDACi-induced apoptosis was compared in cells transfected with 25 nM ATF4, 25 nM POU2F2 and 25 nM SRF siRNA, cells transfected with 25 nM scrambled siRNA and untransfected cells.

7.5.1 ATF4 and POU2F2 appeared to converge on the same apoptotic pathways by 48-hours

The pathway triple knockdown was initially carried out in MDA-MB231 cells, which are believed to be less protected by the HDACi resistance response. The individual knockdown of ATF4 and POU2F2 enhanced the apoptotic population in MDA-MB231 cells. Thus, these factors were knocked down together with SRF to investigate whether this further enhanced the HDACi-sensitivity of this cell-line.

Quantification by qPCR showed that *ATF4* expression was depleted by 52.5%, *POU2F2* by 58% compared with expression in scrambled siRNA treated cells (data not shown; Table 7.2). *SRF* was only depleted by 15% in one of the two replicates. SAHA treatment resulted in a 38.2% loss in viability in scrambled siRNA transfected cells and 51% loss in viability in pathway triple knockdown cells (Figure 7.21). Interestingly, this 12.79% increase resulted in an accumulation of cells in late-stage apoptosis - as had been observed following POU2F2 knockdown. Pathway triple knockdown cells exhibited a reduction in their resulting viable population, alongside an increase in their late apoptotic population in response to SAHA treatment (Figure 7.22A). However, the loss in viability was not increased over either ATF4 or POU2F2 knockdown alone (Figure 7.22B). ATF4 knockdown resulted in a 9.6% increase in the loss in viability over treated scrambled cells, POU2F2 resulted in an 11.1% increase, while triple knockdown resulted in only a 13.76% increase. This highlighted that knockdown across three different pathways only increased the loss in viability by around 2-4% over the individual knockdown of ATF4 or POU2F2. However, differences in knockdown efficiency should be considered compared with the individual ATF4 and POU2F2 knockdown experiments (Table 7.1). ATF4 knockdown depleted expression by 78.5%, while POU2F2 knockdown depleted expression by 89.3%. These represent a 26% greater depletion in *ATF4* and 41.3% greater depletion in *POU2F2* expression. This difference could explain why the pathway triple knockdown resulted in only a 2-4% greater loss in viability. This suggests that with greater knockdown efficiency, a greater loss in viability may be observed.

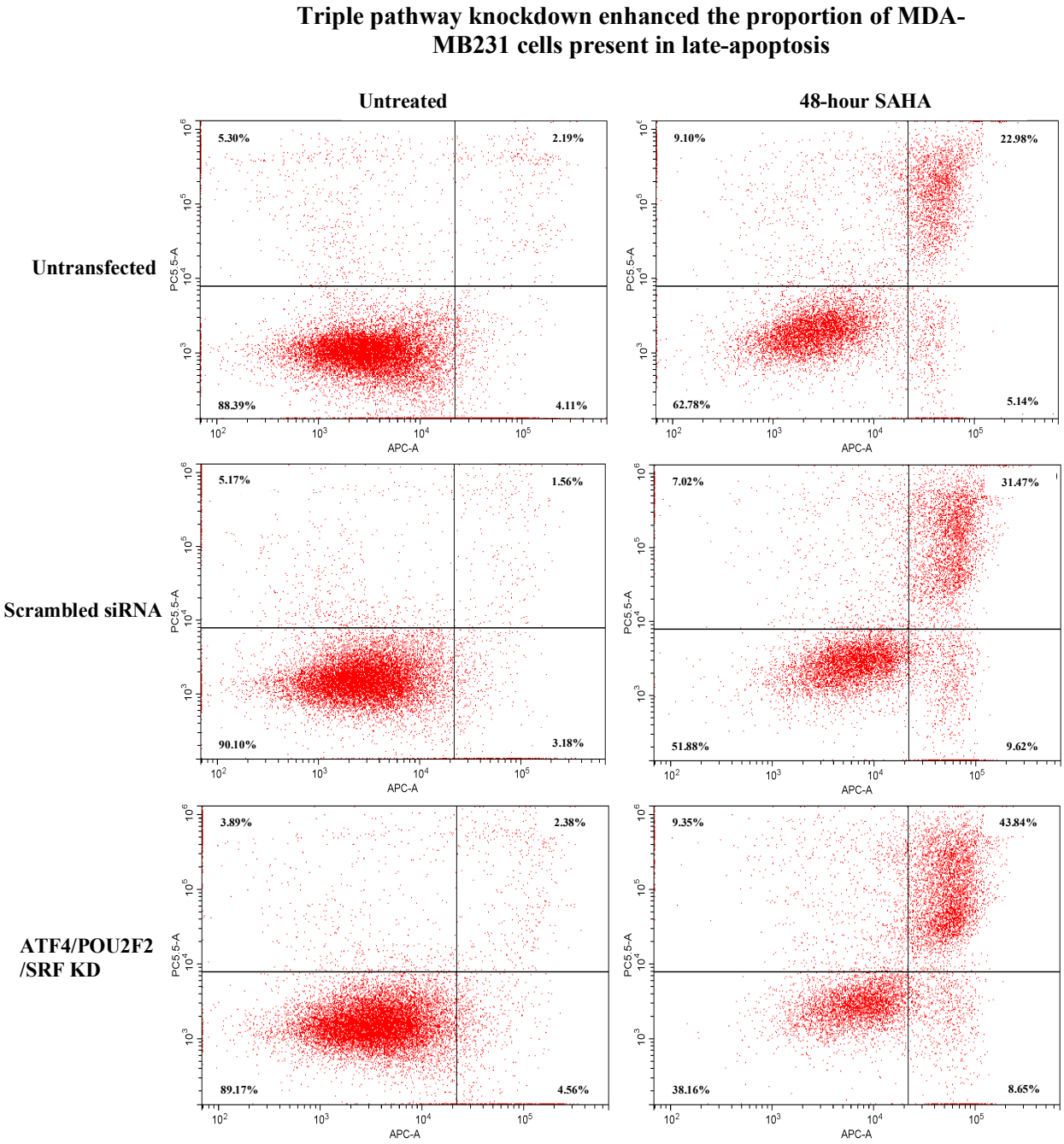


Figure 7.21: ATF4, POU2F2 and SRF knockdown in MDA-MB231 cells reduced the viable population remaining after 48-hour SAHA treatment. *Apoptosis in untransfected, cells transfected with scrambled or ATF4/POU2F2/SRF siRNA was assessed using the annexin V/propidium iodide assay following treatment with 2.5 μM SAHA for 48-hours. Images generated using CytExpert 3.4 Software.*

This experiment concluded that knocking down POU2F2, ATF4 and SRF did not enhance SAHA-induced apoptosis in MDA-MB231 cells over individual knockdown.

As SRF was only knocked down in one replicate, this effect was dependent on only ATF4 and POU2F2. The pathway triple knockdown exhibited the outcome of either ATF4 or POU2F2 knockdown alone. The lack of additive or protective effect observed when knocking them down together suggested that these factors may converge on the same pathways. The limited difference observed between the triple knockdown and individual ATF4 or POU2F2 knockdowns, suggested that these factors converge on similar apoptotic pathways by 48-hours.

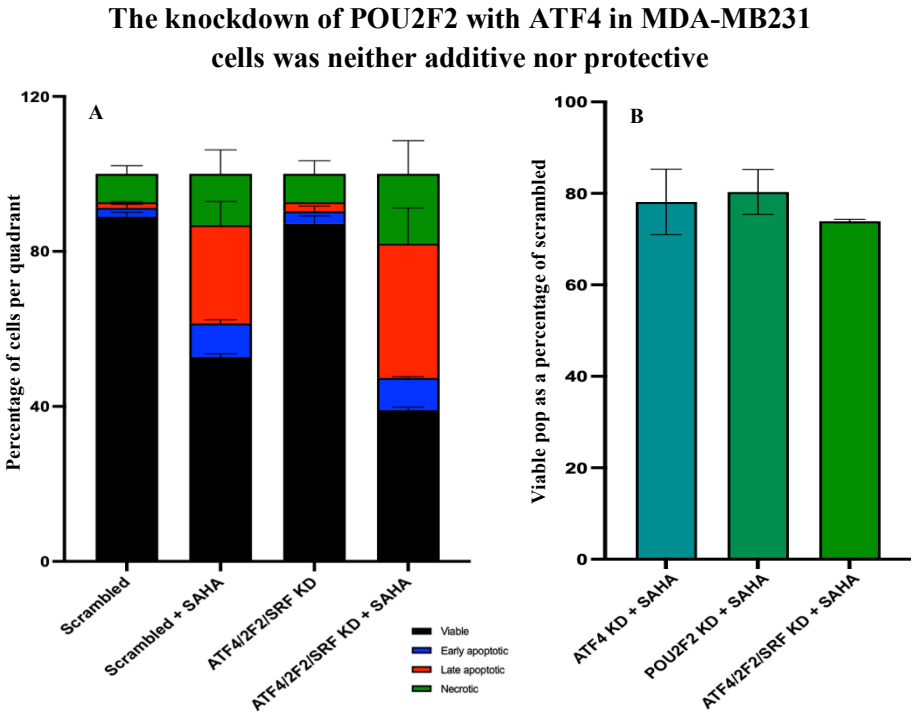


Figure 7.22: Knockdown of ATF4 POU2F2 and SRF together did not result in a significant loss in cell viability over individual knockdown. *A. The percentage of cells per quadrant of the Annexin V Assay in SAHA treated and untreated scrambled and ATF4, POU2F2 and SRF knockdown cells. B. The viable population remaining after SAHA treatment following individual ATF4 or POU2F2 knockdown or pathway triple knockdown cells as a percentage of that in respective scrambled controls. Error bars show SEM of independent experiments (N=2).*

7.5.2 The effect of ATF4 knockdown was lost in MCF7 cells with SRF also knocked down

ATF4, POU2F2 and SRF were then knocked down in MCF7 cells to explore whether knocking down multiple resistance pathways enhanced their sensitivity to HDACi-induced apoptosis. In this cell-line, only ATF4 knockdown of these three factors had significantly enhanced their SAHA sensitivity. This pathway triple knockdown was carried out to be compared with the results observed in the more HDACi sensitive cell-line. However, we were interested to observe whether perturbing a few resistance pathways would reduce the protective effect of the HDACi survival response.

As has been shown previously, *POU2F2* was not expressed in this cell-line. Quantification by qPCR showed that *ATF4* expression was depleted by 45.3% and *SRF* by 47% compared with expression in scrambled siRNA treated cells (data not shown; Table 7.2). SRF knockdown was inconsistent across replicates, with a 10% knockdown achieved in one and an 84% knockdown achieved in the second. Pathway triple knockdown did not affect the distribution of cells per quadrant of the Annexin V assay, with no increase observed in the number of late apoptotic cells (Figure 7.23). However, interpreting these results was confounded by the high percentage of necrotic cells evident (Figure 7.23A). The increase in apoptotic cells following SAHA treatment resulted in a loss from the necrotic and not viable population. Therefore, no difference was observed in the percentage of viable cells remaining across the treatments. Pathway triple knockdown did not increase apoptosis above that induced in scrambled siRNA transfected cells (Figure 7.23B). Interestingly, the effect of ATF4 knockdown in increasing the SAHA-sensitivity of MCF7 cells was lost upon pathway triple pathway knockdown. 7.6% of cells were in late apoptosis following individual

ATF4 knockdown. In the pathway triple knockdown with a 10% loss in SRF expression, 7.8% cells were in late apoptosis. The percentage of cells in late apoptosis was reduced to 6.8% with an 84% loss in SRF expression (Figure 7.23). Though further replicates are needed, this suggests that SRF knockdown may reduce the effect observed following ATF4 knockdown. The high percentage of cells in late apoptosis in SAHA treated scrambled cells in the pathway triple knockdown, compared with the ATF4 knockdown experiment, affected the direct comparison of these results. This led to the question of whether SRF knockdown protected from the effect induced following ATF4 loss, or whether SRF perturbed ATF4 related signalling?

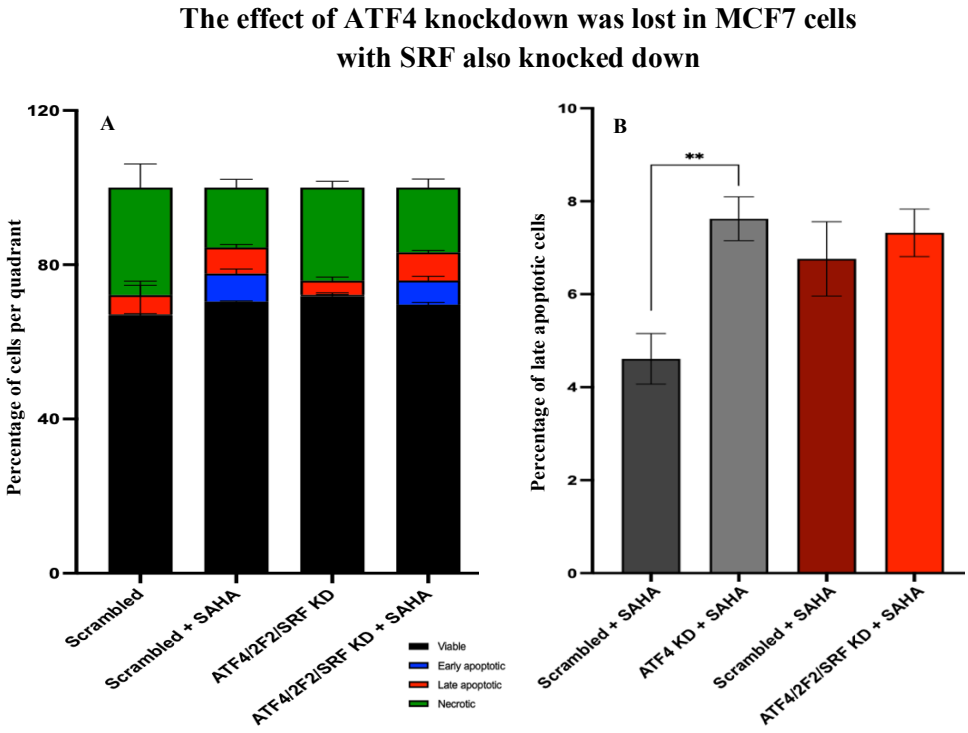


Figure 7.23: Knockdown of ATF4, POU2F2 and SRF did not enhance the SAHA sensitivity of MCF7 cells. *A. The percentage of cells per quadrant of the Annexin V Assay in untreated and SAHA treated scrambled and ATF4, POU2F2 and SRF knockdown cells. B. The late apoptotic population in SAHA treated ATF4 knockdown or triple pathway knockdown cells alongside their respective scrambled control. Paired, one-tailed T-test **p<0.01. Error bars show SEM of independent experiments (N=2; ATF4 N=4).*

Table 7.2: Knockdown efficiency in triple pathway knockdown

Transcription Factor	Percentage knockdown in MCF7 cells	Percentage knockdown in MDA-MB231 cells
ATF4	45.3%	52.5%
POU2F2	-	58%
SRF	47%	15%

The pathway triple knockdown exhibited the effect of either ATF4 or POU2F2 knockdown in MDA-MB231 cells, highlighting that these TFs were neither protective nor additive when knocked down together. This suggested that they may converge on the same apoptotic pathways by 48-hours. On the other hand, when SRF and ATF4 were knocked down together – the effect of ATF4 knockdown was lost. This raised the question of whether a downstream effect of SRF knockdown interacted with the transcriptional effects of ATF4 at 48-hours.

The knockdown of an *ATF/CREB* gene may affect the expression of other bZIP TF genes. This was controlled for in initial experiments, which considered the expression of *ATF4, ATF5* and *CREB3L4* in response to each individual knockdown. Following ATF4 knockdown in MDA-MB231 cells, *ATF5* expression was upregulated while CREB3L4 expression was reduced by 33.5%. Following ATF5 knockdown, *ATF4* expression was reduced by 13% in one replicate while *CREB3L4* expression was reduced by 38%. CREB3L4 knockdown did not affect *ATF4* expression while *ATF5* was reduced in expression only in one replicate (data not shown). In MCF7 cells, CREB3L4 expression was reduced by 50% in one ATF4 knockdown replicate while ATF4 expression was reduced by around 24% following CREB3L4 knockdown (data

not shown). Considering the efficiency observed in our experiments, these results suggest that our knockdowns were more specific to the ATF/CREB target gene of interest (Table 7.1). However, the expression of additional bZIP TF members was affected which makes it difficult to identify the effect from individual gene knockdowns.

In addition, functional redundancy is evident within the ATF/CREB family (Hau and Hartman, 2001). Members of this family recognise the same DNA binding sequence and readily form homo and hetero dimers. For example, ATF4 form heterodimers with members of the ATF, FOS/JUN and C/EBP transcription factor families (Wortel *et al.,* 2017; Chen *et al*., 2022). This suggests that other bZIP TF genes may compensate for the loss of *ATF4, ATF5* or *CREB3L4* and prevent the effect of individual knockdowns being observed.

7.6 Our model system was representative of the comparison between luminal A and triple-negative tumours

The final step in this project involved comparing our samples to a patient cohort to understand whether MCF7 and MDA-MB231 cells are representative of their molecular subtype. MCF7 cells represent a luminal A subtype (ER/PR+, HER2-) and MDA-MB231 a triple-negative (ER/PR/HER2-) (Riaz *et al.,* 2013; Cailleau *et al.,* 1978). This project directly compared the SAHA-induced transcriptional changes in one sensitive and one more resistant cell-line. This comparison does not consider the inherent differences between them that do not affect how they respond to HDACi treatment. This project would have benefitted from assessing a large cell-line panel, to establish correctly what

could be assigned as characteristic of this response. As this was not possible, the model was validated by comparing it to a patient cohort using the CBioPortal database. The genetic profiles of triple-negative and luminal A tumours were investigated – considering copy number variations, mutations, and the mRNA expression of gene families which had been identified for knockdown analysis. The question asked was whether our model system represented tumour cell populations and whether the TF genes of interest were differentially expressed between luminal A and triple-negative samples.

HDACi have not been effective in the treatment of solid tumours. It is believed that their clinical use could be enhanced through their personalisation to receptive tumours. The identification of differential gene expression profiles in sensitive tumours could be an avenue through which tumours could be screened prior to treatment.

This comparison only considered breast tumour samples, corresponding to our knockdown work in a breast line model. The expression, mutation, and gene amplification profiles of *SRF, CREB3L4, ATF1, ATF3, ATF4, ATF5, ATF6, POU2F1* and *POU2F2* were queried in all 25 breast cancer studies included in CBioPortal (Cerami *et al.*, 2012; Gao *et al.,* 2013). These genes represent those which were selected for knockdown, alongside additional members of the ATF family – as this family significantly affected the SAHA sensitivity of both cell-lines. The queried genes were altered in 17% of the 11632 total samples, with gene amplification the most common alteration observed across all samples (Figure 7.24). This was perhaps not surprising, as copy number and single nucleotide variation have been shown generating most driver mutations in breast cancer (Shlien and Malkin, 2009). What was interesting to observe was the co-occurrence of gene amplifications among these genes of interest in the patient

samples. Though most obvious with *CREB3L4, ATF3, ATF6* and *POU2F1*, significant co-occurrence was observed across all the genes analysed. This was an initial validation of our model system. The genes selected for this analysis, which had been identified through motif and subsequent knockdown analysis, appeared to be relevant in these cancers.

Genes of interest were predominantly amplified in breast cancer samples

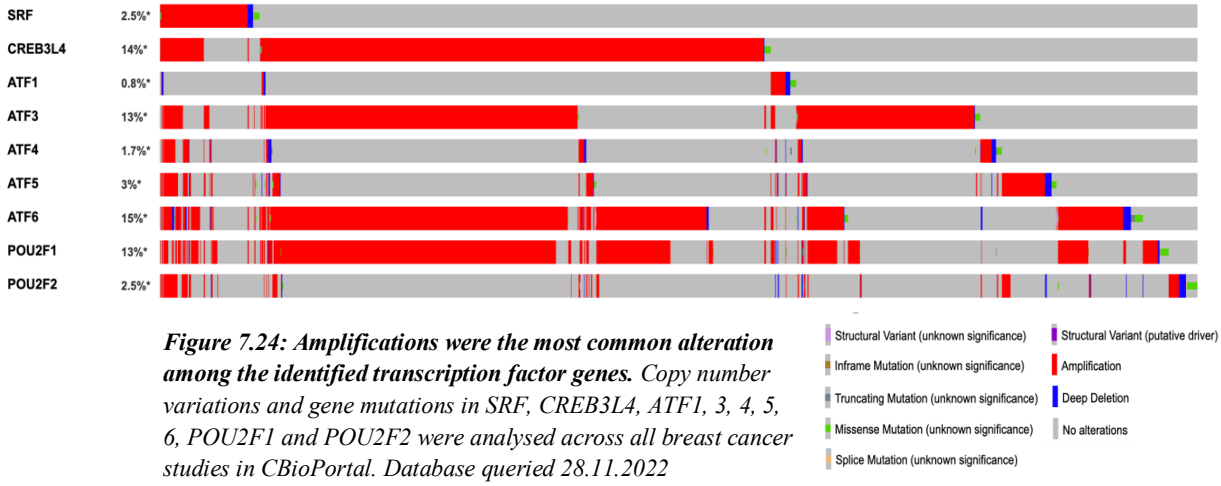


Figure 7.24: Amplifications were the most common alteration among the identified transcription factor genes. *Copy number variations and gene mutations in SRF, CREB3L4, ATF1, 3, 4, 5, 6, POU2F1 and POU2F2 were analysed across all breast cancer studies in CBioPortal. Database queried 28.11.2022*

Based on this co-occurrence, the chromosomal position of our TF genes of interest was then considered. Analysis of the literature confirmed that the regions at which the genes identified for this analysis were located were commonly amplified in cancers. For example, five of these genes were located on the q arm of Chromosome 1 – a region commonly amplified in breast cancers (Figure 7.25; Chen e*t al*., 2020; Shadeo and Lam, 2006). Analysis of 31 primary tumours of advanced breast cancer showed that 1q11-23 was amplified in 48% and 1q25-31 in 45% of cases - the region in which the *CREB3L4* gene is located (Nessling *et al.* 2005). In addition, amplifications were observed at 6p21- where *SRF* is located – as well as 19q13 - where *ATF5* and *POU2F2* are found and 22q13 – the region at which *ATF4* is located (Figure 7.25).

Commonly amplified genes are located at similar chromosomal positions

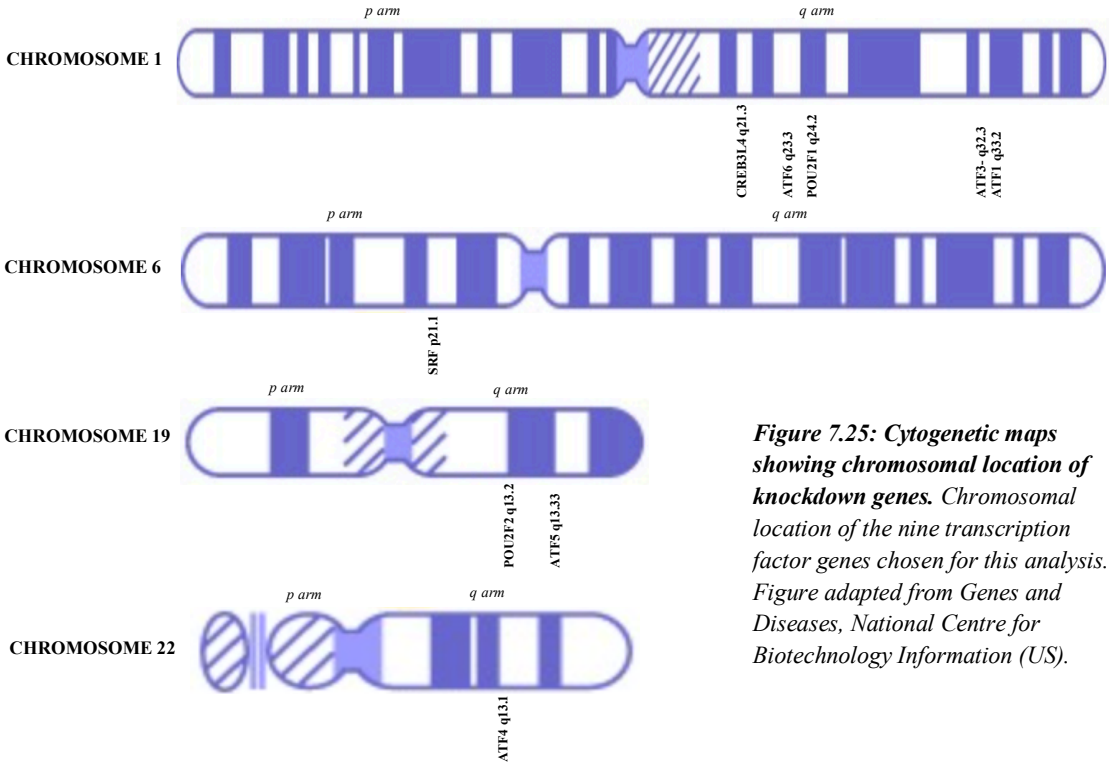


Figure 7.25: Cytogenetic maps showing chromosomal location of knockdown genes. *Chromosomal location of the nine transcription factor genes chosen for this analysis. Figure adapted from Genes and Diseases, National Centre for Biotechnology Information (US).*

Interest then turned to assessing whether the molecular subtypes were associated with a particular copy number profile. The overall breast cancer dataset in CBioPortal does not contain information on the receptor status of each patient, so this analysis used the TCGA Nature 2012 dataset. By incorporating tracks for the ER and PR as well as HER2 status, the mutation and copy number profile associated with the molecular subtypes of breast cancer were assessed. Interestingly, triple-negative and luminal A samples could not be easily distinguished when patients were separated by receptor status (Figure 7.26). For example, *CREB3L4, ATF6* and *POU2F1* were similarly amplified in both subtypes. Some differences were suggested in these genes. A greater number of *ATF3* or *ATF5* amplifications were evident in our luminal A samples. Overall, this indicated that the molecular subtypes could not be easily distinguished by gene copy number or mutation.

This led to the consideration of whether the gene copy numbers correlated to the resulting gene expression.

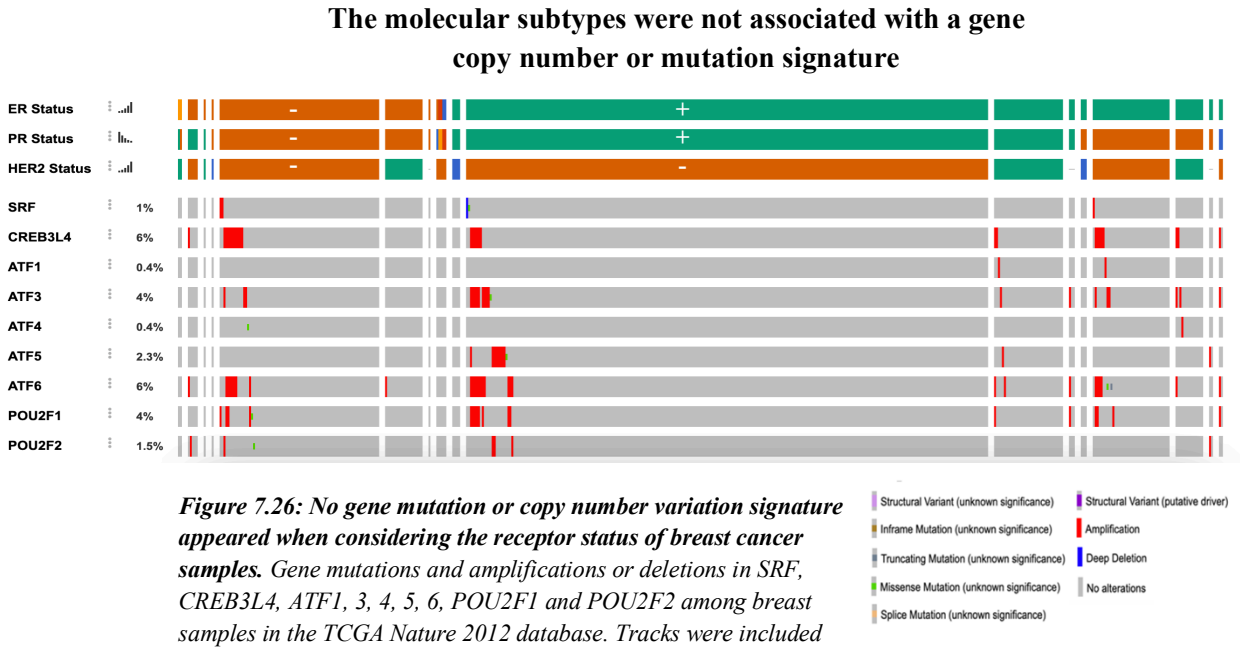


Figure 7.26: No gene mutation or copy number variation signature appeared when considering the receptor status of breast cancer samples. *Gene mutations and amplifications or deletions in SRF, CREB3L4, ATF1, 3, 4, 5, 6, POU2F1 and POU2F2 among breast samples in the TCGA Nature 2012 database. Tracks were included for ER, PR and HER2 status with orange depicting a negative status and green a positive status. Databased queried on 29.11.2022.*

Pollack *et al.,* in 2002 showed a link between DNA copy number changes and increased gene expression in cancers. However, it was not known whether this would be the case in these breast cancer samples. To query this, a heatmap was used to visualise the gene expression patterns in triple-negative and luminal A samples (Figure 7.27). This showed that copy number variation did not correlate with gene expression changes, indicating that additional mechanisms were involved in their transcriptional activation. However, this identified the initial difference between the subtypes. Our molecular subtypes could be distinguished when considering gene expression patterns. The greatest difference in expression between the two subtypes was evident in *CREB3L4*. This gene appeared to be downregulated in triple-negative compared with luminal A samples. The heatmap indicated that there were several differences between the subtypes. For example, *ATF4* and *POU2F2* were predominantly downregulated among luminal A samples.

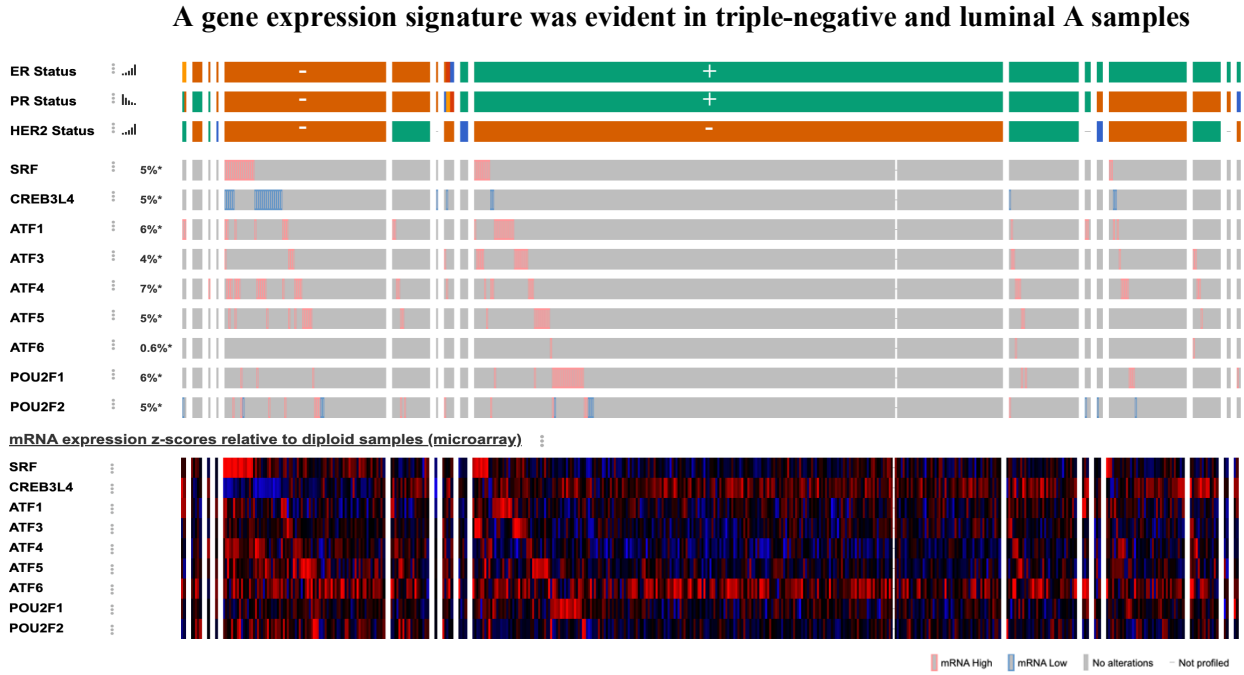


Figure 7.27: A gene expression signature was evident when considering the receptor status of breast cancer samples. *The gene expression of SRF, CREB3L4, ATF1, ATF3, ATF4, ATF5, ATF6, POU2F1 and POU2F2 was considered in triple-negative and luminal A breast cancer subtypes in the TCGA Nature 2012 database. Shown is a heatmap depicting z-scores relative to the diploid samples. Queried on 29.11.2022.*

The TCGA Nature 2012 database contained a greater number of luminal A samples. Therefore, differential expression between subtypes could not be quantified from the resulting oncoprint (Figure 7.27). Thus, mRNA microarray data from each patient sample was used to compare gene expression across the subtypes. Figure 7.28 depicts those genes exhibiting a significant difference in their expression between the triple-negative and luminal A samples (p<0.001). These violin plots show that differential expression is evident between triple-negative and luminal A samples. *CREB3L4* provided the most striking difference. This was clearly highlighted with the difference in their median expression values. This figure also shows that the spread of *ATF4* and *SRF* expression values is much smaller, than was observed with genes such as *ATF3*. What was most interesting was that these expression differences often correlated with those which had been observed in our RNA-Sequencing data. This is best represented with *CREB3L4* and

POU2F2 expression. *CREB3L4* was more highly expressed in luminal A samples. This correlates with its selection for knockdown analysis based on being more highly expressed in MCF7 cells. *POU2F2* was more highly expressed in triple-negative samples. POU2F2 was selected as a target for knockdown as it was only expressed in our triple negative cell-line. This suggests that our model system, MCF7 and MDA-MB231, is transcriptionally representative of these two molecular subtypes – when we consider these selected genes.

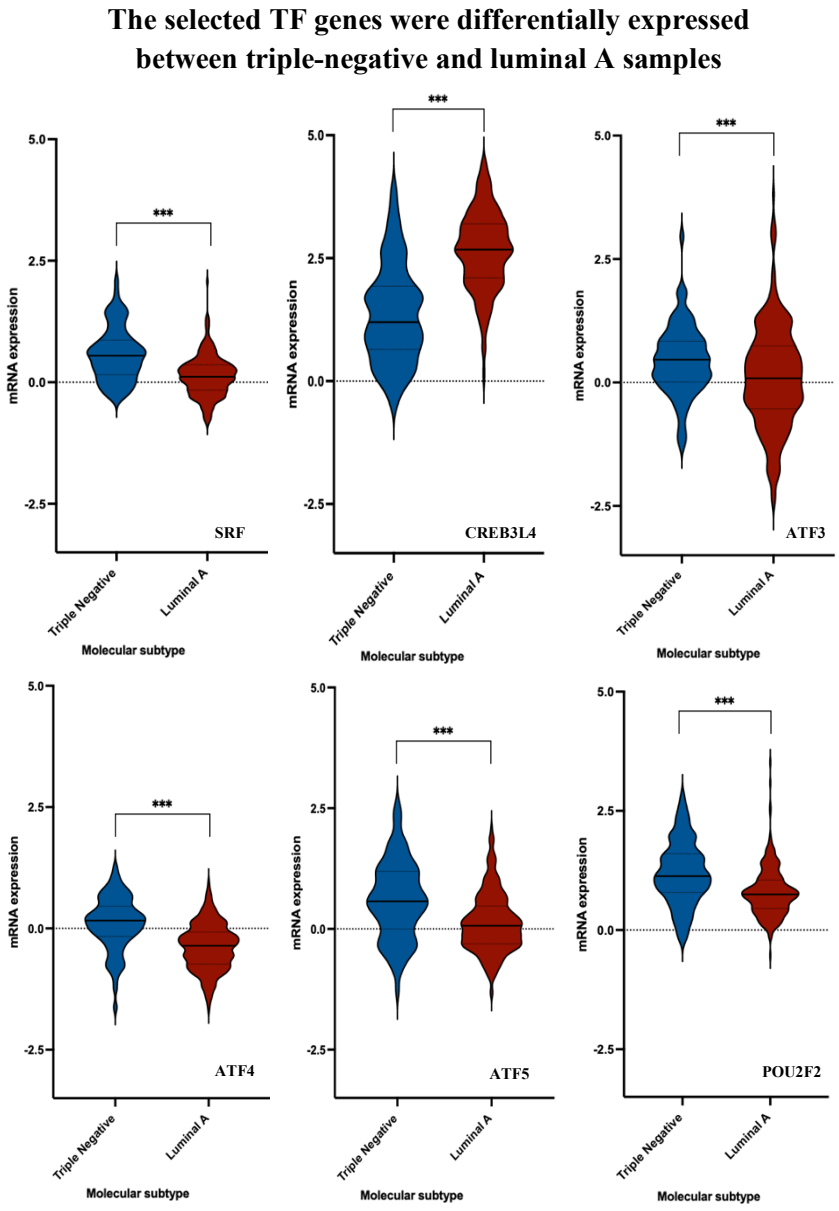


Figure 7.28: The transcription factor genes were significantly differentially expressed by molecular subtype. *The expression of SRF, CREB3L4, ATF3, ATF4, ATF5 and POU2F2 was compared in triple-negative and luminal A breast cancer samples using the TCGA Nature 2012 mRNA microarray data. The shape of the kernel indicates the distribution of data – with the steeper sides indicating a greater concentration of data points. The solid horizontal line depicts the median and dotted lines the quartiles ***p<0.001 (Welch's correction).*

The final question asked was whether the basal expression of *HSP* genes differed between triple-negative and luminal A samples. This analysis was designed to explore the idea that the MDA-MB231 cell-line was inherently more stressed. The gene mutation, copy number and expression profile of *HSPA1A*, *HSP90AA1*, *HSP90AB1* and *HSP90B1* were considered with tumour samples separated by molecular subtype (Figure 7.29). The expression of the four *HSP* genes differed between the triple-negative and luminal A samples. This was most clearly observed with *HSPA1A*, which was predominantly downregulated in the triple-negative compared with luminal A samples. Assessment of their expression from the mRNA microarray data indicated that three of the *HSP* genes were significantly differentially expressed between triple-negative and luminal A samples (Figure 7.30; $p<0.01$, $p<0.001$). This analysis showed higher basal expression of *HSP* genes in triple-negative samples.

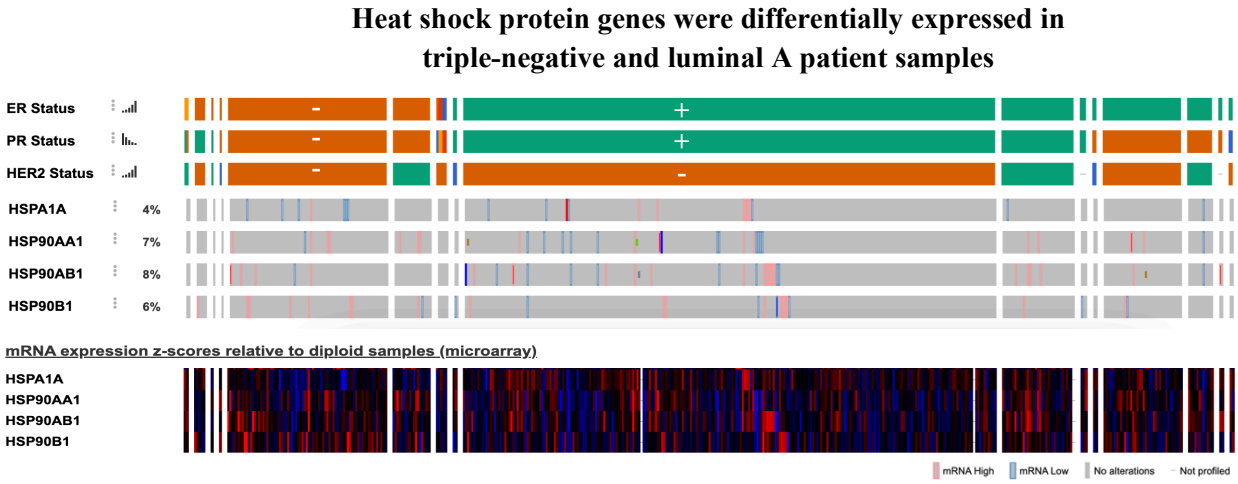


Figure 7.29: Heat shock protein gene expression differed by molecular subtype. *The gene copy number variations, mutations, and expression of HSPA1A, HSP90AA1, HSP90AB1 and HSP90B1 was considered in triple-negative and luminal A breast cancer patient samples in the TCGA Nature 2012 database. Queried on 15.12.2022.*

HSPA1A, HSP90B1 and HSP90AB1 were differentially expressed in triple-negative and luminal A samples

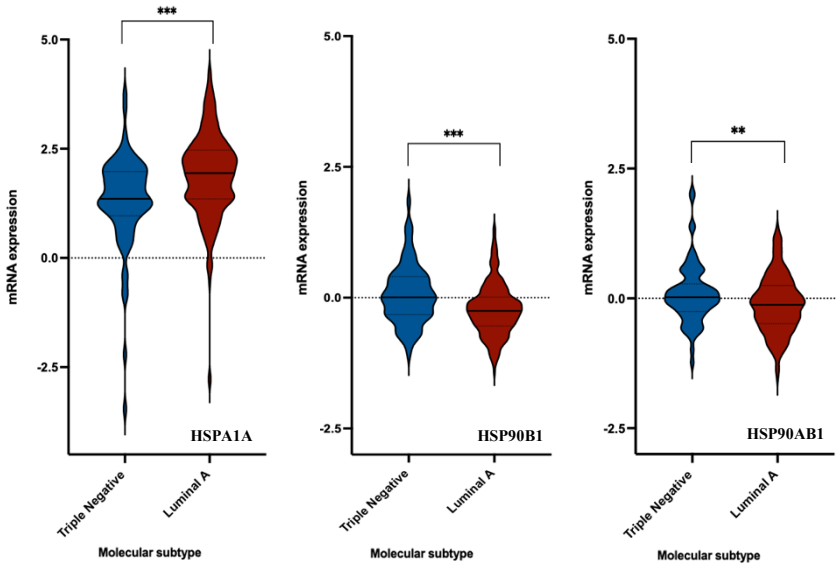


Figure 7.30: Heat shock protein genes were significantly differentially expressed by molecular subtype. *The expression of HSPA1A, HSP90B1 and HSP90AB1 was compared in triple-negative and luminal A breast cancer patient samples. The shape of the kernel indicates the distribution of data – with the steeper sides indicating a greater concentration of data points. The solid horizontal line depicts the median and dotted lines the quartiles. ***p<0.001 **p<0.01 (Welch's correction).*

Comparing our samples to a patient cohort suggested that the transcriptional landscape in our model cell-lines was representative of a tumour cell population. MCF7 and MDA-MB231 cells appeared to be representative of their luminal A and triple-negative subtypes in terms of expression of the key genes identified. The genes of interest for this analysis were selected based on their differential expression between our cell-lines and their ability to alter their HDACi sensitivity. A molecular subtype signature was identified when considering the expression of our nine identified genes of interest.

The database analysis suggested that the identified knockdown genes were differentially expressed between the two subtypes. It was important to see that their expression patterns – specifically those of *CREB3L4* and *POU2F2* - matched what was observed in our qPCR and RNA-Sequencing work. This suggests that gene expression signatures may make it possible to target HDACi therapy to receptive tumours.

8. DISCUSSION

The first chapter developed a solid tumour model of HDACi resistance - consisting of the more HDACi sensitive MDA-MB231, more HDACi resistant MCF7, alongside the immortalised but non-transformed MCF10A cells. Their response to SAHA treatment was then compared. The same alterations were observed in the MCF7 and MDA-MB231 cell-cycles in response to SAHA, confirming that MCF7 resistance could not be explained by a difference at the level of the cell-cycle. Western Blot and Flow Cytometry analysis of histone modifications confirmed that acetylation occurred in both cell-lines within 2-hour SAHA treatment.

In the next chapter the results of an RNA-Sequencing experiment comparing the response of our two cell-lines to treatment with SAHA for 30, 60 or 120-minutes were analysed. An analysis of the differentially expressed genes across the time-course highlighted that a greater transcriptional response was induced in MCF7 cells following SAHA treatment. Ontology analysis suggested that a common response was induced in both cell-lines, occurring more slowly in the MDA-MB231 cells. Motif analysis investigated the TFs driving early gene expression change in MCF7 cells. This identified potential driver genes for knockdown analysis, including SRF as well as ATF, SMAD and POU TF families.

The following chapter investigated the DNA methylation response induced following HDACi treatment. Our analysis indicated that DNA methylation was not involved in the early transcriptional response following HDACi treatment. However, dynamic methylation changes were induced in both cell-lines in response to 24 and 48-hour SAHA treatment. A

greater overall change in methylation was observed in MDA-MB231 cells. Though similar methylation patterns were observed in both cell-lines, no common set of genes was identified.

The role of the POU family members in mediating the response of our cell-lines to SAHA treatment were then considered. It was shown that POU2F2 knockdown further enhanced the HDACi sensitivity of MDA-MB231 cells. POU2F2 did not play a transcriptional role during their early response to HDACi treatment – with HAT gene downregulation not perturbed following knockdown. This does not explain the difference in sensitivity between our two cell-lines which led us to the investigation of the next target identified from the motif analysis.

The role of the ATF/CREB family members in mediating the response of our cell-lines to SAHA treatment was then considered. Our knockdown experiments highlighted key differences between the cell-lines (Table 8.1). Knockdown of ATF4 and ATF5 further enhanced the sensitivity of MDA-MB231 cells to SAHA. However, ATF4 and CREB3L4 knockdown increased the SAHA sensitivity of MCF7 cells. ATF4 did not play a transcriptional role during their early response to HDACi treatment – with HAT gene downregulation and ATF gene expression not perturbed following knockdown. This was followed by an investigation of knockdown across resistance pathways – involving SRF, ATF4 and POU2F2. In MDA-MB231 cells, ATF4 and POU2F2 knockdown was not additive or protective. In MCF7 cells, the effect of ATF4 knockdown alone was not observed with SRF also knocked down. Comparison of our samples to a patient cohort in the CBioPortal database confirmed that our model system was representative of cancer. MCF7 and MDA-MB231 cell-lines represented their luminal A and triple-negative subtype

in terms of expression of the key genes we identified. The genes selected for analysis exhibited differential expression between the two subtypes, often matching our experimental observations. This suggested that transcriptional signatures may make it possible to target HDACi to receptive tumours.

Table 8.1 Summary of gene knockdown effect in each cell-line

Transcription Factor	MCF7	MDA-MB231
ATF4	** ↑ Late apoptosis/ ↓ viability	* ↓ viability
ATF5	NS change	* ↑ Late apoptosis/↓viability
CREB3L4	* ↑ Late apoptosis/ ↓ viability	NS change
ATF4/ATF5	NS change	** ↓ viability
ATF4/CREB3L4	NS change	-
ATF4/ATF5/CREB3L4	-	* ↓viability
POU2F1	NS change	NS change
POU2F2	-	** ↑ Late apoptosis/ ↓ viability
POU2F1/POU2F2	NS change	NS change
ATF4/POU2F2/SRF	NS change	** ↓ viability

**p<0.05, **p<0.01*

8.1 Are there multiple drivers of the HDACi survival response?

This project was built on the hypothesis that non-histone protein acetylation drives a transcriptional response enabling some cells to survive in the presence of an HDACi (Halsall *et al.,* 2015). Thus, our aim was to identify the genes and signalling pathways driving the resistance observed in many tumours to these drugs. The clinical endpoint we

were aiming for was to inhibit this crucial driver and then treat with an HDAC inhibitor. This would provide a mechanism to kill HDACi resistant cell-lines. Through sensitising tumours to HDAC inhibition, this would enhance the number of tumours against which they could be used. This was along the same lines as the aims of Chang *et al.* in 2012, who investigated the phenotypic differences between HDACi sensitive and resistant cell-lines to identify potential biomarkers of drug sensitivity.

However, it is highly unlikely that this evolutionarily conserved pathway is driven by one gene and resulting signalling pathway. We now believe that this response is complex, likely involving multiple driver proteins as well as multiple pathways of resistance. Thus, the loss of more than one factor would be needed to perturb this response. This complexity is highlighted by the number of non-histone proteins with which HDACs interact (Glozak *et al.,* 2005).

Our experimental work highlighted the likelihood of there being multiple drivers. The knockdown of ATF4 and CREB3L4 was shown to enhance the sensitivity of our HDACi resistant MCF7 cells to SAHA-induced apoptosis at 48-hours. They went from being resistant to HDAC inhibition, to being slightly more sensitive. In the case of CREB3L4, the viable population was reduced from 77.2% to 69.7% comparing scrambled with CREB3L4 knockdown cells (Figure 7.4). This was not the silver bullet idea whereby we would have seen conversion to this cell-type being receptive to HDAC inhibition.

This approach could have additional clinical implications. Firstly, would this also sensitise normal cells to these drugs? An important positive for their use currently is that most tumour cells seem more sensitive to HDACi than normal cells (Ungerstedt *et al.,* 2005;

Marks *et al.,* 2001). Secondly, going down this route would require the development of additional inhibitors for the identified driver proteins.

8.2 Is our goal still achievable?

Is converting an HDACi resistant cell-line to an HDACi sensitive cell-line still an achievable goal? No one individual target in the resistant cell-line appeared to be alone in driving this survival response. It could, of course, be argued that we just did not locate the correct one. However, the differing effects observed following ATF5 and CREB3L4 knockdown in our two cell-lines argues against the idea that there is only one driver. ATF5 knockdown enhanced the sensitivity of MDA-MB231 cells to HDACi inhibition, while not affecting the response in MCF7 cells (Figure 7.3; Figure 7.8). The knockdown of CREB3L4 displayed the opposite effect in our cell-lines (Figure 7.4; Figure 7.9). This knockdown work instead highlighted several proteins altering the apoptotic response induced in our cell-lines at 48-hours. It was suggested that the knockdown of ATF4, ATF5 and POU2F2 created MDA-MB231 cells even more sensitive to HDACi while ATF4 and CREB3L4 knockdown enhanced the sensitivity of MCF7 cells to HDACi. These identified TFs provide part of the answer as to what is involved in driving this survival response. Considering what our experimental work showed, it was perhaps simplistic to imagine we could make HDACi resistant cell-lines more sensitive through the knockdown of one key driver TF. We believe that the survival response is more complex, with multiple components involved in mediating how cells respond to HDAC inhibition. This also makes sense considering how cells react biochemically when treated with these drugs. HDAC inhibition induces cell-cycle arrest, impairs the DNA damage response, and induces apoptosis (Singh *et al.*, 2018).

It seems that we can identify characteristics of more responsive tumours. Our results suggest that the expression of a few select TFs correlated with how the MCF7 and MDA-MB231 cell-line responded to HDAC inhibition. Therefore, it could be possible to screen for the downregulation of these selected TFs in these two cell-lines to select cells more likely to be receptive to this form of treatment. What was most interesting was that our work showed the HDACi sensitive triple-negative MDA-MB231 cell-line could be made more sensitive to these drugs. The knockdown work suggested that the effectiveness of HDAC inhibitors in these cells could potentially be enhanced by considering those with a lower expression of *ATF4, ATF5* and *POU2F2.*

8.3 Could HDAC inhibitors be targeted to triple-negative tumours?

Is it possible to apply these results more generally to breast cancer rather than just in these two cell-lines? This is where the CBioPortal database was necessary. Our experimental work was limited in comparing only two cell-lines, MCF7 and MDA-MB231. It was through the comparison with a cohort of breast tumour samples from the CBioPortal database that this work was widened from its starting point. Prior to this, all the identified differences may be just differences between our cell-lines and may not contribute at all to how these cells respond to HDAC inhibition. This additional analysis suggested that the transcriptional landscape in our model could represent breast cancer samples. MCF7 cells were representative of their luminal A subtype and MDA-MB231 cells of their triple-negative subtype in their expression of the key genes we had identified. This validated our selected model system and was a hugely encouraging step towards the idea of HDACi

personalisation. We could more confidently say the characteristics we identified experimentally could be attributed to a molecular subtype, not just the cell-line.

The first indication giving us confidence in our selected knockdown targets was that the genes of interest identified through our experimental work were also altered across the cohort. We identified amplifications, mutations, and gene expression patterns in these nine genes of interest across all 25 breast cancer studies included in the database (Figure 7.24). These genes were selected based on their differential expression between our two cell-lines and their ability to alter the HDACi sensitivity of these cell-lines. They appeared to be differentially expressed between molecular subtypes in the database. Six of these nine genes were significantly differentially expressed between luminal A and triple-negative samples (Figure 7.28). This was a pointer towards the idea that gene expression signatures may be associated with tumours receptive to HDAC inhibition. This also suggests that HDACi response could be predicted based on existing diagnostic tests. Not only that but their expression often matched what was observed in our RNA-Sequencing and qPCR data. This was most clearly observed with *CREB3L4*. This was one of our initial targets identified for knockdown and it was selected based on its higher expression in MCF7 cells (Figure 7.1). Examination of all the tumour samples contained in CBioPortal correlated this greater expression of *CREB3L4* with luminal A subtypes (Figure 7.28). The second gene we looked at was *POU2F2.* This gene was also differentially expressed between luminal A and triple-negative samples. It appeared that a higher expression of *POU2F2* was associated with triple-negative subtypes, while this gene was mostly downregulated in luminal A samples (Figure 7.27). Knockdown of *POU2F2* had significantly enhanced SAHA-induced apoptosis in our triple-negative MDA-MB231 cells (Figure 6.14). In addition, our experimental work had shown that *POU2F2* was not expressed in MCF7

cells (Figure 6.3). This difference in *POU2F2* expression between our cell-lines therefore seemed to be representative of differences between these two molecular breast cancer subtypes. Additionally, higher *ATF4* and *ATF5* expression appeared to be associated with triple-negative subtypes (Figure 7.28). This was a promising discovery. It suggested that expression patterns are potentially an avenue by which receptive tumours could be identified.

With this indication that our MDA-MB231 cells were representative of triple-negative tumours – could we hypothesise that triple-negative tumours as a subtype may be more responsive to HDAC inhibition? Our experimental work showed that the triple-negative cell-line was more sensitive than the luminal A cell-line to HDAC inhibition. This was observed in the Annexin V and MTS Assays following 48-hour SAHA treatment (Figure 3.4A; Figure 3.5). This was also alluded to in the RNA-Sequencing, with this cell-line mounting a smaller transcriptional response following 2-hour SAHA treatment and fewer DEGs being identified between the treatment timepoints (Figure 4.1; Figure 4.3). Not only that, but the knockdown work then showed that this cell-line could be made even more sensitive to SAHA. The knockdown of ATF4, ATF5 and POU2F2 resulted in MDA-MB231 cells even more sensitive to HDAC inhibition. If we consider this a potential transcriptional signature, it would be important to understand how these genes could interact. The triple pathway knockdown (ATF4, SRF and POU2F2) carried out produced results matching individual ATF4 or POU2F2 knockdown (Figure 7.22). This indicated that these TFs converged on similar apoptotic pathways by 48-hours, but importantly that they did not protect against the other knockdown.

Targeting triple-negative tumours could have wide ranging clinical implications. There are currently very few treatment options in these tumours, beyond chemotherapy and radiotherapy which have limited efficacy (Yin *et al.,* 2020). As they do not express ER, PR or HER2 – they are not receptive to endocrine or molecular targeted therapies (Yin *et al.,* 2020). This sets them apart from other breast molecular subtypes. However, this is not to say that targeted therapy has not been attempted in these cell types. Researchers have tried to use the combination of an HDACi and DNMTi to re-express the ER in triple-negative cells (Salahuddin *et al.,* 2022). This would make these cells more amenable to targeted treatments. However, this would be difficult to achieve as this expression may be reversed once the drugs are discontinued (Pathiraja *et al.,* 2011). The fact that this has been attempted highlights how few treatments are available to attack this cancer subtype. HDACi personalisation is potentially a means by which these aggressive and currently difficult to treat triple-negative tumours could be targeted in the clinic.

This work has given us a different way of thinking. What we could do with these results is slightly different from what we set out to do. This project looked for a way to make HDAC inhibitors effective in all tumours. However, a better strategy towards their personalisation would be to select within a group of patients those who are more receptive. This work indicates that it may be possible to outline several components required to get a clinical response.

This leads us to consider additional reasons why we might label triple-negative cells as potentially more sensitive to SAHA. Could the involvement of the heat shock response be important in mediating sensitivity? It was shown that *HSPs* were more highly expressed basally in our MDA-MB231 cell-line. However, their basal expression was variable across

the replicates. This could be explained by the fact that they are stress responsive genes and would operate differently based on the context of the cells. Comparison with samples from the CBioPortal database indicated that triple-negative cells express *HSP90B1* and *HSP90AB1* more highly basally (Figure 7.30). This suggested that a higher basal expression of these selected *HSPs* was a characteristic of triple-negative tumours. This leaves us considering whether these cells were more inherently stressed – and whether they rely more heavily on the HSR? If this were the case, does this point to them being less able to survive HDAC inhibition as it would impact on the HSR. The HSR is intrinsically linked to acetylation. Many key players of this response, such as HSP70 and HSP90, are regulated through acetylation (Seo *et al.,* 2016; Scroggins *et al.,* 2007). HDAC inhibitors, through altering the acetylation balance in cells, will interfere with the function of the HSR. This may give us additional characteristic to add to the list of sensitivity criteria we have already considered. Basal expression of *HSPs* could be considered alongside gene expression patterns (e.g., *ATF4* and *POU2F2*).

8.4 What is the future for HDAC inhibitors in the clinic*?*

HDAC inhibitors have had a patchy history as anti-cancer therapies, only really displaying clinical benefit in a small number of haematological cancers (Halsall and Turner, 2016). Out with this clinical area, they are only currently used in combination therapies. As outlined in the introduction, their favourable safety profile means that they can be used to sensitize cells to additional therapies or lower the dose of cytotoxic drugs needed (Suraweera *et al.,* 2018). They do exhibit significant anti-cancer properties, inducing apoptosis and anti-proliferative effects in receptive tumour types (Singh *et al.,* 2018). They

could be more useful in a clinical setting if it were possible to identify characteristics of sensitive tumours.

Drawing up a list of sensitivity criteria, starting with what was identified in this work could allow specific tumours to be targeted based on their likelihood of responding. Knockdown work indicated that HDACi could be targeted to a subset of triple-negative tumours by looking for patients exhibiting a downregulation in *ATF4, ATF5* and *POU2F2* and *CREB3L4* expression. This suggests that a transcriptional profile may exist indicating cells that are more HDACi sensitive. It would be clinically beneficial if this transcriptional profile could be identified even in a small subpopulation of triple-negative tumours.

We set out to investigate whether it would be possible to personalise HDACi use in the clinic. It appears that this is a possibility – transcriptional profiles could potentially be used to indicate a subpopulation of triple-negative tumours more likely to respond to HDAC inhibition. This is a promising start but is far from the end of this story.

9. LIST OF REFERENCES

Albanell, J and Baselga, J. (2001). Unraveling resistance to trastuzumab (Herceptin): insulin-like growth factor-I receptor, a new suspect. *J Natl Cancer Inst* 93(24): 1830-2

Allfrey, V.G., Faulkner, R and Mirksy, A.E. (1964). Acetylation and methylation of histones and their possible role in the regulation of RNA synthesis. *Proc Natl Acad Sci USA* 51(5): 786-94

Alseksek, R.K., Ramadan, W.S., Saleh, E and El-Awady, R. (2022). The Role of HDACs in the Response of Cancer Cells to Cellular Stress and the Potential for Therapeutic Intervention. I*nt. J. Mol. Sci* 23(15), 8141 https://doi.org/10.3390/ ijms23158141

Ameri, K and Harris, A.L. (2008). Activating transcription factor 4. *Int J Biochem Cell Biol.* 40(1): 14-21

Andrews, J.M., Schmidt, J.A., Carson, K.R., Musiek, A.C., Mehta-Shah and Payton, J.E. (2019). Novel cell adhesion/migration pathways are predictive markers of HDAC inhibitor resistance in cutaneous T cell lymphoma. *EBioMedicine* 46: 170-183

Annunziato, A.T. (2008) DNA Packaging: Nucleosomes and Chromatin. *Nature Education* 1(1):26

Arzenani, M.K., Zade, A.E., Ming, Y *et al.* (2011). Genomic DNA hypomethylation by histone deacetylase inhibition implicates DNMT1 nuclear dynamics. *Mol Cell Biol* 31(19): 4119-28

Avvakumov, N., Lalonde, M-E., Saksouk, N *et al*. (2012). Conserved Molecular Interactions within HBO1 Acetyltransferase Complexes Regulate Cell Proliferation. *Mol Cell Biol*. 32(3): 689-703

Ayturk, U.M., Jacobsen, C.M., Christodoulou, D.C *et al.* (2013). An RNA-seq Protocol to Identify mRNA Expression Changes in Mouse Diaphyseal Bone: Applications in Mice with Bone Property Altering *Lrp5* Mutations. *J Bone Miner Res* 28(10): 2081-93

Bachman, K.E., Park, B.H, Rhee, I *et al.* (2003). Histone modifications and silencing prior to DNA methylation of a tumor suppressor gene. *Cancer Cell* 3: 89-95

Bali, P., Pranpat, M., Swaby, R., Fiskus, W., Yamaguchi, H., Balasi, M., Rocha, K., Wang, H-G., Richon, V and Bhalla, K. (2005). Activity of Suberoylanilide Hydroxamic Acid Against Human Breast Cancer Cells with Amplification of Her-2. *Clin Cancer Res* 11(17): 6382-9

Bannister, A.J and Kouzarides, T. (2011). Regulation of chromatin by histone modifications. *Cell Research* 21: 381-395

Bassett, S.A and Barnett, M.P.G. (2014). The Role of Dietary Histone Deacetylases (HDACs) Inhibitors in Health and Disease. *Nutrients* 6(10): 4273-301

Baylin, S.B and Jones, P.A. (2011). A decade of exploring the cancer epigenome – biological and translational implications. *Nat Rev Cancer* 11(10): 726-34

Baylin, S.B., Herman, J.G., Graff, J.R., Vertino, P.M and Issa, J-P. (1998). Alterations in DNA methylation: A fundamental aspect of neoplasia. *Adv Cancer Res* 72: 141-96

Bell, O., Tiwari, V.K., Thomä, N.H and Schübeler, D. (2011). Determinants and dynamics of genome accessibility. *Nat Rev Genet.* 12(12): 554-64

Bentrari, F., Chantôme, A., Knights, A., Jeannin, J-F and Pance, A. (2015). Oct-2 forms a complex with Oct-1 on the iNOS promoter and represses transcription by interfering with recruitment of RNA PolII by Oct-1. *Nucleic Acids Research* 43(20): 9757-9765

Berger, S.L. (2007). The complex language of chromatin regulation during transcription. *Nature* 447: 407- 412

Bernstein, B.E., Mikkelsen, T.S., Xie, W. *et al.* (2006). A bivalent chromatin structure marks key developmental genes in embryonic stem cells. *Cell* 125(2): 315-26

Bertos, N.R., A.H. Wang, and X.J. Yang. (2001). Class II histone deacetylases: Structure, function, and regulation. *Biochem Cell Biol* 79(3): 243–52

Bertrand, P. (2010). Inside HDAC with HDAC inhibitors. *Eur J Med Chem* 45(6): 2095–116

Bestor, T.H (2000). The DNA methyltransferases of mammals. *Hum Mol Genet* 9(16):2395–402

Bird A. (2002). DNA methylation patterns and epigenetic memory. *Genes Dev* 16(1):6–21

Black, J.C., Van Rechem, C and Whetstine, J.R. (2012). Histone lysine methylation dynamics: establishment, regulation, and biological impact. *Mol Cell* 48(4): 491-507

Blagosklonny, M.V., Robey, R., Sackett, D.L., Du, L., Traganos, F., Darzymkiewicz, Z., Fojo, T and Bates, S.E. (2002). Histone deacetylase inhibitors all induce p21 but differentially cause tubulin acetylation, mitotic arrest, and cytotoxicity. *Mol Cancer Ther* 1(11):937–41

Bogdanova, E.A., Barsova, E.E., Shagina, I.A *et al.* (2011). Normalization of Full-Length-Enriched cDNA. *Methods Mol Biol* 729: 85-98

Bojang Jr, P and Ramos, K.S. (2014). The promise and failures of epigenetic therapies for cancer treatment. *Cancer Treat Rev* 40(1): 153-69

Boslaugh, S and Waters, P.A. (2008). *Statistics in a Nutshell*. First Edition. O'Reilly Media, Inc. Sebastopol, CA.

Boudadi, E., Stower, N., Halsall, J.A., Rutledge, C.E., Leeb, M., Wutz, A., O'Neill, L.P., Nightingale, K.P and Turner, B.M. (2013). The histone deacetylase inhibitor sodium valproate causes limited transcriptional change in mouse embryonic stem cells but selectively overrides Polycomb-mediated *Hoxb* silencing. *Epigenetics Chromatin* 6:11 http://www.epigeneticsandchromatin.com/content/6/1/11

Bradbury, C.A., Khanim, F.L., Hayden, R., Bunce, C.M., White, D.A., Drayson, M.T., Craddock, C and Turner, B.M. (2005). Histone deacetylases in acute myeloid leukaemia show a distinctive pattern of expression that changes selectively in response to deacetylase inhibitors. *Leukemia* 19(10): 1751–9

Brenner, C., Deplus, R., Didelot, C *et al*. (2005). Myc represses transcription through recruitment of DNA methyltransferase corepressor. *EMBO J* 24: 336-346

Brownell, J.E., Zhou, J., Ranalli, T., Edmondson, D.G., Roth, S.Y and Allis, C.D. (1996). Tetrahymena Histone Acetyltransferase A: A Homolog to Yeast Gcn5p Linking Histone Acetylation to Gene Activation. *Cell* 84(6): 843-51

Cailleau, R., Olivé, M and Cruciger, Q.V. (1978). Long-term human breast carcinoma cell lines of metastatic origin: preliminary characterization. *In Vitro* 14(11): 911-5

Cannan, W.J and Pederson, D.S. (2017). Mechanisms and Consequences of Double-strand DNA Break Formation in Chromatin. *J Cell Physiol* 231(1): 3-14

Carrozza, M.J., Utley, R.T., Workman, J.L and Côté, J. (2003). The diverse functions of histone acetyltransferase complexes. *Trends Genet.* 19(6): 321-9

Cerami, E., Gao, J., Dogrusoz *et al.* (2012). The cBio cancer genomics portal: an open platform for exploring multidimensional cancer genomics data. *Cancer Discov* 2(5): 401-404

Chai, J and Tarnawski, A.S. (2002). Serum response factor: discovery, biochemistry, biological roles and implications for tissue injury healing. *J Physiol Pharmacol* 53(2): 147-57

Chambers, A.E., Banerjee, S., Chaplin, T., Dunne, J., Debernardi, S., Joel, S.P and Young, B.D. (2003). Histone acetylation-mediated regulation of genes in leukaemia cells. *Eur J Cancer.* 39(8): 1165-75

Chang, J., Varghese, D.S., Gillam, M.C *et al.* (2012). Differential response of cancer cells to HDAC inhibitors Trichostatin A and depsipeptide. *Br J Cancer.* 106(1): 116-125

Chavez, K.J., Garimella, S.V and Lipkowitz, S. (2010). Triple Negative Breast Cancer Cell Lines: One Tool in the Search for Better Treatment of Triple Negative Breast Cancer. *Breast Dis* 32(1-2): 35-48

Chen, M., Liu, Y., Yang, Y., Qiu, Y., Wang, Z., Li, X and Zhang, W. (2022). Emerging roles of activating transcription factor (ATF) family members in tumourigenesis and immunity: Implications in cancer immunotherapy. *Genes Dis* 9(4): 981-999

Chen, Y-Y., Ge, J-Y., Xhu, S-Y., Shao, Z-M and Yu, K-D. (2020). Copy number amplification of ENSA promotes the progression of triple-negative breast cancer via cholesterol biosynthesis. *Nat Commun.* 13(1): 791 doi: 10.1038/s41467-022-28452-z

Cheung, P., Allis, C.D and Sassone-Corsi, P. (2000). Signaling to Chromatin through Histone Modifications. *Cell* 103(2): 263-71

Chueh, A.C., Tse, J.W.T., Tögel, L and Mariadason, J.M. (2015). Mechanisms of Histone Deacetylase Inhibitor-Regulated Gene Expression in Cancer Cells. *Antioxid Redox Signal* 23(1): 66-84

Chun, P. (2015). Histone deacetylase inhibitors in hematological malignancies and solid tumors. *Arch Pharm Res* 38(6): 933-49

Clerc, R.G., Corcoran, L.M., LeBowitz, J.H., Baltimore, D and Sharp, P.A. (1988). The B-cell specific Oct-2 protein contains POU box- and homeo box-type domains. *Genes Dev* 2(12A): 1570-81

Comsa, S., Cimpean, A.M and Raica, M. (2015). The Story of MCF-7 Breast Cancer Cell Line: 40 years of Experience in Research. *Anticancer Res* 35(6): 3147-54

Covault, J and Chalkley, R. (1980). The identification of Distinct Populations of Acetylated Histones. *J Biol Chem* 225(19): 9110-6

Crosio, C., Fimia, G.M., Loury, R., Kimura, M., Okano, Y., Zhou, H., Sen, S., Allis, C.D and Sassone-Corsi, P. (2002). Mitotic Phosphorylation of Histone H3: Spatio-Temporal Regulation by Mammalian Aurora Kinases. *Mol Cell Biol* 22(3): 874-85

Cui, X., Cui, M and Asada, R. *et al.* (2016). The androgen-induced protein AIbZIP facilitates proliferation of prostate cancer cells through downregulation of p21 expression. *Sci Rep* 6:37310 https://doi.org/10.1038/srep37310

Cusack, M., King, H.W., Spingardi, P *et al.* (2020). Distinct contributions of DNA methylation and histone acetylation to the genomic occupancy of transcription factors. *Genome Res* 30(10): 1393-1406

Cutter, A.R and Hayes, J.J. (2015). A brief review of nucleosome structure. *FEBS Lett.* 589: 2914-22

D'Anselmi, F., Masiello, M.G., Cucina, A. *et al.* (2013). Microenvironment Promotes Tumour Cell Reprogramming in Human Breast Cancer Cell Lines. *PLoS One* 8(12): e83770 doi: 10.1371/journal.pone.0083770

Damaskos, C., Garmpis, N., Valsami, S. *et al*. (2017). Histone Deacetylase Inhibitors: An Attractive Therapeutic Strategy Against Breast Cancer. *Anticancer Res.* 37(1): 35-46

Dangond, F and Gullans, S.R. (1998). Differential Expression of Human Histone Deacetylase mRNAs in Response to Immune Cell Apoptosis Induction by Trichostatin A and Butyrate. *Biochem Biophys Res Commun.* 247(3): 833-7

Davie, J.R. (1997). Nuclear matrix, dynamic histone acetylation and transcriptionally active chromatin. *Mol Biol Rep* 24(3): 197-207

de Bustros, A., Nelkin, B.D., Silverman, A., Ehrlich, G., Poiesz, B and Baylin, S.B (1988). The short arm of chromosome 11 is a "hot spot" for hypermethylation in human neoplasia. *Proc Natl Acad Sci USA* 85(15): 5693–5697

de Ruijter, A.J.M., van Gennip, A.H., Caron, H.N., Kemp, S and van Kuilenburg, A.B.P. (2003). Histone deacetylases (HDACs): characterization of the classical HDAC family. *Biochem J.* 370(Pt3): 737-49

Deaton, A.M and Bird, A. (2011). CpG island and the regulation of transcription. *Gens Dev.* 25(10): 1010-22

Dluzen, D., Li, G., Tacelosky, D., Moreau, M and Liu, D.X. (2011). BCL-2 Is a Downstream Target oof ATF5 That Mediates the Prosurvival Function of ATF5 in a Cell Type-dependent Manner. *J Biol Chem.* 286(9): 7705-13

Dong, B and Zhao, F-Q. (2007). Expression of the Oct-2 transcription factor in mouse mammary gland and cloning and characterization of a novel Oct-2 isoform. *Cell Tissue Res* 328(3): 595-606

Dovey, O.M., Foster, C.T and Cowley, S.M. (2010). Emphasizing the positive: A role for histone deacetylases in transcriptional activation. *Cell Cycle* 9(14): 2700-1

Du, Z., Song, J., Wang, Y., Zhao, Y *et al.* (2010). DNMT1 Stability Is Regulated by Proteins Coordinating Deubiquitination and Acetylation-Driven Ubiquitination. *Sci Signal* 3(146): doi: 10.1126/scisignal.2001462

Ellis, D.J.P., Lawman, Z.K and Bonham, K. (2008). Histone acetylation is not an accurate predictor of gene expression following treatment with histone deacetylase inhibitors. *Biochem Biophys Res Commun.* 367(3): 656-62

Esteller, M. (2008). Epigenetics in Cancer. *N Engl J Med* 358(11): 1148-59

Fan, Y., Nikitina, T., Morin-Kensicki, E.M., Zhao, J., Magnuson, T.R., Woodcock, C.L and Skoultchi, A.I. (2003). HI linker histones are essential for mouse development and affect nucleosome spacing in vivo. *Mol. Cell. Biol* 23(13): 4559-72

Fandy, T.E. (2009). Development of DNA methyltransferase inhibitors for the treatment of neoplastic diseases. *Curr Med Chem* 16(17): 2075-85

Fang, Z., Martin, J and Wang, Z. (2012). Statistical methods for identifying differentially expressed genes in RNA-Seq experiments. *Cell Biosci* 2:26 http://www.cellandbioscience.com/content/2/1/26

Fantin, V.R.; Richon, V.M. (2007) Mechanisms of Resistance to Histone Deacetylase Inhibitors and Their Therapeutic Implications. *Clin. Cancer Res* 13(24): 7237–42.

Feinberg, A.P and Tycko, B. (2004). The history of cancer epigenetics. *Nat Rev Cancer* 4(2): 143-53

Feinberg, A.P. (2005). Cancer epigenetics is no Mickey Mouse. *Cancer Cell* 8(4): 267-8

Feinberg, A.P. and Vogelstein, B. (1983) Hypomethylation distinguishes genes of some human cancers from their normal counterparts. *Nature* 301: 89–92 https://doi.org/10.1038/301089a0

Feinberg, A.P., Ohlsson, R and Henikoff, S. (2006). The epigenetic progenitor origin of human cancer. *Nat Rev Genet*. 7(1): 21-33

Feng, H and Wu, H. (2019). Differential methylation analysis for bisulfite sequencing using DSS. *Quant Biol* 7(4): 327-334

Finnin, M.S., Donigian, J.R., Cohen, A., Richon, V.M., Rifkind, R.A., Marks, P.A, Breslow, R and Pavletich, N.P. (1999). Structures of a histone deacetylase homologue bound to the TSA and SAHA inhibitors. *Nature* 401(6749): 188-93

Flanagan, J.F., Mi, L-Z., Chruszcz, M. *et al.* (2005). Double chromodomains cooperate to recognize the methylated histone H3 tail. *Nature* 438(7071): 1181-5

Flavahan, W.A., Gaskell, E and Bernstein, B.E. (2017). Epigenetic plasticity and the hallmarks of cancer. *Science* 357(6348): doi:10.1126/science.aal2380

Friedl, E.M and Matthias, P. (1995). Transcriptional activation and repression, two properties of the lymphoid-specific transcription factor Oct-2a. *Eur J Biochem* 234(1): 308-16

Fuino, L., Bali, P., Wittmann, S., Donapaty, S., Guo, F., Yamaguchi, H., Wang, H-G., Atadja, P and Bhalla, K. (2003). Histone deacetylase inhibitor LAQ824 down-regulates Her-2 and sensitizes human breast cancer cells to trastuzumab, Taxotere, gemcitabine, and epothilone B. *Mol Cancer Ther* 2(10): 971-84

Fuks, F., Burgers, W.A., Brehm, A., Hughes-Davies, L and Kouzarides, T. (2000). DNA methyltransferase Dnmt1 associates with histone deacetylase activity. *Nat Genet* 24(1):88–91

Gajria, D and Chandarlapaty, S. (2011). HER2-amplified breast cancer: Mechanisms of trastuzumab resistance and novel targeted therapies. *Expert Rev. Anticancer Ther* 11(2): 263-275

Gama-Sosa, M.A., Slagel, V.A., Trewyn, R.W *et al.* (1983). The 5-methylcytosine content of DNA from human tumors. *Nucleic Acids Res* 11(19): 6883-6894

Gao, J., Aksoy, B.A., Dogrusoz, U *et al.* (2013). Integrative analysis of complex cancer genomics and clinical profiles using cBioPortal. Sci Signal 6(269): p11. doi:10.1126/scisignal.2004088

Gest, C., Joimel, U., Huang, L., Pritchard, L-L *et al.* (2013). Rac3 induced a molecular pathway triggering breast cancer cell aggressiveness: differences in MDA-MB-231 and MCF-7 breast cancer cell lines. *BMC Cancer* 13:63 doi: 10.1186/1471-2407-13-63

Ghoshal, K., Datta, J., Majumder, S., Bai, S., Dong, X., Parthun, M and Jacob. S.T. (2002). Inhibitors of histone deacetylase and DNA methyltransferase synergistically activate the methylated metallothionein I promoter by activating the transcription factor MTF-1 and forming an open chromatin structure. *Mol Cell Biol* 22(23): 8302-19

Gius, D., Cui, H., Bradbury, M., Cook, J. *et al.* (2004). Distinct effects on gene expression of chemical and genetic manipulation of the cancer epigenome revealed by a multimodality approach. *Cancer Cell* 6(4): 361-71

Glaser, K.B., Staver, M.J., and Waring, J.F., Stender, J., Ulrich, R.G and Davidsen, S.K. (2003). Gene Expression Profiling of Multiple Histone Deacetylase (HDAC) Inhibitors: Defining a Common Gene Set Produced by HDAC Inhibition in T24 and MDA Carcinoma Cell Lines. *Mol Cancer Ther* 2(2): 151-63

Glozak, M.A., Sengupta, N., Zhang, X and Seto, E. (2005). Acetylation and deacetylation of non-histone proteins. *Gene* 363: 15-23

Goldenberg, M.M. (2010). Overview of Drugs Used for Epilepsy and Seizures. *P T* 35(7): 392-415

Göttlicher, M., Minucci, S., Zhu, P *et al*. (2001). Valproic acid defines a novel class of HDAC inhibitors inducing differentiation of transformed cells. *EMBO J* 20(24):6969-78

Govers, A.M.A.P., Wiggers, C.R.M., van Boxtel, R., Mokry, M. *et al.* (2019). Transcriptomic and Epigenomic Profiling of Histone Deacetylase Inhibitor Treatment Reveals Distinct Gene Regulation Profiles Leading to Impaired Neutrophil Development. *HemaSphere* 3:4 e270 http://dx.doi.org/10.1097/HS9.0000000000000270

Gray, S.G., Qian, C-N., Furge, K., Guo, X and Teh, B.T. (2004). Microarray profiling of the effects of histone deacetylase inhibitors on gene expression in cancer cell lines. *Int J Oncol.* 24(4): 773-95

Greene, L.A., Lee, H.Y and Angelastro, J.M. (2009). The transcription factor ATF5: role in neurodevelopment and neural tumors. *J. Neurochem*. 108(1):11–22

Gregoretti, I.V., Lee, Y-M and Goodson, H.V. (2004). Molecular evolution of the histone deacetylase family: functional implications of phylogenetic analysis. *J Mol. Biol* 338(1): 17-31

Groselj, B., Sharma, N.L., Hamdy, F.C., Kerr, M and Kiltie, A.E. (2013). Histone deacetylase inhibitors as radiosensitisers: effects on DNA damage signalling and repair. *Br J Cancer* 108(4): 748-754

Gryder, B.E., Pomella, S., Sayers, C *et al*. (2019). Histone hyperacetylation disrupts core gene regulatory architecture in rhabdomyosarcoma. *Nat Genet* 51(12): 1714-1722

Gu, H., Smith, Z.D., Bock, C. *et al.* (2011). Preparation of reduced representation bisulfite sequencing libraries for genome-scale DNA methylation profiling. *Nat Protoc*. 6: 468-81

Hai, T. (2006). The ATF Transcription Factors in Cellular Adaptive Responses. In: Ma, J. (eds) *Gene Expression and Regulation*. Springer, New York, NY

Hai, T and Hartman, M.G. (2001). The molecular biology and nomenclature of the activating transcription factor/cAMP responsive element binding family of transcription factors: activating transcription factor proteins and homeostasis. *Gene* 273: 1-11

Hai, T.W., Liu, F., Coukos, W.J. and Green, M.R. (1989). Transcription factor ATF cDNA clones: an extensive family of leucine zipper proteins able to selectively form DNA-binding heterodimers. *Genes Dev* 3(12B): 2083-90

Halsall, J.A and Turner, B.M. (2016). Histone deacetylase inhibitors for cancer therapy: An evolutionarily ancient resistance response may explain their limited success. *Bioessays* 38(11): 1102-1110

Halsall, J.A., Gupta, V., O'Neill, L.P., Turner, B.M and Nightingale, K.P. (2012). Genes Are Often Sheltered from the Global Histone Hyperacetylation Induced by HDAC Inhibitors. *PLoS ONE* 7(3): e33453. doi:10.1371/journal.pone.0033453

Halsall, J.A., Turan, N., Wiersma, M and Turner, B.M (2015). Cells adapt to the epigenomic disruption caused by histone deacetylase inhibitors through a coordinated, chromatin-mediated transcriptional response. *Epigenetics & Chromatin* 8:29 DOI 10.1186/s13072-015-0021-9

Hanahan, D and Weinberg, R.A. (2011). Hallmarks of cancer: the next generation. *Cell* 144(5): 646-74

Hansen, B.K., Gupta, R., Baldus, L. *et al.* (2019). Analysis of human acetylation stoichiometry defines mechanistic constraints on protein regulation. *Nat Commun* 10, 1055 https://doi.org/10.1038/s41467-019-09024-0

Harari, D and Yarden, Y. (2000). Molecular mechanisms underlying ErbB2/HER2 action in breast cancer. *Oncogene* 19(53):6102-14

hbctraining. (2023). Introduction to DGE – Archived. Accessed from: https://hbctraining.github.io/DGE_workshop/lessons/08_DGE_LRT.html on 12/02/2023.

He, F., Xiao, H., Cai, Y and Zhang, N. (2021). ATF5 and HIF1α cooperatively activate HIF1 signalling pathway in esophageal cancer. *Cell Commun Signal* 19: 53 doi: 10.1186/s12964-021-00734-x

Héberle, E and Bardet, A.F. (2019). Sensitivity of transcription factors to DNA methylation. *Essays Biochem* 63(6): 727-741

Herr, W., Sturm, R.A., Clerc, R.G *et al.* (1988). The POU domain: a large conserved region in the mammalian pit-1, oct-1, oct-2, and Caenorhabditis elegans unc-86 gene products. *Genes Dev* 2(12A): 1513-6

Hontecillas-Prieto, L., Flores-Campos, R., Silver, A., de Álava, E., Hajji, N and García-Domínguez, D.J. (2020) Synergistic Enhancement of Cancer Therapy Using HDAC Inhibitors: Opportunity for Clinical Trials. *Front. Genet*. 11:578011. doi: 10.3389/fgene.2020.578011

Huang, D.W., Sherman, B.T and Lempicki, R.A. (2009a). Systematic and integrative analysis of large gene lists using DAVID Bioinformatics Resources. *Nature Protoc*. 4(1): 44-57

Huang, D.W., Sherman, B.T and Lempicki, R.A. (2009b). Bioinformatics enrichment tools: paths toward the comprehensive functional analysis of large gene lists. *Nucleic Acids Res* 37(1):1-13

Huang, L and Pardee, A.B. (2000). Suberoylanilide Hydroxamic Acid as a Potential Therapeutic Agent for Human Breast Cancer Treatment. *Mol Med.* 6(10): 849-66

Huang, Z., Zhou, W., Li, Y *et al*. (2018). Novel hybrid molecule overcomes the limited response of solid tumours to HDAC inhibitors via suppressing JAK1-STAT3-BCL2 signalling. *Theranostics* 8(18): 4995-5011

Hull, E.E., Montgomery, M.R and Leyva, K.J. (2016). HDAC Inhibitors as Epigenetic Regulators of the Immune System: Impacts on Cancer Therapy and Inflammatory Diseases. *BioMed Research International* 4:1-15

Hyland, E.M., Cosgrove, M.S., Molina, H., Wang, D., Pandey, A., Cottee, R.J and Boeke, J.D. (2005). Insights into the role of histone H3 and histone H4 core modifiable residues in Saccharomyces cerevisiae. *Mol Cell Biol* 25(22): 10060–70

Hynes, N.E and Lane, H.A. (2005). ERBB receptors and cancer: the complexity of targeted inhibitors. *Nat Rev Cancer* 5(5): 341-54

Hyun, K., Jeon, J., Park, K and Kim, J. (2017). Writing, erasing and reading histone lysine methylations. *Exp Mol Med* 49 e324 doi:10.1038/emm.2017.11

Imai, S., Armstong, C.M., Kaeberlein, M and Guarente, L. (2000). Transcriptional silencing and longevity protein Sir2 is an NAD-dependent histone deacetylase. *Nature* 403(6771): 795-800

Inagaki, Y., Yasui, K., Endo, M., Nakajima, T., Zen, K., Tsuji K, *et al*. (2008). CREB3L4, INTS3, and SNAPAP are targets for the 1q21 amplicon frequently detected in hepatocellular carcinoma. *Cancer Genet Cytogenet* 180(1): 30–6

Inoue, Y., Itoh, Y., Abe, K., Okamoto, T., Daitoku, H., Fukamizu, A., Onozaki, K and Hayashi, H. (2007). Smad3 is acetylated by p300/CBP to regulate its transactivation activity. *Oncogene* 26: 500-8

Iqbal, N and Iqbal, N. (2014). Human Epidermal Growth Factor Receptor 2 (HER2) in Cancers: Overexpression and Therapeutic Implications. *Mol Biol Int*. https://doi.org/10.1155/2014/852748

Issa, J-P.J and Kantarjian, H.M. (2009). Targeting DNA Methylation. *Clin Cancer Res* 15(12): 3938-46

Ito, S., D'Alessio, A.C., Taranova, O.V., Hong, K., Sowers, L.C and Zhang, Y. (2010). Role of Tet proteins in 5mC to 5hmC conversion, ES-cell self-renewal and inner cell mass specification. *Nature* 466(7310): 1129-33

Jacobson, E.M., Li, P., Leon-del-Rio, A., Rosenfeld, M.G and Aggarwal, A.K. (1997). Structure of Pit-1 POU domain bound to DNA as a dimer: unexpected arrangement and flexibility. *Genes Dev* 11(2): 198-212

Jaksik, R., Iwanaszko, M., Rzeszowska-Wolny, J and Kimmel, M. (2015). Microarray experiments and factors which affect their reliability. *Biol Direct* 10:46 DOI 10.1186/s13062-015-0077-2

Jones, P.A and Baylin, S.B. (2002). The Fundamental Role of Epigenetic Events in Cancer. *Nat Rev Genet.* 3(6): 415-28

Jones, P.A and Laird, P.W. (1999). Cancer epigenetics comes of age. *Nat Genet* 21(2): 163-7

Jones, P.L., Veenstra, G.J., Wade, P.A., Vermaak, D., Kass, S.U., Landsberger, N., Strouboulis, J and Wolffe, A.P. (1998). Methylated DNA and MeCP2 recruit histone deacetylase to repress transcription. *Nat Gene* 19(2): 187-91

Kalebic, T. (2003). Epigenetic transitions: towards therapeutic targets. *Expert Opin Ther Targets* 7(6): 693-9

Kamato, D., Do, B.H., Osman, N., Ross, B.P., Mohamed, R., Xu, S and Little, P.J. (2020). Smad linker region phosphorylation is a signalling pathway in its own right and not only a modulator of canonical TGF-β signalling. *Cell Mol Life Sci* 77: 243-151

Kang, J.S., Alliston, T., Delston, R., and Derynck, R. (2005). Repression of Runx2 function by TGF-β through recruitment of class II histone deacetylases by Smad3. *EMBO J*. 24(14): 2543–2555.

Karagiannis, T.C and El-Osta, A. (2006). Modulation of cellular radiation response by histone deacetylase inhibitors. *Oncogene* 25(28): 3885-93

Kass, S.U., Pruss, D and Wolffe, A.P. (1997). How does DNA methylation repress transcription? *Trends Genet*. 13(11): 444-9

Katoh, M and Katoh, M. (2009). Integrative genomic analyses of ZEB2: transcriptional regulation of ZEB2 based on SMADs, ETS1, HIF1alpha, POU/OCT, and NF-kappaB. *Int. J. Oncol*. 34(6): 1737-42

Kawai, H., Li, H., Avraham, S., Jiang, S and Avraham, H.K. (2003). Overexpression of histone deacetylase HDAC1 modulates breast cancer progression by negative regulation of estrogen receptor alpha. *Int J Cancer* 107(3):353–8

Kawamata, N., Chen, J and Koeffler, H.P. (2007). Suberoylanilide hydroxamic acid (SAHA; Vorinostat) supresses translation of cyclin D1 in mantle cell lymphoma cells. *Blood* 110(7): 2667-2673

Kelly, R.D.W. and Cowley, S.M. (2012) The physiological roles of histone deacetylase (HDAC) 1 and 2: complex co-stars with multiple leading parts. *Biochem. Soc. Trans*. 41(3): 741–749

Khachigian, L.M and Collins, T. (1997) Inducible expression of Egr-1-dependent genes: a paradigm of transcriptional activation in vascular endothelium. *Circ Res* 81(4):457-61

Kiernan, R., Brès, V., Ng, R.W.M., Coudart, M-P. *et al.* (2003). Post-activation Turn-off of NF-B-dependent Transcription Is Regulated by Acetylation of p65. *J Biol Chem* 278(4): 2758-66

Kim, G.D., Choi, Y.H., Dimtchev, A., Jeong, S.J., Dritschilo, A and Jung, M. (1999). Sensing of ionizing radiation-induced DNA damage by ATM through interaction with histone deacetylase. *J Biol Chem* 274:31127-30

Kim, T-H., Park, J-M., Kim, M-Y and Ahn, Y-H. (2017). The role of CREB3L4 in the proliferation of prostate cancer cells. *Scientific Reports* 7: 45300 https://doi.org/10.1038/srep45300

Kitano, H. (2003). Cancer robustness: Tumour tactics. *Nature* 426, 125 https://doi.org/10.1038/426125a

Kondo, Y. (2009). Epigenetic Cross-Talk between DNA Methylation and Histone Modifications in Human Cancers. *Yonsei Med J* 50(4): 455-63

Kozera, B and Rapacz, M. (2013). References genes in real-time PCR. *J Appl Genet* 54(4): 391-406

Krusche, C.A., Wülfing, P., Kersting, C., Vloet, A., Böcker, W., Kiesel, L., Beier, H.M and Alfer, J. (2005). Histone deacetylase-1 and -3 protein expression in human breast cancer: a tissue microarray analysis. *Breast Cancer Res Treat* 90(1): 15-23

Kuzmichev, A., Nishioka, K., Erdjument-Bromage, H., Tempst, P and Reinberg, D. (2002). Histone methyltransferase activity associated with a human multiprotein complex containing the Enhancer of Zeste protein. *Genes Dev.* 16(22): 2893-905

Lassot, I., Estrabaud, E., Emiliani, S., Benkirane, M., Benarous, R and Margottin-Goguet, F. (2005). p300 Modulates ATF4 Stability and Transcriptional Activity Independently of Its Acetyltransferase Domain. *J Biol Chem* 280(50): 41537-45

Latchman, D.S. (1999). POU Family Transcription Factors in the Nervous System. *J Cell Physiol.* 179(2): 126-33

Laubach, J.P., Moreau, P., San-Miguel, J.F and Richardson, P.G. (2015). Panobinostat for the treatment of multiple myeloma. *Clin. Cancer Res*. 21(21): 4767-73

Lee, H-Z., Kwitkowski, V.E., Del Valle, P.L *et al* (2015). FDA Approval: Belinostat for the Treatment of Patients with Relapsed or Refractory Peripheral T-cell Lymphoma. *Clin Cancer Res* 21(12): 2666-70

Lee, H., Lee, S., Bæk, M., Kim, H-Y and Jeoung, D-I. (2002). Expression profile analysis of Trichostatin A in human gastric cancer cells. *Biotechnology Letters* 24(5): 377-381

Lee, K.K and Workman, J.L. (2007). Histone acetyltransferase complexes: one size doesn't fit all. *Nat Rev Mol Cell Biol* 8(4):284–95

Leu, Y-W., Yan, P.S., Fan, M. *et al.* (2004). Loss of Estrogen Receptor Signaling Triggers Epigenetic Silencing of Downstream Targets in Breast Cancer. *Cancer Res* 64(22): 8184-8193

Li, G., Xu, Y., Guan, D., Liu, Z., and Liu, D.X. (2011). HSP70 promotes survival of C6 and U87 glioma cells by inhibition of ATF5 degradation. *J. Biol.Chem*. 286(23): 20251–20259

Liu, D.X., Qian, D., Wang, B., Yang, J-M and Lu, Z. (2011). p300-Depdendent ATF5 Acetylation Is Essential for Egr-1 Gene Activation and Cell Proliferation and Survival. *Mol Cell Biol.* 31(18): 3906-3916

Liu, F., Hata, A., Baker, J.C., Doody, J., Cárcamo, J., Harland, R.M and Massagué, J. (1996). A human Mad protein acting as a BMP-regulated transcriptional activator. *Nature* 381:620–623

Love, M.I., Huber, W and Anders, S. (2014). Moderated estimation of fold change and dispersion for RNA-seq data with DESeq2. *Genome Biol* 15(550) https://doi.org/10.1186/s13059-014-0550-8

Lu., X., Ning, Z., Li, Z., Cao, H and Wang, X. (2016). Development of chidamide for peripheral T-cell lymphoma, the first orphan drugs approved in China. *Intractable Rare Dis Res* 5(3): 185-91

Luger, K., Dechassa, M.L and Tremethick, D.J. (2012). New insights into nucleosome and chromatin structure: an ordered state or a disordered affair? *Nat Rev Mol Cell Biol* 13(7): 436-47

Luger, K., Mäder, A.W., Richmond, R.K., Sargent, D.F and Richmond, T.J. (1997). Crystal structure of the nucleosome core particle at 2.8Å resolution. *Nature* 389: 251-260

Luo, X., Zhang, T., Zhai, Y *et al.* (2021). Effects of DNA Methylation on TFs in Human Embryonic Stem Cells. *Front Genet* 12: 639461. doi: 10.3389/fgene.2021.639461

Majchrzak-Celińska, A., Warych, A and Szoszkiewicz, M. (2021). Novel Approaches to Epigenetic Therapies: From Drug Combinations to Epigenetic Editing. *Genes* 12, 208 https://doi.org/10.3390/genes12020208

Mann, B.S., Johnson, J.R., Cohen, M.H., Justice, R and Pazdur, R. (2007). FDA approval summary: Vorinostat for treatment of advanced primary cutaneous T-cell lymphoma. *Oncologist* 12(10): 1247-52

Manohar, M., Mooney, A.M., North, J.A. *et al.* (2009). Acetylation of histone H3 at the nucleosome dyad alters DNA-histone binding. *J. Biol. Chem* 284(35): 23312–23321.

Marchion, D.C., Bicaku, E., Daud, A.I., Richon, V., Sullivan, D.M and Munster, P.N. (2004). Sequence-Specific Potentiation of Topoisomerase II Inhibitors by the Histone Deacetylase Inhibitor Suberoylanilide Hydroxamic Acid. *J Cell Biochem* 92(2):223-37

Mariadason, J.M., Corner, G.A and Augenlicht, L.H. (2000). Genetic Reprogramming in Pathways of Colonic Cell Maturation Induced by Short Chain Fatty Acids: Comparison with Trichostatin A, Sulindac, and Curcumin and Implications for Chemoprevention of Colon Cancer. *Cancer Res* 60(16): 4561-4572

Marin-Muller, C., Li, D., Bharadwaj, U., Li, M. *et al.* (2013). A Tumorigenic Factor Interactome Connected through Tumour Suppressor MicroRNA-198 in Human Pancreatic Cancer. *Clin Cancer Res* 19(21): 5901-5913

Marks, P.A. (2010). Histone Deacetylase Inhibitors: A Chemical Genetics Approach to Understanding Cellular Functions. *Biochim Biophys Acta* 1779(10-12): 717-25

Marks, P.A., Richon, V.M., Miller, T and Kelly, W.K. (2004). Histone Deacetylase Inhibitors. *Adv Cancer Res* 91: 137-68

Marks, P.A., Rifkind, R.A., Richon, V.M., Breslow, R., Miller, T and Kelly, W.K. (2001). Histone deactylases and cancer: causes and therapies. *Nat Rev Cancer* 1(3): 194-202

Marmostein, R. (2001). Structure and function of histone acetyltransferases. *Cell. Mol. Life Sci* 58 (5-6): 693-703

Massagué, J., Seoane, J and Wotton, D. (2005). Smad transcription factors. *Genes Dev* 19(23): 2783-810

Mazzio, E.A and Soliman, K.F.A. (2018). Whole-transcriptomic Profile of SK-MEL-3 Melanoma Cells Treated with the Histone Deacetylase Inhibitor: Trichostatin A. *Cancer Genomics Proteomics* 15(5): 349-364

Mead, A. (1992). Review of the development of Multidimensional Scaling Methods. *The Statistician* 41(1): 27-39

Miano, J.M., Long, X and Fujiwara, K. (2007). Serum response factor: master regulator of the actin cytoskeleton and contractile apparatus. *Am. J. Physiol. Cell Physiol*. 292: C70-81 doi: 10.1152/ajpcell.00386.2006

Millard, C.J., Watson, P.J., Fairall, L and Schwabe, J.W.R. (2017). Targeting Class I Histone Deacetylases in a "Complex" Environment. *Trends Pharmacol Sci* 38(4): 363- 377

Milutinovic, S., D'Alessio, A.C., Detich, N and Szyf, M. (2007). Valproate induces widespread epigenetic reprogramming which involves demethylation of specific genes. *Carcinogenesis* 28(3): 560-71

Minucci, S and Pelicci, P.G. (2006). Histone deacetylase inhibitors and the promise of epigenetic (and more) treatments for cancer. *Nature Rev Cancer.* 6(1): 38-51

Mitsiades, C.S., Mitsiades, N.S., McMullan, C.J. *et al*. (2004). Transcriptional signature of histone deacetylase inhibition in multiple myeloma: biological and clinical implications. *Proc Natl Acad Sci USA* 101(2): 540-5

Mohammad, H.P., Barbash, O., Creasy, C.L. (2019). Targeting epigenetic modifications in cancer therapy: erasing the roadmap to cancer. *Nature Medicine* 25: 403-418

Mokhtari, R.B., Homayouni, T.S., Baluch, N., Morgatskaya, E., Kumar, S., Das, B and Yeger, H. (2017). Combination Therapy in Combating Cancer. *Oncotarget* 8: 38022- 328043

Momparler, R.L and Bovenzi, V. (2000). DNA methylation and cancer. *J Cell Physiol*. 183(2): 145-54

Monaco, S.E., Angelastro, J.M., Szabolcs, M and Greene, L.A. (2007). The transcription factor ATF5 is widely expressed in carcinomas, and interference with its function selectively kills neoplastic, but not nontransformed, breast cell lines. *Int. J. Cancer* 120(9): 1883-90

Moore, P.S., Barbi, S., Donadelli, M., Constanzo, C. *et al.* (2004). Gene expression profiling after treatment with the histone deacetylase inhibitor trichostatin A reveals altered expression of both pro- and anti-apoptotic genes in pancreatic adenocarcinoma cells. *Biochimia et Biophysica Acta* 1693(3): 167-176

Mossman, T. (1983). Rapid Colorimetric Assay for Cellular Growth and Survival: Application to Proliferation and Cytotoxicity Assays. *J Immunol Methods* 65(1-2): 55-63

Müller, B.M., Jana, L., Kasajima, A. *et al.* (2013). Differential expression of histone deacetylases HDAC1, 2 and 3 in human breast cancer – overexpression of HDAC2 and HDAC3 is associated with clinicopathological indicators of disease progression. *BMC Cancer* 13: 215 https://doi.org/10.1186/1471-2407-13-215

Munshi, A., Kurland, J.F., Nishikawa, T. *et al.* (2005). Histone deacetylase inhibitors radiosensitize human melanoma cells by suppressing DNA repair activity. *Clin Cancer Res* 11(13): 4912-22

Munster, P.N., Thurn, K.T., Thomas, S., Raha, P. *et al*. (2011). A phase II study of the histone deacetylase inhibitor Vorinostat combined with tamoxifen for the treatment of patients with hormone therapy-resistant breast cancer. *Br J Cancer* 104(12): 1828-35

Munster, P.N., Troso-Sandoval, T., Rosen, N., Rifkind, R., Marks, P.A and Richon, V.M. (2001). The Histone Deacetylase Inhibitor Suberoylanilide Hydroxamic Acid Induces Differentiation of Human Breast Cancer Cells. *Cancer Res* 61(23): 8492-7

Mutskov, V and Felsenfeld, D. (2004). Silencing of transgene transcription precedes methylation of promoter DNA and histone H3 lysine 9. *EMBO J* 1: 1-12

Nagarajan, A., Roden, C and Wajapeyee. (2014). Reduced Representation Bisulfite Sequencing to Identify Global Alteration of DNA Methylation. *Methods Mol Biol* 1176: 23-31

Nahta, R and Esteva, F.J. (2006). Herceptin: mechanisms of action and resistance. *Cancer Lett* 232(2): 123-38

Nan, X., Ng, H.H., Johnson, C.A., Laherty, C.D., Turner, B.M., Eisenman, R.N and Bird, A. (1998). Transcriptional repression by the methyl-CpG-binding protein MeCP2 involves a histone deacetylase complex. *Nature* 393(6683): 386-9

Nepali, K and Liou, JP. (2021) Recent developments in epigenetic cancer therapeutics: clinical advancement and emerging trends. *J Biomed Sci* 28, 27 https://doi.org/10.1186/s12929-021-00721-x

Nervi, C., De Marinis, E and Codacci-Pisanelli, G. (2015). Epigenetic treatment of solid tumours: a review of clinical trials. *Clin Epigenet* 7, 127 https://doi.org/10.1186/s13148-015-0157-2

Nessling, M., Richter, K., Schwaenen, C., Roerig, P. *et al.* (2005). Candidate Genes in Breast Cancer Revealed by Microarray-Based Comparative Genomic Hybridization of Archived Tissues. *Cancer Res* 65(2): 439-47

Neuwald, A.F and Landsman, D. (1997). GCN5-related histone N-acetyltransferases belong to a diverse superfamily that includes the yeast SPT10 protein. *Trends Biochem Sci* 22(5):154–5

Nightingale, K.P. (2016). Epigenetics – What it is and Why it Matters? *Epigenetics for Drug Discovery.* RSC Cambridge

Nightingale, K.P., Gendreizig, S., White, D.A., Bradbury, C., Hollfelder, F and Turner, B.M. (2007). Cross-talk between Histone Modifications in Response to Histone Deacetylase Inhibitors. *J Biol Chem* 282(7): 4408-4416

Nightingale, K.P., O'Neill, L.P and Turner, B.M. (2006). Histone modifications: signalling receptors and potential elements of a heritable epigenetic code. *Curr Opin Genet Dev* 16(2): 125-36

Nishioka, K., Chuikov, S., Sarma, K. *et al.* (2002). Set9, a novel histone H3 methyltransferase that facilitates transcription by precluding histone tail modifications required for heterochromatin formation. *Genes Dev* 16(4): 479-89

Noh, E.J and Lee, J-S. (2003). Functional interplay between modulation of histone deacetylase activity and its regulatory role in G2-M transition. *Biochem Biophys Res Commun* 310(2):267–73

Nolan, L., Johnson, P.W.M., Ganesan, A., Packham, G and Crabb, S.J. (2008). Will Histone Deacetylase Inhibitors Require Combination with Other Agents to Fulfil Their Therapeutic Potential? *Br J Cancer* 99(5): 689–94.

Norman, C., Runswick, M., Pollock, R and Treisman, R. (1988). Isolation and properties of cDNA clones encoding SRF, a transcription factor that binds to the c-fos serum response element. *Cell* 55(6): 989-1003

Ogryzko, V.V., Schiltz, R.L., Russanova, V., Howard, B.H and Nakatani, Y. (1996). The transcriptional coactivators p300 and CBP are histone acetyltransferases. *Cell* 87(5): 953–9

Okano, M., Bell, D.W., Haber, D.A and Li, E. (1999). DNA methyltransferases Dnmt3a and DNMT3b are essential for de novo methylation and mammalian development. *Cell* 99(3): 247-57

Oki, Y., Aoki, E and Issa, J-P.J. (2007). Decitabine – Bedside to bench. *Crit Rev Oncol Hematol* 61(2): 140-52

Oliveros, J.C. (2007). VENNY. *An interactive tool for comparing lists with Venn Diagrams.* *https://bioinfogp.cnb.csic.es/tools/venny/index.html*

Ou, J-N., Torrisani, J., Unterberger, A. (2007). Histone deacetylase inhibitor Trichostatin A induces global and gene-specific DNA demethylation in human cancer cell lines. *Biochem Pharmacol* 73(9): 1297-307

Paerhati, P., Liu, J., Jin, Z., Jakoš, T., Zhu, S., Qian, L., Zhu, J and Yuan, Y. (2022). Advancements in Activating Transcription Factor 5 Function in Regulating Cell Stress and Survival. *Int J Mol Sci* 23(13), 7129 https://doi.org/10.3390/ijms23137129

Park, S-Y and Kim, J-S. (2020). A short guide to histone deacetylases including recent progress on class II enzymes. *Exp Mol Med* 52: 204-212

Park, S.Y., Jun, J.A., Jeong, K.J. *et al.* (2011). Histone deacetylase 1,6 and 8 are critical for invasion in breast cancer. *Oncol Rep* 25(6): 1677-81

Parthun, M.R., Widom, J and Gottschling, D.E. (1996). The major cytoplasmic histone acetyltransferase in yeast: links to chromatin replication and histone metabolism. *Cell.* 87(1): 85–94.

Pathiraja, T.N., Stearns, V and Oesterreich, S. (2011). Epigenetic Regulation in Estrogen Receptor Positive Breast Cancer – Role in Treatment Response. *J Mammary Gland Biol Neoplasia* 15(1): 35-47

Peart, M.J., Smyth, G.K., van Laar, R.K. *et al*. (2005). Identification and functional significance of genes regulated by structurally different histone deacetylase inhibitors. *Proc Natl Acad Sci USA* 102(10): 3697-702

Peng, L., Yuan, Z., Ling, H. *et al*. (2011). SIRT1 Deacetylates the DNA Methyltransferase 1 (DNMT1) Protein and Alters Its Activities. *Mol Cell Biol.* 31(23): 4720–34

Piekarz, R.L., Frye, R., Prince, H.M., Kirschbaum. M.H. *et al*. (2011). Phase 2 trial of romidepsin in patients with peripheral T-cell lymphoma. *Blood* 117(22): 5827-34

Pollack, J.R., Sørlie, T., Perou, C.M., Rees, C.A. *et al.* (2002). Microarray analysis reveals a major direct role of DNA copy number alteration in the transcriptional program of human breast tumors. *Proc Natl Acad Sci USA* 99(20): 12963-8

Pouponnot, C., Jayaraman, L and Massagué, J. (1998). Physical and Functional Interaction of SMADs and p300/CBP. *J Biol Chem* 273(36): 22865-8

Prat, A., Parker, J.S., Karginova, O. *et al*. (2010). Phenotypic and molecular characterization of the claudin-low intrinsic subtype of breast cancer. *Breast Cancer Res* 12: R68 https://doi.org/10.1186/bcr2635

Pu, Q., Lu, L., Dong, K. *et al.* (2020). The Novel Transcription Factor CREB3L4 Contributes to the Progression of Human Breast Carcinoma. *J Mammary Gland Biol Neoplasia* 25(1): 37-50

Puleo, J and Polyak, K. (2021). The MCF10 Model of Breast Tumour Progression. *Cancer Res* 81(16): 4183-4185

Qin S., Shi X., Wang C., Jin P., Ma F. (2019). Transcription factor and miRNA interplays can manifest the survival of ccRCC patients. *Cancers* 11(11): 1668 doi: 10.3390/cancers11111668

Qin, X-F., Luo, Y., Suh, H. *et al*. (1994). Transformation by homeobox genes can be mediated by selective transcriptional repression. *EMBO J* 13(24): 5967-5976

Rada-Iglesias, A., Enrouth, S., Ameur, A. *et al.* (2007). Butyrate mediates decrease of histone acetylation centered on transcription start sites and down-regulation of associated genes. *Genome Res* 17(6):708-19

Rafehi, H., Balcercyzk, A., Lunke, S *et al*. (2014). Vascular histone deacetylation by pharmacological HDAC inhibition. *Genome Res* 24(8): 1271-1284

Rakyan, V.K., Down, T.A., Balding, D.J *et al.,* (2011). Epigenome-wide association studies for common human diseases. *Nat Rev Genet* 12(8): 529-41

Raudvere, U., Kolberg, L., Kuzmin, I. *et al.* (2019). g:Profiler: a web server for functional enrichment analysis and conversions of gene lists (2019 update) *Nucleic Acids Res* 47(W1): W191-198 doi:10.1093/nar/gkz369

Riaz, M., van Jaarsveld, M.T.M., Hollestelle, A. *et al.* (2013). miRNA expression profiling of 51 human breast cancer cell lines reveals subtype and driver mutation-specific miRNAs. *Breast Cancer Res* 15(2): R33 doi: 10.1186/bcr3415

Richon, V.M. (2006). Cancer biology: mechanism of antitumour action of Vorinostat (suberoylanilide hydroxamic acid), a novel histone deacetylase inhibitor. *Br J Cancer* 95(S1): S2-S6

Riss, T.L., Moravec, R.A., Niles, A.L. *et al.* (2013). Cell Viability Assays. In *The Assay Guidance Manual.* Bethesda (MD): Eli Lilly & Company and the National Center for Advancing Translational Sciences; 2004. Available from: https://www.ncbi.nlm.nih.gov/books/NBK144065/

Robey, R.W., Chakraborty, A.R., Basseville, A, *et al*. (2011). Histone deacetylase inhibitors: emerging mechanisms of resistance. *Mol Pharm* 8(6): 2021–31

Rouillard, A.D., Gundersen, G.W., Fernandez, N.F. *et al*. (2016). The harmonizome; a collection of processed dataset gathered to serve and mine knowledge about genes and proteins. *Database (Oxford)* https://doi.org/10.1093/database/baw100

Ryan, D. (2022). *MethylDackel*. Available at: https://github.com/dpryan79/MethylDackel. (Accessed on 23/05/2023).

Rzymski, T., Milani, M., Singleton, D.C and Harris, A.L. (2009). Role of ATF4 in regulation of autophagy and resistance to drugs and hypoxia. *Cell Cycle* 8(23): 3838-47

Saint-André, V *et al.,* (2016). Models of human core transcriptional regulatory circuitries. *Genome Res* 26(3): 385-396

Salahuddin, A., Ghanem, H., Omran, G.A and Helmy, M.W. (2022). Epigenetic restoration and activation of ERβ: an inspiring approach for treatment of triple-negative breast cancer. *Med Oncol* 39, 150 https://doi.org/10.1007/s12032-022-01765-1

Santi, D.V., Norment, A and Garrett, C.E. (1984). Covalent bond formation between a DNA-cytosine methyltransferase and DNA containing 5-azacytosine. *Proc. Natl. Acad. Sci USA* 81(22): 6993-7

Santini, V., Kantarjian, H.M and Issa, J-P. (2001). Changes in DNA Methylation in Neoplasia: Pathophysiology and Therapeutic Implications. *Ann Intern Med* 134(7) 573-86

Sarkar, S., Goldgar, B., Byler, S. *et al*. (2013). Demethylation and re-expression of epigenetically silenced tumour suppressor genes: sensitization of cancer cells by combination therapy. *Epigenomics* 5(1): 87-94

Sasakawa, Y., Naoe, Y., Sogo, N. *et al*. (2005). Marker genes to predict sensitivity to FK228, a histone deacetylase inhibitor. *Biochem Pharmacol* 69(4): 603-16

Sato, T., Cesaroni, M., Chung, W *et al.* (2017). Transcriptional Selectivity of Epigenetic Therapy in Cancer. *Cancer Res* 77(2): 470-481

Schöler, H.R. (1991). Octamania: The POU factors in murine development. *Trends Genet* 7(10): 323-9

Schöler, H.R., Hatzopoulos, A.K., Balling, R., Suzuki, N and Gruss, P. (1989). A family of octamer-specific proteins present during mouse embryogenesis: evidence for germline-specific expression of an Oct factor. *EMBO J* 8(9):2543–50

Schreiber, J., Enderich, J, Sock, E. *et al.* (1997). Redundancy of Class III POU Proteins in the Oligodendrocyte Lineage. *The Journal of Biochemistry* 272(51): 32286-32293

Scott, G.K., Marden, C., Xu, F., Kirk, L and Benz, C.C. (2002). Transcriptional repression of ErbB2 by histone deacetylase inhibitors detected by a genomically integrated ErbB2 promoter-reporting cell screen. *Mol Cancer Ther* 1(6): 385-92

Scroggins, B.T., Robzyk, K., Wang, D. *et al.* (2007). An Acetylation Site in the Middle Domain of Hsp90 Regulates Chaperone Function. *Mol Cell* 25(1): 151-9

Seidel, C., Schnekenburger, M., Dicato, M and Diederich, M. (2012). Histone deacetylase modulators provided by Mother Nature. *Genes Nutr* 7(3): 357-367

Sengupta, N and Seto, E. (2004). Regulation of histone deacetylase activities. *J Cell Biochem.* 93(1): 57–67

Seo, J., Min, S.K., Park, H-R. *et al.* (2014). Expression of Histone Deacetylases HDAC1, HDAC2, HDAC3, and HDAC6 in Invasive Ductal Carcinomas of the Breast. *J Breast Cancer* 17(4): 323-31

Seo, J.H., Park, J-H., Li, E.J. *et al*. (2016). ARD1-mediated Hsp70 acetylation balances stress-induced protein refolding and degradation. *Nat Commun.* 7: 12882 doi: 10.1038/ncomms12882

Shadeo, A and Lam, W.L. (2006). Comprehensive copy number profiles of breast cancer cell model genomes. *Breast Cancer Res* 8, R9 https://doi.org/10.1186/bcr1370

Shahbazian, M.D and Grunstein, M. (2007) Functions of Site-Specific Histone Acetylation and Deacetylation. *Annu. Rev. Biochem* 76: 75-100

Shakya, A., Kang, J., Chumley, J., Williams, M.A and Tantin, D. (2011). Oct1 Is a Switchable, Bipotential Stabilizer of Repressed and Inducible Transcriptional States. *J Biol Chem* 286(1): 450-459

Shi, Y. and Massagué, J. (2003). Mechanisms of TGF-signaling from cell membrane to the nucleus. *Cell* 113(6):685–700

Shlien, A and Malkin, D. (2009). Copy number variations and cancer. *Genome Med* 1, 62 https://doi.org/10.1186/gm62

Shogren-Knaak, M., Ishii, H., Sun, J-M. *et al*. (2006) Histone H4-K16 acetylation controls chromatin structure and protein interactions. *Science* 311(5762): 844–7

Shore, P and Sharrocks, A.D. (1995). The MADS-box family of transcription factors *Eur. J. Biochem*. 229(1): 1–13

Simonsson, M., Heldin, C-H., Ericsson, J and Grönroos, E. (2005) The Balance between Acetylation and Deacetylation Controls Smad7 Stability. *J Biol Chem* 280(23): 21797- 803

Simonsson, M., Kanduri, M., Grönroos, E., Heldin, C-H and Ericsson, J. (2006). The DNA Binding Activities of Smad2 and Smad3 Are Regulated by Coactivator-mediated Acetylation. *J Biol Chem* 281(52): 39870-80

Singh, A.K., Bishayee, A and Pandey. A.K. (2018). Targeting Histone Deacetylases with Natural and Synthetic Agents: An Emerging Anticancer Strategy. *Nutrients* 10(6): 731 doi: 10.3390/nu10060731.

Smalley, J.P., Cowley, S.M and Hodgkinson, J.T. (2020). Bifunctional HDAC Therapeutics: One Drug to Rule Them All? *Molecules* 25(19), 4394 https://doi.org/10.3390/molecules25194394

Smith, Z.D., Gu, H., Bock, C *et al.* (2009). High throughput bisulfite sequencing in mammalian genomes. *Methods* 48: 226-32

Smith, Z.D and Meissner, A. (2013). DNA methylation: roles in mammalian development. *Nat Rev Genet* 14: 204-20

Soule, H.D., *et al*. (1973). A human cell line from a pleural effusion derived from a breast carcinoma. *J Natl Cancer Inst* 51(5): 1409-16

Soule, H.D., Maloney, T.M., Wolman, S.R. *et al.* (1990). Isolation and characterization of spontaneously immortalized human breast epithelial cell-line, MCF10A. *Cancer Res* 50(18): 6075-86

Stockert, J.C., Horobin, R.W., Colombo, L.L and Blázquez-Castro, A. (2018). Tetrazolium salts and formazan products in Cell Biology: Viability assessment, fluorescence imaging, and labelling perspectives. *Acta Histochemica* 120(3): 159-167

Strahl, B.D and Allis, D. (2000). The language of covalent histone modifications. *Nature* 403: 41-45

Strunnikova, M., Schagdarsurengin, U and Kehlen, A. (2005). Chromatin Inactivation Precedes De Novo DNA Methylation during the Progressive Epigenetic Silencing of the RASSF1A Promoter. *Mol Cell Biol*. 25(10): 3923-3933

Sun (2019). Bioinformatics Methodology Development for the Whole Genome Bisulfite Sequencing. *Computational Epigenetics and Diseases.* Academic Press.

Suraweera, A., O'Byrne, K.J and Richard, D.J. (2018). Combination Therapy With Histone Deacetylase Inhibitors (HDACi) for the Treatment of Cancer: Achieving the Full Therapeutic Potential of HDACi. *Front. Oncol* 8:92 doi: 10.3389/fonc.2018.00092

Tantin, D. (2013). Oct transcription factors in development and stem cells: insights and mechanisms. *Development* 140(14): 2857-66

Tantin, D., Schild-Poulter, C., Wang, V. *et al.* (2005). The Octamer Binding Transcription Factor Oct-1 Is a Stress Sensor. *Cancer Res* 65(23): 10750-8

Taunton, J., Hassig, C.A and Schreiber, S.L. (1996). A Mammalian Histone Deacetylase Related to the Yeast Transcriptional Regulator Rpd3p. *Science* 272(5620): 408-11

Thiagalingam, S., Cheng, K-H., Lee, H.J. *et al.* (2003). Histone Deacetylases: Unique Players in Shaping the Epigenetic Histone Code. *Ann N Y Acad Sci* 983: 84-100

Thomas, S., Thurn, K.T., Bicaku, E., Marchion, D.C and Munster, P.N. (2011) Addition of a histone deacetylase inhibitor redirects tamoxifen-treated breast cancer cells into apoptosis, which is opposed by the induction of autophagy. *Breast Cancer Res Treat* 130(2): 437-47

Thurn, K.T., Thomas, S., Moore, A., Munster, P.N. (2011). Rational therapeutic combinations with histone deacetylase inhibitors for the treatment of cancer. *Future Oncol*. 7(2): 263-83

Thurn, K.T., Thomas, S., Raha, P., Qureshi, I and Munster, P.N. (2013). Histone Deacetylase Regulation of ATM-Mediated DNA Damage Signaling. *Mol Cancer Ther* 12(10): 2078-87

Treisman, R. (1987). Identification and purification of a polypeptide that binds to the c-fos serum response element. *EMBO J* 6(9): 2711-7

Treisman, R., Marais, R. and Wynne, J. (1992) Spatial flexibility in ternary complexes between SRF and its accessory proteins. *EMBO J* 11(12):4631–4640

Troester, M.A., Herschkowitz, J.I., Oh, D.S. *et al.* (2006). Gene expression patterns associated with p53 status in breast cancer. *BMC Cancer* 6: 276 https://doi.org/10.1186/1471-2407-6-276

Tu, A.W and Luo, K. (2007). Acetylation of Smad2 by the co-activator p300 regulates activin and transforming growth factor beta response. *J Biol Chem* 282(29): 21187–96.

Turner, B.M. (1993). Decoding the nucleosome. *Cell* 75(1): 5-8

Turner, B.M. (2014). Nucleosome signalling; An evolving concept. *Biochimica et Biophysica Acta* 1839(9): 623-6

Turner, B.M., Birley, A.J and Lavender, J. (1992). Histone H4 isoforms acetylated at specific lysine residues define individual chromosomes and chromatin domains in Drosophila polytene nuclei. *Cell* 69(2): 375-84

Turner, B.M., Franchi, L and Wallace, H. (1990). Islands of acetylated histone H4 in polytene chromosomes and their relationship to chromatin packaging and transcriptional activity. *J Cell Sci* 96(Pt2): 335-46

Turner, B.M and Jeppesen, P. (1993). The inactive X chromosome in female mammals is distinguished by a lack of histone H4 acetylation, a cytogenic marker for gene expression. *Cell* 74(2): 281-9

Ungerstedt, J.S., Sowa, Y., Xu, W-S. *et al.* (2005). Role of thioredoxin in the response of normal and transformed cells to histone deacetylase inhibitors. *Proc Natl Acad Sci USA* 102(3): 673-8

Vaissière, T., Sawan, C and Herceg, Z. (2008). Epigenetic interplay between histone modifications and DNA methylation in gene silencing. *Mutat Res* 659(1-2): 40-8

Vallejo, M., Ron, D., Miller, C.P and Habener, J.F. (1993). C/ATF, a member of the activating transcription factor family of DNA-binding proteins, dimerizes with CAAT/enhancer-binding proteins and directs their binding to cAMP response elements. *Proc. Natl. Acad. Sci USA* 90(10): 4679-83

Van Dam, H and Castellazzi, M. (2001). Distinct roles of Jun:Fos and Jun:ATF dimers in oncogenesis. *Oncogene* 20: 2453-2464

van Holde, K.E. (1989). *Chromatin*. Springer Verlag, New York.

Van Lint, C., Emiliani, S and Verdin, E. (1996). The Expression of a Small Fraction of Cellular Genes Is Changed in Response to Histone Hyperacetylation. *Gene Expr* 5(4-5): 245-53

Veenstra, G.J., van der Vliet, P.C. and Destrée, O.H. (1997). POU domain transcription factors in embryonic development. *Mol Bio Rep.* 24(3): 139-55

Villar-Garea, A and Esteller, M. (2004). Histone deacetylase inhibitors: Understanding a new wave of anticancer agents. *Int J Cancer* 112(2): 171-8

Vinson, C.R., Hai, T and Boyd, S.M (1993). Dimerization specificity of the leucine zipper-containing bZIP motif on DNA binding: Prediction and rational design. *Genes Dev* 7(6): 1047–58

Viré, E., Brenner, C., Deplus, R *et al.* (2006). The Polycomb group protein EZH2 directly controls DNA methylation. *Nature* 439: 871-874

Vogelstein, B and Kinzler, K.W. (2004) Cancer genes and the pathways they control. *Nat Med* 10(8): 789-99

Walerych, D., Napoli, M., Collavin, L and Del Sal, G. (2012). The rebel agent: mutant p53 as the driving oncogene in breast cancer. *Carcinogenesis* 33(11): 2007-2017

Wang, S-M., Tie, J., Wang, W-L. *et al.* (2016). POU2F2-oriented network promotes human gastric cancer metastasis. *Gut* 65(9): 1427-38

Wang, Y and Leung, F.C.C. (2004). An evaluation of new criteria for CpG islands in the human genome as gene markers. *Bioinformatics* 20(7): 1170-7

Wang, Z., Gerstein, M and Snyder, M. (2010). RNA-Seq: a revolutionary tool for transcriptomics. *Nat Rev Genet 10*(1): 57-63

Wang, Z., Zang, C., Cui, K. *et al.* (2009). Genome-wide Mapping of HATs and HDACs Reveals Distinct Functions in Active and Inactive Genes. *Cell* 138(5): 1019-31

Wapenaar, H and Dekker, F.J. (2016). Histone acetyltransferases: challenges in targeting bi-substrate enzymes. *Clinical Epigenetics* 8, 59 https://doi.org/10.1186/s13148-016-0225-2

Wawruszak, A., Luszczki, J.J., Grabarska, A. *et al.* (2015). Assessment of Interactions between Cisplatin and Two Histone Deacetylase Inhibitors in MCF7, T47D and MDA-MB231 Human Breast Cancer Cell Lines – An Isobolographic Analysis. *PLoS ONE* 10(11): e0143013. doi:10.1371/journal.pone.0143013

Weichert, W., Denkert, C., Noske, A. *et al*. (2008). Expression of Class I Histone Deacetylases Indicates Poor Prognosis in Endometrial Subtypes of Ovarian and Endometrial Carcinomas. *Neoplasia* 10(9): 1021-7

Weichert, W., Röske, A., Gekeler, V. *et al.* (2008b). Association of patterns of class I histone deacetylase expression with patient prognosis in gastric cancer: a retrospective analysis. *Lancet Oncol* 9(2): 139-48

Wen, Y.D., Perissi, V., Staszewski, L.M. *et al.* (2000). The histone deacetylase-3 complex contains nuclear receptor corepressors. *Proc. Natl. Acad. Sci USA* 97(13): 7202-7

Whyte, W.A *et al.* (2013). Master transcription factors and mediator establish super-enhancers at key cell identity genes. *Cell* 153: 307-319

Wilson, A.J., Chueh, A.C., Tögel, L *et al*. (2010). Apoptotic Sensitivity of Colon Cancer Cells to Histone Deacetylase Inhibitors Is Mediated by an Sp1/Sp3-Activated Transcriptional Program Involving Immediate-Early Gene Induction. *Cancer Res* 70(2): 609-20

Winston, F and Allis, C.D. (1999). The bromodomain: a chromatin-targeting module? *Nat Struct Biol.* 6(7): 601-4

Witt, O., Deubzer, H.E., Milde, T and Oehme, I (2009). HDAC family: What are the cancer relevant targets? *Cancer Lett* 277(1): 8-21

Workman, J.L. and Kingston, R.E. (1998). Alteration of nucleosome structure as a mechanism of transcriptional regulation. *Annu Rev Biochem* 67: 545-79

Wortel, I.M.N., van der Meer, L.T., Kilberg, M.S and van Leeuwen, F.N. (2017). Surviving Stress: Modulation of ATF4-Mediated Stress Responses in Normal and Malignant Cells. *Trends Endocrinol Metab* 28(11): 794-806

Xu, L., Glass, C.K., and Rosenfeld, M.G. (1999). Coactivator and corepressor complexes in nuclear receptor function. *Curr. Opin. Genet. Dev* 9(2): 140–7

Yang, H., Liu, Y., Bai, F. *et al*. (2013). Tumor development is associated with decrease of TET gene expression and 5-methylcytosine hydroxylation. *Oncogene* 32(5): 663-9

Yang, X-J and Seto, E. (2008). Lysine Acetylation: Codified Crosstalk with Other Posttranslational Modifications. *Mol Cell* 31(4): 449-461

Yang, X. *et al.* (2001). Synergistic activation of functional estrogen receptor (ER)-by DNA methyltransferase and histone deacetylase inhibition in human ER-negative breast cancer cells. *Cancer Res* 61(19): 7025-9

Yang, X., Lay, F., Han, H and Jones, P.A. (2010). Targeting DNA methylation for epigenetic therapy. *Trends Pharmacol Sci* 31(11): 536-46

Yin, L., Duan, J-J., Bian, X-W and Yu, S-C. (2020). Triple-negative breast cancer molecular subtyping and treatment progress. *Breast Cancer Res* 22, 61 https://doi.org/10.1186/s13058-020-01296-5

Yun, M., Wu, J., Workman, J.L and Li, B. (2011). Readers of histone modifications. *Cell Res.* 21(4): 564-78

Zentner , G.E and Henikoff, S. (2013). Regulation of nucleosome dynamics by histone modifications. *Nat Struct Mol Biol* 20(3): 259–66

Zhang, H., Zhang, N., Liu, Y. *et al*. (2019). Epigenetic Regulation of *NAMPT* by *NAMPT-AS* Drives Metastatic Progression in Triple-Negative Breast Cancer. *Cancer Res* 79(13): 3347-59

Zhang, Y.W., Wang, Z., Xie, W. *et al*. (2017). Acetylation Enhances TET2 Function in Protecting Against Abnormal DNA Methylation during Oxidative Stress. *Mol Cell* 65(2): 323-335

Zhang, Z., Yamashita, H., Toyama, T. *et al.* (2004). HDAC6 Expression Is Correlated with Better Survival in Breast Cancer. *Clin Cancer Res.* 10(20): 6962-8

Zhang, Z., Yamashita, H., Toyama., T. *et al*. (2005). Quantitation of HDAC1 mRNA expression in invasive carcinoma of the breast. *Breast Cancer Res Treat* 94(1): 11-16

Zhao, F-Q., Zheng, Y., Dong, B and Oka, T. (2004). Cloning, genomic organization, expression, and effect on beta-casein promoter activity of a novel isoform of the mouse Oct-1 transcription factor. *Gene* 326: 175–87

Zhou, Q., Agoston, A.T., Atadja, P., Nelson, W.G and Davidson, N.E. (2008). Inhibition of Histone Deacetylase Promotes Ubiquitin-Dependent Proteasomal Degradation of DNA Methyltransferase 1 in Human Breast Cancer Cells. *Mol Cancer Res* 6(5): 873-883

Zhou, Q., Atadja, P and Davidson, N.E. (2007) Histone deacetylase inhibitor LBH589 reactivates silenced estrogen receptor alpha (ER) gene expression without loss of DNA hypermethylation. *Cancer Biol Ther* 6(1):64–69

10. APPENDICES

10.1 Treatment with DAC for less than 96-hours did not induce apoptosis in our cell-lines

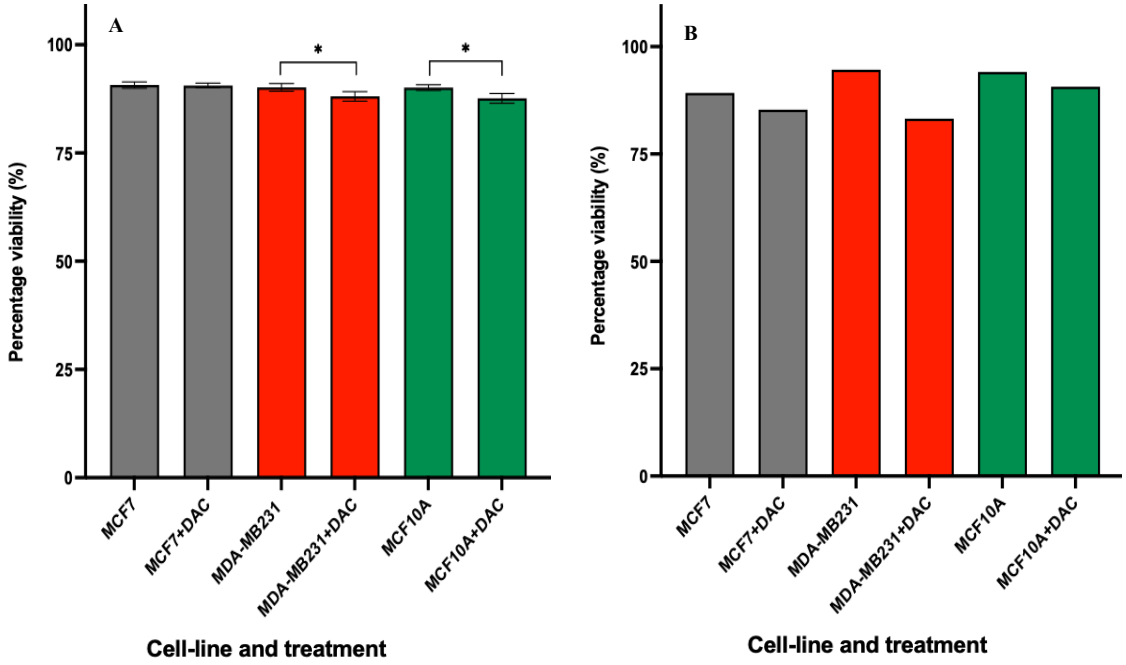


Figure 10.1: 96-hour DAC treatment was required to observe an apoptotic response in our solid tumour cell-lines. *The viable population remaining in untreated MCF7, MDA-MB231 and MCF10A cells versus that remaining following treatment with 1 μM DAC for A. 48-hours and B. 72-hours was assessed using the Annexin V/PI apoptosis assay. One-tailed, paired T-test *p<0.05. Error bars show SEM of independent experiments (N=3).*

10.2 Both cell-lines responded similarly to SAHA treatment at the level of the cell-cycle

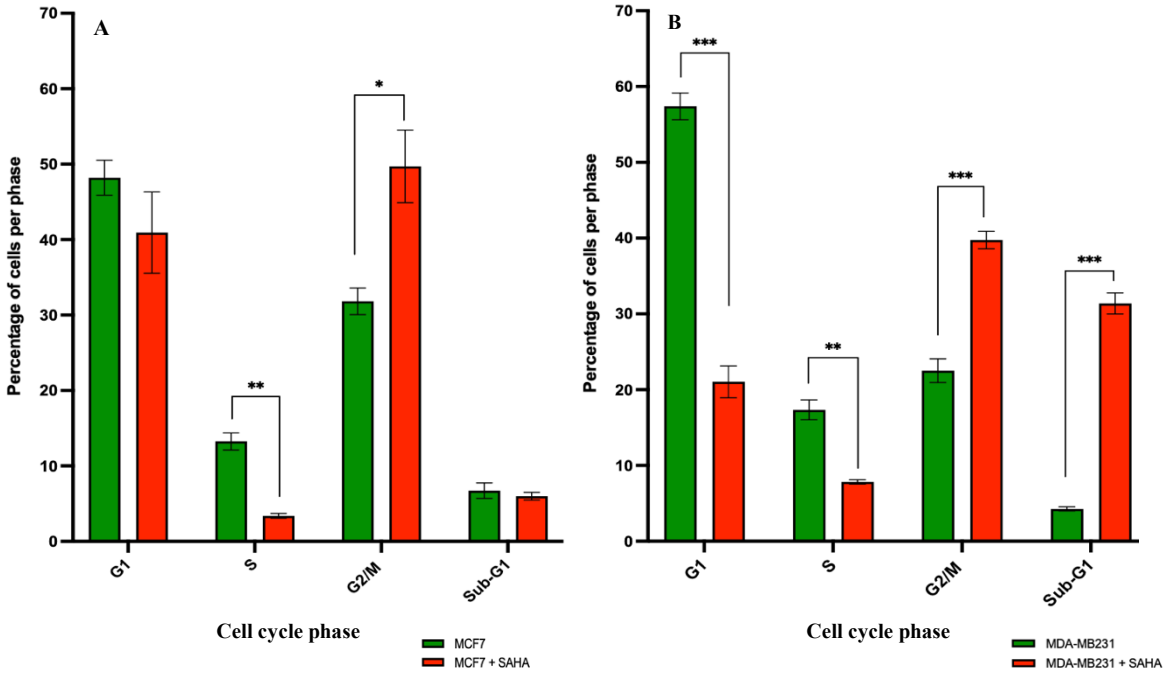


Figure 10.2: MCF7 and MDA-MB231 cells exhibited similar cell-cycle alterations following 48-hour SAHA treatment. *The proportion of A. MCF7 and B. MDA-MB231 cells present in G1, S, G2/M and Sub-G1 in cells treated with 2.5μM SAHA for 48-hours (red) versus the untreated cells (green) was assessed by Flow Cytometry. Two-tailed, paired T-test *p<0.05, **p<0.01, ***p<0.001 Error bars show SEM of independent experiments (N=4).*

10.3 2-hour SAHA treatment induced histone hyperacetylation in both cell-lines

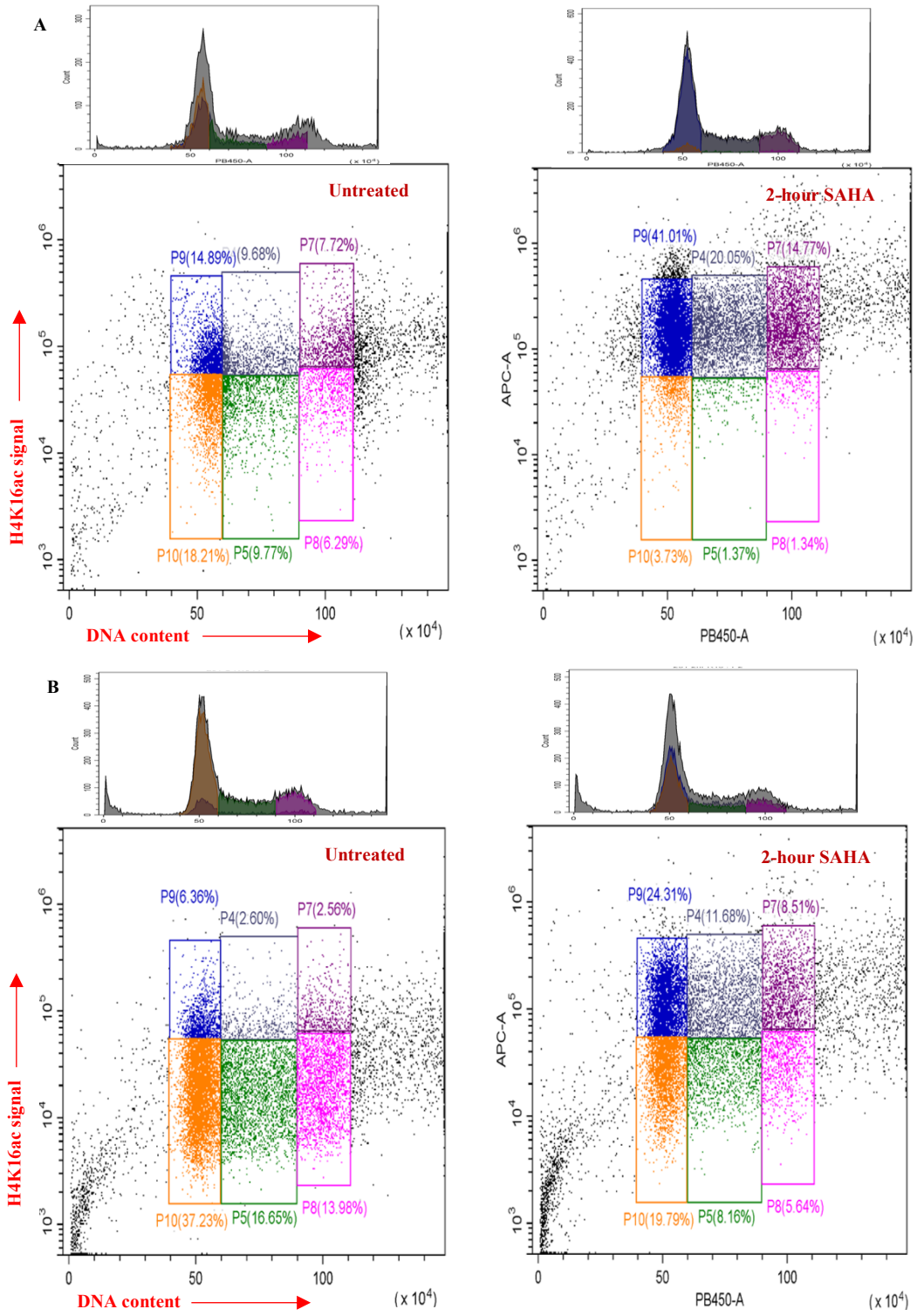


Figure 10.3: H4K16 hyperacetylation was evident after 2-hour SAHA treatment in both cell-lines. *Flow Cytometry analysis of the H4K16ac signal obtained from A. MCF7 and B. MDA-MB231 cells either untreated or following treatment with 2.5 μM SAHA for 2-hours.*

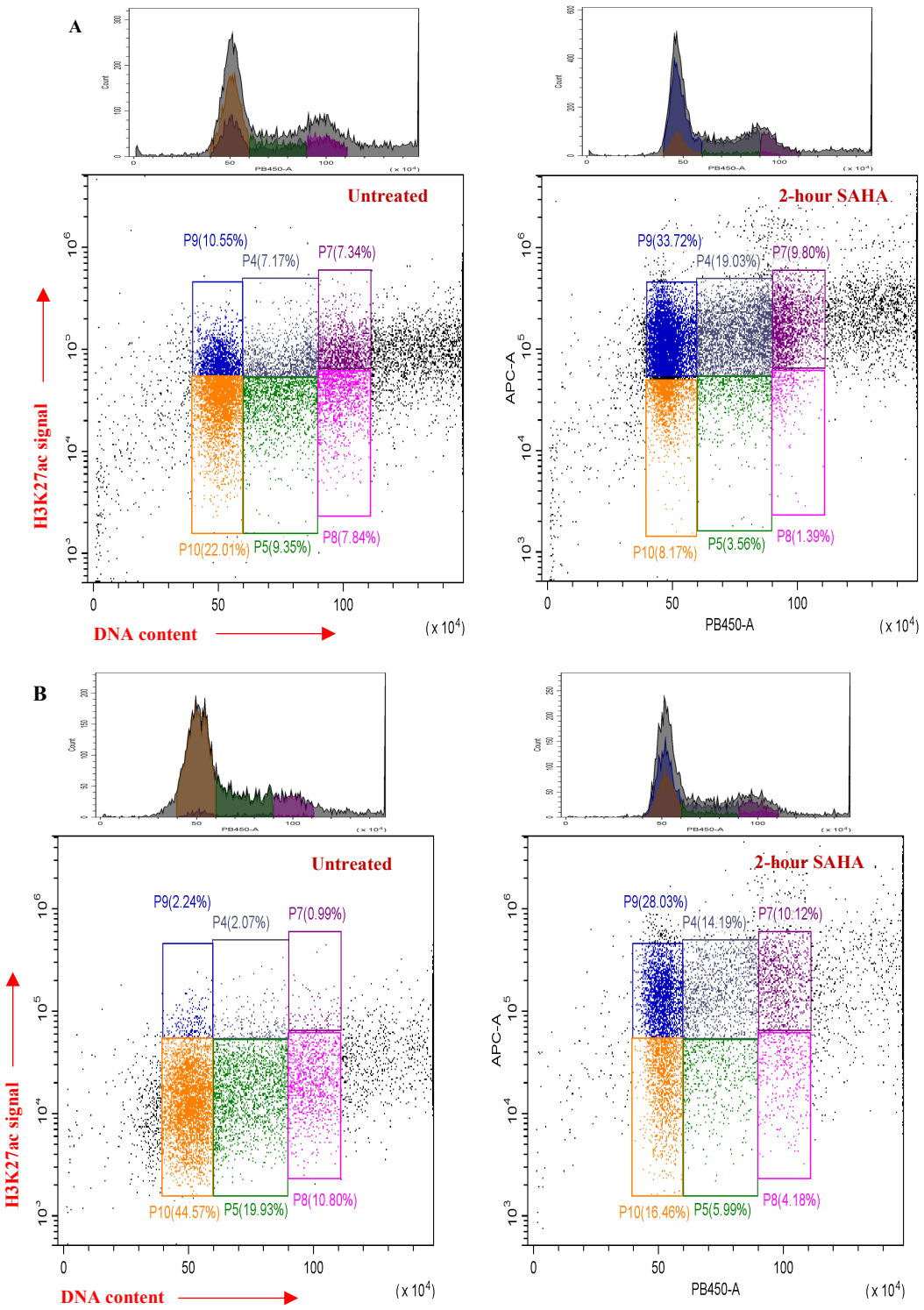


Figure 10.4: Hyperacetylation of H3K27 was observed in both cell-lines after 2-hour SAHA treatment. *Flow Cytometry analysis of the H3K27ac signal obtained from A. MCF7 cells and B. MDA-MB231 treated with 2.5 μM SAHA for 2-hours.*

10.4 IgG and C-terminal staining were not affected by SAHA treatment

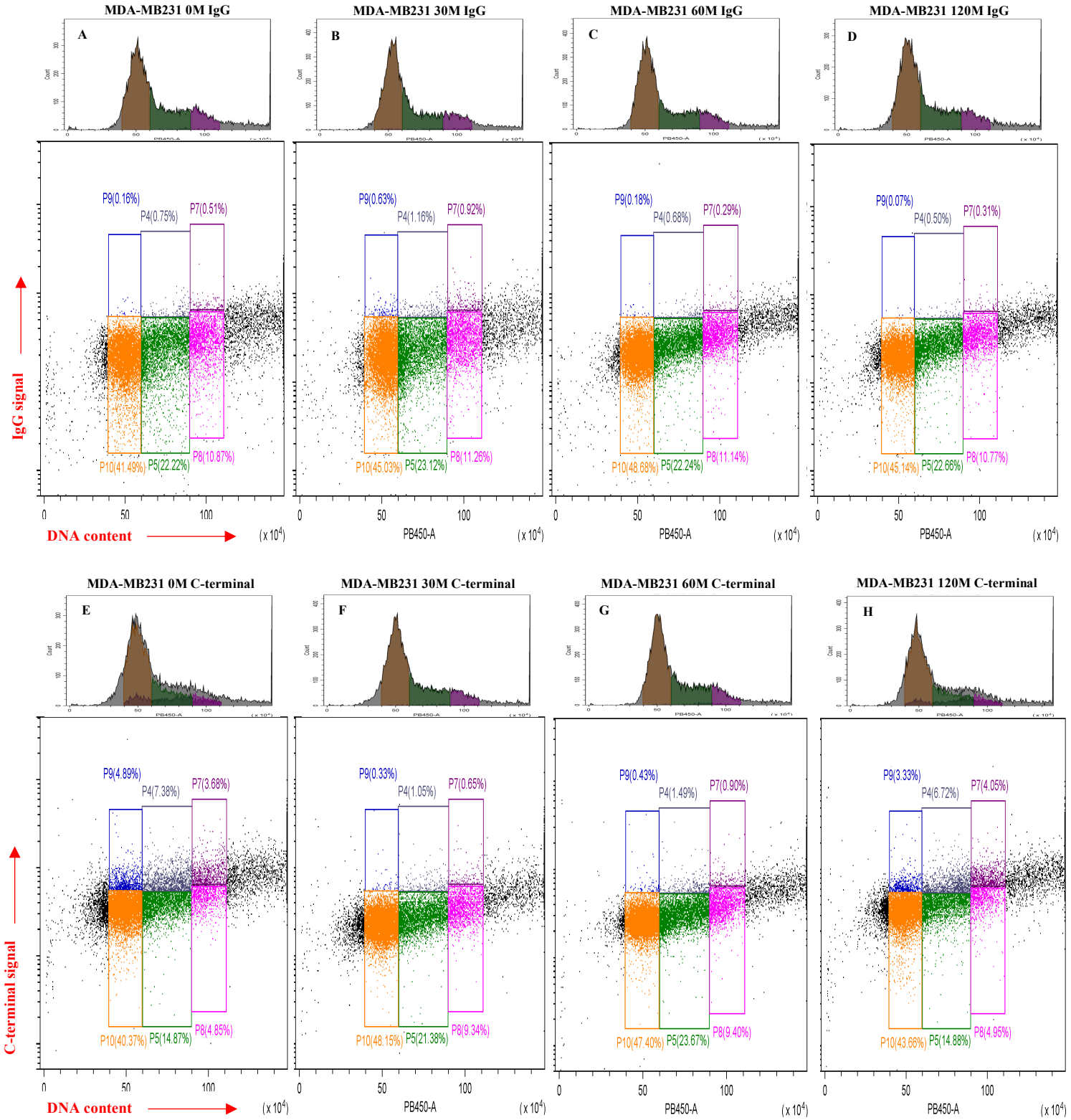


Figure 10.5: The IgG and C-terminal signal did not increase during the 2-hour SAHA treatment time course. *Flow Cytometry analysis of the IgG signal in A. untreated and MDA-MB231 cells treated with 2.5 μM SAHA for B. 30-minutes, C. 60-minutes and D. 120-minutes and the binding of the C-terminal antibody in E. untreated and MDA-MB231 cells treated with 2.5μM SAHA for F. 30-minutes, G. 60-minutes and H. 120-minutes.*

10.5 Correlation was observed between the MDA-MB231 timepoint samples in the RNA-Sequencing

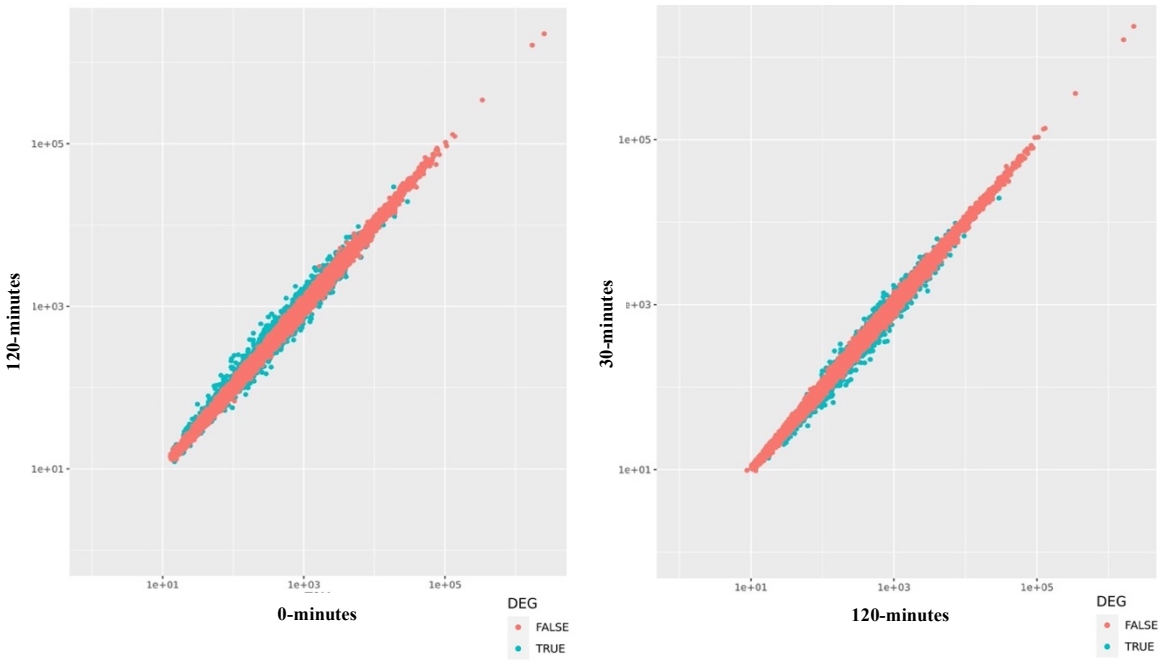


Figure 10.6: The MDA-MB231 RNA Sequencing timepoint samples correlate. *Comparison of the gene expression patterns between A. 120-minute and 0-minute and B. 120-minute, and 30-minute SAHA treated MDA-MB231 timepoint samples. Orange depicts non differentially expressed genes and green depicts those differentially expressed.*

10.6 The Lipofectamine 3000 transfection protocol was optimised for use in MCF7 and MDA-MB231 cells

The Lipofectamine 3000 transfection protocol was optimised using a GFP expressing plasmid. This allowed the appropriate Lipofectamine concentration for use in both cell-lines to be determined, as well as the optimal incubation time and seeding density. This involved the transformation of a GFP vector pmax plasmid. To ensure there would be sufficient colonies, 1 and 5 ng of plasmid were incubated with 50 µl of DH5α. 20µl and 200 µl of both cultures were then streaked onto Kanamycin selective plates. A colony from the 5 ng and 20 µl plate was selected to be grown and concentrated, producing plasmid at a concentration of 0.33 µg/µl.

Cells were initially transfected with 2.5 µg plasmid for 24-hours using 5 µl Lipofectamine 3000. To confirm plasmid incorporation, the presence of GFP in cells was assessed using the EVOS Microscope (AMG). The presence of GFP within cell nuclei showed that the plasmid incorporated into both cell-lines (Figure 10.7). However, 24-hour incubation with Lipofectamine was toxic to the cells. Thus, the seeding density was increased to ensure a greater density of cells on the day of transfection and the Lipofectamine incubation time was reduced to 4-hours.

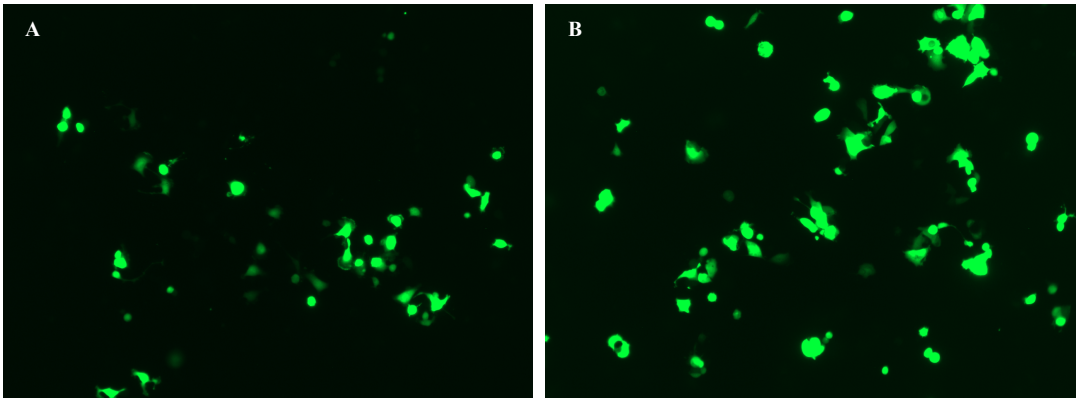


Figure 10.7: The GFP expressing plasmid transfected efficiently into both cell-lines following 24-hour incubation with Lipofectamine 3000. *GFP expression in A. MDA-MB231 and B. MCF7 cells following transfection with 2.5 µg plasmid DNA using 5 µl Lipofectamine for 24-hours. Images acquired at 10x objective on the EVOS Microscope.*

The next step involved determining the most effective concentration of Lipofectamine for use in each cell-line. Cells were transfected with 2.5 µg plasmid using 2.5 µl, 5 µl or 7.5 µl Lipofectamine and fresh media applied after 4-hours. 24-hours post transfection, the incorporation of GFP was quantified by Flow Cytometry to determine the transfection efficiency. The greatest efficiency was observed using 2.5 µl in MCF7 cells, while MDA-MB231 cells required 5 µl of Lipofectamine (Figure 10.8). Toxicity was evident in the cells exposed to 7.5 µl Lipofectamine, leading to the question of whether Lipofectamine was toxic to the cells. Cells incubated with 2.5 µl Lipofectamine only for 2-hours exhibited no loss in viability, indicating that Lipofectamine was not toxic to the cells.

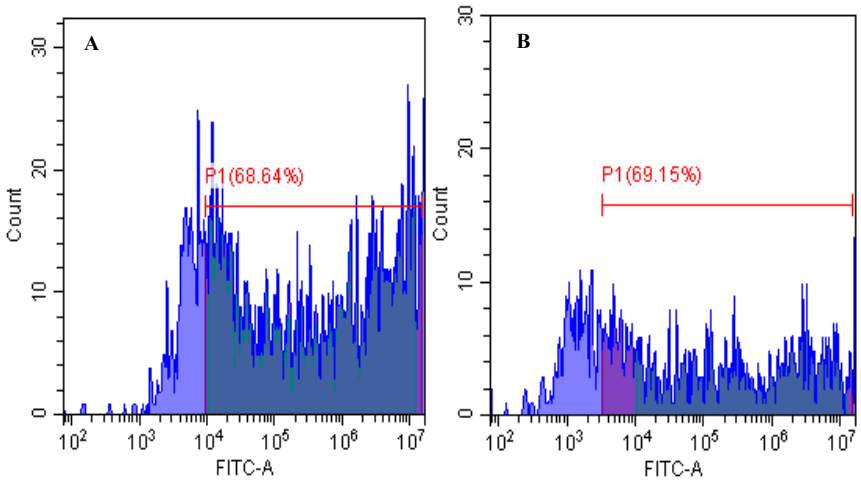


Figure 10.8: Efficient GFP transfection was achieved in MCF7 cells using 2.5µl Lipofectamine in MDA-MB231 using 5 µl Lipofectamine in. *The percentage of GFP expressing cells was assessed by Flow Cytometry in A. MCF7 cells transfected using 2.5 µl Lipofectamine and B. MDA-MB231 cells transfected using 5µl Lipofectamine with 2.5 µg plasmid DNA for 4-hours. P1 was set on the untransfected cell population.*

The effect of seeding density on transfection efficiency was then assessed. Initial experiments analysed GFP incorporation after 48-hours; however, future work would require cells to be grown for 96-hours. MCF7 cells were seeded in 6-well plates at densities of approximately $2.5x10^5$, $1.9x10^5$ and $1.4x10^5$ cells per well and transfected with the Cy3-labelled fluorescent transfection control siRNA duplex (ORIGENE). After 4-hours fresh DMEM was applied, with the transfection efficiency quantified after 48-hours. Cell density on the day of transfection did not affect the resulting transfection efficiency (Figure 10.9). The percentage of transfected cells ranged from 89.5% when seeded at the greatest density ($2.5x10^5$ cells) to 93.4% when seeding at the lowest density ($1.4x10^5$ cells). This experiment confirmed that cells would be incubated with Lipofectamine for

only 4-hours, and that sufficient transfection could be obtained in cells seeded at a density for 96-hours of growth.

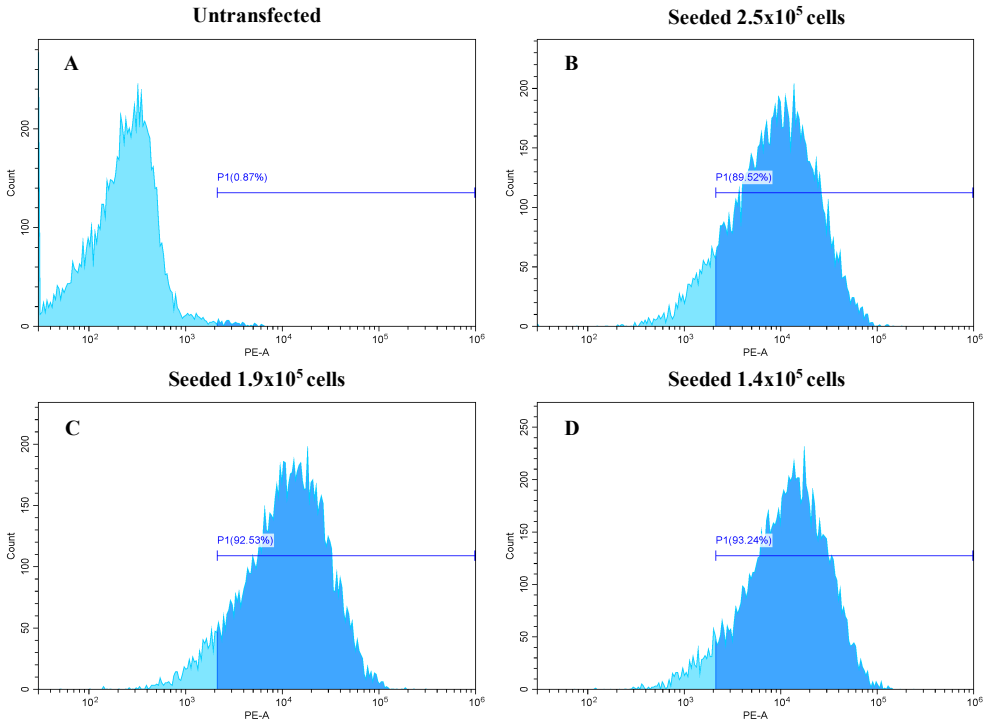


Figure 10.9: Seeding density on the day of transfection did not affect the efficiency of siRNA incorporation into MCF7 cells. *The percentages of cells transfected with the Cy3-labelled siRNA control assessed by Flow Cytometry when seeded at B. 2.5x10^5 C. 1.9x10^5 and D. 1.4x10^5 cells per well with PE-A gating set on the A. untransfected MCF7 cell population. Images generated using CytExpert software.*

10.7 Primers were designed to identify the unique exon structures of the POU2F2 transcript variants

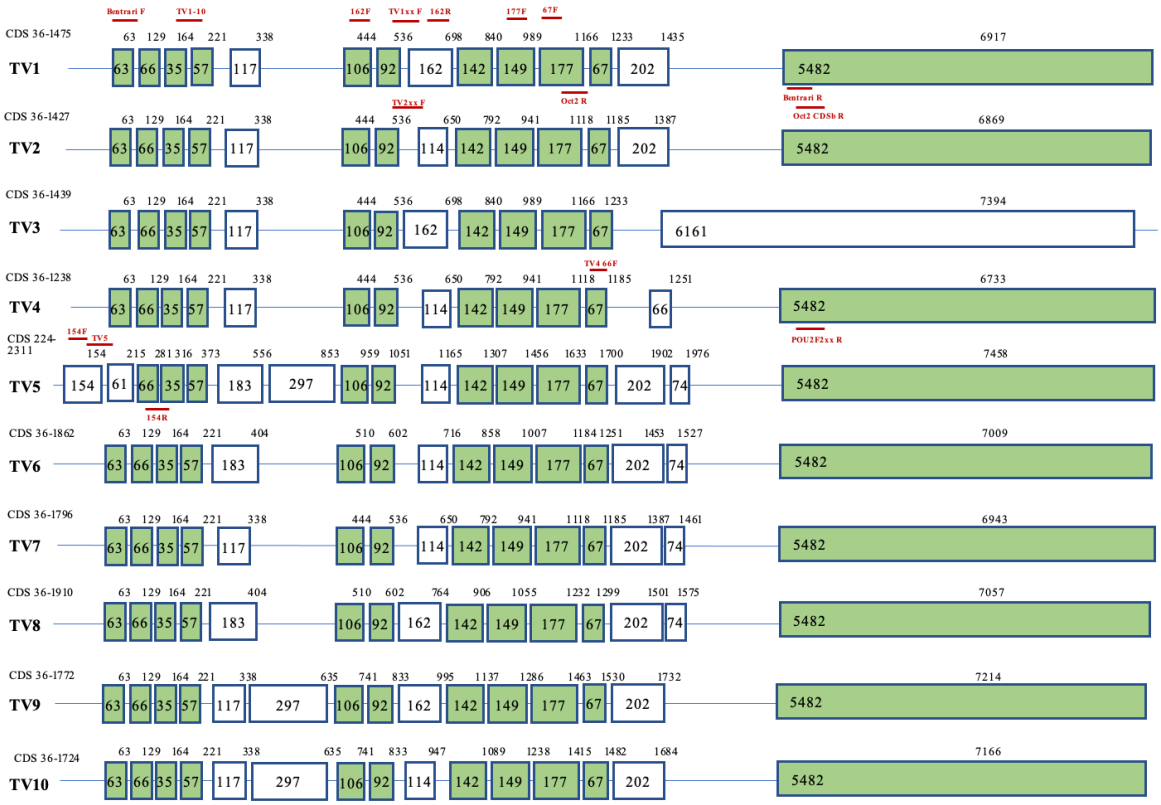


Figure 10.10: The exon structure of the ten POU2F2 transcript variants. *Indicated are the exons included in the individual variants and depicted in red are the sites targeted by the individual primer sets.*

Primer set	Transcript Size
TV1-10	TV1/2/3/4/7:256 bp
TV5 + Bentrari R	1891 bp
Bentrari F/R	TV1:1437 bp, TV2:1389 bp, TV3:1914 bp, TV4:1253 bp, TV6:1529 bp, TV7:1463 bp, TV8:1577 bp, TV9:1734 bp, TV10:1686 bp
TV5 154F/R	167 bp
TV5 154F +Bentrari R	1819 bp
Bentrari F + Oct2 CDSb R	TV1:1445 bp, TV2:1397 bp, TV3:1922 bp, TV4:1261 bp, TV6:1537 bp, TV7:1471 bp, TV8:1585 bp, TV9: 1742 bp, TV10:1694 bp
TV1xx F/R	TV1/3/8/9:592 bp
TV2xxF + POU2F2xx R	TV2/10:995 bp, TV4:859 bp, TV5/6/7:1069 bp
TV4 66F + POU2F2xx R	TV1/2/9/10:361 bp, TV3: 838 bp, TV4:225 bp, TV5:435 bp, TV6/7/8:435 bp
162F/R	TV2/4/5/6/7/10: 198 bp or TV1/3/8/9:246 bp

10.8 Primers were designed to identify the unique exon structures of the POU2F1 transcript variants

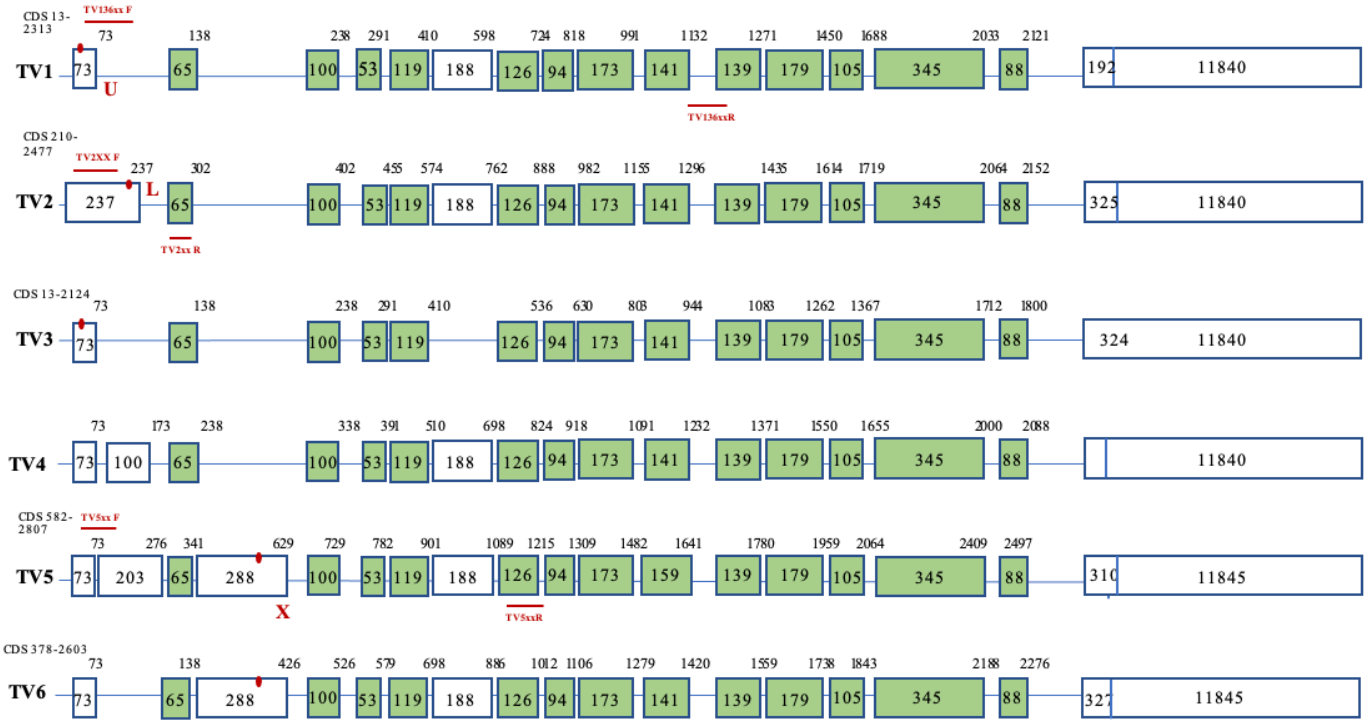


Figure 10.11: The exon structure of the six POU2F1 transcript variants. *The five variants coding for proteins are transcribed from alternate promoters U, L or X. The regions targeted by the TV136xxF, Oct1R, TV2xxF/R and TV5xxF primers are indicated in red.*

Primer set	Transcript Size
TV136xx F/R	TV1:1084 bp, TV3:895 bp, TV5/6:1373 bp
TV2xx	237 bp
TV5xx	1060 bp